
Mechanics and information of macromolecules

Semiflexible polymer dynamics and enzymatic self-replication

Benedikt Obermayer



München 2010

Mechanics and information of macromolecules

Semiflexible polymer dynamics and enzymatic self-replication

Benedikt Obermayer

Dissertation
an der Fakultät für Physik
der Ludwig–Maximilians–Universität
München

vorgelegt von
Benedikt Obermayer
aus Gräfelfing

München, den 25. März 2010

Erstgutachter: Prof. Dr. E. Frey

Zweitgutachter: Prof. Dr. K. Kroy

Tag der mündlichen Prüfung: 10. Mai 2010

Contents

Zusammenfassung	ix
Abstract	xi
1. Introduction	1
1.1. Semiflexible polymers in cell division and the cytoskeleton	2
1.2. Prebiotic self-replication at the origin of life	7
2. Nonlinear dynamic response of semiflexible polymers	13
2.1. Wormlike chain dynamics	14
2.1.1. Equations of motion	14
2.1.2. The weakly-bending limit	15
2.1.3. The dynamics on the linear level	16
2.1.4. Failure of the linear theory	18
2.2. Tension dynamics for wormlike chains	18
2.2.1. Multiple-scale perturbation theory	19
2.2.2. Coarse-grained equation of motion for the tension	20
2.3. Longitudinal response	21
2.4. Transverse response	24
2.5. Relaxation dynamics	26
2.6. Microstructure corrections	30
2.6.1. Backbone extensibility	30
2.6.2. Backbone discretization	32
2.7. Conclusions	33
2.8. Outlook	33
2.9. B. Obermayer and O. Hallatschek, <i>Phys. Rev. Lett.</i> 99 , 098302 (2007) . . .	35
2.10. B. Obermayer, W. Möbius, O. Hallatschek, E. Frey, and K. Kroy, <i>Phys. Rev. E</i> 79 , 021804 (2009)	39
2.11. B. Obermayer and E. Frey, <i>Phys. Rev. E</i> 80 , 040801(R) (2009)	53
3. Quasispecies theory for specific enzymatic replication	57
3.1. Eigen's quasispecies theory	58
3.1.1. Fitness landscapes	58
3.1.2. Formal solution	59
3.1.3. Simple symmetric fitness landscapes	60

3.1.4. The error threshold	62
3.1.5. Neutrality in fitness landscapes	65
3.2. Enzymatic catalysis	66
3.2.1. Non-enzymatic vs. enzymatic replication	66
3.2.2. The replicator-mutator equation	67
3.2.3. Hypercycles	69
3.3. Specific enzymatic replication	70
3.3.1. Recognition regions and high specificity	71
3.3.2. General specificity functions	73
3.4. Conclusions	74
3.5. Outlook	75
3.6. B. Obermayer and E. Frey, <i>Europhys. Lett.</i> 88 , 48006 (2009)	77
3.7. B. Obermayer and E. Frey, submitted (2010)	83
A. Calculation details for Chapter 2	107
A.1. Asymptotic force-extension relations	107
A.2. Discretization effects	107
A.2.1. Small force	108
A.2.2. Intermediate force	109
A.2.3. Large force	111
Bibliography	113
Danksagung	133
Curriculum Vitae	135

List of Figures

1.1. Sketch of DNA replication	3
1.2. Single-molecule experiments on DNA	3
1.3. Mitotic spindle	5
1.4. Semiflexible polymers in the cytoskeleton	6
1.5. Non-enzymatic polymerization and ligation	8
1.6. RNA polymerase ribozyme	9
1.7. Emergence of cells	10
1.8. Mutation rate and genome sizes across species	11
2.1. Force scenario for the longitudinal response	21
2.2. Asymptotic regimes for the longitudinal response	23
2.3. Force scenario for the transverse response	24
2.4. Different setups for relaxation experiments	27
3.1. Mutant distributions for exemplary fitness landscapes	61
3.2. Non-enzymatic vs. enzymatic replication	68

Zusammenfassung

In seinem Buch “Was ist Leben?” beschreibt Erwin Schrödinger die DNA-Stränge, die die Erbinformation enthalten, aus der Perspektive eines Physikers als “aperiodische Kristalle”. Tatsächlich zeichnet sich DNA auf kleinen Längenskalen durch eine zwar irreguläre und aperiodische, aber dezidiert nicht-zufällige Unordnung in der Basensequenz aus, um als Träger für genetische Information dienen zu können, während die regelmäßige und daher kristalline Struktur auf größeren Skalen für die besonderen mechanischen Eigenschaften dieses Makromoleküls verantwortlich ist. In der vorliegenden Arbeit werden mittels theoretischer Modelle aus der biologischen und statistischen Physik die Mechanik und Information von Makromolekülen untersucht, im ersten Teil insbesondere die nichtlineare Dynamik halbsteifer Polymere, im zweiten Teil mit Fokus auf dem maximalen Informationsgehalt enzymatisch selbst-replizierender Polynukleotide.

Der erste Teil der Arbeit befasst sich mit Biopolymeren relativ großer Biegesteifigkeit. Dies trifft nicht nur auf DNA, sondern auch auf die Konstituenten des Zellskeletts zu. Ihre mechanischen Eigenschaften werden ausgezeichnet durch das sogenannte “wormlike-chain”-Modell beschrieben, in dem die Polymerkontur als kontinuierliche Raumkurve konstanter Länge idealisiert wird. In viskosem Lösungsmittel folgt ihre Brownsche Dynamik überdämpften Bewegungsgleichungen, die wegen der lokalen Undehnbarkeits-Zwangsbedingung nichtlinear sind. Simple Näherungsverfahren versagen bei plötzlichen äußeren Störungen aufgrund der vernachlässigten Spannungspropagation. Eine Mehrskalens-Störungstheorie erlaubt die Berechnung der Spannungsdynamik über eine nichtlineare partielle Integro-Differentialgleichung. Wir verwenden und erweitern diese Methodik, um drei relevante Szenarien der nichtlinearen Polymerdynamik zu untersuchen. Zuerst behandeln wir Kräfte transversal zur Kontur, die aufgrund der Undehnbarkeit an die longitudinale Dynamik koppeln, was sich über eine effektive Randbedingung berechnen lässt. Zweitens betrachten wir die Relaxation anfänglich gestreckter Polymere, ein Standardexperiment der Polymerphysik. Unsere Analyse kombiniert Theorie und Computersimulation und zeigt, dass verschiedene gebräuchliche Streckmethoden (etwa mit mechanischen, elektrischen oder hydrodynamischen Kräften) zu spezifischer Kurzzeit- und universeller Langzeitdynamik führen, so dass ein systematischer Vergleich erstmals möglich ist. Drittens untersuchen wir Mikrostrukturkorrekturen, die wegen endlicher Elastizität oder Diskretisierung der Kontur bei größeren Kräften beobachtet werden. Diese Erkenntnisse sind besonders für den korrekten Entwurf von Computersimulationen relevant.

Der zweite Teil dieser Arbeit konzentriert sich auf den maximalen Informationsgehalt selbst-replizierender Polynukleotide wie z. B. RNA. Dieses Molekül enthält genetische Information und kann zugleich enzymatische Funktionen ausführen, weshalb man vermutet, dass die ersten replizierenden Makromoleküle am Ursprung des Lebens aus RNA

bestanden. Berechnungen innerhalb der Quasispezies-Theorie zeigen, dass ihre maximale Länge, also ihr Informationsgehalt, wegen der unvermeidlich fehlerhaften Replikation durch die sogenannte Fehlerkatastrophe stark beschränkt ist. Allerdings wurden diese Modelle für nicht-enzymatische Replikation entwickelt, die als autokatalytischer Prozess in einer präbiotischen Umgebung eher unwahrscheinlich ist. Die plausiblere Replikation durch RNA-Enzyme ist aber nur dann für das Enzym selbst von evolutionärem Vorteil, wenn es in einer *spezifischen* Reaktion vorzugsweise funktionale Substrate repliziert. Wir analysieren zwei Modelle für spezifische enzymatische Replikation. Im ersten Fall, der eine gesonderte Spezifitätsregion des Moleküls berücksichtigt, zeigt sich, dass der maximale Informationsgehalt deutlich reduziert ist, da die effektive Replikationsrate mit der Konzentration funktionaler Enzyme sinkt. In der zweiten Arbeit werden diese Ergebnisse auf generelle Spezifitätsfunktionen verallgemeinert. Techniken aus der statistischen Physik erlauben eine systematische theoretische Analyse, die die vollständige Abhängigkeit der maximal zulässigen Fehlerrate von allen Modellparametern liefert. Ihre Zunahme mit dem Spezifitätsgrad unterstreicht die Bedeutung spezifischer enzymatischer Replikation. Eine grobe numerische Abschätzung zeigt, dass auch in diesem Fall die maximale Länge stark durch die Fehlerkatastrophe beschränkt ist.

Die Arbeit gliedert sich wie folgt: In der Einleitung geben wir einerseits einen Überblick der wichtigsten experimentellen und theoretischen Literatur zur Rolle halbsteifer Biopolymere während der Zellteilung und im Zellskelett, andererseits diskutieren wir gegenwärtige Hypothesen und Laborergebnisse zum Ursprung des Lebens, zur Entstehung selbst-replizierender Moleküle und Protozellen und zur Fehlerkatastrophe. Kapitel 2 behandelt die Dynamik von halbsteifen Polymeren und ihre theoretische Beschreibung, und stellt nach einer kurzen Rekapitulation einer früheren Arbeit die Hauptergebnisse unserer drei Publikationen zu diesem Themengebiet vor, die am Ende des Kapitels abgedruckt sind. Die Details zu einigen dieser Rechnungen sind im Anhang ausgeführt. In Kapitel 3 geben wir zuerst eine Einführung in die Quasispezies-Theorie und ihre Vorhersagen für verschiedene gebräuchliche Fitnesslandschaften, danach betrachten wir die Besonderheiten enzymatischer Replikation. Schließlich werden unsere beiden Veröffentlichungen zu dieser Thematik zusammengefasst und am Ende des Kapitels abgedruckt.

Abstract

Erwin Schrödinger describes the DNA strands coding for hereditary information in his book “What is Life?” as “aperiodic crystals”. On small length scales, DNA indeed shows an irregular and aperiodic, yet decidedly non-random disorder, thus coding for genetic information, while the regular and therefore crystal-like structure on larger scales is responsible for the particular mechanical properties of this macromolecule. In this thesis, we analyze the mechanics and information of macromolecules by means of theoretical models from biological and statistical physics. We first concentrate on the nonlinear dynamics of semiflexible polymers, and focus on the maximal information content of enzymatically self-replicating polynucleotides in a second part.

The first part of this thesis is concerned with biopolymers of relatively large bending stiffness, which is the case not only for DNA, but also for the constituents of the cytoskeleton. The mechanical properties of these polymers can be described accurately by means of the so-called “wormlike-chain” model, where the polymer contour is idealized as continuous space curve of constant length. In a viscous solvent, the Brownian dynamics of these chains obeys overdamped equations of motion, which are nonlinear due to a local inextensibility constraint. Simple approximation techniques fail in the case of sudden external perturbations because tension propagation is neglected. An improved multiple-scale perturbation theory allows to calculate the dynamics of this tension from a nonlinear partial integro-differential equation. We use and extend this method to investigate three relevant scenarios of nonlinear polymer dynamics. First, we discuss transverse forces perpendicular to the contour. As a consequence of the inextensibility constraint, these forces couple nonlinearly to the longitudinal dynamics, which can be quantified through an effective boundary condition for the tension. Secondly, we address the relaxation of initially straight polymers, which is a standard experiment in polymer physics. Combining theory and computer simulations, our analysis shows that different commonly employed stretching methods (such as mechanical, electrostatic, or hydrodynamic forces) give rise to specific short-time but universal long-time dynamics, facilitating a systematic comparison of results obtained with different setups. Finally, we investigate microstructure corrections due to a finite backbone elasticity or discretization, which become observable for stronger forces. These results are especially relevant for the proper design of computer simulations.

The second part is concerned with the maximal information content of self-replicating polynucleotides such as RNA. This molecule both contains genetic information and exhibits catalytic functions, such that the first replicating macromolecules at the origin of life were presumably made of RNA. Theoretical considerations within quasispecies theory show that their maximal length, i.e., their information content, is strongly limited due to a so-called error catastrophe caused by the unavoidably erroneous replication process. How-

ever, these models were made for non-enzymatic replication, which is as an autocatalytic process rather unlikely in a prebiotic environment. Replication through RNA enzymes is more plausible, but is of evolutionary advantage for the enzyme itself only if the reaction *specificity* guarantees that it replicates preferably functional substrates. We analyze two models for specific enzymatic replication. In the first case, we consider a distinct recognition region for specificity. It turns out that the maximal information content is significantly reduced, because the effective replication rate decreases with the concentration of functional enzymes. In our second study, we generalize these results to a broad range of specificity functions. Using techniques from statistical physics, a systematic theoretical analysis gives the complete dependence of the maximally tolerable error rate on all model parameters. Generally, it increases with the degree of specificity, highlighting the importance of specific recognition. A rough numerical estimate indicates that the maximal length of enzymatic replicators is strongly limited through the error catastrophe as well.

This thesis is organized as follows: In the introduction, we present an overview of the most important experimental and theoretical findings regarding the role of biopolymers during cell division and in the cytoskeleton. We also discuss current hypotheses and laboratory results for the origin of life, for the emergence of self-replicating molecules and protocells, and the error catastrophe. Chapter 2 is devoted to the dynamics of semiflexible polymers and its theoretical description. After briefly summing up previous work, we present the main results of our three publications in this field, which are reprinted at the end of the chapter. Some technical details of these calculations are summarized in the appendix. In Chapter 3, we give an introduction to quasispecies theory and discuss some commonly used fitness landscapes, before addressing the specific features of enzymatic replication. Finally, we summarize our two publications on this subject, which are reprinted at the end of the chapter.

1. Introduction

A viable definition of “life” encompassing the enormous diversity of the living organisms we are familiar with as well as the possibly fundamentally different life forms yet to be discovered is notoriously difficult [180], but two major features should certainly be observed if something is to be classified as “alive”: *metabolism* and *heredity* [177]. Metabolic chemical reactions allow organisms to use extrinsic energy sources for creating their internal structure and performing vital functions, hence providing the thermodynamic conditions for the very existence of an organism in a local and temporary non-equilibrium process working against global and long-term entropy increase. In contrast, heredity comprises the ability to convey this structural and functional potential to future progeny; supplemented by a capacity for replication and for introducing heritable variation it enables the organism to evolve driven by natural selection.

Commonly believed to have originated spontaneously from primitive anorganic chemistry, the astounding variation and remarkable complexity of life on earth was generated by ongoing Darwinian evolution. Some of the underlying evolutionary processes become more and more understood, others still defy explanation, some are of minor importance, and some constitute “major transitions in evolution”, as phrased in the book of the same title by John Maynard Smith and Eörs Szathmáry [177]. The authors count among these

- the organization of single replicating molecules into compartmentalized populations,
- the cooperative integration of independent replicators into chromosomes,
- the development of the genetic code,
- the evolution of eukaryotes from prokaryotes,
- the progression from asexual to sexual replication,
- the invention of differentiated cells in multi-cellular organisms, and of specialized individuals in large colonies,
- cultural innovations such as language and social behavior.

Especially the first few of these transitions are intimately linked to various properties of the constituent biological macromolecules, which we will discuss in the two following sections. From a physicist’s perspective, e.g., the one taken by Erwin Schrödinger in his book “What is life?” [227], such macromolecules can be classified as “aperiodic crystals”. For instance, the hereditary information of a DNA molecule is contained in its sequence.

But this particular aperiodic and highly non-random disorder is linked to and dependent on a (on a larger scale) quite regular crystal-like structure giving rise to unique mechanical properties. If this DNA is to provide heredity, both its mechanical integrity as well as its information content need to be maintained over many rounds of replication, by a replication apparatus again largely dependent on the specific mechanical properties of certain biopolymers. In this thesis, we investigate different theoretical models for these macromolecular constituents and discuss generic aspects of their mechanics and information. The remainder of this chapter presents a short introduction to the biological systems we are interested in, concentrating on important experimental evidence and some general theoretical results, while a more detailed review of the theoretical literature will be presented in Chapters 2 and 3.

1.1. Semiflexible polymers in cell division and the cytoskeleton

All known life is organized into smaller compartments, a feature that has been evolved at a very early stage. Compartmentalization, as this essential characteristic is usually labeled, describes the confinement to a limited volume, bounded by a surface like a lipid membrane, in order to maintain substances necessary for this “cell” on the inside at sufficiently high concentrations, and keep unwanted or deleterious material outside. Reproduction thus implies replication of genome and container in a coordinated manner, a nontrivial task that has been perfected to a high degree of sophistication in living organisms. Their cell division has to ensure the proper replication of a very long and typically highly compacted DNA sequence, while maintaining the intricate cellular organization both in mother and daughter cells. Many aspects of this remarkable process are now well understood, and it has been discovered that it is determined to a large extent by the biophysical properties of various involved biopolymers. We will now review some of the experimental and theoretical research that has enhanced our understanding of such aspects of cell division.

At the center of cell division stands replication of DNA, schematically depicted in Fig. 1.1, which is orchestrated by a large number of different protein enzymes. The two strands are unzipped by a helicase, resulting in the so-called replication fork with leading and lagging strand, which are decorated by single strand binding proteins to avoid formation of secondary structure. Because DNA is a helical molecule, unzipping creates twist, which is released through the action of topoisomerase enzymes. The leading strand is oriented in the usual direction 5' to 3', and a DNA polymerase can therefore produce the appropriate complementary strand in a straightforward manner. On the lagging strand with opposite orientation, RNA is added in short separated segments functioning as primer for another DNA polymerase, producing so-called Okazaki fragments that are finally joined by a DNA ligase.

Valuable insight into the detailed interaction between DNA and some of these proteins has been obtained in the last 15 years through single-molecule experiments (for reviews,

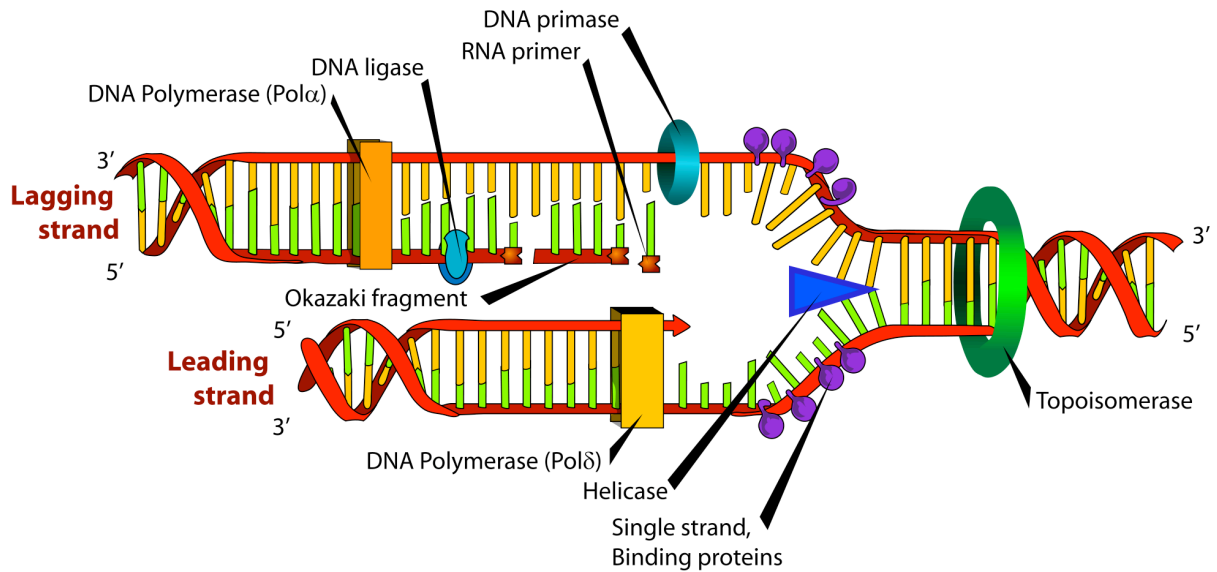


Figure 1.1: The DNA replication fork with the various enzymes that are involved in replication. A helicase enzyme unwinds the two strands, building up twist that is released through topoisomerase action. The leading strand is copied by a DNA polymerase in the ordinary 5' to 3' direction, while the lagging strand with its opposite orientation is completed through the sequential ligation of Okazaki fragments, produced from short intermediate RNA primers. Image source: Wikipedia.

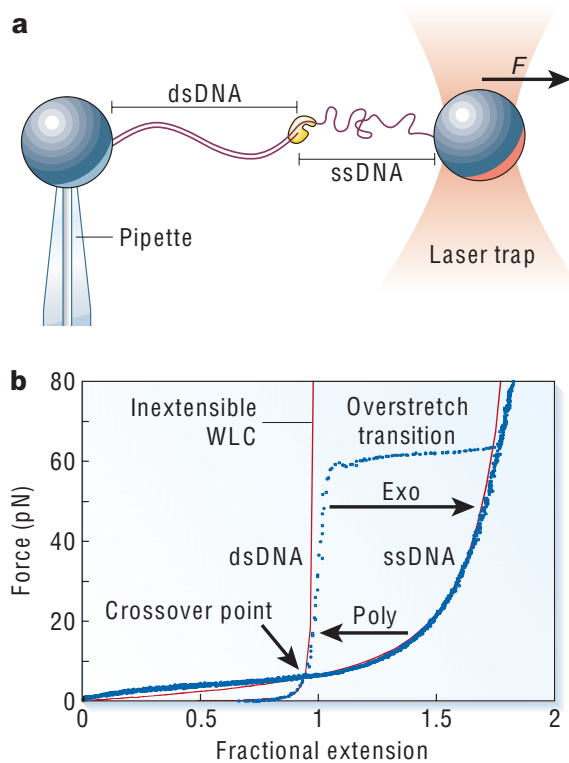


Figure 1.2: Single-molecule experiments on DNA. (a) A DNA molecule composed of single-stranded (ss) and double-stranded (ds) DNA is stretched by means of beads held between a micropipette and a force-measuring optical trap. The activity of enzymes bound to the DNA can be assessed from the respective force-extension curves shown in part (b) by the transitions indicated by arrows, e.g., resulting from DNA polymerization (Poly) or force-induced exonuclease activity (Exo). Reprinted by permission from Macmillan Publishers Ltd: Nature [28], copyright (2003).

see [28, 29, 31, 173, 252]). Schematically shown in Fig. 1.2, such setups use stretched single- and double-stranded DNA attached to two beads, which are usually held by a micropipette and a force-measuring optical trap, respectively. From the force-extension response of the DNA, the effects of DNA-binding enzymes can be assessed. For instance, it has been found that the DNA-cleaving activity of restriction enzymes strongly depends on the tension on the DNA. In this way, conformational changes of the DNA induced by these enzymes [26] and the influence of DNA looping [82] can be quantified. Further, the details of DNA ligase action have been elucidated through a single-molecule assay similar to the one shown in Fig. 1.2, but exploiting signatures of supercoiling dynamics [44]; these experiments also allow one to study DNA uncoiling by topoisomerases [253], and to detect the obstruction of this process by antitumor drugs [139]. Finally, DNA polymerase activity has been investigated, finding its rate strongly tension-dependent [88, 167, 285], and identifying distinct signals of proofreading dynamics [120].

Not surprisingly, the extraordinary success of these experimental methods would not have been possible without a thorough and quantitative understanding of DNA mechanics in the absence of proteins. The first results obtained from DNA stretching experiments using magnetic tweezers [245] prompted a very successful theoretical analysis of DNA elasticity by means of the wormlike chain (WLC) model [30]. Dating back to early work by Kratky and Porod [141], this model provides a simple description of semiflexible polymers as continuous inextensible space curves $\mathbf{r}(s)$ of length L with bending modulus κ . The corresponding Hamiltonian penalizes bending deformations expressed through changes in the tangent vectors $\mathbf{t}(s) = \mathbf{r}'(s)$, where s is the arclength and the prime denotes an arclength derivative:

$$\mathcal{H} = \frac{\kappa}{2} \int_0^L ds \mathbf{t}^2(s). \quad (1.1)$$

The statistical mechanics of this model was to a great deal developed by Saitô et al. [226], who exploited an analogy to path integrals well-known in quantum mechanics, in order to (re)derive a few pertinent observables like the first moments of the end-to-end distance. Central to these derivations is a very characteristic correlation function, namely the one for tangent orientations:

$$\langle \mathbf{t}(s) \mathbf{t}(s') \rangle = e^{-|s-s'|/\ell_p}. \quad (1.2)$$

It decays over a length scale given by the *persistence length* $\ell_p = \kappa/k_B T$, which is a measure for the bending stiffness of the polymer and can be used to distinguish stiff ($L \ll \ell_p$), semiflexible ($L \approx \ell_p$) and flexible polymers ($L \gg \ell_p$).

Which of these cases applies to DNA with its persistence length of about 50 nm depends of course on the length of the molecule under consideration. Importantly, however, the early stretching studies, even though performed on comparably long DNA molecules ($L \approx 30 \mu\text{m}$), clearly indicated that the WLC model for semiflexible polymers provides a significantly better fit than the freely-jointed chain model (appropriate for many flexible polymers) [30], in particular because these models have different asymptotes for the force needed to obtain full stretching (which diverges like $(1-r)^{-2}$ for the WLC and $(1-r)^{-1}$ for the freely-jointed chain, where $r = R/L$ is the fractional extension and R the distance

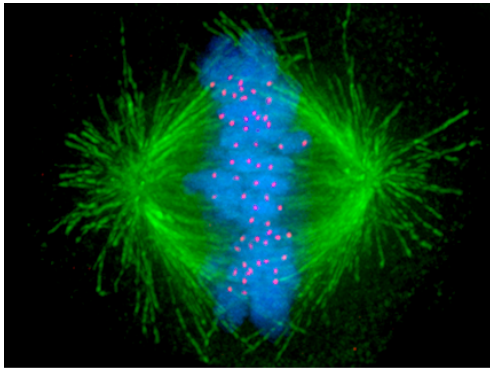


Figure 1.3: Image of a mitotic spindle in human cells. Microtubules (green) extending from organizing centers attach to chromosomally compacted DNA (blue) by way of kinetochores (pink) and pull chromosomes apart. Image source: Wikipedia.

between the two ends). By means of the above mentioned path integral methods, Marko and Siggia rigorously validated this result by computing the full force-extension relation for DNA [174], which is well approximated by the famous interpolation formula

$$\frac{f\ell_p}{k_B T} = \frac{1}{4(1 - R/L)^2} - \frac{1}{4} + \frac{R}{L}, \quad (1.3)$$

where f is the applied force, k_B is Boltzmann's constant and T is the temperature. Notably, the exceptional quality of the above cited stretching experiments exceeds the accuracy of this interpolation formula, which is only about 7% [174] and has later been quantitatively improved [23].

Many aspects of DNA replication depend strongly on mechanical properties of DNA, and the association of replication with the enclosing cell also relies heavily on semiflexible biopolymers. In particular, a reliable and efficient method for a fair distribution of the two genome replicas to the two container replicas is indispensable for successful cell division. Segregation of intertwined polymers may be driven largely by entropic repulsion alone [127], but most organisms have evolved additional means for efficient chromosome segregation (reviewed in [20]). In prokaryotes, the segregation of the two genome copies is mainly forced through the growth of semiflexible actin filaments attached at both ends to the DNA plasmids. In contrast, it is commonly believed that the major evolutionary transition from prokaryotes to eukaryotes was accompanied by the invention of an intricate chromosome separation machinery, allowing DNA replication to start simultaneously at several origins and thus facilitating an increase in genome complexity through more efficient replication pathways [177]. At the heart of this mechanism lies the mitotic spindle, depicted in Fig. 1.3. It is composed of a dynamical array of microtubules (a rather stiff class of biopolymers), which extend from organizing centers at opposite poles of the eukaryotic cell. Attaching to chromosomes at a protein structure called the kinetochore, these microtubules provide an outward force of about 5 pN to drive chromosome segregation [20].

Gaining a solid understanding of these biopolymers is not only essential because they are involved at crucial stages in cell division, but even more because they are integral constituents of the cytoskeleton, an interconnected network of various semiflexible polymers and many different regulatory proteins (see, e.g., Refs. [18, 68] for reviews). Its main filamentous constituents are three classes of semiflexible biopolymers, shown in Fig. 1.4:

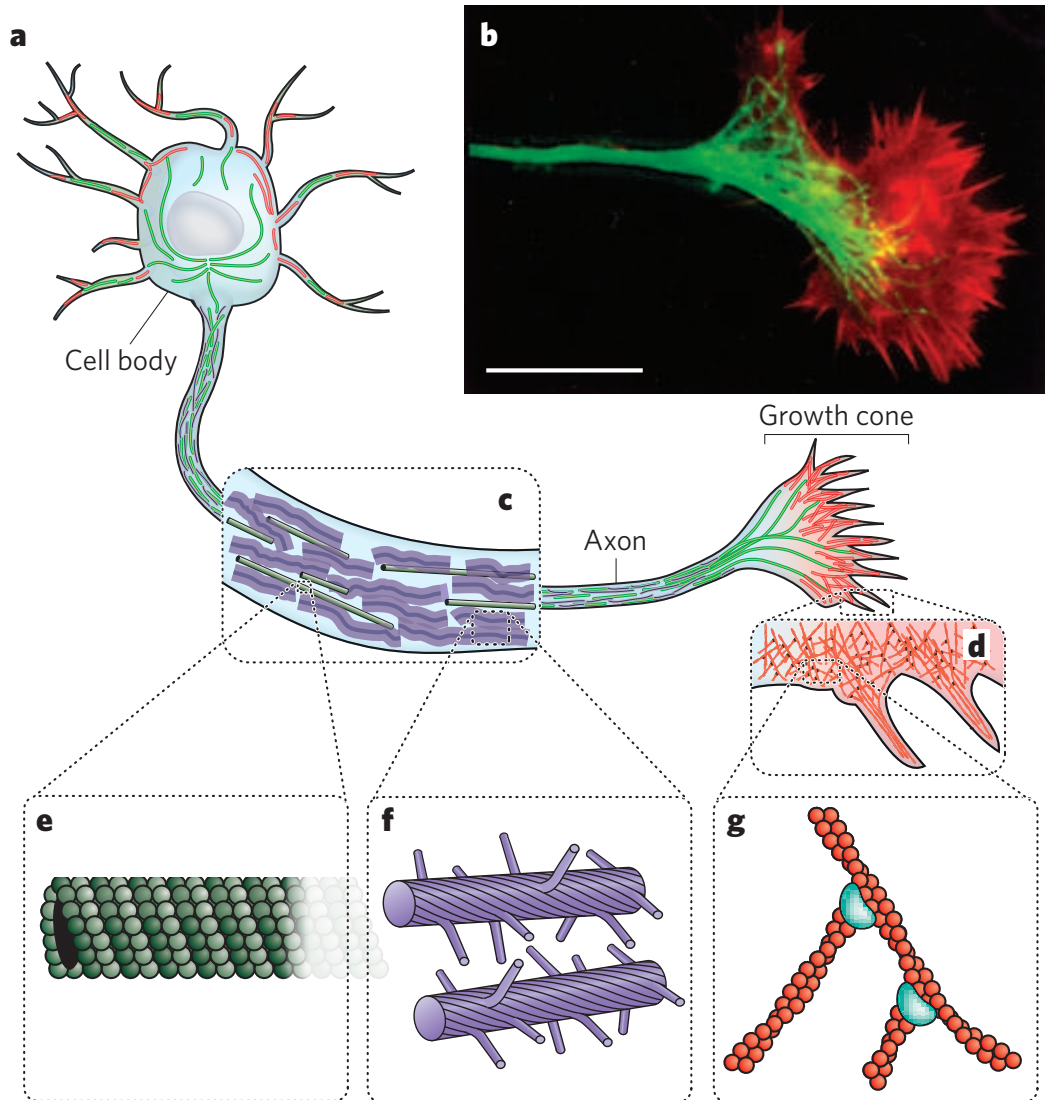


Figure 1.4: Semiflexible polymers in the cytoskeleton. (a) Sketch of a neuronal cell. Its cytoskeleton consists of microtubules (green), actin filaments (red) and intermediate filaments (purple). (c) Intermediate filaments form a structural matrix embedding microtubules in the axon, which ends in the growth cone containing an actin network (d). The polymers in this structure can be observed in the fluorescence micrograph shown in part (b) (scale bar: $20 \mu\text{m}$; picture reproduced with permission from Ref. [222]). Schematic drawings of microtubules, intermediate neurofilaments and actin networks are shown in parts (e), (f), and (g), respectively. Reprinted by permission from Macmillan Publishers Ltd: Nature [68], copyright (2010).

stiff microtubules ($\ell_p \approx 5 \text{ nm}$), actin filaments with $\ell_p \approx 15 \mu\text{m}$, usually organized into networks or bundles, and a broad class of more flexible intermediate filaments. This dynamic and adaptive structure determines the unique mechanical properties of eukaryotic cells and their ability to change their shapes, and provides an intracellular transportation network. The cytoskeleton takes care of the spatial organization of cellular contents, it supplies physical and biochemical connections to the external environment, is able to generate coordinated forces, and has even been speculated to realize a form of cytoskeletal epigenetics by passing on a structural memory of external conditions to future progeny [68].

Under a broad range of conditions, not only DNA but also these cytoskeletal filaments are well described by the WLC model. Many of its aspects, to be detailed in Chapter 2, have been studied extensively during the last two decades, and significant progress to understand more complex polymeric structures such as networks and gels has been made. Still, some quite elementary issues even on the single molecule level remain mysterious, which is in most cases due to a fundamental nonlinearity casually disregarded in the preceding paragraphs: the WLC model represents semiflexible polymers as *inextensible* space curves, which is a reasonably accurate description for the extremely high stretching stiffness of these very thin filaments in experimentally relevant parameter regimes. However, this inextensibility constraint presents severe complications for theoretical analysis, in particular if external forces are involved and if the dynamics is of interest. Based on a singular perturbation theory for an appropriate treatment of the resulting nonlinearities [97], we present our results for some generic scenarios for the nonlinear dynamic response of semiflexible polymers in Chapter 2.

1.2. Prebiotic self-replication at the origin of life

As heredity and metabolism are two main ingredients in almost any definition of life, there are correspondingly two different theories of which came first. The proponents of the “metabolism-first” theory claim that autocatalytic reaction networks, apart from performing metabolic functions, can replicate by fission and provide hereditary information [77, 234, 235]. In contrast, the supporters of the “genes-first” theory hold that these ensemble replicators provide only limited hereditary potential (their state space is small) and lack therefore true evolvability [266], while the inherent variability of polynucleotides is virtually unlimited (there are more possibilities for a sequence of about 140 letters from a four-letter alphabet than there are atoms in the universe). Assuming the existence of an abiotic metabolism for the continuous synthesis of necessary energy-rich substrates, this theory accordingly argues that polynucleotides with their ability for complementary base pairing constituted the first replicators, just as DNA replication in present-day life operates through template-directed polymerization (see Fig. 1.5 for an illustration of template-directed processes). However, DNA replication is catalyzed by protein enzymes such as DNA polymerases, and these proteins themselves are produced by decoding DNA, such that neither can arise without the other, resulting in a “chicken-and-egg” problem that was resolved by suggesting that RNA functions both as gene (providing heredity) and enzyme

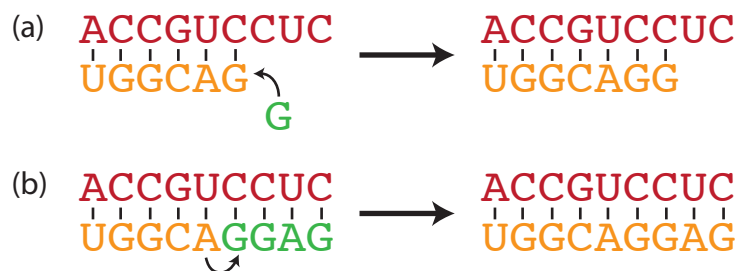


Figure 1.5: Non-enzymatic template-directed polymerization and ligation reactions. (a) Polymerization proceeds via the successive addition of monomers (green) to a primer (orange), which is complementary to a template (red). This process can also be catalyzed by an RNA polymerase ribozyme as the one shown in Fig. 1.6. (b) Ligation results from catalyzing the formation of a backbone bond between two oligomers (orange and green) both complementary to the template (red). Both schemes can result in chemical self-replication, if the product (the complement of the template) itself is able to catalyze complementary polymerization or ligation reactions, but self-replication may be inhibited strongly if template and product strand do not separate quickly enough in order to be able to catalyze new reactions.

(involved in metabolism and replication). Only after a major evolutionary transition, viz. the invention of the genetic code, the general-purpose molecule RNA was largely superseded by a system based on different macromolecules more specialized for these respective tasks, namely DNA and proteins. The idea that the first self-replicating molecules were RNA-like polynucleotides, called the “RNA world theory” (see the book [84]) became famous during the 1980s shortly after remarkable discoveries of enzymatic activity of RNA [85]. Starting with the initial observation of self-splicing RNA in the organism *Tetrahymena* [35], a large number of RNA enzymes (ribozymes) catalyzing diverse chemical reactions were found in subsequent years (for review see, e.g., Refs. [49, 157]), and more were evolved *in vitro* [126].

The literature on RNA chemistry and possible self-replication under prebiotic conditions is extensive (see the reviews [125, 206, 207, 208] and the book [84]), and we will only touch upon the findings most relevant for the theory developed in chapter 3. Even though it is still unclear how single nucleotides can be synthesized *de novo* under prebiotic conditions, their polymerization is with reasonable efficiency catalyzed through lipids [218], clay [65], or water [129] (which is also a catalyst for ligation [216]), albeit the resulting sequence repertoire is strongly limited and regio-specificity (i.e., the preference of 3',5'- over 2',5'-phosphodiester bonds) is not always properly maintained. Unfortunately, non-enzymatic template-directed polymerization (see Fig. 1.5(a)), previously hypothesized as important replication mode, has been demonstrated only for specific sequences [1] or structures [284], and with discouragingly small rates. A more promising route is based on template-directed ligation of RNA oligomers catalyzed through the RNA template itself [50, 179] (see Fig. 1.5(b)), and if suitable building blocks are provided, this approach can be upgraded to chemical self-replication [131, 134, 158, 212, 213], even though such replicators provide only limited heredity and may be affected by product inhibition due to insufficient separation of template and product strand [132]. Probably the most auspicious



Figure 1.6: Sequence and secondary structure of an RNA polymerase. This ribozyme catalyzes the successive extension of a primer (orange strand) by up to 14 nucleotides complementary to an RNA template (red strand). It was derived from an RNA ligase ribozyme by 18 rounds of *in vitro* evolution (relevant changes compared to prior rounds are indicated in pink). Its overall replication accuracy is 96.7% per nucleotide, and the rate of nucleotide addition is on the order of 0.6 nt/hour. From Ref. [124]. Reprinted with permission from AAAS.

development is the recent observation of RNA-catalyzed RNA polymerization on an RNA template [58, 124, 288]: polymerase ribozymes such as the one depicted in Fig. 1.6 take the lead in the hunt for a true RNA replicase.

Further experimental research concerns environmental conditions: in dilute solution, the small concentrations of single monomers and polynucleotides will probably not allow fast enough polymerization or replication reactions to beat ongoing degradation. As a possible remedy, hydrothermal vents have recently been shown to cause extreme accumulation of nucleotides owing to an asymmetric superposition of thermal convection and thermodiffusion [14, 138], and also to frequently initiate convectively driven temperature oscillations, which could speed up dissociation of template and product strands and reduce the effects of product inhibition. Low-dimensional or structured environments like mineral surfaces or porous materials have also been speculated to provide surroundings more favorable for the spontaneous emergence of replicators. Another direction pursues the demonstration of prebiotic compartmentalization by creating protocells with self-replicating genomes contained in a self-replicating membrane [36, 258] (see Fig. 1.7). Such fatty acid vesicles have been shown to spontaneously grow and divide [39]. Active genome replication would generate osmotic pressure [38], leading to membrane growth at the expense of other membranes enclosing less-efficient replicators [37], complemented by the creation of a pH gradient that in turn could be used to drive intracellular processes [40]. In this way, a coupling between the replication of the genome and the replication of the enclosing membrane could be achieved purely based on physical principles [36].

While the emergence of self-replicating RNA-like polynucleotides under prebiotic conditions has not yet been experimentally demonstrated, a fundamental understanding of universal principles governing these replicators has been initiated by the pioneering work of Manfred Eigen. In seminal papers published in the 1970s [52, 55, 56, 57], he presented a theoretical framework to describe the self-replication of information-carrying macromolecules such as polynucleotides. We will discuss this theory, which is based on high-dimensional

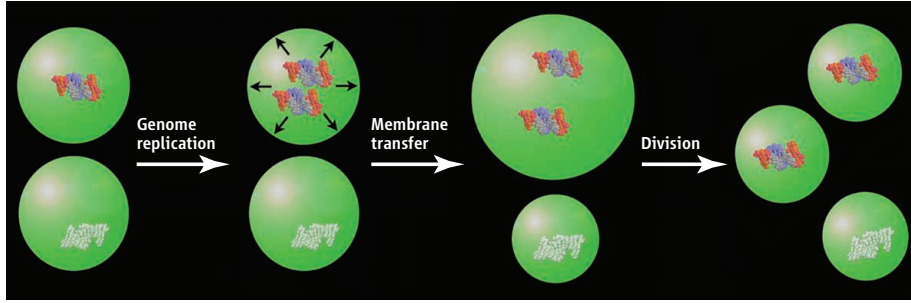


Figure 1.7: The emergence of cells during the origin of life. Protocell membranes containing actively replicating genomes grow at the expense of other cells containing inactive replicators, spontaneously inducing division. From Ref. [36]. Reprinted with permission from AAAS.

deterministic rate equations for the concentrations of macromolecules with a certain sequence, in more detail in Chapter 3 and present only some generic results here. A strongly simplified version displaying the essential features assumes the existence of an efficiently self-replicating “master” molecule of L nucleotides, which is present in concentration x_0 . Replication occurs with rate r_0 , and involves stepwise polymerization reactions implying the incorporation of erroneous nucleotides with a certain mutation probability μ . From such errors result “mutants”, present in concentration x' and replicating with reduced rate $r' < r_0$, without chance of regaining the master sequence through backmutations (which are unlikely if L is large). Normalizing the concentrations, $x_0 + x' = 1$, we can write $x' = 1 - x_0$, and readily set up the dynamics of the master sequences:

$$\dot{x}_0 = (1 - \mu)^L r_0 x_0 - x_0 [r_0 x_0 + r' (1 - x_0)]. \quad (1.4)$$

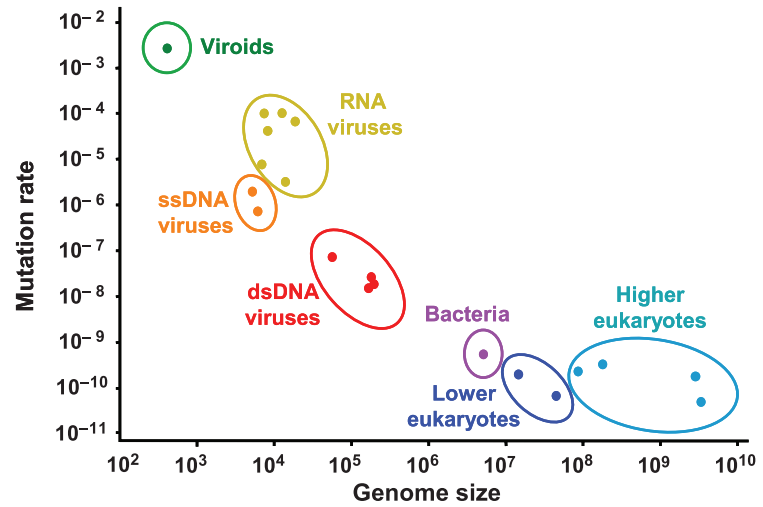
This equation describes the change in concentration through error-free replication of the master with rate r_0 and probability $(1 - \mu)^L$ (the probability not to introduce an error at any of L positions). The second term in brackets involves the mean replication rate $r_0 x_0 + r' x'$ and has been subtracted to keep the concentrations normalized at all times. In the stationary state $\dot{x}_0 = 0$, we find $x_0 = [(1 - \mu)^L r_0 - r'] / (r_0 - r')$. As function of mutation rate μ , the concentration of the master sequence x_0 is non-negative only if μ is smaller than a critical value μ_c . Using that $(1 - \mu)^L \approx e^{-\mu L}$ for large L , this condition reads

$$\mu < \mu_c = \frac{\ln(r_0/r')}{L}. \quad (1.5)$$

This highly influential result predicts a critical mutation rate, called the “error threshold”, beyond which faithful replication is no longer possible: if the effective rate $(1 - \mu)^L r_0$ of creating the master sequence falls below the replication rate r' of the mutants, the master will be outgrown and ultimately be driven to extinction. Essentially, this implies that the information content that can reliably be transmitted in the process of self-replication is limited by the mutation rate.

In a probably oversimplified attempt to quantify these conclusions, we can estimate the (in the absence of experimental evidence for such self-replicators hardly measurable) logarithmic ratio of master and mutant replication rates in the numerator of Eq. (1.5) casually

Figure 1.8: Mutation rate μ per base per genome replication versus genome size L for different organisms (log-log plot). An inverse proportionality $\mu \propto L^{-1}$ suggesting a relationship to the error threshold Eq. (1.5) can clearly be seen. From Ref. [75]. Reprinted with permission from AAAS.



as number of order 1, and invoke thermodynamic arguments to determine a lower bound on the mutation rate: in equilibrium, the probability of incorporating an (energetically unfavorable) erroneous nucleotide rather than the preferred complementary one depends exponentially on the corresponding free energy difference between the two resulting conformations. The inference is a bit more tricky for polynucleotides due to cooperative stacking interactions between successive base pairs, but measured melting curves place the resulting mutation rates above 1% per base and replication [52] (duly, the polymerase ribozyme shown in Fig. 1.6 has an error rate of about 3%). This has prompted models of “kinetic proofreading” in order to explain the much lower values observed in living organisms by energy-consuming non-equilibrium processes [117]. Indeed, most organisms have evolved such mechanisms for reliable error-correction, yet the inverse proportionality between mutation rate and genome size is still obeyed with remarkable adherence across species, as shown in Fig. 1.8, even though other explanations for the scaling $\mu \propto L^{-1}$ may be proposed. At any rate, with this relatively large value for the mutation rate, the condition Eq. (1.5) can be read as upper bound on the length of the molecule, which would then be somewhere on the order of 100 nucleotides (note that the polymerase ribozyme shown in Fig. 1.6 has a length of 189 nt). Because the absence of enzymatically driven error-correction leads to high mutation rates, which in turn permit only relatively short genomes, prebiotic ribozymes will not be able to perform complex enzymatic functions and will therefore replicate with high mutation rates possibly precluding their very existence, a paradoxical consequence christened the “catch-22 of molecular evolution” by John Maynard Smith [176].

Whether or not these theoretical arguments have any real implications for prebiotic replicators has been heavily debated, since the conclusions drawn from Eq. (1.4) rest on some questionable assumptions to be discussed in more detail in Chapter 3, for instance the premises that the mutants have a finite replication rate r' and that a deterministic treatment is appropriate. Quantitative interpretations are therefore built on somewhat shaky grounds and have accordingly largely been ignored in the experimental literature. For the problems discussed in Chapter 3 more crucial is the assumption that the replication rates

of master and mutants are fixed numbers depending only on their respective genotypes, implying either that replication is not catalyzed by any enzymes, or that concentrations and characteristics of these enzymes are not accounted for. Ignoring essential constituents is obviously not a feasible way to describe the origin of self-replicating molecules, while autocatalytic replication, as for instance in Fig. 1.5, does not appear very plausible under prebiotic conditions given the limited experimental success of non-enzymatic polymerization and ligation reactions discussed before. Self-replication catalyzed by ribozymes such as shown in Fig. 1.6 is the more likely scenario, but it is of evolutionary advantage for the replicase enzyme itself only if it replicates specifically only functional substrates. Accordingly, we develop a theory of *specific* enzymatic self-replication in Chapter 3.

2. Nonlinear dynamic response of semiflexible polymers

In the introduction, we explored some outstanding experimental results for biologically relevant semiflexible polymers like DNA or cytoskeletal filaments such as microtubules or actin, and discussed some aspects of a successful theoretical description by means of the wormlike chain (WLC) model. Proposed in 1949 [141] in order to explain X-ray scattering results on polymeric solutions, many of the theoretical studies on this model developed in the following years were in fact concerned with similar collective properties. Since the 1990s, the advent of experimental single-molecule techniques provided an exciting new application field, as the stretching of single DNA molecules was accomplished by various means, among them optical [270] or magnetic [30, 245] tweezers, so-called “molecular combing” [19], hydrodynamic flows in different geometries [148, 215, 228, 229, 230, 243], electric fields [168], or a combination of both [15]. At the same time, the growing realization that complex network structures composed of semiflexible polymers like actin are largely responsible for the mechanical properties of the cytoskeleton encouraged further research in network properties (see, e.g., Refs. [18, 68, 72, 73, 74] for reviews). A more detailed understanding of single-molecule statistics, such as the full distribution function for the end-to-end distance [277], was complemented by studies of elastic properties of networks and solutions (see, e.g., Refs. [112, 143, 166, 278]). Of course, the range of applicability of the WLC model is not without controversy, as there is an ongoing debate on indications of irregularly high DNA elasticity on small length scales [178, 275, 276, 286] with possibly serious biological implications [78]. Microtubules have as well been shown to exhibit anomalous fluctuations caused by their non-trivial internal architecture [210, 262].

Following this brief account of some prevailing topics in semiflexible polymer physics, this chapter will put particular emphasis on the dynamic properties of wormlike chains (see Ref. [142] for a recent review), and the singularities produced by ordinary perturbation methods in some limits. After summarizing an accordingly improved theory for the propagation and relaxation of backbone tension in such polymers [97, 98, 99] and discussing our previous work on the implications for the longitudinal stretching response [203], this will ultimately lead us to the nonlinear response characteristics investigated in this work: transverse forces [202], the longitudinal relaxation dynamics [204], and microstructure corrections due to a finite backbone extensibility [200] or discretization effects.

2.1. Wormlike chain dynamics

A major complication resulting from a description of the polymer contour as inextensible continuous space curve $\mathbf{r}(s)$ is the ensuing condition that s is actually the arclength coordinate at any moment, i.e., that the tangent vector has always unit length:

$$|\mathbf{r}'(s)| = 1. \quad (2.1)$$

Whereas the obstacles caused by this constraint can for certain statistical mechanics problems be removed by interpreting s as time and the tangent $\mathbf{t}(s) = \mathbf{r}'(s)$ as the position of a particule on the unit sphere [226], this is approach not possible when the *dynamics* is of interest. Early attempts used a global Lagrange multiplier in order to keep the average total contour length $\langle L \rangle$ constant [103, 105, 226], which introduces an effective stretching elasticity and leads to inconsistent equations of motion [8, 246]. Further, for an only locally extensible contour, the underlying Gaussian distance statistics is essentially equivalent to that of a Rouse chain with some bending stiffness. Hence, the strict condition that extensions $R > L$ are unattainable, unless caused by internal structural rearrangements such as the DNA overstretching transition, is violated. This constraint is intrinsically responsible for the observed divergence in the force-extension relation Eq. (1.3), also seen in Fig. 1.2(b). In an attempt to account for the necessary contour length conservation, subsequently developed mean-field theories introduced different additional Lagrange multipliers in order to fix some suitably defined thermal and/or spatial averages of the constraint [93, 94, 101, 102, 110, 111, 282]. While these techniques correctly reproduce the first moments of the end-to-end distance in the absence of external forces, they fail to describe the properties of stretched polymers, in particular because the characteristic anisotropy of transverse and longitudinal fluctuations is overlooked (a recent effort to include these effects arrives at a theory based on 7 Lagrange multipliers that can only be computed numerically [109]).

2.1.1. Equations of motion

A more systematic approach observes that the local constraint Eq. (2.1) requires a correspondingly local Lagrange multiplier function $f(s)$ [89], which is readily interpreted as *backbone tension* preventing the stretching of backbone bonds. Adding a constraint term to the Hamiltonian Eq. (1.1) and switching to a formulation in terms of position vectors \mathbf{r} instead of tangents gives

$$\mathcal{H} = \frac{1}{2} \int_0^L ds [\kappa \mathbf{r}''^2(s) + f(s) \mathbf{r}'^2(s)]. \quad (2.2)$$

Due to the very small Reynolds numbers associated with these biopolymers, the overdamped motion of the polymer contour is not affected by inertia. Further, within the *free-draining* approximation [48], hydrodynamic interactions between different parts of the contour give only rise to logarithmic corrections that can be neglected (we will briefly come

back to this point in Sec. 2.5). This implies local anisotropic dissipation, accounted for in the friction matrix

$$\zeta = \zeta_{\perp}(1 - \mathbf{r}'\mathbf{r}') + \zeta_{\parallel}\mathbf{r}'\mathbf{r}' \quad (2.3)$$

For a straight and slender rod of length L and diameter $a \ll L$ in a solvent with viscosity η , the transverse and longitudinal friction coefficients ζ_{\perp} and ζ_{\parallel} are given to leading order in $\ln(L/a)^{-1}$ by [17]

$$\zeta_{\parallel} = \hat{\zeta}\zeta_{\perp} = \frac{2\pi\eta}{\ln(L/a)}, \quad (2.4)$$

with $\hat{\zeta} \approx 1/2$.

The stochastic equations of motion now result from a balance of viscous forces $\zeta\partial_t\mathbf{r}$, elastic forces $-\delta\mathcal{H}/\delta\mathbf{r}$ and thermal noise ξ :

$$\zeta\partial_t\mathbf{r} = -\kappa\mathbf{r}'''' + (f\mathbf{r}')' + \xi, \quad (2.5)$$

where the noise correlations are fixed through the fluctuation-dissipation theorem [48]:

$$\langle \xi_i(s, t) \rangle = 0 \quad (2.6a)$$

$$\langle \xi_i(s, t)\xi_j(s', t') \rangle = 2k_{\text{B}}T\zeta_{ij}\delta(s - s')\delta(t - t'). \quad (2.6b)$$

Choice of units. For the remainder of this chapter, we will change units such that all quantities are powers of a length. Hence, we set $\kappa = \zeta_{\perp} = 1$, which makes time a length⁴ and forces such as the tension f a length⁻². Also, $k_{\text{B}}T = \ell_{\text{p}}^{-1}$ in these units.

2.1.2. The weakly-bending limit

The equations of motion Eq. (2.5) are highly nonlinear, given that the Lagrange multiplier function $f(s)$ has to be determined from the inextensibility constraint Eq. (2.1). Other authors have dealt with this problem by introducing two constraints (for inextensibility and connectivity) [161], or by formulating stochastic equations of motion in mode space [189]. A more popular method to tackle these nonlinearities is based on expanding the contour about a straight line, amounting to a perturbation theory in the *weakly-bending limit* of a straight rod [62]. To this end, we decompose the contour into small displacements transverse and longitudinal to the initial axis, and introduce a small parameter ε to be defined more precisely below by requiring the relative transverse excursions to be small:

$$\mathbf{r}(s) = (\mathbf{r}_{\perp}(s), s - r_{\parallel}(s))^T \quad \text{with } \mathbf{r}_{\perp}^2 = \mathcal{O}(\varepsilon) \ll 1. \quad (2.7)$$

Expanding the inextensibility constraint Eq. (2.1) to leading order,

$$r'_{\parallel} = \frac{1}{2}\mathbf{r}_{\perp}^{\prime 2} + \mathcal{O}(\varepsilon^2), \quad (2.8)$$

we recognize that the longitudinal displacements are of higher order than the transverse ones. Up to order ε , the accordingly decomposed equations of motion Eq. (2.5) read:

$$\partial_t\mathbf{r}_{\perp} = -\mathbf{r}_{\perp}'''' + (f\mathbf{r}'_{\perp})' + \xi_{\perp}, \quad (2.9a)$$

$$\hat{\zeta}\partial_t r_{\parallel} + (1 - \hat{\zeta})\mathbf{r}'_{\perp}\partial_t\mathbf{r}_{\perp} = -r_{\parallel}'''' - f' + (fr'_{\parallel})' + \xi_{\parallel}. \quad (2.9b)$$

where the longitudinal part obtains a transverse contribution from the anisotropic projection operators in the friction matrix Eq. (2.3), vanishing for isotropic friction ($\hat{\zeta} = 1$).

2.1.3. The dynamics on the linear level

Because the longitudinal displacements are subdominant for weakly-bending wormlike chains, the longitudinal part Eq. (2.9b) reduces in the absence of bulk forces and to leading order $\mathcal{O}(\varepsilon^{1/2})$ to the simple condition

$$f' = 0, \quad (2.10a)$$

which implies that the tension across the contour is a constant determined by the forces applied at the polymer's ends. In this section, we will only discuss the force-free case $f = 0$. Further, the transverse part Eq. (2.9a) becomes a linear equation formally equivalent to the versions used previously, but now resulting from a systematic expansion:

$$\partial_t \mathbf{r}_\perp = -\mathbf{r}_\perp'''' + \boldsymbol{\xi}_\perp. \quad (2.10b)$$

Quantities of interest such as correlation functions of transverse displacements relevant for the dynamic structure factor [62, 144, 162] or the shear modulus [86, 185, 186] can now be obtained by a normal mode decomposition of Eq. (2.10b). Writing

$$\mathbf{r}_\perp(s, t) = \sum_n \mathbf{r}_n(t) w_n(s) \quad (2.11)$$

with an orthonormal set of eigenfunctions to the biharmonic operator ∂_s^4 [8, 274], such that $w_n''''(s) = q_n^4 w_n(s)$, the equation of motion for the mode amplitudes is readily solved:

$$\mathbf{r}_n(t) = \int_{-\infty}^t dt' \boldsymbol{\xi}_{\perp, n}(t') e^{-(t-t')/\tau_n}, \quad (2.12)$$

where the relaxation times $\tau_n = q_n^{-4}$ scale with the fourth power of the wave length. Using the noise correlation $\langle \boldsymbol{\xi}_{\perp, n}(t) \boldsymbol{\xi}_{\perp, m}(t') \rangle \propto (\ell_p L)^{-1} \delta_{nm} \delta(t - t')$ obtained from accordingly transforming Eq. (2.6a) gives the spatially averaged correlation function of transverse displacements as:

$$\begin{aligned} \langle \delta \mathbf{r}_\perp^2(t) \rangle &\equiv \int_0^L \frac{ds}{L} \langle [\mathbf{r}_\perp(s, t) - \mathbf{r}_\perp(s, 0)]^2 \rangle \\ &\propto \frac{1}{L \ell_p} \sum_n \frac{1 - e^{-t/\tau_n}}{q_n^4} \sim \frac{L^3}{\ell_p} \left(\frac{t}{t_L^\perp} \right)^{3/4} \quad \text{for } t \ll t_L^\perp. \end{aligned} \quad (2.13)$$

Approximating the sum by an integral readily yields the characteristic subdiffusive $t^{3/4}$ -growth of transverse fluctuation amplitudes [91] for times shorter than the longest relaxation time $t_L^\perp \simeq L^4$.

Dynamic scaling. Note that Eq. (2.13) can be written on the scaling level as

$$\langle \delta r_{\perp}^2(t) \rangle \simeq \frac{\ell_{\perp}(t)^3}{\ell_p}, \quad (2.14)$$

if we define a *transverse correlation length*

$$\ell_{\perp}(t) = \begin{cases} t^{1/4}, & \text{for } t \ll t_L^{\perp}, \\ L, & \text{for } t \gtrsim t_L^{\perp}. \end{cases} \quad (2.15)$$

A useful interpretation of $\ell_{\perp}(t)$, which can easily be read off from Eq. (2.10b) as characteristic dynamic length scale, is that it denotes the length of *segments* that are equilibrated up to this time. We can also use the result Eq. (2.14) to obtain one possible definition of the small parameter ε , by noting that the mean square amplitude of the transverse modes saturates at a value $\langle r_{\perp}^2 \rangle \simeq L^3/\ell_p$. For the relative excursions, this means that $\langle r_{\perp}^2 \rangle \simeq L/\ell_p \equiv \varepsilon$, making explicit the intuitive observation that stiff polymers with $L \ll \ell_p$ are weakly-bending.

Longitudinal fluctuations. Because longitudinal displacements are of higher order in ε as a consequence of Eq. (2.8), their mean square amplitudes in equilibrium accordingly must scale as $\langle r_{\parallel}^2 \rangle \simeq L^4/\ell_p^2$, i.e., they are a factor ε smaller than the transverse ones. Considering a long filament as chain of L/ℓ_{\perp} equilibrated segments of length ℓ_{\perp} , their contributions can be averaged to give a scaling law for the dynamical correlation of the longitudinal fluctuations

$$\langle \delta r_{\parallel}^2(t) \rangle \sim \frac{L\ell_{\perp}(t)^3}{\ell_p^2}. \quad (2.16)$$

The relations (2.14) and (2.16) express on the scaling level the characteristic anisotropy of transverse and longitudinal fluctuations mentioned at the beginning of this section.

Experimental observations. The success of the WLC model for describing static properties of semiflexible polymers largely carries over to dynamical features in the linear regime: the anisotropy of transverse and longitudinal displacements has indeed been measured on DNA by high-resolution optical-tweezer experiments [181, 217] and by fluorescence correlation spectroscopy [165]. In actin solutions [87, 159] and networks [5], the subdiffusive $t^{3/4}$ -fluctuations were seen, and also microtubules were found to obey this scaling [34], even though deviations at small length scales are indicative of their complex architecture causing nontrivial shear elasticity and internal friction [262]. Finally, calculations along these lines, but with a more detailed treatment of boundary conditions, give the autocorrelation function of the end-to-end distance of a free polymer, again in excellent agreement with experimental observations on actin filaments [152].

2.1.4. Failure of the linear theory

A failure of this linear theory for short times has been observed by several authors [2, 25, 60, 185, 186, 236]. We will present the linear response argument made by Everaers et al. [60] here and briefly discuss another more general derivation in Section 2.3 below. Their reasoning invokes the fluctuation-dissipation theorem to observe that within linear response a weak longitudinal force f_{\parallel} applied to a filament would produce a longitudinal displacement $\delta r_{\parallel} \simeq f_{\parallel} L \ell_{\perp}^3 / \ell_p \simeq f_{\parallel} L t^{3/4} / \ell_p$. However, the resulting drag force $\hat{\zeta} L \delta r_{\parallel} / t$ falling off over the filament's length L exceeds the driving force f_{\parallel} for times smaller than $t_{\star} \simeq \hat{\zeta}^4 L^8 / \ell_p^4$ [60, 185, 186]. Because a violation of this force balance between friction and driving force is certainly unphysical, the authors argue that not the whole filament is set into motion at once, but only a smaller section of length $\ell_{\parallel}(t)$. Replacing $L \rightarrow \ell_{\parallel}(t)$ in the above scaling argument gives a result consistent with the friction balance if this length is chosen as $\ell_{\parallel}(t) \simeq (\ell_p / \hat{\zeta})^{1/2} t^{1/8}$ [60, 211].

Accordingly, the difference between transverse and the much weaker longitudinal fluctuations manifests itself in qualitatively different scaling laws: replacing $L \rightarrow \ell_{\parallel}(t)$ in Eq. (2.16), we find $\langle \delta r_{\parallel}^2 \rangle \propto t^{7/8}$ in contrast to the scaling law $\langle \delta \mathbf{r}_{\perp}^2 \rangle \propto t^{3/4}$ for the transverse fluctuations. Moreover, reading $\ell_{\parallel}(t)$ as a correlation length for longitudinal fluctuations reveals that these fluctuations live on *much larger scales* than transverse ones, since $\ell_{\perp}(t) / \ell_{\parallel}(t) \propto \varepsilon^{1/2}$ for times on the order of t_{\star} .

We emphasize that responsible for the failure of the linear theory is the omission of longitudinal friction $\hat{\zeta} \partial_t r_{\parallel}$ in the linearized equations of motion (2.10). This point has also been observed by other authors for different scenarios involving stronger forces where linear response theory is not applicable [2, 25, 236], leading to different scaling laws for an analogously defined dynamic length scale $\ell_{\parallel}(t)$. Because neglecting longitudinal friction leads to divergencies that can not be removed by including the next-order terms in Eq. (2.9) [236], an ordinary perturbation expansion of the equations of motion in powers of ε gives singular results: it is not possible to take the limit $t \rightarrow 0$ while holding ε constant [98]. The above linear response argument indicates that an underlying scale separation between transverse and longitudinal dynamics causes these problems, and the next section will present a correspondingly improved “multiple-scale” perturbation theory.

2.2. Tension dynamics for wormlike chains

For an inextensible polymer, the backbone cannot actually be stretched, but the thermally excited transverse excursions discussed above cause the contour to exhibit bending undulations. These thermal fluctuations can be straightened by applying external forces, and the tension f , introduced as constraint force, is a measure of the force necessary to ensure that only fluctuations are straightened but the backbone itself remains at constant length; accordingly, the tension diverges as the extension approaches the contour length (cf. Eq. (1.3) with f as tension). Hence, a reciprocal relation between contour length “stored” in thermal undulations (“stored length”), and tension arises: external forces can

pull out stored length and create tension; once the thermal undulations are re-introduced, the tension relaxes.

By Eq. (2.10a), the absence of longitudinal friction and bulk forces means that the leading-order tension is just a constant and stored length is thus homogeneously distributed along the contour. If a sudden stretching force is applied, the above introduced correlation length $\ell_{\parallel}(t)$ gains another, much more intuitive interpretation: stored length is pulled out, but limited by longitudinal friction this happens at first only near the boundary, over distances of length $\ell_{\parallel}(t)$. Likewise, the increased tension induced by the applied force accordingly penetrates the contour only within a growing region of size $\ell_{\parallel}(t)$. In this sense, the physics missed within the linear theory is entirely contained in a proper description of the propagation and relaxation of backbone tension.

Realizing these important features, a theory of tension dynamics on the linear level has been developed by Morse et al. [211, 238], while the case of large force has been discussed both based on a “taut-string” approximation by Seifert et al. [236], as well as using the somewhat complementary “quasi-static” approximation by Brochard-Wyart et al. [25]. Together with accordingly refined mean-field models [153] and other studies based on scaling arguments [2, 60, 236], “adiabatic” approximations [219, 236] or computer simulations [190, 269], these approaches lead to an incomplete and, due to partly contradicting assumptions, also somewhat inconsistent picture of tension propagation under different conditions. Aiming to provide a unified and systematic theoretical description, Hallatschek et al. [97, 98, 99] developed a general theory of tension dynamics in the weakly-bending limit based on a rigorous multiple-scale perturbation theory (for an introduction to this method see the book [108]).

2.2.1. Multiple-scale perturbation theory

This approach, explained in detail in Ref. [98], exploits the previously observed scale separation $\ell_{\perp}/\ell_{\parallel} \propto \varepsilon^{1/2}$ to introduce two different small- and large-scale arclength coordinates s and $\bar{s}\varepsilon^{1/2}$. Writing dynamic variables such as $\mathbf{r}(s)$ and $f(s)$ as an expansion in functions of these two *formally independent* variables gives a system of equations of motion in each power of $\varepsilon^{1/2}$. In order to obtain a uniformly convergent expansion, the coefficients in each order should be bounded in the formal limit $s \rightarrow \infty$. Most importantly, this condition yields that the tension is a function of the large-scale variable \bar{s} only. This finding suggests to spatially average the longitudinal part over small-scale fluctuations, which causes most terms in Eq. (2.9b) to vanish and results in the simple equations of motion:

$$\partial_t \mathbf{r}_{\perp} = -\mathbf{r}_{\perp}'''' + \bar{f} \mathbf{r}_{\perp}'' + \boldsymbol{\xi}_{\perp}, \quad (2.17a)$$

$$\hat{\zeta} \partial_t \bar{r}'_{\parallel} = -\partial_{\bar{s}}^2 \bar{f}, \quad (2.17b)$$

where the prime is an s -derivative and the overbar denotes the spatial average. The latter is performed over many *uncorrelated* segments of length ℓ_{\perp} and thus effectively produces an ensemble average [98]. Hence, the longitudinal part Eq. (2.17b) can be written as

$$\partial_{\bar{s}}^2 \bar{f} = -\hat{\zeta} \partial_t \langle \bar{\varrho} \rangle, \quad (2.18)$$

where $\varrho = \frac{1}{2}r_{\perp}'^2 \approx r'_{\parallel}$ is the local density of contour length stored in thermal undulations, i.e., the stored length density. The transverse equation of motion Eq. (2.17a) for small-scale transverse fluctuations contains a locally constant tension, whose large-scale arclength dependence follows from Eq. (2.18), which describes the deviations of the tension profile from its constant equilibrium value. Integrating over arclength suggests the interpretation that *changes in stored length produce tension gradients* against longitudinal friction.

2.2.2. Coarse-grained equation of motion for the tension

Using that Eq. (2.17a) is linear, because the large-scale arclength dependence of the tension enters only adiabatically, a mode decomposition of $\mathbf{r}_{\perp}(s, t)$ in terms of eigenmodes $w_q(s)$ to the eigenvalues $-q^2[q^2 + \bar{f}(\bar{s}, t)]$ provides a solution via the response function

$$\chi_{\perp}(q; t, t') = e^{-2q^2[q^2(t-t') + \int_{t'}^t d\tau \bar{f}(\bar{s}, \tau)]} \Theta(t - t'). \quad (2.19)$$

It is the appropriate extension of the function $\chi_{\perp}^0(q; t, t') = e^{-q^4(t-t')} \Theta(t - t')$ used for solving the linear force-free case Eq. (2.10b) in Sec. 2.1.3. Hence, the expectation value $\langle \varrho \rangle = \langle \frac{1}{2}r_{\perp}'^2 \rangle$ is given by

$$\langle \varrho \rangle = \left\langle \frac{1}{2} \left[\sum_q \int_{-\infty}^{\infty} dt' \xi_{\perp, q}(t') \chi_{\perp}(q; t, t') w_q'(s) \right]^2 \right\rangle. \quad (2.20)$$

In order to proceed from here, we have to specify the scenarios we will be interested in. Let us assume that the polymer is for $t < 0$ equilibrated under a possibly inhomogeneous tension profile $\bar{f}_0(\bar{s})$ and with a possibly different persistence length $\theta \ell_p$. Further, we assume that the boundary conditions on the contour are such (e.g., hinged) that a spatial average over the squared first derivatives of the eigenmodes gives a constant (this point will be discussed further in Sec. 2.5):

$$\overline{w_q'^2(s)} \approx \frac{q^2}{L}. \quad (2.21)$$

In this case, we can evaluate Eq. (2.20) by using the noise correlation as for Eq. (2.13) to find the spatially averaged stored length $\langle \bar{\varrho} \rangle$ as

$$\langle \bar{\varrho} \rangle = \sum_q \left[\frac{\chi_{\perp}^2(q; t, 0)}{L\theta \ell_p [q^2 + \bar{f}_0(\bar{s})]} + \frac{2q^2}{L\ell_p} \int_0^t dt' \chi_{\perp}^2(q; t, t') \right]. \quad (2.22)$$

To obtain an explicit coarse-grained equation of motion for the backbone tension from Eq. (2.18), we switch to the time-integrated tension

$$\bar{F}(\bar{s}, t) = \int_0^t dt' \bar{f}(\bar{s}, t'). \quad (2.23)$$

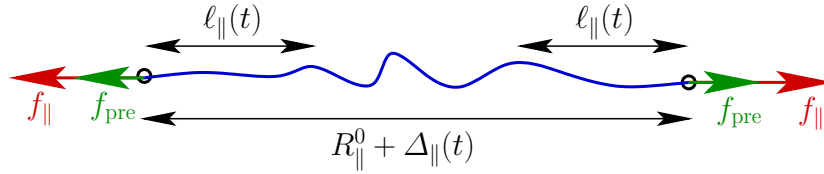


Figure 2.1: Force scenario for the longitudinal response. A filament is equilibrated under a prestretching force f_{pre} , which is suddenly changed to f_{\parallel} . The resulting change in projected length $\Delta_{\parallel}(t)$ arises due to contour straightening, first in boundary layers of size $\ell_{\parallel}(t)$.

For most of the scenarios analyzed in the following, we can additionally perform the continuum limit $L \rightarrow \infty$, because we are interested in time regimes where all relevant length scales (e.g., correlation lengths) are much smaller than L . Since the small-scale s -dependence has now been transferred to mode space, we can drop the overbars, and finally find that $F(s, t)$ obeys a nonlinear partial integro-differential equation:

$$\partial_s^2 F(s, t) = \hat{\zeta} \int_0^\infty \frac{dq}{\pi \ell_p} \left[\frac{1 - \chi_{\perp}^2(q; t, 0)}{\theta[q^2 + f_0(s)]} - 2q^2 \int_0^t dt' \chi_{\perp}^2(q; t, t') \right]. \quad (2.24)$$

Its scenario-specific initial and boundary conditions are discussed in more detail in Refs. [99, 202, 203, 204]. In the remaining sections, we will analyze this equation for different experimentally relevant situations, and also extend the underlying theory by important correction terms where necessary.

2.3. Longitudinal response

Developing a numerical algorithm to solve the partial integro-differential equation (2.24) for the tension and analyzing the dynamic longitudinal response of prestretched semiflexible polymers was the subject of the author's diploma thesis, later published in Ref. [203]. Here, we recapitulate the essential results, because they provide a thorough understanding of the asymptotes of Eq. (2.24) in various regimes. Moreover, the scaling laws derived in Ref. [203] are also relevant for the qualitative discussion of the transverse response in the next section.

Our setup, schematically shown in Fig. 2.1, is motivated by the observation that the physics of semiflexible polymers is significantly changed by externally applied prestress. For instance, the previously discussed transverse mode amplitudes of polymers under tension follow the anomalously slow growth law $t^{1/2}$ [91], which has been confirmed experimentally on prestressed microtubules [34]. More importantly, it has recently been shown that prestressed actin networks *in vitro* provide a realistic model for the viscoelasticity of living cells [64, 80, 81, 130], and that stresses generated by the activity of motor proteins in such networks produce distinct prestress signatures in viscoelastic response quantities [182, 183]. These observations also prompted other theoretical studies based on computer simulations [169, 223]. We were additionally encouraged by the predictions

that the tension propagation length $\ell_{\parallel}(t)$ should follow different growth laws for free and prestressed polymers [25, 236], which were, however, derived by means of contradicting assumptions.

In order to elucidate the change $\Delta_{\parallel}(t)$ in projected length R_{\parallel} in response to a change of the longitudinal force from f_{pre} to f_{\parallel} , we first observe that this change has to equal the amount of stored length $\varrho\ell_{\parallel}$ that has been created in the boundary layer. On the scaling level, Eq. (2.18) reads $\bar{f}/\ell_{\parallel}^2 \simeq \hat{\zeta}\varrho/t$, where \bar{f} is the relevant force scale in the filament. In this case, it is given by the driving force f_{\parallel} (remember that Eq. (2.18) is essentially a friction balance), and the change in projected length reads therefore:

$$\Delta_{\parallel}(t) \simeq \frac{tf_{\parallel}}{\hat{\zeta}\ell_{\parallel}}. \quad (2.25)$$

Hence, we only need to determine the scaling of $\ell_{\parallel}(t)$. This was done in Ref. [203] by means of a ‘‘blob picture’’ for stretching dynamics. Inspired by the famous analogon for flexible polymers [45], this intuitive picture derives from the observation that bending and tension contributions to the WLC Hamiltonian Eq. (2.2) balance on length scales of the order of the blob size $f^{-1/2}$ [133], such that the contour is dominated by bending forces (i.e., it is essentially free) within blobs, while the tension contributes only on larger scales. The scaling argument draws again on the notion of equilibration segments of size $\ell_{\perp} \ll L$, which, however, now follow from a scaling analysis of Eq. (2.17a) as [97]

$$\ell_{\perp}(t) \simeq \begin{cases} t^{1/4}, & \text{for } t \ll f^{-2}, \\ (ft)^{1/2}, & \text{for } t \gg f^{-2}. \end{cases} \quad (2.26)$$

This dynamic force balance between transverse friction forces \mathbf{r}_{\perp}/t and bending $\mathbf{r}_{\perp}/\ell_{\perp}^4$ or tension terms $f\mathbf{r}_{\perp}/\ell_{\perp}^2$ displays a crossover between ‘‘free’’ (bending-dominated) relaxation within blobs and ‘‘forced’’ (tension-driven) relaxation on larger scales. In the more interesting case $f_{\text{ext}} \gg f_{\text{pre}}$, scaling laws for the boundary layer size ℓ_{\parallel} follow now from decomposing the contour into segments of size ℓ_{\perp} . The amount δ by which each of these segments is stretched depends on whether it is smaller or larger than a blob, because this determines the relative magnitude of the effective stretching force. Applying the friction balance to the total stretching $(\ell_{\parallel}/\ell_{\perp})\delta$ of these segments gives:

$$\ell_{\parallel}(t) \simeq \begin{cases} (\ell_{\text{p}}/\hat{\zeta})^{1/2}t^{1/8} \text{ [60, 97, 211]}, & \text{for } t \ll f_{\parallel}^{-2} & (2.27\text{a}) \\ (\ell_{\text{p}}/\hat{\zeta})^{1/2}(f_{\parallel}t)^{1/4} \text{ [2, 97, 236]}, & \text{for } f_{\parallel}^{-2} \ll t \ll (f_{\parallel}f_{\text{pre}})^{-1} & (2.27\text{b}) \\ (\ell_{\text{p}}/\hat{\zeta})^{1/2}f_{\text{pre}}^{1/4}(f_{\parallel}t)^{1/2}, & \text{for } (f_{\parallel}f_{\text{pre}})^{-1} \ll t. & (2.27\text{c}) \end{cases}$$

It turns out that the first asymptote, previously obtained only for small forces [60, 211], is now always attained for short enough times [97]. The intermediate $t^{1/4}$ -regime emerges only for vanishing prestretching force or for strong force scale separation $f_{\parallel} \gg f_{\text{pre}}$, and allows one to apply a so-called ‘‘taut-string’’ approximation [236], where bending and thermal

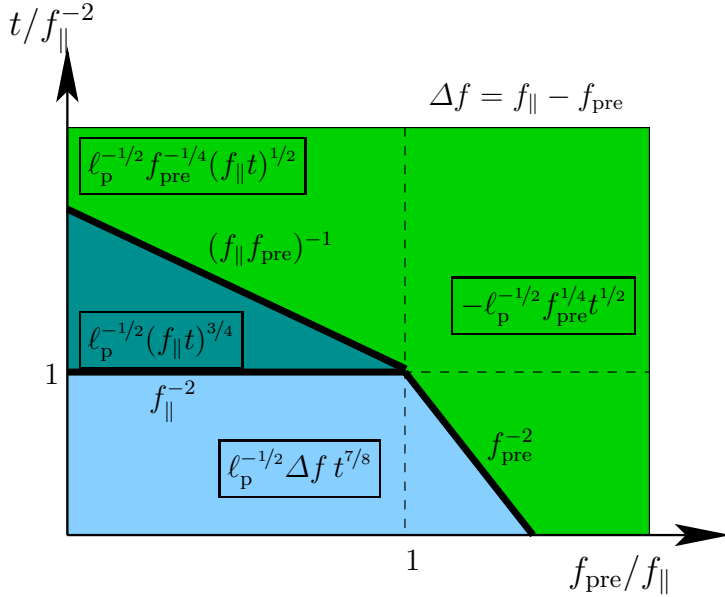


Figure 2.2: Regimes of intermediate asymptotics for the change in projected length $\Delta_{\parallel}(t)$ in the propagation regime $\ell_{\parallel}(t) \ll L$: time t in units of f_{\parallel}^{-2} vs. force ratio $f_{\text{pre}}/f_{\parallel}$ (log-log-scale). For simplicity, we use isotropic friction $\hat{\zeta} = 1$. For a given force ratio, the time evolution of $\Delta_{\parallel}(t)$ corresponds to a vertical trajectory through the diagram. Figure adapted from Fig. 5 of Ref. [203].

forces can be neglected after the preparation of an initial equilibrium conformation. However, this simplification is rigorously valid only for $f_{\text{pre}} = 0$. For long times $t \gg (f_{\parallel} f_{\text{pre}})^{-1}$, our result has the same $t^{1/2}$ -time scaling as in Ref. [25] but a different force dependence. These authors used the “quasi-static” assumption of a locally equilibrated tension, but failed to correctly account for the limit $f_{\text{pre}} \rightarrow 0$. The inconsistencies arising from the complementary approaches of Refs. [25, 236] are thus traced back to a relevant subtlety of the limit of vanishing prestress, underlining its crucial influence.

Using these results gives via Eq. (2.25) readily the scaling laws for the change in projected length $\Delta_{\parallel}(t)$ shown in Fig. 2.2 (in the case $f_{\parallel} < f_{\text{pre}}$, corresponding to a force reduction, the subdominant force f_{\parallel} is largely irrelevant). Here, we have set $\hat{\zeta} = 1$ for simplicity. Given a specific ratio between f_{\parallel} and f_{pre} , the time evolution of $\Delta_{\parallel}(t)$ corresponds to a vertical cut through the figure. For instance, stretching a previously unstretched chain (with $f_{\text{pre}} = 0$), which has been termed “pulling” [97, 236], produces an initial growth $\Delta_{\parallel}(t) \simeq f_{\parallel} t^{7/8} / \ell_p^{1/2}$ for times $t \ll f_{\parallel}^{-2}$, corresponding to the growth law obtained through the linear response argument of Ref. [60] (note, however, that the actual linear response limit $f_{\parallel} \rightarrow 0$ cannot be taken just like that because stochastic tension fluctuations neglected to leading order in the multiple scale perturbation theory become relevant [99]). Afterwards, the longitudinal extension grows like $(f_{\parallel} t)^{3/4} / \ell_p^{1/2}$ [236]. In contrast, completely removing the stretching force (i.e., $f_{\parallel} = 0$), which has been termed “release” [25, 97], gives a corresponding linear response like growth law for the longitudinal contraction, $\Delta_{\parallel}(t) \simeq -f_{\text{pre}} t^{7/8} / \ell_p^{1/2}$, crossing over to $\Delta_{\parallel}(t) \simeq -f_{\text{pre}}^{1/4} t^{1/2} / \ell_p^{1/2}$ at times $t \simeq f_{\text{pre}}^{-2}$. If the effective change in force is small compared to the prestress, $|\Delta f| = |f_{\parallel} - f_{\text{pre}}| \ll f_{\text{pre}}$, the entire calculation can be performed in Fourier space for oscillatory force variations $\Delta f e^{i\omega t}$ by means of a linearization in Δf , which gives analytical expression for the viscoelastic modulus $G^* = G' + iG''$ of a single semiflexible chain [113, 200]. These laws are all valid as long the tension has not

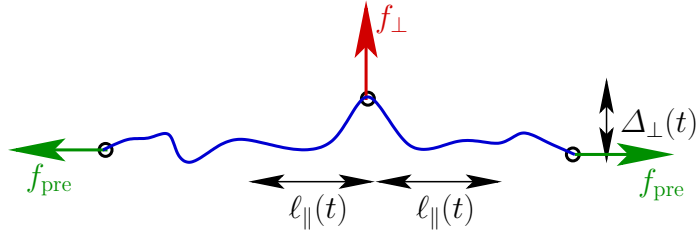


Figure 2.3: Force scenario for the transverse response. A filament is equilibrated under a pre-stretching force f_{pre} , and a sudden transverse force f_{\perp} is applied in the middle of the contour, producing a bulge of height $\Delta_{\perp}(t)$ in response. Via an effective longitudinal force $f_{\parallel}(t)$, this leads to a straightening of the rest of the contour, at first in small regions of size $\ell_{\parallel}(t)$.

yet propagated through the filament, i.e., as long as $\ell_{\parallel} \ll L$. Evaluating the condition $\ell_{\parallel}(t_L^{\parallel}) = L$ yields a second characteristic crossover time t_L^{\parallel} separating the propagation from the relaxation regime [203].

Our previous study also established the applicability of the weakly-bending approximation for two different experimentally relevant situations. The case of *stiff* polymers with $L \ll \ell_p$ gives the small parameter $\varepsilon = L/\ell_p$ as before, appropriate for microtubules, actin, or entire chromosomes. In contrast, a prestretching force f_{pre} can significantly straighten a filament as well. From the force-extension relation Eq. (1.3), we read off the high-force asymptote $1 - R_{\parallel}/L \sim (4\ell_p^2 f_{\text{pre}})^{-1/2}$ [174]. Accordingly, the weakly-bending limit for *stretched* polymers is expressed through the small parameter $\varepsilon = f_{\text{pre}}^{-1/2}/\ell_p$, which is easily attained for forces of about 0.1 pN in the case of DNA. In the outlook Sec. 2.8, we will briefly discuss another example of weakly-bending polymers: those in strong confinement.

2.4. Transverse response

As a first extension of the theory of tension dynamics outlined in Sec. 2.2, we analyzed the transverse response of semiflexible polymers. As shown in Sec. 2.1.3, their stiff backbones lead to the characteristic anisotropy between transverse fluctuation amplitudes (which, in equilibrium, grow like $t^{3/4}/\ell_p$), and longitudinal ones (scaling like $Lt^{3/4}/\ell_p^2$ for times larger than $t_{\star} \simeq L^8/\ell_p^4$, and like $t^{7/8}/\ell_p^{3/2}$ before that). However, due to the inextensibility of the contour, fluctuations in these two directions evolve independently only on the linear level. This implies a coupling of transverse and longitudinal response for stronger forces, which was neglected in previous studies of transverse fluctuations and response [5, 274], because it does not enter the linearized equations of motion Eq. (2.10). We have analyzed such couplings for the dynamic response of single polymers, and we expect them to be relevant also for the force transduction in more complex structures such as single crosslinks [60], crosslinked networks [81], and prestressed “tensegrity” structures: the peculiar elastic properties of the cytoskeleton have been speculated to arise due to its specific architecture reminiscent of these interconnected networks composed of compressed and

tensed elements under prestress [121, 122, 271].

The setup analyzed in our study [202], which is reprinted in Sec. 2.9, is shown in Fig. 2.3. We consider a weakly-bending contour, either for a stiff polymer with $L \ll \ell_p$ or due to an externally applied prestretching force $f_{\text{pre}} \gg \ell_p^{-2}$. At time $t = 0$, a transverse point force f_{\perp} is applied in the middle of the contour. In response to this force, the contour develops a bulge of height $\Delta_{\perp}(t)$ and width $\ell_{\perp}(t)$. Because of the backbone's inextensibility, the bulge can continue growing only by *pulling in* contour length stored in thermal undulations from the filament's tails. Hence, the transverse force f_{\perp} translates into an effective time-dependent longitudinal force $f_{\parallel}(t)$, which pulls in stored length from the tails, hindered by longitudinal friction and therefore initially only from limited regions of size $\ell_{\parallel}(t)$. This longitudinal force, in turn, is equivalent to a backbone tension decaying over a length $\ell_{\parallel}(t)$, which feeds back on the dynamics of the bulge growth and tends to *slow down* the bulge growth (remember that the transverse fluctuations of prestretched filaments grow more slowly than those of free chains). In order to quantify these ideas, our study presents a scaling argument and a rigorous derivation based on the theory of tension dynamics discussed in Sec. 2.2.

Our scaling argument revisits known growth laws for the linear transverse response with and without prestress (the latter case can easily be obtained via a fluctuation-dissipation theorem from Eq. (2.14)) [91]. Since the contour length used for producing the bulge must have been pulled out from the tails, the resulting friction has to balance the unknown longitudinal pulling force $f_{\parallel}(t)$. In a first step, the ‘‘athermal’’ case without thermal contour undulations is discussed, where the tails are pulled in along their entire length L . Self-consistent growth laws for the effective longitudinal force $f_{\parallel}(t)$ and the transverse response $\Delta_{\perp}(t)$ indicate that the coupling is irrelevant for times less than a certain crossover time t_f , whereas at later times the growing longitudinal force feeds back onto the transverse dynamics and slows down the bulge growth. A simple back reference to the longitudinal response readily yields results for the thermal case, where stored length is pulled out only from smaller regions of size $\ell_{\parallel}(t)$: because the growth laws Eq. (2.27) derived in Ref. [203] can be generalized to weakly time-dependent forces such as $f_{\parallel}(t)$, replacing $L \rightarrow \ell_{\parallel}(t)$ gives self-consistent scaling laws for $f_{\parallel}(t)$, and therefore also growth laws for $\Delta_{\perp}(t)$, summarized in a phase diagram quite similar to Fig. 2.2, but with numerically less simple fractions in the exponents. Quantitative estimates for microtubules, actin and DNA indicate that the nonlinearities due to the coupling of transverse and longitudinal response can be observed under many experimental circumstances.

A rigorous approach invokes the above developed theory for the dynamics of the tension along the contour, which can then be related to observables of interest. The essential idea is to treat the localized perturbation f_{\perp} as *boundary condition* on a contour effectively split in half. Further, because the bulge width ℓ_{\perp} follows as characteristic length scale of bending undulations described through the transverse equation of motion Eq. (2.17a), the stored length contained in the bulge gives actually only a *microscopic* and therefore negligible contribution to the spatially averaged quantity $\langle \bar{\rho} \rangle$ entering the right hand side of the coarse-grained equation of motion for the tension, Eq. (2.18). It is important for the boundary conditions, though: demanding that the average longitudinal velocity at the

origin should vanish, $\langle \partial_t r_{\parallel} \rangle = 0$, the inextensibility constraint implies a relation between the first derivative of the tension profile at the origin and the integrated difference in spatially averaged and full stored length density:

$$\partial_s \bar{f}|_{s=0} = -\hat{\zeta} \int_0^L ds \partial_t \langle \varrho - \bar{\varrho} \rangle. \quad (2.28)$$

This boundary condition for the tension profile (which can explicitly be given in terms of the response function Eq. (2.19)), quantifies the feedback between “bulge” and “tail” dynamics. It depends on small-scale contributions to the stored length density ϱ that drop out when spatially averaged. However, for a singular perturbation like a transverse point force, they may still be relevant. By way of the analytical methods discussed in the previous section, it is possible to compute tension profiles in certain intermediate asymptotic regimes, in order to quantitatively verify the previously obtained scaling laws. Numerical solutions, using the algorithm presented in Ref. [203], give solutions for intermediate regimes and more insight into the crossover scenario. In the next section, we will encounter another example where small-scale contributions to stored length density resulting from boundary effects have a quantitative influence.

2.5. Relaxation dynamics

Measuring the relaxation of polymer chains from an initially straight conformation is a standard experiment in polymer rheology (see Ref. [239] for a review on DNA relaxation dynamics in shear flow). As mentioned at the beginning of this chapter, many different setups have been used to straighten polymers, and for most of them, the relaxation dynamics has been investigated as well: for DNA straightened by linear elongational flows [214], by shear flows [170], by electric fields [168] or a combination of fields and flows [15], and for DNA within nanochannels [220] or other nanostructures [265], or stretched with optical tweezers [22, 43, 63, 90]. *In vivo*, relaxation has been observed on stress fibers following laser severing [146] and on DNA after chromosome breakage [66]. Moreover, different computer simulations have been performed: some authors used an initially perfectly straight conformation and bead-rod Brownian dynamics simulations [46, 47, 269], others employed bead-spring models and used shear flows [119, 151] or forces [149, 241] for stretching. Theoretical studies have modeled these chains by elastic dumbbells [116, 240], as flexible polymers [24, 104], and as wormlike chains by means of different quasi-static approximations [22, 25, 43].

Generally, the relaxation of an initially straight polymer is a prime example for the stretch-coil transition, and so far the analysis concentrated for the most part on determining how its key identifier, the longest relaxation time t_R , is influenced by hydrodynamic interactions. Here, we are interested in the dynamics on much shorter scales, especially because the results of Sec. 2.3 suggest that removing a stretching force gives rise to propagation and relaxation of backbone tension: the contour starts to coil up first in boundary layers of size $\ell_{\parallel}(t)$, because building up thermal undulations in the bulk would require to

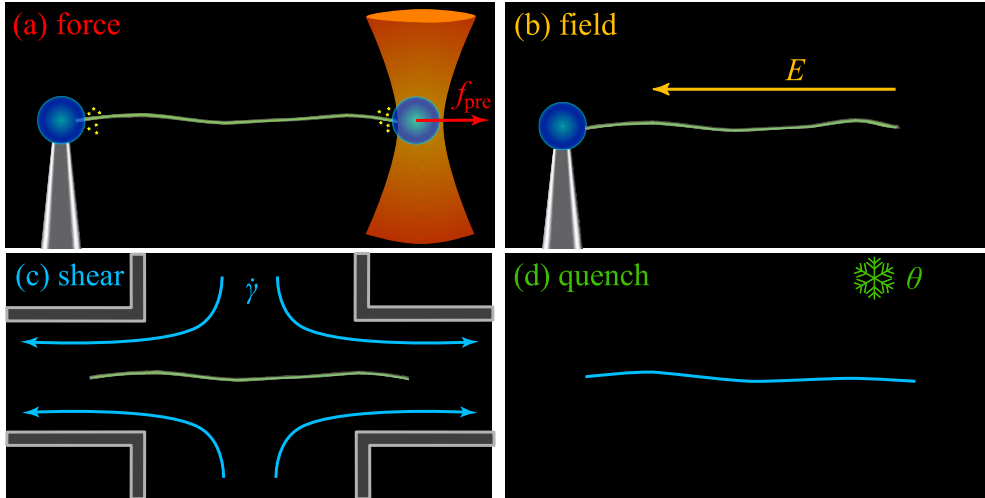


Figure 2.4: Possible experimental setups for relaxation experiments. (a) In the “force” scenario, optical tweezers are used to stretch a filament fixed between two beads with a force f_{pre} . Restriction enzymes could be used to cut the filament loose. (b) In the “field” setup, an electric field of strength E is used to straighten the chain, which remains attached to a bead at one end. Using linear extensional flow of velocity v for stretching gives rise to largely equivalent relaxation dynamics. (c) The “shear” case describes the straightening of polymers by a symmetric shear flow with shear rate $\dot{\gamma}$. (d) In the “quench” experiment, the filament is equilibrated at low temperature, which is then suddenly increased by a factor θ . Figure adapted from Fig. 1 of Ref. [204].

pull in the filament’s tails against longitudinal friction. Accordingly, the tension relaxes from its initially high value at first only near the ends. Primarily, we want to investigate the influence of the exact initial conditions resulting from the quite different commonly employed experimental setups, which was previously not discussed. Because *exactly* straight initial conditions, repeatedly used in computer simulation [46, 47, 269], cannot be realized in practice due to the presence of thermal noise, relaxation will always start from an initially only “nearly” straight conformation containing some “memory” of the stretching mechanism, but in all cases it will be driven exclusively by stochastic forces. To which extent the initial conditions influence the longitudinal dynamics, and how results obtained with different setups should be compared, were the main questions addressed in our own study [204], which is reprinted in Section 2.10.

For the four different setups shown in Fig. 2.4, we employed Brownian dynamics simulations using a simple free-draining bead-spring model (simulations were carried out by Wolfram Möbius). We measured two observables: the time-dependent change $\Delta_{\parallel}(t) = R_{\parallel}(t) - R_{\parallel}(0)$ in end-to-end distance projected onto the initial longitudinal axis (note that it is defined with a minus sign in Ref. [204]; here, we ignore the sign if only the scaling is of interest), and the bulk tension $f_b(t)$ in the filament, which gives a measure of the bulk stress in a polymer solution. The parameter values for the different setups were cho-

sen such that the initial extension is approximately identical and close to full stretching, $\Delta_{\parallel}(0) \approx 0.97L$ (see Appendix A.1 for a simple estimation of force-extension relations for different setups). Our results show distinct differences between the four setups for short times and universal scaling for longer times, which can be explained on a qualitative level based on the results of Sec. 2.3.

The “force” case is identical to the “release” scenario briefly mentioned in Sec. 2.3. While the bulk tension f_b , initially equal to the external force f_{pre} , stays approximately constant for times $t \ll t_L^{\parallel}$, the boundary layer size $\ell_{\parallel}(t)$ and from Eq. (2.25) also the change in projected length $\Delta_{\parallel}(t) \simeq t f_b(t) / (\hat{\zeta} \ell_{\parallel}(t))$ undergo at $t_f = f_{\text{pre}}^{-2}$ a crossover from a linear regime ($\Delta_{\parallel} \propto t^{7/8}$) to a nonlinear regime ($\Delta_{\parallel} \propto f_{\text{pre}}^{1/4} t^{1/2}$), see Fig. 2.1. At time $t = t_L^{\parallel}$, when the tension has propagated through the filament ($\ell_{\parallel}(t_L^{\parallel}) = L$), the dynamics enters the universal relaxation regime discussed below.

For the “field” and “shear” cases, the initial tension profiles have a different shape (linear and parabolic, respectively), and we can estimate their magnitude from a force analog f_{pre}^* : the total Stokes friction $\hat{\zeta} v L$ in a linear flow of velocity v and the total friction $\hat{\zeta} L^2 \dot{\gamma}$ in an extensional shear flow of shear rate $\dot{\gamma}$ give a measure of the resulting tension in a filament. If an electric field is used for stretching, the effective force resulting from the applied field E is not so easily quantified due to complicated counterion effects [107, 163, 164, 250]. In any case, the resulting tension dynamics also displays a dynamic crossover at a characteristic time $t_f = f_{\text{pre}}^{*-2}$. However, the longitudinal contraction $\Delta_{\parallel}(t) \propto t$ scales always linearly in time, because the filament’s tails have been equilibrated under a flow profile very similar to the one that is generated as they are “pulled in” with approximately constant speed, such that tension propagation effects are only subdominant.

The “quench” case, finally, describes an experiment where the filament has been equilibrated at low temperature, which is then suddenly increased by a large factor θ . Here, a force analog can only be defined formally to match the resulting crossover time t_L^{\parallel} . In contrast to the other setups, the tension in a quenched filament is initially zero and only produced because the contour is equilibrated under a different temperature than now experienced. This tension can be relaxed by reshuffling stored length between short and long wavelength modes [96], and since it decreases as $f_b \propto t^{-1/2}$, while $\ell_{\parallel} \propto t^{1/8}$, we observe a new growth law $\Delta_{\parallel} \propto t^{3/8}$ in the longitudinal contraction. Note that because the tension even diverges as $t \rightarrow 0$, microstructure corrections that are subdominant for “realistic” values of the tension become observable (see Sec. 2.6 for a discussion of these effects).

At time $t = t_L^{\parallel}$, the tension has propagated through the filament and enters the regime of “homogeneous tension relaxation” [97], where our observables attain the same scaling in all setups. The universal growth law $\Delta_{\parallel} \propto t^{1/3}$, which has been observed in experiments on DNA relaxation from shear flow stretching [229], results from a nontrivial influence of longitudinal friction, which may not be neglected even though the tension is quasi-statically equilibrated [97]. This growth law can readily be motivated in a simple but somewhat unphysical picture based on a strongly stretched polymer with instantaneous extension $L - \Delta_{\parallel}$, where $\Delta_{\parallel} \simeq L f_b^{-1/2} / \ell_p$ is in a quasi-static approximation given by the high-force asymptote of the force-extension relation Eq. (1.3) [174]. Assuming that the

friction $\hat{\zeta}L\Delta_{\parallel}/t$ resulting from the contraction is balanced by the internal tension f_b , we obtain the scaling laws $\Delta_{\parallel} \propto t^{1/3}$ and $f_b \propto t^{-2/3}$ [97]. These results for the universal regime also indicate that for the exactly straight initial condition, which could be realized in all four setups by sending the control parameters to infinity, the propagation regimes with their characteristic differences vanish: $t_L^{\parallel} \rightarrow 0$. At the same time, important microstructure corrections, discussed in the next section, become very relevant.

These qualitative results can be systematically verified by solving the coarse-grained equation of motion for the tension, Eq. (2.24), for the respective setups. While the “force” case has been discussed previously [99, 203], the results for “field”, “shear”, and “quench” require different approximation techniques. Using corresponding numerical solutions, we compare these results to simulation data. It turns out that it is necessary to account for the exact boundary conditions. Our main observable, the longitudinal contraction $\Delta_{\parallel}(t)$, can be expressed as the amount of stored length that has been created in the contour:

$$\begin{aligned} \Delta_{\parallel}(t) &= - \int_0^L ds \int_0^t dt' \partial_{t'} \langle \varrho \rangle (s, t') \\ &= \hat{\zeta}^{-1} [F'(L, t) - F'(0, t)] - \int_0^L ds \int_0^t dt' \partial_{t'} \langle \varrho - \bar{\varrho} \rangle (s, t'). \end{aligned} \quad (2.29)$$

While the first term involving $\langle \bar{\varrho} \rangle$ follows via Eq. (2.18) from the tension profile, the second term measures the difference between spatially averaged and full stored length density, which was already relevant for the transverse response (see Eq. (2.28)), but has been neglected in our scaling arguments for the longitudinal response in Sec. 2.3. Revisiting the simplification $\overline{w_q^2(s)} \approx q^2/L$ made in Eq. (2.21), this term can be approximately computed by using the correct eigenmodes for “free” ends, resulting in a quantitatively relevant even though on the scaling level subdominant contribution that gives altogether good quantitative agreement between simulation results and analytical theory over almost 6 decades in time *without free parameters*.

Moreover, we briefly quantify experimentally relevant time and force scales: e.g., for typical DNA a stretching force of about 2 pN would be sufficient to see tension propagation effects on time scales below 50 ms. We also discuss the onset of the stretch-coil transition: the well-known stem-flower picture by Brochard-Wyart [24] for a flexible polymer predicts a longitudinal contraction $\Delta_{\parallel}(t) \propto (t/t_R)^{1/2}$, where t_R is the Rouse time, due to the formation of coil-like “flowers” at the ends of a still relatively straight “stem”. For the dominating bulk (i.e., stem) relaxation of strongly stretched semiflexible polymers (in the relevant regime of homogeneous tension relaxation, $\Delta_{\parallel}(t) \simeq (t/t_R)^{1/3}$), the scaling argument has to be modified and gives an even more subdominant contraction that scales like $(t/t_R)^{2/3}$. Finally, we argue that hydrodynamic interactions could be phenomenologically included by replacing the length L in the logarithms of the denominators of the friction coefficients, Eq. (2.4), with appropriately time-dependent hydrodynamic correlation lengths.

2.6. Microstructure corrections

The previous section has shown that corrections to the inextensible continuous WLC model may become relevant if relatively large stretching forces are involved. In this section, we present two theoretical approaches to study corrections to nonlinear WLC dynamics due to a finite backbone extensibility [200] and a discretized backbone, respectively. These corrections are particularly important when comparing to simulation data: conventional simulation models for semiflexible polymers are usually not realistic enough to correctly account for these effects, which are essentially caused by the very microstructure that has been neglected in the coarse-grained model. Hence, a semi-quantitative understanding is important for choosing simulation parameters such that microstructure contributions, which are essentially simulation artefacts, are not observable.

Basically, two different approaches for Brownian dynamics simulations of semiflexible polymers are commonly used [67, 92, 247]: bead-spring algorithms, which model the polymer as a chain of beads connected by extensible (Hookean or nonlinear) springs, have the advantage that equations of motion are easily written down and straightforwardly integrated numerically; however, to correctly account for the actually very large backbone stiffness of realistic biopolymers, unfeasibly small time steps are necessary in order to resolve the resulting high-frequency dynamics. In contrast, bead-rod models, where the beads are connected by strictly inextensible rods, are supposed to avoid this problem, but the formulation of the resulting “constrained” dynamics is far from trivial [92, 184, 187] and requires the introduction of unintuitive metric correction forces; moreover, the time step cannot be chosen as large as desired due to a regrettably poor numerical stability of available implementations.

In both cases, the necessary trade-off between simulation accuracy and computational efficiency can lead to an overestimated prominence of extensibility and discretization effects, and a theoretical account of their quantitative relevance is therefore desirable. Previous studies have investigated static properties [133, 160] and some aspects of the dynamics in the linear regime [172], but the nonlinear tension dynamics remain unexplored.

2.6.1. Backbone extensibility

Almost 15 years ago, experiments have shown that DNA is an extensible molecule [42]. If stretched with forces of about 65 pN, DNA undergoes the so-called overstretching transition, observable also in Fig. 1.2, which is caused by internal structural rearrangements (the double helix changes from the B to the S form). This transition has been studied in great detail experimentally [42, 244] and theoretically [41, 191, 251]. However, even for smaller forces, DNA exhibits a finite backbone extensibility coupled to its twist elasticity [171, 172]. Other semiflexible polymers like actin are of course also not strictly inextensible [135], even though the backbone bonds are indeed very stiff.

In the previous sections, we have analyzed the nonlinear dynamic response of semiflexible polymers and provided a theoretical description based on an interplay of stored length and backbone tension. If the backbone is extensible, the tension is no longer a formally

introduced Lagrange multiplier but an actual spring force proportional to the backbone strain. Although for a stiff backbone the stretching modes connected to longitudinal strain relax much faster than the bending modes related to stored length [246], they do so against the background of a potentially inhomogeneous and not necessarily equilibrated stored length profile, which in turn can still be related to backbone tension. For a non-equilibrium relaxation experiment like the “force” scenario discussed in Sec. 2.5, the tension dynamics is thus a reflection of the competition between the creation of thermal stored length and the relaxation of mechanical backbone strain.

Our study [200], reprinted in Sec. 2.11, presents a systematic theoretical analysis of these phenomenological ideas. We use an extensible WLC Hamiltonian [172],

$$\mathcal{H} = \frac{1}{2} \int_0^L ds \left[\mathbf{r}'^2 + \frac{k_x}{\ell_p} u^2 \right], \quad (2.30)$$

where the combination k_x/ℓ_p (which reads $k_B T k_x$ in real units) is the energetic penalty for elongational strain $u = |\mathbf{r}'| - 1$, and k_x is the stretching elastic constant. Strictly speaking, s is no longer the proper arclength, but the difference is negligible on our level of approximations. For a filament under large prestress $f_{\text{pre}} \gg \ell_p^{-2}$, this Hamiltonian gives rise to an asymptotic force extension relation [172]

$$1 - \frac{R_{\parallel}}{L} = -\langle u \rangle + \langle \frac{1}{2} \mathbf{r}'_{\perp}{}^2 \rangle = -\frac{\ell_p f_{\text{pre}}}{k_x} + \frac{1}{2\ell_p f_{\text{pre}}^{1/2}}, \quad (2.31)$$

which suggests to define two small parameters: $\varepsilon_{\text{th}} = f_{\text{pre}}^{-1/2}/\ell_p$ expresses the weakly-bending limit of small contour undulations, and $\varepsilon_x = \ell_p f_{\text{pre}}/k_x$ formalizes a corresponding “weakly-stretching” asymptote of small longitudinal strain. For our analysis, we assume that the contribution due to backbone stretching is subdominant against bending, i.e., that $\varepsilon_x \ll \varepsilon_{\text{th}} \ll 1$. Our theory exploits that stretching modes relax faster than bending modes, while the effective tension $f = k_x u/\ell_p$ varies on spatially larger scales than the bending modes. Hence, we introduce small- and large-scale spatial coordinates as in Sec. 2.2.1, but additionally also two independent time variables for the slow bending and fast stretching dynamics, respectively. Performing a multiple-scale analysis similar to Sec. 2.2.1, we arrive at a coarse-grained equation of motion for the tension similar to Eq. (2.18):

$$\partial_s^2 \bar{f} = -\hat{\zeta} \partial_t [\bar{\varrho} - \bar{u}], \quad (2.32)$$

where the thermal stored length density $\varrho = \frac{1}{2} \mathbf{r}'_{\perp}{}^2$ is now reduced by an amount $u = \ell_p f/k_x$ due to the mechanical stretching of backbone bonds.

Our study proceeds to calculate the complex compliance J^* describing the change in end-to-end distance $\Delta_{\parallel}(t)$ in response to an oscillatory perturbation $f_{\parallel} = f_{\text{pre}} + \delta f e^{i\omega t}$, arriving at scaling laws in intermediate asymptotic regimes, similar to the ones shown in Fig. 2.1 (cf. also Ref. [113] for the inextensible case). Here, however, we are more interested in extensibility corrections for the “force” scenario of Sec. 2.5. From Eq. (2.32), we obtain

a diffusive growth law for short times,

$$\Delta_{\parallel}(t) = -\frac{4f_{\text{pre}}}{\sqrt{\pi}} \sqrt{\frac{\ell_{\text{p}} t}{\hat{\zeta} k_{\text{x}}}} \quad \text{for } t \ll t_{\text{X}}, \quad (2.33)$$

where the time scale $t_{\text{X}} = f_{\text{X}}^{-2}$ is related to a characteristic force scale $f_{\text{X}} = (k_{\text{x}}/\ell_{\text{p}}^2)^{2/3}$ [133, 270]: if $f_{\text{pre}} \ll f_{\text{X}}$ (equivalent to $\varepsilon_{\text{x}} \ll \varepsilon_{\text{th}}$), thermal stored length (from bending) contributes more to extension than longitudinal strain, and in this case the dynamics for later times $t \gg t_{\text{X}}$ is unperturbed by extensibility effects. Given that $f_{\text{X}} \approx 50$ pN for DNA [172], which is close to the overstretching transition, extensibility effects are indeed not relevant for experiments on DNA in reasonable parameter regimes, but the condition $f_{\text{pre}} \ll f_{\text{X}}$ is much harder to obey in bead-spring simulations (see, for instance, Ref. [190]).

2.6.2. Backbone discretization

In order to estimate the relevance of discretization or microstructure effects, which are generally inevitable in experiments and computer simulations, we introduce an ultraviolet mode cutoff $q_{\text{max}} \simeq \pi/b$ in the explicit formulation of Eq. (2.18) (see Eq. (2.24) and Eq. (A.3)), where $b \ll L$, ℓ_{p} is an appropriate microscopic length scale. A detailed analysis of the “force” scenario of Sec. 2.5 is presented in Appendix A.2, where the resulting intermediate asymptotic growth laws are summarized in Table A.1. As noted previously [269], the maximum “reasonable” stretching force is given by the force scale $f_{\text{D}} = b^{-2}$: larger forces $f_{\text{pre}} \gg f_{\text{D}}$ have a correspondingly smaller blob size $f_{\text{pre}}^{-1/2} \ll b$ [203] below the spatial resolution.

For small enough forces $f_{\text{pre}} \ll f_{\text{D}}$, we find relevant effects only on very short times, where they contribute a linear growth of the end-to-end distance, masking the predictions of Ref. [204] for the ideal case:

$$\Delta_{\parallel}(t) = -\sqrt{\frac{8}{\hat{\zeta} \ell_{\text{p}} b}} f_{\text{pre}} t \quad \text{for } t \ll t_{\text{D}}, \quad (2.34)$$

with a characteristic time $t_{\text{D}} = f_{\text{D}}^{-2}$. In contrast, for an *exactly straight* initial conformation as in Refs. [46, 47, 269], which we model as the limit $f_{\text{pre}} \rightarrow \infty$ in Appendix A.2, we find initially parabolic tension profiles with maximum (bulk) magnitude $f_{\text{b}} = L^2/(\ell_{\text{p}} b^3)$ proportional to the squared number of beads (in agreement with Ref. [92]). These results suggest that for a discrete model any force larger than $L^2/(\ell_{\text{p}} b^3)$ amounts to the infinite force limit.

While for DNA the characteristic force $f_{\text{D}} \approx 50$ pN is again in the neighborhood of the overstretching transition, the consequences of these bounds have not always been properly realized in computer simulations [47, 190]: if $f_{\text{pre}} \gg f_{\text{D}}$, discretization effects dominate the relaxation for times up to $\hat{\zeta} L^2 b^3 / \ell_{\text{p}}$, which can be much larger than the microscopic time scale $\ell_{\text{p}} b^3$ associated with the Brownian dynamics of the single beads [92].

2.7. Conclusions

This chapter presented a theoretical discussion of the nonlinear dynamic response of semiflexible polymers. Methodically based on a multiple-scale perturbation theory [97, 98, 99], developed to systematically account for the failures of the linearized dynamics in the short time response to sudden perturbations, we summarized in Section 2.3 our previously obtained results for the longitudinal response [203], illuminating the strong and intricate influence of prestress on the semiflexible polymer response. In the following Section 2.4, the nonlinear response to transverse forces was analyzed by means of scaling laws, which shed light on the coupling between transverse and longitudinal response and the resulting feedback. In a systematic and quantitative calculation, we treated the effects of the transverse point force via a boundary condition on the backbone tension [202]. In Section 2.5, we discussed a paradigmatic experiment in polymer rheology: the relaxation of a polymer chain from an initially straight conformation. Comparing different experimental realizations of “initially straight” (e.g., by forces, fields, or flows), we elaborated the resulting differences in the relaxation dynamics: while it is scenario-specific for short times, where tension propagation is relevant, it becomes universal for longer times. Supplemented by a more accurate treatment of the exact boundary conditions, our parameter-free theory curves are in good agreement with simulation data from Brownian dynamics simulations. We also discussed the influence of hydrodynamic interactions, the onset of the stretch-coil transition, and quantitative implications for experiments [204]. The following Section 2.6 was concerned with microstructure corrections due to a finite backbone extensibility or a discretized backbone, which are especially relevant for computer simulations. We developed a theory of tension dynamics for extensible wormlike chains that accounts for the interplay of bending and stretching modes, and yields critical time and force scales relevant for simulation design [200]. Further, we analyzed the influence of discretization corrections by means of a mode cutoff, and found that the relaxation dynamics may be completely dominated by discretization effects if the stretching force is chosen too large.

2.8. Outlook

Building up on this and previous work, current research on the nonlinear response of semiflexible polymers focuses on three directions: “glassy” dynamics, confinement and discretization effects.

“Glassy” dynamics. The “glassy” wormlike chain model has been proposed in order to account for the slow relaxation of long-wavelength bending modes in polymeric solutions [142, 145, 237]. The complicated collective effects of polymeric interactions and molecular crowding, giving rise to distinct signatures of “glassy” dynamics [61], are phenomenologically accounted for by an exponential stretching of the relaxation times of all modes with wavelength longer than a certain cutoff length Λ . This provides an accurate quantitative description of rheological data from actin solution [237]. Analyzing the longi-

tudinal and transverse response discussed in Sections 2.3 and 2.4 within this model reveals distinct signatures beyond a characteristic crossover time t_A [254].

Confinement. Recent technological advances have allowed to study static and dynamic properties of single polymers such as actin [140] or DNA [221] confined in micro- or nanochannels. Theoretical research has so far focused on scaling properties [205] and certain static observables such as the tangent correlation and the mean end-to-end distance and its distribution [156, 264, 267]. Several experimental studies also investigated the dynamic response of confined DNA [15, 16, 221], but the influence of confinement on tension dynamics remained unexplored. Recent work extends the analysis of the longitudinal response to polymers in confinement [263], recognizing dynamic signatures reminiscent of those caused by external prestress. Interestingly, suddenly removing the confinement walls, as another theoretically conceivable setup to measure the relaxation of an initially straight filament, leads to a new superlinear growth law $\Delta_{\parallel}(t) \propto t^{9/8}$ for the initial longitudinal contraction.

Discretization effects. Understanding the effects of a finitely discretized backbone is crucial for the proper design of computer simulations. In order to compare the performance and accuracy of bead-spring vs. bead-rod algorithms, we have simulated the “force” scenario discussed in Sec. 2.5. If simulation parameters are chosen such that the bounds established in Sec. 2.6 are respected, the resulting differences in $\Delta_{\parallel}(t)$ for these two algorithms are indeed smaller than the error bars. While introducing a suitably adjusted mode cutoff as in Ref. [111] gives quantitative agreement between simulation and theory for the autocorrelation function of the end-to-end distance [152], a cutoff within the continuum approximation as in Sec. 2.6.2 describes the strong short-time deviations expected for the relaxation from a perfectly straight initial conformation (see Appendix A.2) only qualitatively [150].

Coupling of Transverse and Longitudinal Response in Stiff Polymers

Benedikt Obermayer^{1,*} and Oskar Hallatschek^{2,†}

¹Arnold Sommerfeld Center and Center for NanoScience, Ludwig-Maximilians-Universität München, Theresienstr. 37, 80333 München, Germany

²Lyman Laboratory of Physics, Harvard University, Cambridge, Massachusetts 02138, USA

(Received 25 April 2007; published 31 August 2007)

The time-dependent transverse response of stiff inextensible polymers is well understood on the linear level, where transverse and longitudinal displacements evolve independently. We show that for times beyond a characteristic time t_f , longitudinal friction considerably *weakens* the response compared to the widely used linear response predictions. The corresponding feedback mechanism is explained by scaling arguments and quantified by a systematic theory. Our scaling laws and exact solutions for the transverse response apply to cytoskeletal filaments as well as DNA under tension.

DOI: 10.1103/PhysRevLett.99.098302

PACS numbers: 82.35.Lr, 87.15.He, 87.15.La

In tracing back the viscoelasticity of the cell to properties of its constituents, a detailed understanding of the mechanical response of single cytoskeletal filaments is indispensable. Because of their large bending stiffness, these filaments exhibit highly anisotropic static [1] and dynamic [2–4] features, such as the anomalous $t^{3/4}$ -growth of fluctuation amplitudes in the transverse direction [5,6], i.e., perpendicular to the local tangent. The related response to a localized transverse driving force has so far been examined only by neglecting longitudinal degrees of freedom [6,7], although these polymers are virtually inextensible, and transverse and longitudinal contour deformations therefore coupled. In this Letter, we show that longitudinal motion strongly affects the transverse response even for weakly-bending filaments and leads to relevant nonlinearities beyond a characteristic time t_f .

The physical key factors controlling the transverse response may be understood from Fig. 1, which shows a weakly-bending polymer (bending undulations are exaggerated for visualization) shortly after a transverse driving force f_{\perp} has been applied in the bulk. In response to this force, the contour develops a bulge. Because of the backbone inextensibility, this bulge can continue growing only by *pulling in* contour length from the filament's tails. This effectively reduces the thermal roughness of the contour [8–10] at a rate substantially limited by longitudinal solvent friction. The resulting coupling to the longitudinal response tends to *slow down* the bulge growth. In order to describe this feedback mechanism, we start with a scaling analysis and treat the simpler *athermal* case first. To connect to the biologically important situations of prestressed actin networks [11] and prestretched DNA [12], we then extend a recent theory of tension dynamics [13] to calculate the nonlinear response for unstretched and prestretched initial conditions.

Consider the overdamped dynamics of an initially straight stiff rod of total length L . Suddenly applying a transverse pulling force f_{\perp} , for simplicity in the center of

the rod, leads to the growth of a bulge deformation. The generated friction in the transverse and longitudinal direction needs to be balanced by corresponding driving forces. Viscous solvent friction is modeled via anisotropic friction coefficients (per length) ζ_{\perp} and $\zeta_{\parallel} = \zeta\zeta_{\perp}$ with $\zeta \approx \frac{1}{2}$ [7] for transverse and longitudinal motion, respectively. After a time t , the resulting bulge has some characteristic height $\Delta_{\perp}(t)$ and width $\ell_{\perp}(t)$. The transverse force f_{\perp} balances the drag force $\zeta_{\perp}\ell_{\perp}\Delta_{\perp}/t$ acting on a polymer section of length ℓ_{\perp} moving transversely with velocity Δ_{\perp}/t through the solvent; hence, $\Delta_{\perp} \simeq f_{\perp}t/(\zeta_{\perp}\ell_{\perp})$. Naturally, the contour length along the deformed rod section is larger than its longitudinal extent ℓ_{\perp} . Assuming a simple “triangle” geometry as in the blowup in Fig. 1, the difference is roughly given by $\Delta_{\perp}^2/\ell_{\perp}$. In order to provide this *stored* (or excess) length, the filament's tails are pulled in by a longitudinal force f_{\parallel} . The latter has to balance the longitudinal friction that acts on the filament's tails of length L

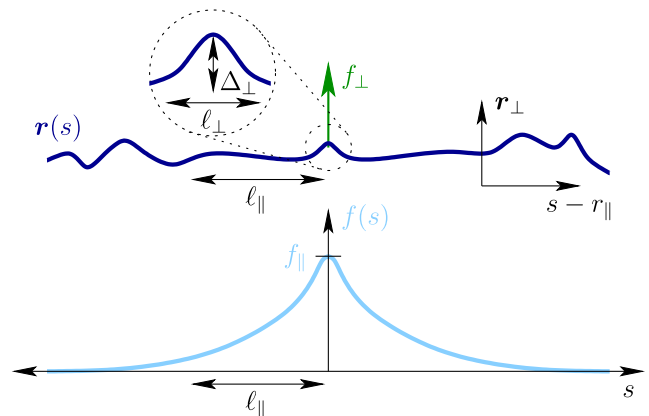


FIG. 1 (color online). A transverse point force f_{\perp} applied to the contour $r(s)$ (dark) translates, through the formation of a bulge of height Δ_{\perp} and width ℓ_{\perp} , into a longitudinal pulling force f_{\parallel} acting on the polymer's tails. This force induces backbone tension $f(s)$ (light) that penetrates the contour within a region of size ℓ_{\parallel} where thermal undulations are straightened.

moving longitudinally with a velocity given by the temporal change of the excess contour length contained in the bulge. Estimating $f_{\parallel} \approx \zeta_{\parallel} L \Delta_{\perp}^2 / (\ell_{\perp} t)$, we plug in Δ_{\perp} from above and get $f_{\parallel} \approx \zeta_{\parallel} L f_{\perp}^2 t / (\zeta_{\perp}^2 \ell_{\perp}^3)$.

The yet unknown time-dependent width $\ell_{\perp}(t)$ of the bulge is controlled by the relaxation spectrum of bending deformations. In the weakly-bending limit, the transverse displacement field $\mathbf{r}_{\perp}(s, t)$ of an overdamped inextensible rod with bending stiffness κ obeys [5]

$$\zeta_{\perp} \partial_t \mathbf{r}_{\perp} = -\kappa \mathbf{r}_{\perp}'''' + f_{\parallel}(t) \mathbf{r}_{\perp}'', \quad (1)$$

in the presence of a longitudinal pulling force $f_{\parallel}(t)$. Primes denote derivatives with respect to the arclength coordinate $s \in [-\frac{L}{2}, \frac{L}{2}]$. In the following, we set κ and ζ_{\perp} to unity, such that time is a length⁴ and force a length⁻². From a simple scaling analysis of Eq. (1), $\mathbf{r}_{\perp}/t \approx \mathbf{r}_{\perp}(\ell_{\perp}^{-4} + f_{\parallel} \ell_{\perp}^{-2})$, we deduce the growing size $\ell_{\perp}(t)$ of a bending deformation (assuming $\ell_{\perp} \ll L$). Inserting appropriate formulas [13] for $\ell_{\perp}(t)$ into the relations for Δ_{\perp} and f_{\parallel} derived before finally yields the self-consistent scaling laws for $f_{\parallel}(t)$ and the nonlinear response $\Delta_{\perp}(t)$ summarized in Table I(a). For short times, the coupling effect is irrelevant, and $\Delta_{\perp}(t)$ is linear in f_{\perp} . However, this requires the small force f_{\parallel} to pull in more and more contour length from the tails and increases the longitudinal friction to be balanced by f_{\parallel} . At the crossover time t_f , this force becomes large enough (typically, $f_{\parallel} \approx \gamma f_{\perp} \gtrsim f_{\perp}$) to feed back onto the transverse dynamics, which is manifest in nonlinear dependencies [14] on f_{\perp} . In particular, it considerably slows down the bulge growth, which in turn requires f_{\parallel} to pull in contour length at a slower rate and eventually makes it decrease.

The essential difference for nonzero temperatures is the presence of thermal contour undulations, see Fig. 1, which are correlated over the persistence length $\ell_p = (k_B T)^{-1}$, and straightened out by the longitudinal force f_{\parallel} . Still counteracted by longitudinal friction, this happens first only within a small but growing region of size $\ell_{\parallel}(t)$ (see

Refs. [3,8–10,13]). Correspondingly, the force $f_{\parallel}(t)$ from above has to be generalized to a tension field $f(s, t)$, which decays over the length scale $\ell_{\parallel}(t)$. Crossover scaling laws for $\ell_{\parallel}(t)$, shown in Table I(b), were derived for constant external force in Ref. [13] and can be generalized to (weakly) time-dependent “external” forces such as $f_{\parallel}(t)$. The thermal problem is essentially analogous to the athermal case for late times $t > t_L^{\parallel}$ where t_L^{\parallel} is defined via $\ell_{\parallel}(t_L^{\parallel}) = L$. However, if the region $\ell_{\parallel}(t)$, where the contour straightens, does not yet extend to the filament’s ends ($\ell_{\parallel} \ll L$, or $t \ll t_L^{\parallel}$), the “thermal” rod has only an effective time-dependent length of $\ell_{\parallel}(t)$. Hence, scaling laws for the nonlinear response are then obtained simply by replacing $L \rightarrow \ell_{\parallel}$ in Table I(a), which gives the results summarized in Table I(b). These apply to initially unstretched filaments while the general case of prestretched initial conditions is discussed below and summarized in Fig. 3. Naturally, the replacement $L \rightarrow \ell_{\parallel}$ affects only the long-time scaling of the nonlinear response $\Delta_{\perp}(t)$ —on short times $t \ll t_f$, the transverse dynamics evolves undisturbed by the longitudinal one. We expect the anomalously slow long-time response to be observable in many biological situations. In aqueous solution, we roughly estimate a crossover time $t_f \approx 10^{-2} \text{ s}/f_{\perp} [\text{pN}]^{8/3}$ for typical microtubules with $L \approx 10 \mu\text{m}$ [15] (representing the athermal case). Under thermal conditions, where the “interesting” time window is between t_f and t_L^{\parallel} , we get $t_f \approx 10^{-3} \text{ s}/f_{\perp} [\text{pN}]^{16/7}$ and $t_L^{\parallel} \approx 0.2 \text{ s}/f_{\perp} [\text{pN}]$ for (unstretched) actin filaments of about $20 \mu\text{m}$ length [4], which implies that the actin response to myosin motors becomes nonlinear on time scales comparable to the duration of a single power stroke [16]. Filaments in actin networks (mesh size $\xi \approx \frac{1}{10} L \approx 0.5 \mu\text{m}$) under stresses of about 1 Pa [11] are usually so short that $t_f \gg t_L^{\parallel} \approx 10^{-4} \text{ s}$, but the coupling nonlinearity should be observable in the viscoelastic response [3]. Finally, $t_f \approx 10^{-5} \text{ s}/f_{\perp} [\text{pN}]^{16/7}$ and $t_L^{\parallel} \approx 0.05 \text{ s}/[(f_{\perp} [\text{pN}])(f_{\text{pre}} [\text{pN}]^{5/8})]$ for DNA ($L \approx 20 \mu\text{m}$ [12]) prestretched with $f_{\text{pre}} \ll f_{\perp}$.

TABLE I. Summary of crossover scaling laws for an initially unstretched filament. The crossover time t_f is implicitly defined through $t_f = f_{\parallel}^{-2}(t_f)$, $f_{\parallel}(t)$ is the induced longitudinal force, $\Delta_{\perp}(t)$ is the transverse response, and $\ell_{\perp/\parallel}$ is the transverse/longitudinal correlation length [8,9,13]. (a) Athermal case. f_{\parallel} pulls in the filament’s tails of length L . $t_f = (\gamma_0 f_{\perp})^{-2}$ with $\gamma_0 = (\zeta L)^{2/3} f_{\perp}^{1/3}$. (b) Thermal case. The filament’s tails have effective length $\ell_{\parallel} \ll L$. $t_f = (\gamma f_{\perp})^{-2}$ with $\gamma = (\zeta \ell_p)^{2/7} f_{\perp}^{1/7}$.

(a)	$\ell_{\perp}(t)$	$f_{\parallel}(t)$	$\Delta_{\perp}(t)$	
$t \ll t_f$	$t^{1/4}$	$\zeta L f_{\perp}^2 t^{1/4}$	$f_{\perp} t^{3/4}$	
$t \gg t_f$	$[t f_{\parallel}(t)]^{1/2}$	$(\zeta L)^{2/5} f_{\perp}^{4/5} t^{-1/5}$	$(\zeta L)^{-1/5} (f_{\perp} t)^{3/5}$	
(b)	$\ell_{\perp}(t)$	$\ell_{\parallel}(t)$	$f_{\parallel}(t)$	$\Delta_{\perp}(t)$
$t \ll t_f$	$t^{1/4}$	$(\ell_p/\zeta)^{1/2} t^{1/8}$	$(\zeta \ell_p)^{1/2} f_{\perp}^2 t^{3/8}$	$f_{\perp} t^{3/4}$
$t \gg t_f$	$[t f_{\parallel}(t)]^{1/2}$	$(\ell_p/\zeta)^{1/2} [t f_{\parallel}(t)]^{1/4}$	$(\zeta \ell_p)^{2/9} f_{\perp}^{8/9} t^{-1/9}$	$(\zeta \ell_p)^{-1/9} (f_{\perp} t)^{5/9}$

In order to support and quantify the scaling picture developed above, we proceed with a systematic approach similar to Ref. [13] based on the length scale separation $\ell_{\parallel}(t) \gg \ell_{\perp}(t)$. As long as the dynamics induced by the transverse force is not influenced by end effects ($\ell_{\parallel} \ll L$), we consider a semi-infinite arclength interval, $s \in [0, \infty)$, and represent the transverse force as a *boundary condition* at $s = 0$. In the wormlike chain Hamiltonian, $\mathcal{H} = \frac{1}{2} \times \int ds [\mathbf{r}'^2 + f \mathbf{r}^2]$, the tension $f(s, t)$ enforces the local inextensibility constraint $\mathbf{r}^2(s, t) = 1$. Parametrizing the contour $\mathbf{r}(s, t) = (\mathbf{r}_{\perp}, s - r_{\parallel})^T$ by its transverse and longitudinal displacements from a straight line (see Fig. 1), the weakly-bending limit of small contour gradients $\mathbf{r}'_{\perp} = \mathcal{O}(\varepsilon) \ll 1$ is realized for very stiff polymers ($\varepsilon \equiv L/\ell_p$), alternatively for semiflexible filaments strongly pre-stretched with a force f_{pre} ($\varepsilon \equiv f_{\text{pre}}^{-1/2}/\ell_p$).

The conformational dynamics in solution follows from a balance of elastic and tensile forces $-\delta\mathcal{H}/\delta\mathbf{r}$, thermal noise $\boldsymbol{\xi}$, and anisotropic friction $[\mathbf{r}'\mathbf{r}' + \zeta(1 - \mathbf{r}'\mathbf{r}')] \partial_t \mathbf{r}$ [7]. Within the weakly-bending limit, transverse and longitudinal fluctuations have strongly different correlation lengths: $\ell_{\perp}/\ell_{\parallel} = \mathcal{O}(\varepsilon^{1/2})$; cf. Table I(b). An adiabatic approximation (justified via a multiple scale analysis) exploits this scale separation. The resulting equations of motion [13] are written in terms of formally independent rapidly and slowly varying arclength parameters s and $\bar{s}\varepsilon^{1/2}$, respectively:

$$\partial_t \mathbf{r}_{\perp} = -\partial_s^4 \mathbf{r}_{\perp} + \bar{f} \partial_s^2 \mathbf{r}_{\perp} + \boldsymbol{\xi}_{\perp} + \mathbf{f}_{\perp} \delta(s) \Theta(t), \quad (2a)$$

$$\partial_s^2 \bar{f} = -\zeta \langle \partial_t \bar{\varrho} \rangle. \quad (2b)$$

Equation (2a) gives the small-scale dynamics of the transverse displacements $\mathbf{r}_{\perp}(s, t)$ for *locally constant* tension $f \equiv \bar{f}(\bar{s}, t)$, cf. Eq. (1). Using a Cosine transform with respect to s , it is readily solved by the response function

$$\chi_{\perp}(q; t, t') = e^{-q^2[q^2(t-t') + \int_{t'}^t d\tau \bar{f}(\bar{s}, \tau)]} \Theta(t - t'). \quad (3)$$

Equation (2b) describes the coarse-grained tension variations on the large scale $\bar{s}\varepsilon^{1/2}$: it relates curvature in the tension to (average) changes in stored length density $\langle \bar{\varrho} \rangle \times (\bar{s}, t) \equiv \langle \frac{1}{2} \mathbf{r}'_{\perp}{}^2 \rangle(\bar{s}, t)$. Averaged both thermally and spatially (on the small scale s), $\langle \bar{\varrho} \rangle$ inherits its remaining \bar{s} -dependence from the tension \bar{f} in Eq. (3):

$$\langle \bar{\varrho} \rangle = \left\langle \frac{1}{2} \left[\int_0^{\infty} \frac{dq}{\pi} \int_{-\infty}^t dt' q \chi_{\perp}(q; t, t') \boldsymbol{\xi}_{\perp}(q, t') \right]^2 \right\rangle. \quad (4)$$

Reintroducing a single unique arclength variable, $\bar{s} \equiv s$, Eqs. (2b) and (4) result in a nonlinear partial integro-differential equation (PIDE) for $\bar{f}(s, t)$ that was analyzed in Ref. [13] for explicitly prescribed boundary conditions. In the present case, however, the boundary condition at $s = 0$ has to be determined implicitly. The polymer's inextensibility requires that the bulge be created using stored length from the tails. To formalize this condition, we demand at any time a vanishing average longitudinal ve-

locity $\langle \partial_t r_{\parallel} \rangle$ at the origin where the force is applied, and also at infinity. Inextensibility ($r'_{\parallel} = \frac{1}{2} \mathbf{r}'_{\perp}{}^2 + \mathcal{O}(\varepsilon^2) \approx \varrho$) gives $0 = \int_0^{\infty} ds \langle \partial_t r'_{\parallel} \rangle = \int_0^{\infty} ds \langle \partial_t \varrho \rangle$. With $\partial_s \bar{f}|_{s \rightarrow \infty} = 0$ and Eq. (2b), this constraint implies

$$\partial_s \bar{f}|_{s=0} = -\zeta \int_0^{\infty} ds \partial_t \langle \varrho - \bar{\varrho} \rangle. \quad (5)$$

The difference $\langle \varrho - \bar{\varrho} \rangle$ represents the excess length stored in the bulge on the small length scale ℓ_{\perp} . Consequently, it did not contribute to Eq. (4) which was spatially coarse-grained on intermediate scales $\ell_{\perp} \ll l \ll \ell_{\parallel}$. It can be obtained, though, from the right hand side of Eq. (4) upon replacing $\boldsymbol{\xi}_{\perp} \rightarrow -\mathbf{f}_{\perp} \sin qs \Theta(t)$. Evaluating the s -integral in Eq. (5) to leading order yields our central analytical result—a boundary condition for the tension that quantifies the feedback between “bulge” and “tail” dynamics:

$$\partial_s \bar{f}|_{s=0} = -\frac{\zeta f_{\perp}^2}{4} \int_0^{\infty} \frac{dq}{\pi} \partial_t \left[\int_0^t dt' q \chi_{\perp}(q; t, t') \right]_{s=0}^2. \quad (6)$$

In terms of the response function $\chi_{\perp}(q; t, t')$ of Eq. (3), the average displacement $\Delta_{\perp}(t)$ induced by the transverse force (i.e., the nonlinear response) reads

$$\Delta_{\perp}(t) = f_{\perp} \int_0^{\infty} \frac{dq}{\pi} \int_0^t dt' \chi_{\perp}(q; t, t')|_{s=0}, \quad (7)$$

which is evaluated at $s = 0$ after the tension profiles $\bar{f}(s, t)$ are computed from Eqs. (2b), (4), and (6). To this end, we introduce two-variable scaling forms [13] that remove any parameter dependence: $\bar{f}(s, t) = \gamma f_{\perp} \varphi(s/s_f, t/t_f)$, with the crossover scales t_f and s_f and γ as in Fig. 2. Numerical solutions are obtained by mapping the PIDE onto a system of nonlinear equations [17]. Selected tension profiles are displayed in Fig. 2 and describe one half of

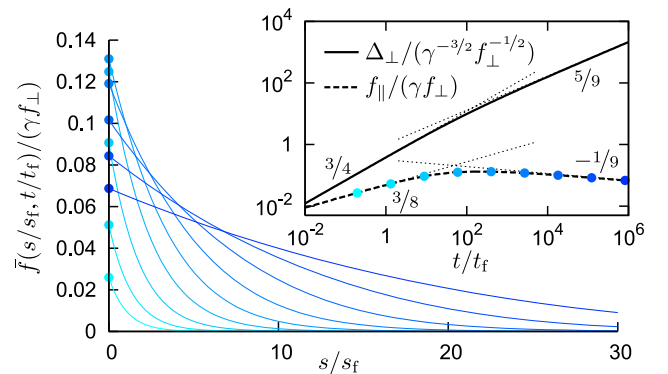


FIG. 2 (color online). Numerical solutions $\bar{f}(s, t)$ to Eqs. (2b), (4), and (6) for $f_{\text{pre}} = 0$, time is increasing from light to dark color. Inset: log-log plot of the effective longitudinal force $f_{\parallel}(t) = \bar{f}(0, t)$ (dashed line with circles), and of the nonlinear response $\Delta_{\perp}(t)$ from Eq. (7) (solid line). Dotted lines indicate the asymptotes of Table I(b). The crossover scales are $t_f = (\gamma f_{\perp})^{-2}$ and $s_f = (\ell_p/\zeta)^{1/2} (\gamma f_{\perp})^{-1/4}$, with $\gamma = (\zeta \ell_p)^{2/7} f_{\perp}^{1/7}$.

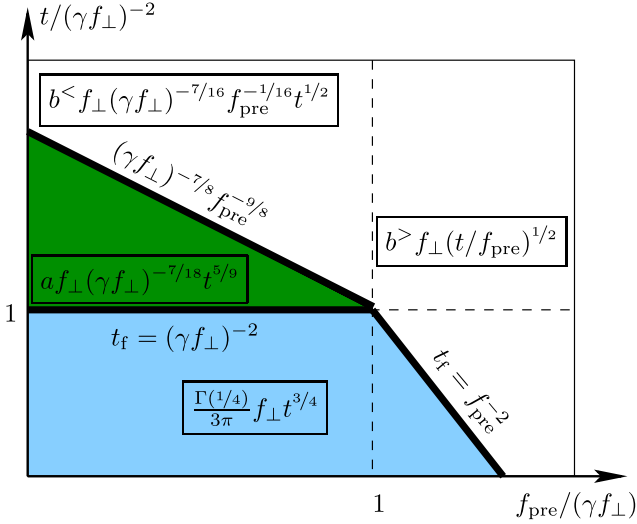


FIG. 3 (color online). Regimes of intermediate asymptotics (separated by thick black lines) for the nonlinear response $\Delta_{\perp}(t)$ (boxed formulas); time $t/(\gamma f_{\perp})^{-2}$ vs. force ratio $f_{\text{pre}}/(\gamma f_{\perp})$ (log-log scale). The universal initial regime [5] (light shaded) is followed by a quasistatic regime (white) with different force scaling for asymptotically small ($<$) and large ($>$) [5] force ratio; in these limits, the respective prefactors are $b^{<} \sim [8(1 + \sqrt{2})^2/\pi^3]^{1/8}$ and $b^{>} \sim \pi^{-1/2}$. An intermediate taut-string regime (dark shaded) emerges for very small force ratio. The prefactor is $a = [3(2 + \sqrt{2})/\pi^2]^{2/9}$ if $f_{\text{pre}} = 0$.

the filament with f_{\perp} being applied at the origin. Our analytical approach is based on reducing the scaling forms $\varphi(s/s_f, t/t_f)$ to one-variable scaling functions $\varphi \sim (t/t_f)^{\alpha} \hat{\varphi}[s/\ell_{\parallel}(t)]$ with $\ell_{\parallel}(t) = s_f(t/t_f)^z$ in the asymptotic limits of short and long times. In the latter limit $t \gg t_f$, we recover either the taut-string approximation of Ref. [8] and may neglect bending and thermal forces, or the quasistatic approximation of Ref. [10], which lets us treat the tension as locally equilibrated. Which approximation is valid depends quite strongly on the prestretching force f_{pre} through the ratio $f_{\text{pre}}/(\gamma f_{\perp})$, similar to the related scenario of longitudinal stretching forces applied to prestretched filaments [17]. The resulting intermediate asymptotic scaling laws for $\Delta_{\perp}(t)$ are summarized in Fig. 3, including analytical prefactors. For a given ratio $f_{\text{pre}}/(\gamma f_{\perp})$, the evolution of $\Delta_{\perp}(t)$ corresponds to a vertical path through Fig. 3. The exact solutions quickly converge to these asymptotes, as shown in the inset of Fig. 2 for the limiting case $f_{\text{pre}} = 0$.

In summary, we argue that the coupling between transverse and longitudinal response affects not only single polymers, but also single crosslinks, crosslinked networks, and tensegrity structures [3,9,11,18]. For completeness, we note that our self-consistent approach both for the heuristic bulge idea as well as for the systematic derivation of Eq. (6) applies only to the *nonlinear* [13] response on sufficiently small times $t \ll t_L^{\parallel}$, t_c . At t_L^{\parallel} , end effects become important, and at t_c , the weakly-bending assumption

breaks down: the contour gradients become large when $\Delta_{\perp} \approx \ell_{\perp}$. We find that $t_c \geq t_L^{\parallel}$ for initially weakly-bending filaments (as those in the above discussed situations) [19]. Our analysis of the generic coupling mechanism is not constrained by the details of the relaxation regime $t \gg t_L^{\parallel}$ (which is similar to the athermal case).

We thank K. Kroy, E. Frey, T. Munk, and C. Heussinger for helpful discussions. O.H. acknowledges financial support by the German Academic Exchange Program (DAAD) and by the Deutsche Forschungsgemeinschaft (DFG) through Grant No. Ha 5163/1. B.O. is supported by the DFG through SFB 486, by the German Excellence Initiative via the program ‘‘Nanosystems Initiative Munich (NIM),’’ and through BayEFG.

*obermayer@physik.lmu.de

†ohallats@physics.harvard.edu

- [1] F. C. MacKintosh, J. Käs, and P. A. Janmey, Phys. Rev. Lett. **75**, 4425 (1995); K. Kroy and E. Frey, Phys. Rev. Lett. **77**, 306 (1996); G. Lattanzi, T. Munk, and E. Frey, Phys. Rev. E **69**, 021801 (2004).
- [2] F. Gittes and F. C. MacKintosh, Phys. Rev. E **58**, R1241 (1998).
- [3] D. C. Morse, Phys. Rev. E **58**, R1237 (1998).
- [4] L. LeGoff, O. Hallatschek, E. Frey, and F. Amblard, Phys. Rev. Lett. **89**, 258101 (2002).
- [5] R. Granek, J. Phys. I (France) **7**, 1761 (1997).
- [6] F. Amblard *et al.*, Phys. Rev. Lett. **77**, 4470 (1996).
- [7] C. H. Wiggins, D. Riveline, A. Ott, and R. E. Goldstein, Biophys. J. **74**, 1043 (1998).
- [8] U. Seifert, W. Wintz, and P. Nelson, Phys. Rev. Lett. **77**, 5389 (1996).
- [9] R. Everaers, F. Jülicher, A. Ajdari, and A. C. Maggs, Phys. Rev. Lett. **82**, 3717 (1999).
- [10] F. Brochard-Wyart, A. Buguin, and P. G. de Gennes, Europhys. Lett. **47**, 171 (1999).
- [11] M. L. Gardel *et al.*, Proc. Natl. Acad. Sci. U.S.A. **103**, 1762 (2006).
- [12] Y. Bohbot-Raviv *et al.*, Phys. Rev. Lett. **92**, 098101 (2004).
- [13] O. Hallatschek, E. Frey, and K. Kroy, Phys. Rev. Lett. **94**, 077804 (2005); Phys. Rev. E **75**, 031905 (2007); **75**, 031906 (2007).
- [14] Since the weakly-bending assumption still holds at $t = t_f$, longitudinal friction is the only relevant nonlinearity, and higher-order terms $\propto r_{\perp}^3$ in Eq. (2a) are negligible.
- [15] F. Pampaloni *et al.*, Proc. Natl. Acad. Sci. U.S.A. **103**, 10248 (2006).
- [16] M. J. Tyska and D. M. Warshaw, Cell Motil. Cytoskeleton **51**, 1 (2002).
- [17] B. Obermayer, O. Hallatschek, E. Frey, and K. Kroy, Eur. Phys. J. E (to be published).
- [18] D. E. Ingber, J. Cell Sci. **116**, 1157 (2003).
- [19] $t_c \approx (\ell_p/L)^9 t_L^{\parallel}$ if $f_{\perp} \gg \ell_p^{-2}$ and $f_{\text{pre}} \leq \ell_p^{-2}$; otherwise, $t_c \gg t_L^{\parallel}$. For $f_{\perp} \gg \ell_p^{3/2}/L^{7/2}$ ($f_{\text{pre}} \gg \ell_p^2/L^4$), t_L^{\parallel} falls into the taut-string (quasistatic) regime (cf. Figure 3).

Freely relaxing polymers remember how they were straightened

Benedikt Obermayer,¹ Wolfram Möbius,^{1,2} Oskar Hallatschek,³ Erwin Frey,^{1,*} and Klaus Kroy^{4,†}

¹Arnold Sommerfeld Center and Center of NanoScience, Ludwig-Maximilians-Universität München, Theresienstrasse 37, 80333 München, Germany

²Institut für Theoretische Physik, Universität zu Köln, Zùlpicher Strasse 77, 50937 Köln, Germany

³Max Planck Institute for Dynamics and Self-Organization, 37073 Göttingen, Germany

⁴Institut für Theoretische Physik, Universität Leipzig, Postfach 100920, 04009 Leipzig, Germany

(Received 11 June 2008; revised manuscript received 15 December 2008; published 26 February 2009)

The relaxation of initially straight semiflexible polymers has been discussed mainly with respect to the longest relaxation time. The biologically relevant nonequilibrium dynamics on shorter times is comparatively poorly understood, partly because “initially straight” can be realized in manifold ways. Combining Brownian dynamics simulations and systematic theory, we demonstrate how different experimental preparations give rise to specific short-time and universal long-time dynamics. We also discuss boundary effects and the onset of the stretch-coil transition.

DOI: 10.1103/PhysRevE.79.021804

PACS number(s): 82.35.Pq, 87.15.H–, 87.15.ap

I. INTRODUCTION

The mechanical properties of semiflexible polymers, which form an integral part of the cell structure, are of high relevance to the understanding of cell elasticity and motility [1,2]. External stress not only remarkably changes static and dynamic features [3–5], but has also important biological implications, e.g., for enzyme activity on DNA [6–8]. Particularly intriguing aspects of stress-controlled behavior can be observed for the relaxation of semiflexible filaments from initially nearly straight (i.e., highly stressed) conformations. In recent years, many experimental and theoretical studies have addressed this paradigmatic problem of polymer rheology (see, e.g., Refs. [9–28]), often primarily focused on the influence of hydrodynamic interactions on the longest relaxation time t_R , which is a key identifier of the stretch-coil transition. However, on much shorter times the polymer dynamics is predominantly controlled by the highly nontrivial *internal* conformational relaxation [29,30], which plays a relevant role in many biological situations ranging from the viscoelastic response of polymer networks [31] to molecular motor kinetics [32] and DNA supercoiling dynamics [27,33]. This aspect of the relaxation is still poorly understood, the more so as standard analytical techniques based on linearized equations of motion fail due to inherent nonlinearities initiated by strong perturbations [34,35]. Further, because a *completely* straightened polymer conformation can in practice not be realized in the presence of thermal noise from the environment, the short-time dynamics of an initially “nearly” straight filament will reflect the way it was straightened: filaments can be stretched by optical tweezers [20,26], by electric fields [13,17,18,23,36], or by flows of different geometry [9,11,13,16,19,22,28,37], but a straightened contour can also result from low initial temperatures. In any case the relaxation dynamics is driven exclusively by stochastic forces. This raises the question how results obtained with different

setups should be compared and when the dependence on initial conditions fades out.

In the following, we present results from computer simulations combined with a thorough and exhaustive theoretical analysis to explain how fundamental differences in the short-time relaxation emerge from different experimental preparation methods but give way to universal long-time relaxation. Four idealized initial conditions (see Fig. 1) are shown to lead to qualitatively distinct behavior despite superficial similarities. “Force” refers to mechanical stretching, i.e., a strong external stretching force f_{pre} that is suddenly removed on both ends, for instance, in a setup using λ -DNA, optical tweezers, and restriction enzymes [8]. Second, the term “field” is used for experiments employing an electric field [17] of strength E for stretching, where one end is always kept fixed. Once switched off, such fields give rise to relaxation dynamics similar to the one in setups using homogeneous elongational flows [9] of velocity v . Further, we denote by “shear” the stretching by planar extensional shear flows of shear rate $\dot{\gamma}$ in a symmetric geometry [19,22], see Fig. 1(c). Finally, “quench” refers to a scenario where the

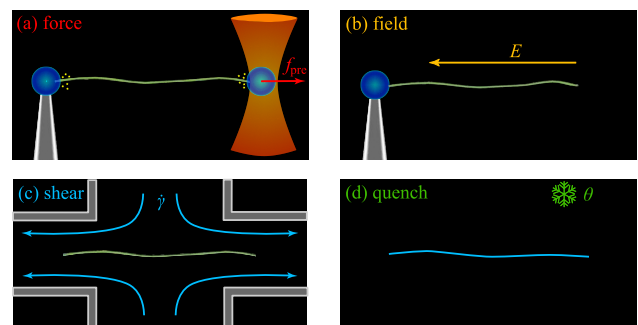


FIG. 1. (Color online) In the “force” scenario (a), a stretching force f_{pre} is suddenly removed at both ends. In the “field” setup (b), one end is held fixed and the electric field of strength E (or homogeneous elongational flow of velocity v) is switched off, similar to the “shear” case (c) with a symmetric extensional shear flow of shear rate $\dot{\gamma}$. In the “quench” experiment (d), the temperature is suddenly increased by a large factor θ from an initially small value.

*frey@physik.lmu.de

†kroy@itp.uni-leipzig.de

temperature is suddenly increased by a large factor θ from a small value T/θ near zero to its final value T . This setup is more feasible for computer simulations, but the equivalent sudden drop in persistence length ℓ_p might be experimentally realizable by chemical reactions.

The paper is organized as follows. In Sec. II, we show results from Brownian dynamics simulations for each of the four different setups. Section III presents a qualitative discussion of the underlying theoretical model, resulting in scaling laws for pertinent observables which readily suggest intuitive explanations for the qualitative differences between the scenarios and their universal long-time asymptote. A detailed and somewhat technical derivation of these asymptotic scaling laws is contained in Sec. IV, where we also analyze the effect of different boundary conditions. In Sec. V, we present a quantitative comparison between simulation results and theory. At the end of the paper, we discuss experimental implications including quantitative estimates of control parameters in typical realizations, the onset of the stretch-coil transition, and the influence of hydrodynamic interactions.

II. SIMULATION RESULTS

In the Brownian dynamics simulation, we employ the standard free-draining bead-spring algorithm for wormlike chains, where different environmental conditions during equilibration of the chains correspond to the four scenarios introduced above. The equations of motion for a chain of total length $L=Nb$ with $N+1$ beads of size b and mobility μ are given by

$$\partial_t \mathbf{r}_i - \mathbf{v}_i = -\mu \nabla_i U + \boldsymbol{\eta}_i(t), \quad (1)$$

where the potential $U=U_s+U_b+U_f$ contains a stretching part

$$U_s = \frac{k_B T \gamma_s}{2b} \sum_i (|\mathbf{r}_{i+1} - \mathbf{r}_i| - b)^2, \quad (2)$$

a bending part

$$U_b = \frac{k_B T \ell_p}{b} \sum_i (1 - \mathbf{t}_{i+1} \cdot \mathbf{t}_i), \quad (3)$$

and an external potential U_f . Here, ℓ_p is the persistence length, $\mathbf{t}_i = \frac{\mathbf{r}_i - \mathbf{r}_{i-1}}{|\mathbf{r}_i - \mathbf{r}_{i-1}|}$ is a normalized tangent vector, and γ_s is the stretching elastic constant, which is chosen such as to avoid visible artifacts from backbone stretching in our simulation results. We use Gaussian noise with strength $\langle \boldsymbol{\eta}_i(t) \boldsymbol{\eta}_j(t') \rangle = 6\mu k_B T \delta_{ij} \delta(t-t')$. The time step is $10^{-5} \tau_0$, where $\tau_0 = b^2 / (k_B T \mu)$ is the self-diffusion time of the beads. The chains are equilibrated along the x axis symmetrically to the origin under the respective stretching mechanism. In the force case, $U_f = -f_{\text{pre}}(x_N - x_0)$ and $\mathbf{v}_i = 0$, while $U_f = 0$ and $\mathbf{v}_i = (v, 0, 0)^T$ for field setups. For shear, we take $\mathbf{v}_i = \dot{\gamma}(x_i, -y_i, -z_i)^T$, and in order to prevent the polymer from diffusing out of the stagnation point, an additional harmonic potential $U_f = \frac{1}{2} \dot{\gamma} \mu^{-1} x_{\text{COM}}^2$ drives the center-of-mass coordinate x_{COM} back to the origin (cf. the feedback control system in Ref. [19]). In these scenarios, we equilibrate for 10^4 time steps, while initial conformations are generated directly us-

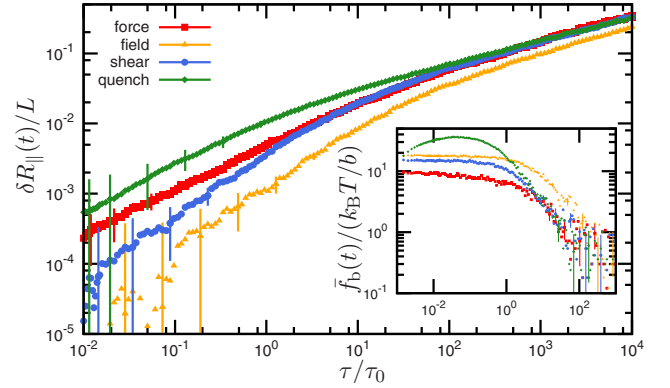


FIG. 2. (Color online) Quantitative results: change in projected length $\delta R_{\parallel}(t)$ and mean bulk tension $\bar{f}_b(t)$ (inset) for computer simulations of a force (squares), field (triangles), shear (circles), and quench (diamonds) scenario, respectively. Simulation parameters were $L=200b$, $\ell_p=40b$, $\gamma_s=6000/b$, $f_{\text{pre}}=10k_B T/b$, $v=0.18b/\tau_0$, $\dot{\gamma}=0.0046/\tau_0$, and $\theta=35.7$, such that $R_{\parallel}(0) \approx 0.97L$ in all cases.

ing the equilibrium tangent correlations in the quench case. In all cases, $U_f=0$ and $\mathbf{v}_i=0$ upon release. Ensemble averages were taken over 150 realizations.

To characterize the relaxation dynamics, we concentrate on two observables. One is the time-dependent change $\delta R_{\parallel}(t) = R_{\parallel}(0) - R_{\parallel}(t)$ in the ensemble average of the filament's end-to-end distance R_{\parallel} , projected onto the initial longitudinal axis. Note that with this definition, δR_{\parallel} is positive and increasing, while the actual end-to-end distance shrinks during relaxation. The second observable is the mean tension $\bar{f}_b(t)$ in the filament, proportional to the bulk stress $\sigma(t)$ in a polymer solution. Figure 2 shows simulation results for $\delta R_{\parallel}(t)$, measured from the projection on the initial longitudinal axis, and for $\bar{f}_b(t)$ (proportional to the sum of the spring displacements from their equilibrium position). Parameter values are given in the caption of Fig. 2 and were chosen such that the initial extension is close to full stretching [$R_{\parallel}(0) \approx 0.97L$ in all cases]. While the universal scaling for longer times is evident (the apparent systematic offset in the field case arises simply because there is only one free end), substantial differences between the scenarios for shorter times are clearly observable as well.

III. QUALITATIVE THEORETICAL RESULTS

From Fig. 2 it is obvious that the time evolution of $\delta R_{\parallel}(t)$ and $\bar{f}_b(t)$ does not obey simple power-law scaling. Simplifying approaches based on scaling arguments [10,17], elastic dumbbell models [16,22], or quasiequilibrium approximations [14,27] have sometimes been used successfully for specific situations and parameter ranges. In contrast, we employ a systematic formalism [35] based on the wormlike chain model, which allows one to generally account for the complex dynamics resulting from different environmental perturbations. Here, we first present qualitative results for all four scenarios in order to illustrate their differences and discuss exact analytical and numerical results in the next section.

In the wormlike chain model [38], semiflexible polymers are represented as inextensible smooth space curves $\mathbf{r}(s, t)$ of length L . Bending energy is proportional to the squared local curvature $(\partial_s^2 \mathbf{r})^2$, such that in equilibrium, tangent orientations are correlated over the persistence length $\ell_p = \kappa/k_B T$, where κ is the bending rigidity. The initially straight polymer is supposed to be equilibrated at times $t < 0$ and released at $t = 0$. After that, the longitudinal contraction is driven energetically uphill via the creation of contour undulations by entropic forces. Considering the conservation of contour length due to the (near) inextensibility of the backbone bonds, these transverse wrinkles are conveniently referred to in terms of their excess contour length, or *stored length*, with an associated line density ϱ . Mathematically, the inextensibility is enforced by the *backbone tension* f which counteracts stretching, and the creation of stored length is accompanied by the relaxation of tension. The theory of Refs. [35,39] relates the tension $f(s, t)$ to the stored length density $\varrho(s, t)$, based on the *weakly bending* limit of small contour deviations from a straight line. In practice, this can easily be realized by choosing the control parameters f_{pre} , E or v , or γ sufficiently strong (as in typical experiments), or the quenching factor θ sufficiently large. It also justifies the free-draining approximation, where hydrodynamic effects are captured by anisotropic local friction coefficients $\zeta_{\perp, \parallel}$ (per length) for transverse and longitudinal friction, respectively [40]. However, ordinary perturbation theory is applicable only for late times $t \gg t_* \approx \zeta_{\parallel} L^3 / (k_B T \ell_p^5)$ [35], because to lowest order it allows only a linear spatial dependence of ϱ and f and neglects longitudinal friction forces [34]. Further, except for quite stiff filaments with $\ell_p \geq L$, the time t_* is usually larger than the filament's longest relaxation time $t_R \approx \zeta_{\parallel} \ell_p L^2 / k_B T$ [41], which within our approximations is given by the Rouse time of a polymer with Kuhn length $2\ell_p$. Nevertheless, with an improved formalism [35,39] including nontrivial spatial variations in f and ϱ , the conformational relaxation at times $t \ll t_R$ can be analyzed even for quite flexible polymers. This leads to the remarkable insight that weakly bending polymers constitute self-averaging systems: the small stochastic fluctuations average out along the contour and the coarse-grained tension dynamics follows from the deterministic relation

$$\partial_s^2 \bar{f} = -\zeta_{\parallel} \partial_s \langle \bar{\varrho} \rangle, \quad (4)$$

where the overbar denotes a (local) spatial average that produces effectively an ensemble average (denoted by $\langle \cdot \rangle$) [39]. Driven by tension gradients, stored length propagates subdiffusively from the filament's ends into the bulk—limited to boundary layers of size $\ell_{\parallel}(t)$ by longitudinal solvent friction. In more intuitive terms, the filament starts to “coil up” first at the boundaries, and only later in the bulk, see also Fig. 3.

In general, $\langle \bar{\varrho} \rangle$ is a nonlinear functional of \bar{f} , see Eq. (10) below for a detailed expression. Exact analytical results for the boundary layer size $\ell_{\parallel}(t)$, the bulk tension $\bar{f}_b(t)$, and the change in projected length $\delta R_{\parallel}(t)$ will be obtained as leading-order results of a systematic asymptotic expansion of Eq. (4) in the next section. However, the *scaling* of the dominant part $\delta \bar{R}_{\parallel}(t)$ of $\delta R_{\parallel}(t)$, which is independent of boundary con-

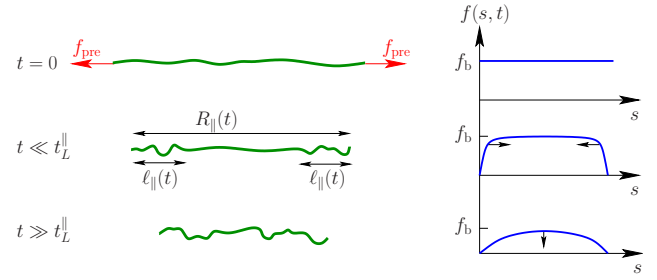


FIG. 3. (Color online) Schematic representation of conformational (left) and tension relaxation (right) in a force setup. For $t = 0$, the filament is equilibrated under the force f_{pre} . As the ends are released, the contour coils up in two growing boundary layers of size $\ell_{\parallel}(t)$ where the tension relaxes. At $t = t_L^{\parallel}$, the dynamics crosses over from the propagation to the relaxation regime and the tension relaxes to zero.

ditions and an effectively deterministic quantity, can be found from a simple dimensional argument: the change in end-to-end distance equals the amount of stored length $\varrho \ell_{\parallel}$ that has been created in the boundary layer. On the scaling level, Eq. (4) reads $\bar{f}_b / \ell_{\parallel}^2 \approx \zeta_{\parallel} \varrho / t$, and we obtain

$$\delta \bar{R}_{\parallel} \approx \frac{t \bar{f}_b}{\zeta_{\parallel} \ell_{\parallel}}. \quad (5)$$

Note that the change $\delta R_G(t)$ in the gyration tensor's largest eigenvalue, which is frequently identified with δR_{\parallel} [21,42], obeys a different scaling law $\delta R_G \approx t \bar{f}_b / (\zeta_{\parallel} L)$ for short times $t \ll t_L^{\parallel}$ [43]. Additional subdominant contributions to $\delta R_{\parallel}(t)$ from end fluctuations will be analyzed in Sec. IV.

Figure 4 summarizes the scaling results of Sec. IV for $\ell_{\parallel}(t)$, $\bar{f}_b(t)$, and $\delta \bar{R}_{\parallel}(t)$ in various intermediate asymptotic regimes, which are separated by different crossover times that have been matched by an appropriate choice of the respective control parameters for better comparison. Clearly, the time $t_L^{\parallel} = \zeta_{\parallel} L^2 [k_B T / (\ell_p f_{\text{pre}}^3)]^{1/2}$ is of key importance since it separates scenario-specific and universal relaxation. To understand the origin of the differences for times $t \ll t_L^{\parallel}$, we will consider the different scenarios separately before we address the universal regime $t \gg t_L^{\parallel}$.

(a) *Force setup.* After the stretching force has been shut off, the polymer starts to build up contour undulations driven by thermal noise. These transverse undulations appear first in growing boundary layers of size $\ell_{\parallel}(t) \ll L$ near the ends: assuming an inextensible backbone, the immediate creation of undulations in the bulk would require the ends to be pulled inwards against longitudinal solvent friction with a force exceeding the actual backbone tension. This phenomenon of *tension propagation* ends after a time t_L^{\parallel} , defined via $\ell_{\parallel}(t_L^{\parallel}) = L$, where the boundary layers extend over the whole polymer length, see Fig. 3. A more detailed analysis [35] shows that the longitudinal relaxation depends on whether the internal tension (initially equal to the stretching force f_{pre}) represents a relevant perturbation to the transverse conformational dynamics. The latter undergoes a dynamic crossover from a bending-dominated regime with $\ell_{\parallel} \propto t^{1/8}$ [44] for the shortest times $t \ll t_f$ to a tension-driven regime with $\ell_{\parallel} \propto t^{1/2}$ [14] for

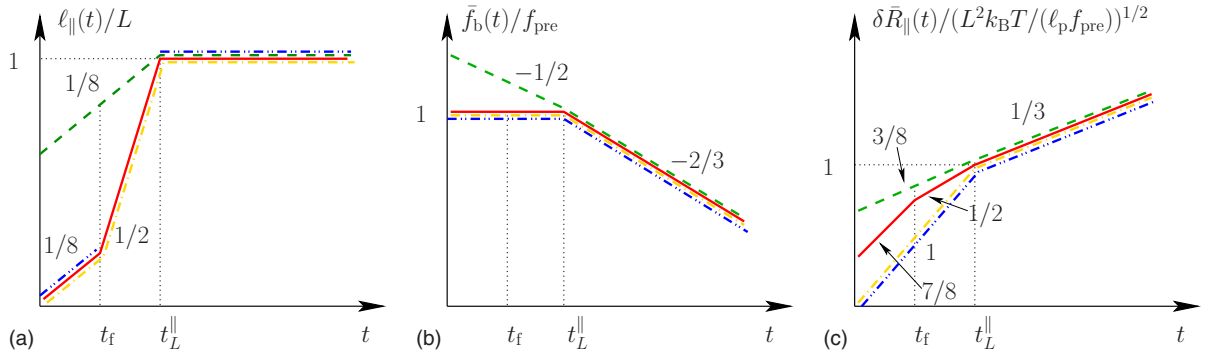


FIG. 4. (Color online) Qualitative results. Asymptotic scaling laws for the boundary layer size $\ell_p(t)$ (a), the mean bulk tension $\bar{f}_b(t)$ or the bulk stress (b), and for the change in projected length $\delta\bar{R}_{\parallel}(t)$ (c) in force (solid line), field (dot-dashed line), shear (dot-dot-dashed line), or quench (dashed line) setups, respectively.

longer times $t \gg t_f$, where the dynamics becomes inherently nonlinear. Here, $t_f = \zeta_{\perp} k_B T \ell_p / f_{\text{pre}}^2$ is a crossover time that obeys $t_f \ll t_L^{\parallel}$ for reasonably large prestress f_{pre} .

(b) *Field and shear setup.* Similarly, one can define a force equivalent in field or shear experiments and corresponding expressions for t_f and t_L^{\parallel} : the hydrodynamic equivalent of f_{pre} is simply the total Stokes friction $\zeta_{\parallel} \nu L$ in a homogeneous flow, and $\zeta_{\parallel} \dot{\gamma} L^2$ is the longitudinal friction in an extensional shear flow. Flow conditions may straightforwardly be recast into the equivalent language of external (e.g., electrical) fields. However, complicated counterion effects [45–47] prevent the quantitative prediction of the equivalent electrophoretic field strength E for typical experimental realizations. Although field-type perturbations induce dynamic crossovers at t_f similar to the force case, the change $\delta\bar{R}_{\parallel}(t)$ in projected length increases always linearly with time. This can be understood by a simple change in perspective: the polymer’s ends are pulled inwards by an approximately constant bulk tension, i.e., with roughly constant velocity. This corresponds in the frame of reference of the ends to an external *flow* field. The resulting friction forces are properly balanced and the initial polymer conformations are already equilibrated under such a flow field in field and shear setups, in contrast to the force scenario. Tension propagation is therefore not a dominant effect in the former [Eq. (5) applies with $\ell_{\parallel} \equiv L$ because of the large-scale spatial variation of the tension], and the constant drag gives $\delta\bar{R}_{\parallel} \propto t$.

(c) *Quench setup.* Here, finally, there is no external force scale and therefore no dynamic crossover ($\ell_{\parallel} \propto t^{1/8}$ for $t \ll t_L^{\parallel}$), although the parameter combination $k_B T \ell_p^3 \theta^4 / L^4$ plays the role of f_{pre} in the crossover time t_L^{\parallel} . The tension in a quenched filament is produced solely by the suddenly increased thermal noise from the environment (if the external temperature increases), or by the suddenly higher “sensitivity” to this noise (if the quenching is achieved by a sudden drop in bending rigidity). Hence its magnitude depends on the “mismatch” between the current conformation and an equilibrium conformation corresponding to the current environment. Therefore the quenched filament can relax tension *even in the bulk* by reshuffling stored length between long and short wavelength modes in a way similar to the mechanical stress relaxation in buckled rods [43], while the bulk

tension stays constant for $t \ll t_L^{\parallel}$ in the other setups.

(d) *Universal regime.* At long times $t \gg t_L^{\parallel}$, when the tension has propagated through the filament, the dynamics enters the universal regime of homogeneous tension relaxation [35]. Contrary to previous assumptions [20], longitudinal friction may not generally be neglected, but dominates the dynamics in this regime. The tension has a nontrivial spatial dependence, but it can for asymptotically large forces be treated as quasistatically equilibrated [14,35]. The characteristic universality of the long-time relaxation is then simply a consequence of the right-hand side of Eq. (4) being independent of initial conditions: $\bar{\varrho} \approx [k_B T / (4\ell_p \bar{f})]^{1/2}$, where we have used the (static) force-extension relation for wormlike chains [48]. This asymptote readily implies by Eq. (4) the scaling $\bar{f} \propto t^{-2/3}$ and by Eq. (5) the characteristic $t^{1/3}$ growth of $\delta\bar{R}_{\parallel}(t)$, which has indeed been observed in experiments [22]. As an aside, we note that $t_{\star} < t_R$ for stiff polymers with $L \lesssim \ell_p$; the adjoining regime of algebraic relaxation for times $t_{\star} \ll t$ shows a $t^{1/4}$ scaling in $\delta\bar{R}_{\parallel}(t)$ [35,49].

Let us finally comment on the joint limiting scenario: the *exactly* straight initial conformation (as in Ref. [21]). Not only it is quite artificial from a theoretical and experimental perspective, it also appears to be ambiguous, since we could let $f_{\text{pre}} \rightarrow \infty$ in one of the scenarios involving external forces as well as $\theta \rightarrow \infty$ for the quench case. Although $t_L^{\parallel} \rightarrow 0$ in both cases, so that only the universal regime survives and the ambiguity is limited to $t=0$, it gives rise to observable effects as soon as one takes into account some microstructure corrections important for real experimental systems and simulation models [50].

After this qualitative discussion of the relaxation dynamics, we will now present a systematic derivation and analysis of Eq. (4), resulting in exact growth laws in various intermediate asymptotic regimes for the observables introduced above. While Ref. [41] only covered the force case, we now obtain results for the other scenarios as well, and include a quantitative analysis of different boundary conditions.

IV. QUANTITATIVE THEORETICAL RESULTS

The starting point for our calculations is the wormlike-chain Hamiltonian

$$\mathcal{H} = \frac{1}{2} \int_0^L ds [\kappa r'^2 + f r'^2], \quad (6)$$

where the backbone tension $f(s, t)$, a Lagrange multiplier function [51], takes care of the local inextensibility constraint $r'(s)^2 = 1$. The equations of motion for the contour result from balancing elastic forces $-\partial\mathcal{H}/\partial\mathbf{r}$ with stochastic noise ξ and anisotropic viscous local friction forces $\zeta[\partial\mathbf{r} - \mathbf{u}]$ with friction matrix $\zeta = [\zeta_\perp \mathbf{r}' \mathbf{r}' + \zeta_\parallel (1 - \mathbf{r}' \mathbf{r}')]^T$ and a velocity field \mathbf{u} of the solvent. The friction coefficients (per length) are $\zeta_\parallel = \hat{\zeta} \zeta_\perp$ with $\hat{\zeta} \approx 1/2$ and $\zeta_\perp \approx 4\pi\eta/\ln(L/a)$ [40], where a is the backbone thickness. Note that the absence of hydrodynamic interactions in our free-draining simulations results in effectively isotropic friction, and we will use $\hat{\zeta} = 1$ in Sec. V when comparing to simulation data. In all of this section, we set $\zeta_\perp = \kappa = 1$ for simplicity, keeping $\kappa = k_B T \ell_p$ constant in the quench scenario. This makes time a length⁴ and the tension a length⁻². Our approach exploits the weakly bending limit. Parametrizing the contour $\mathbf{r} = (\mathbf{r}_\perp, s - r_\parallel)^T$ in terms of small transverse and longitudinal displacements from the straight ground state, this means that $r'^2 = \mathcal{O}(\varepsilon) \ll 1$, with $\varepsilon = f_{\text{pre}}^{-1/2} / \ell_p$ for force setups (and f_{pre} replaced by its equivalents in field or shear scenarios) and $\varepsilon = L / (\theta \ell_p)$ for quench setups, respectively. Up to order ε , the equations of motion for the contour in absence of external forces and for $\mathbf{u} = 0$ read

$$\partial_t \mathbf{r}_\perp = -\mathbf{r}_\perp'''' + (f \mathbf{r}'_\perp)' + \xi_\perp, \quad (7a)$$

$$\hat{\zeta} \partial_t r_\parallel + (1 - \hat{\zeta}) \mathbf{r}'_\perp \partial_t \mathbf{r}_\perp = -r_\parallel'''' - f' + (f r'_\parallel)' + \xi_\parallel. \quad (7b)$$

Because in the weakly bending limit the transverse contour fluctuations are correlated on much shorter length scales than the longitudinal (=tension) dynamics, we can formally introduce “fast” and “slow” arclength coordinates for the small-scale transverse and large-scale longitudinal dynamics, respectively [39]. Taking a local (with respect to ℓ_\parallel) spatial average over the small-scale fluctuations (denoted by an overbar) leads to closed equations:

$$\partial_t \bar{\mathbf{r}}_\perp = -\bar{\mathbf{r}}_\perp'''' + \bar{f} \bar{\mathbf{r}}'_\perp + \bar{\xi}_\perp, \quad (8a)$$

$$\partial_s^2 \bar{f} = -\hat{\zeta} \partial_t \langle \bar{\varrho} \rangle. \quad (8b)$$

The longitudinal part Eq. (8b), where $\varrho = \frac{1}{2} r_\perp'^2$ is the stored length density, follows from the self-averaging property of weakly bending polymers: the spatial coarse graining effectively generates an ensemble average. The transverse part Eq. (8a) contains a locally constant tension \bar{f} [its slow arclength dependence obtained through Eq. (8b) is adiabatically inherited], and can be solved in terms of appropriate eigenmodes $w_q(s)$ with eigenvalue $-q^2[q^2 + f(t)]$ via the response function

$$\chi_\perp(q; t, t') = e^{-2q^2[q^2(t-t') + \int_{t'}^t d\tau f(\tau)]}. \quad (9)$$

Using the noise correlation $\langle \xi_\perp(k, t) \xi_\perp(q, t') \rangle = 4\ell_p^{-1} \delta_{k,q} \delta(t - t')$, we evaluate the expectation value $\langle \frac{1}{2} r_\perp'^2 \rangle$. The different preparation mechanisms discussed in the main text constrain

the polymer only for $t < 0$. Including the initial conditions $\bar{f}(s, t < 0) = \bar{f}_0(s)$ and $\ell_p(t > 0) \equiv \ell_p = \ell_p(t < 0) / \theta$ gives for the stored length density

$$\langle \varrho \rangle = \frac{1}{\ell_p} \sum_q \left[\frac{\chi_\perp^2(q; t, 0)}{q^2 \theta [q^2 + \bar{f}_0(s)]} + 2 \int_0^t dt' \chi_\perp^2(q; t, t') \right] w_q'^2(s). \quad (10)$$

As only the spatially averaged stored length density $\langle \bar{\varrho} \rangle$ enters Eq. (8b), we decompose $w_q'^2(s)$ into a spatially constant and a fluctuating part $c_q(s)$ (the latter will average out upon coarse graining):

$$w_q'^2(s) = \frac{q^2}{L} [1 + c_q(s)]. \quad (11)$$

Taking the continuum limit $L \rightarrow \infty$ and integrating Eq. (8b) over time, we find that the integrated tension $\bar{F}(s, t) = \int_0^t dt' \bar{f}(s, t')$ obeys the partial integrodifferential equation

$$\partial_s^2 \bar{F}(s, t) = \hat{\zeta} \int_0^\infty \frac{dq}{\pi \ell_p} \left[\frac{1 - \chi_\perp^2(q; t, 0)}{\theta [q^2 + \bar{f}_0(s)]} - 2q^2 \int_0^t dt' \chi_\perp^2(q; t, t') \right]. \quad (12)$$

From solutions to this equation in different intermediate asymptotic regimes presented in the next section, we will then infer growth laws for the two observables.

A. Asymptotic results for the tension

1. Force setup

This scenario with $\theta = 1$ and the initial and boundary conditions

$$\bar{f}(s, t < 0) = f_{\text{pre}} \quad \text{and}$$

$$\bar{f}(0, t > 0) = 0, \quad \bar{f}(L, t > 0) = 0, \quad (13)$$

is identical to the “release” scenario which was thoroughly analyzed in Ref. [41]. We will briefly sketch this analysis in order to motivate its application to the other setups. From the response function Eq. (9), we get the asymptotic scaling for the wave number Q of the mode that relaxes at time t :

$$Q \simeq \begin{cases} t^{-1/4} & \text{if } \bar{F}^2/t \ll 1 \text{ (“linear”)}, \\ \bar{F}^{-1/2} & \text{if } \bar{F}^2/t \gg 1 \text{ (“nonlinear”)}. \end{cases} \quad (14)$$

Examining Eq. (8a), one infers that in the first case the tension contribution $Q^2 \bar{F}$ is small compared to the bending contribution $Q^4 t$ and can be treated as perturbation on the linear level. Since the magnitude of the tension is determined by the prestretching force, $\bar{F} \simeq f_{\text{pre}} t$, this asymptote, called “linear regime,” can also be formulated as $t \ll t_f$ with $t_f = f_{\text{pre}}^{-2}$. In the second case $t \gg t_f$, the bending contributions are subdominant which leads to different “nonlinear regimes.”

(a) *Linear propagation* ($t \ll t_f$). We perform an expansion [52] of the right-hand side of Eq. (12) with respect to the integrated tension \bar{F} and to the force f_{pre} :

$$\partial_s^2 \bar{F}(s,t) \approx \hat{\zeta} \int_0^\infty \frac{dq}{\pi \ell_p} \left[-\frac{f_{\text{pre}}}{q^4} (1 - e^{-2q^4 t}) + 2\bar{F}(s,t) - 4q^4 \int_0^t dt' \bar{F}(s,t') e^{-2q^4(t-t')} \right]. \quad (15)$$

Using the Laplace transform $\tilde{F}(s,z) = \mathcal{L}\{\bar{F}(s,t)\}$, this reads

$$\partial_s^2 \tilde{F}(s,z) = \hat{\zeta} \int_0^\infty \frac{dq}{\pi \ell_p} \left[-\frac{2f_{\text{pre}}}{z(z+2q^4)} + \tilde{F}(s,z) \frac{2z}{z+2q^4} \right], \quad (16)$$

which, after performing the q integral, reduces to

$$\lambda^2 \partial_s^2 \tilde{F} = \tilde{F} - \frac{f_{\text{pre}}}{z^2}. \quad (17)$$

Here, $\lambda(z) = 2^{3/8} (\ell_p / \hat{\zeta})^{1/2} z^{-1/8}$ is a dynamic length scale denoting the size of spatial variations in $\tilde{F}(s,z)$. If $L \gg \lambda$, the solution to Eq. (17) varies only close to the boundaries, as it is characteristic for the propagation regime. Near $s=0$ (and correspondingly near $s=L$), it simplifies to

$$\tilde{F}(s,z) \approx \frac{f_{\text{pre}}}{z^2} [1 - e^{-s/\lambda}], \quad (18)$$

which can be backtransformed [41] to

$$\bar{F}(s,t) = f_{\text{pre}} t \{1 - \phi[s/\ell_{\parallel}(t)]\}, \quad (19)$$

where $\phi(\xi) \approx \exp[-2^{-3/8} \xi / \Gamma(15/8)]$ is a scaling function that depends only on the ratio $\xi = s/\ell_{\parallel}(t)$. The length scale λ is directly related to the boundary layer size $\ell_{\parallel}(t) = (\ell_p / \hat{\zeta})^{1/2} t^{1/8}$ [35,41,44], and the requirement $L \gg \lambda$ translates into $t \ll t_L^{\parallel}$.

(b) *Nonlinear propagation* ($t_f \ll t \ll t_L^{\parallel}$). In the nonlinear regime, the $Q^4 t$ bending contributions are small compared to the tension terms $Q^2 \bar{F}$ if $\bar{F}^2/t \gg 1$. This results in $\chi_{\perp}(q;t,t')$ being finite only near $t' \approx t$, see Eq. (9). We can therefore linearize $\bar{F}(s,t) - \bar{F}(s,t') \approx [\partial_t \bar{F}(s,t)](t-t')$ in the exponent. The t' -integral in the second term of Eq. (12) is readily performed [41]:

$$\begin{aligned} \partial_s^2 \bar{F} &\approx \hat{\zeta} \int_0^\infty \frac{dq}{\pi \ell_p} \left[\frac{1 - \chi_{\perp}^2(q;t,0)}{q^2 + f_{\text{pre}}} - \frac{1 - \chi_{\perp}^2(q;t,0)}{q^2 + \partial_t \bar{F}} \right] \\ &\approx \hat{\zeta} \int_0^\infty \frac{dq}{\pi \ell_p} \left[\frac{1}{q^2 + f_{\text{pre}}} - \frac{1}{q^2 + \partial_t \bar{F}} \right] \\ &= \frac{\hat{\zeta}}{2\ell_p} [f_{\text{pre}}^{-1/2} - (\partial_t \bar{F})^{-1/2}]. \end{aligned} \quad (20)$$

In the second line, we let $\chi_{\perp} \rightarrow 0$ because $\bar{F}^2/t \gg 1$. This indicates the underlying ‘‘quasistatic’’ approximation: the relevant modes have already decayed and the tension is quasistatically equilibrated. Taking a time derivative gives [14,41]

$$\partial_s^2 \bar{f} = \frac{\hat{\zeta} \partial_t \bar{f}}{4\ell_p \bar{f}^{3/2}}. \quad (21)$$

Inspired by the result Eq. (19), we expect a scaling form $\bar{f}(s,t) = f_{\text{pre}} \varphi(\xi)$ with $\xi = s/\ell_{\parallel}(t)$ for the tension. Inserting it into Eq. (21) gives $\ell_{\parallel}(t) = (\ell_p / \hat{\zeta})^{1/2} f_{\text{pre}}^{3/4} t^{1/2}$ [14,35] and

$$\partial_{\xi}^2 \varphi = -\frac{1}{8} \xi \varphi^{-3/2} \partial_{\xi} \varphi, \quad (22)$$

with the boundary conditions $\varphi(0)=0$ and $\partial_{\xi} \varphi(\xi \rightarrow \infty)=0$, i.e., we neglect the presence of the second end, where the situation corresponds, and assume just a flat profile in the bulk. Numerical solutions to this equation have been shown in Refs. [14,41] and give $\varphi(\xi \rightarrow \infty)=1$ as expected and $\varphi'(0) \approx 0.62$. The propagation regime ends at $t_L^{\parallel} = L^2 f_{\text{pre}}^{-3/2} / \ell_p$.

(c) *Homogeneous relaxation* ($t_L^{\parallel} \ll t \ll t_R$). After the tension has propagated through the filament, it is no longer constant but expected to decay; but as long as $\bar{F}^2/t \gg 1$ still holds, we can use Eq. (21). Hence we try the separation ansatz $\bar{f}(s,t) = g(t)h(\xi)$ with $\xi = s/L$, which gives [41]

$$g(t) = \left(\frac{\hat{\zeta} L^2}{\ell_p t} \right)^{2/3}, \quad (23)$$

and

$$h'' = -\frac{1}{6} h^{-1/2} \quad \text{with } h(0) = h(1) = 0. \quad (24)$$

The almost parabolic profile $h(\xi)$ is characterized by [41]

$$h'(0) = 12^{-1/3}, \quad h(1/2) = \left(\frac{3}{128} \right)^{2/3}. \quad (25)$$

Using Eq. (23), we find that the condition $\bar{F}^2/t \gg 1$ is violated for $t \geq t_{\star} = L^8 / \ell_p^4$, which is already larger than t_R if $\ell_p \leq L$. Hence this regime lasts until the weakly bending approximation breaks down near the ends due to the onset of the stretch-coil transition.

2. Field setup

For hydrodynamic and/or electrophoretic forces, we find from the longitudinal equation of motion, Eq. (7b), a corresponding nonuniform initial tension profile $\bar{f}(s,t < 0) = g(L-s)$ with $g = \hat{\zeta} v$ for flows or $g \propto E$ for an electric field, where the generally unknown prefactor is some combination of electrophoretic and hydrodynamic mobility. This linearly decreasing prestress would in principle lead to an additional term $\bar{f}' r'_{\perp}$ in Eq. (8a), and the corresponding eigenfunctions would be very complicated. However, because large scale tension variations are irrelevant for the short wavelength transverse dynamics, we can ignore this term by consistently exploiting the scale separation which allowed the derivation of Eq. (8), and use Eq. (12) with the initial linear profile $\bar{f}_0(s) = g(L-s)$. The polymer is supposed to be grafted at $s=0$ and to have a free end at $s=L$, i.e., the boundary conditions are

$$\bar{f}'(0, t > 0) = 0 \quad \text{and} \quad \bar{f}(L, t > 0) = 0. \quad (26)$$

Identifying the force equivalent $f_{\text{pre}}^* = gL$, we expect a linear regime for $t \ll t_f$ with $t_f = f_{\text{pre}}^{*-2}$ and a nonlinear regime for $t \gg t_f$, governed by the respective asymptotic differential equations from the force case.

(a) *Linear propagation* ($t \ll t_f$). Linearizing Eq. (12) in \bar{F} and $\bar{f}_0(s)$ and performing a Laplace transform as in Eqs. (15)–(17), we arrive at the solution

$$\bar{F}(s, t) = gt(L - s) - g\ell_{\parallel}(t)\phi[s/\ell_{\parallel}(t)], \quad (27)$$

with $\ell_{\parallel}(t) = (\ell_p/\hat{\zeta})^{1/2}t^{1/8}$ and $\phi(\xi) \approx \frac{2^{3/8}\exp[-\Gamma(17/8)\xi^{2^{3/8}}]}{\Gamma(17/8)}$. We find a boundary layer at the fixed end where the tension relaxes from its initial value gL only by the small amount $g\ell_{\parallel}$. Near the free end, at $s=L$, we have $F(L, t)=0$ and $F'(L, t)=-gt$ without any algebraic correction terms. Hence, because the tension at the free end is already very small and the contour does not further coil up, there are no boundary layer effects which would give relevant deviations from the linear drift towards the grafted end, in contrast to what has been found in Ref. [17].

(b) *Nonlinear propagation* ($t_f \ll t \ll t_L^{\parallel}$). The assumption $F^2/t \gg 1$ leads again to Eq. (21) except for very small regions near the free end where $\bar{f}_0(s)$ in the denominator of the first term of Eq. (12) is almost zero. Corresponding to the linear case Eq. (27), we assume that the tension deviates only near the fixed end from its initial value $\bar{f}_0(s)$. Hence we insert $\bar{f}(s, t) = \bar{f}_0(s) - g\ell_{\parallel}(t)\varphi(\xi)$ with $\xi = s/\ell_{\parallel}(t)$ and $\ell_{\parallel}(t) = (\ell_p/\hat{\zeta})^{1/2}(gL)^{3/4}t^{1/2}$ into Eq. (21), and expand about $\bar{f}_0(s \ll L)$:

$$\partial_{\xi}^2 \varphi(\xi) \approx \frac{1}{8} [\varphi(\xi) - \xi \partial_{\xi} \varphi(\xi)] \quad (28)$$

with $\varphi'(0) = -1$ and $\varphi(\xi \rightarrow \infty) = 0$. The solution can be given in terms of the complementary error function:

$$\varphi(\xi) = \frac{4}{\sqrt{\pi}} e^{-\xi^2/16} - \xi \operatorname{erfc}(\xi/4). \quad (29)$$

The propagation regime ends at $t_L^{\parallel} = L^2/[\ell_p(gL)^{3/2}]$.

(c) *Homogeneous relaxation* ($t_L^{\parallel} \ll t \ll t_R$). The separation ansatz $\bar{f}(s, t) = g(t)h(\xi)$ with $\xi = s/L$ in Eq. (21) gives $g(t) = [\hat{\zeta}L^2/(\ell_p t)]^{2/3}$ as in Eq. (23) and the spatial function h solves

$$h'' = -\frac{1}{6}h^{-1/2} \quad \text{with} \quad h'(0) = 0, \quad h(1) = 0. \quad (30)$$

We find the following characteristics:

$$h(0) = \left(\frac{3}{32}\right)^{2/3}, \quad h'(1) = 6^{-1/3}. \quad (31)$$

The condition $\bar{F}^2/t \gg 1$ holds until $t = t_R$.

3. Shear setup

In this scenario, the equations of motion $\zeta[\partial_t \mathbf{r} - \mathbf{u}] = -\delta \mathcal{H}/\delta \mathbf{r} + \boldsymbol{\xi}$ are modified in the presence of an extensional

shear flow field $\mathbf{u} = \dot{\gamma}(-\mathbf{r}_{\perp}, s - r_{\parallel} - L/2)^T$, where $\dot{\gamma}$ is the shear rate. To lowest order in ε , and in the stationary state, we obtain from Eq. (7b)

$$-\hat{\zeta}\dot{\gamma}\left(s - \frac{L}{2}\right) = \bar{f}'. \quad (32)$$

As before, we treat this nonuniform tension profile only as large-scale variation and use Eq. (12) with the initial and boundary conditions

$$\bar{f}(s, t < 0) = \frac{1}{2}\hat{\zeta}\dot{\gamma}s(L - s) \quad \text{and}$$

$$\bar{f}(0, t > 0) = \bar{f}(L, t > 0) = 0. \quad (33)$$

As in the ‘‘field’’ case, the time $t_f = f_{\text{pre}}^{*-2}$ with the force equivalent $f_{\text{pre}}^* = \hat{\zeta}\dot{\gamma}L^2$ denotes the linear-nonlinear crossover.

(a) *Linear propagation* ($t \ll t_f$). Here the solution to Eq. (17) reads

$$\bar{F}(s, t) = \frac{1}{2}\hat{\zeta}\dot{\gamma}ts(L - s) - \frac{2^{3/4}\hat{\zeta}\dot{\gamma}\ell_{\parallel}^2 t}{\Gamma(9/4)}\{1 - \phi[s/\ell_{\parallel}(t)]\}, \quad (34)$$

with $\ell_{\parallel} = (\ell_p/\hat{\zeta})^{1/2}t^{1/8}$ as before and $\phi(\xi) \approx \exp[-2^{3/8}\Gamma(9/4)\xi/\Gamma(17/8)]$. We find two small boundary layers at the ends where the tension is slightly smaller than initially.

(b) *Nonlinear regime* ($t_f \ll t \ll t_L^{\parallel}$). The nonlinear regime $t_f \ll t \ll t_L^{\parallel}$ for the shear setup is quite peculiar: if we try (similar to the force and field case) a scaling ansatz $\bar{f}(s, t) = \frac{1}{2}\hat{\zeta}\dot{\gamma}\{s(L - s) + L\ell_{\parallel}(t)\varphi[s/\ell_{\parallel}(t)]\}$ or similarly, we get $\ell_{\parallel}(t) \sim t^2$. This unusual result could be explained by the fact that the ‘‘prestress’’ $\bar{f}(s, t < 0) \approx \frac{1}{2}\hat{\zeta}\dot{\gamma}sL$, which is responsible for the scaling of ℓ_{\parallel} in this regime [52], grows linearly with the distance from the ends. However, we do not get any physically meaningful differential equation for φ under the boundary conditions Eq. (33). We conclude that there is no propagation and *no observable boundary layers*. Looking for a solution spanning the whole arclength interval from 0 to L instead, we insert into Eq. (21) an expansion of the form

$$\bar{f}(s, t) = \frac{1}{2}\hat{\zeta}\dot{\gamma}L^2 \left[\varphi_0(\xi) + \frac{t}{t_L^{\parallel}}\varphi_1(\xi) + O((t/t_L^{\parallel})^2) \right] \quad (35)$$

with $\xi = s/L$ and $t_L^{\parallel} = \hat{\zeta}L^2/[\ell_p(\hat{\zeta}\dot{\gamma}L^2)^{3/2}]$. Solving the resulting differential equations for successive powers of (t/t_L^{\parallel}) gives the leading order terms

$$\varphi_0(\xi) = \xi(1 - \xi), \quad \varphi_1(\xi) = -[2\xi(1 - \xi)]^{3/2}. \quad (36)$$

In contrast to the propagation forms $\bar{f}(s, t) \sim \varphi[s/\ell_{\parallel}(t)]$ of the other scenarios, we now get self-similar and spatially invariant tension profiles. This can probably be attributed to this specific initial condition which allows for self-similar relaxation. Further, to linear order in (t/t_L^{\parallel}) we do not obtain algebraic corrections to the linear growth law of $\delta \bar{R}_{\parallel}(t)$, because $\partial_{\xi}\varphi_1(0) = 0$. Higher-order terms in the expansion (as far as they are analytically tractable) turn out to be ill-behaved near the ends.

(c) *Homogeneous relaxation* ($t_L^{\parallel} \ll t \ll t_R$). The subsequent regime of homogeneous tension relaxation is exactly equivalent to the one of the force case [see the respective boundary conditions, Eqs. (13) and (33)], and the results, Eqs. (23) and (25), apply here as well.

4. Quench setup

This scenario, with the initial and boundary conditions

$$\bar{f}(s, t < 0) = 0 \quad \text{and} \quad \bar{f}(0, t > 0) = \bar{f}(L, t > 0) = 0,$$

$$\ell_p(t < 0) = \theta \ell_p \quad \text{and} \quad \ell_p(t > 0) = \ell_p, \quad (37)$$

has been introduced as “ ℓ_p -quench” in Ref. [35]. In contrast to the scenarios discussed above, we lack a quantity providing a force scale, and the tension attains a simple scaling form in the propagation and relaxation regimes, i.e., there is no linear-nonlinear crossover. However, this scaling form still strongly depends on the value of θ . Physically the limit $\theta \rightarrow 0$ corresponds to suddenly switching off thermal forces for a thermally equilibrated filament, hence purely deterministic relaxation (see Ref. [43]). A small quench $\theta \approx 1$ will not induce strong tension, but the limit $\theta \rightarrow \infty$ describes the scenario of a completely straight contour that equilibrates purely under the action of stochastic forces, and the resulting tension may be very large at short times. In this case, similar approximations as employed when discussing the nonlinear regime in Sec. IV A 1 can be justified. Assuming $\bar{F}^2/t \gg 1$, the response function $\chi_{\perp}(q; t, t')$ from Eq. (9) is finite only near $t' \approx t$ which suggests the linearization $\bar{F}(s, t) - \bar{F}(s, t') \approx [\partial_s \bar{F}(s, t)](t - t')$ in the exponent. Performing the t' integral in the second term of Eq. (12) yields

$$\partial_s^2 \bar{F} \approx \hat{\zeta} \int_0^{\infty} \frac{dq}{\pi \ell_p} \left[\frac{1 - \chi_{\perp}^2(q; t, 0)}{\theta q^2} - \frac{1 - \chi_{\perp}^2(q; t, 0)}{q^2 + \partial_s \bar{F}} \right].$$

In contrast to Eq. (20), we may not set $\chi_{\perp} \rightarrow 0$ in the first term because this would produce an IR divergence; but we can neglect the bending contribution $q^4 t$ in the exponent of the first and set $\chi_{\perp} \rightarrow 0$ only in the second term. This gives

$$\begin{aligned} \partial_s^2 \bar{F} &\approx \hat{\zeta} \int_0^{\infty} \frac{dq}{\pi \ell_p} \left[\frac{1 - e^{-2q^2 \bar{F}}}{\theta q^2} - \frac{1}{q^2 + \partial_s \bar{F}} \right] \\ &= \frac{\hat{\zeta}}{2 \ell_p} \left[\frac{2}{\theta} \sqrt{\frac{2}{\pi}} \bar{F} - (\partial_s \bar{F})^{-1/2} \right]. \end{aligned} \quad (38)$$

(a) *Propagation* ($t \ll t_L^{\parallel}$). Inserting the scaling ansatz $\bar{F}(s, t) = \theta t^{1/2} \phi[s/\ell_{\parallel}(t)]$ with $\ell_{\parallel}(t) = (\ell_p/\hat{\zeta})^{1/2} \theta^{3/4} t^{1/8}$ removes the parameter dependence in Eq. (38):

$$\partial_{\xi}^2 \phi(\xi) = \sqrt{\frac{2}{\pi}} \phi(\xi) - \left[2\phi(\xi) - \frac{1}{2} \xi \partial_{\xi} \phi(\xi) \right]^{-1/2}. \quad (39)$$

Boundary conditions are $\phi(0) = 0$ and $\partial_{\xi} \phi(\xi \rightarrow \infty) = 0$. From a numerical solution we obtain $\phi(\xi \rightarrow \infty) = \sqrt{\pi}/2$ as expected from Eq. (39) and $\phi'(0) \approx 1.44$. The assumption $\bar{F}^2/t \approx \theta \gg 1$ is justified for all times $t \ll t_L^{\parallel} = L^8/(\ell_p^4 \theta^6)$.

(b) *Homogeneous relaxation*. ($t_L^{\parallel} \ll t \ll t_R$). Because we expect universal long time relaxation in the strong quenching limit $\theta \rightarrow \infty$ similar to the force case, we try the ansatz $\bar{F}(s, t) = t^{1/3} (\hat{\zeta} L^2/\ell_p)^{2/3} \phi(\xi)$ with $\xi = s/L$ in Eq. (38):

$$\begin{aligned} \partial_{\xi}^2 \phi &= \left(\frac{\hat{\zeta} L^2}{\ell_p} \right)^{2/3} \theta^{-1} t^{-1/6} \sqrt{\frac{2}{\pi}} \phi - \sqrt{\frac{3}{4\phi}} \\ &\approx -\sqrt{\frac{3}{4\phi}} \quad \text{if } t \gg \frac{L^8}{\ell_p^4 \theta^6} = t_L^{\parallel}. \end{aligned} \quad (40)$$

Because now $\bar{f}(s, t) = \partial_t \bar{F}(s, t) = g(t)h(\xi)$ with $g(t) = (\hat{\zeta} L^2/\ell_p t)^{2/3}$ and $h(\xi) = \phi(\xi)/3$ as in Eqs. (23) and (24), this regime of homogeneous relaxation is identical to the one in the force case. The condition $\bar{F}^2/t \gg 1$ holds until $t \approx t_{\star} = L^8/\ell_p^4 = \theta^6 t_L^{\parallel}$, which is usually already larger than t_R if $\ell_p \ll L$.

B. Results for pertinent observables

The maximum bulk tension $f_b(t) = \bar{f}(L/2, t)$ [in the field case, we prefer to use the grafting force $f_g(t) = f(0, t)$] can be obtained directly from the tension profiles computed in the preceding section. The change in end-to-end distance $\delta R_{\parallel}(t)$ follows from a simple formula: With the sign convention used before, this change has to equal the total amount of stored length that has been created. Hence we integrate the ensemble averaged change in stored length density $\partial_t \langle \varrho \rangle(s, t)$ over s and t :

$$\delta R_{\parallel}(t) = \int_0^L ds \int_0^t dt' \partial_t \langle \varrho \rangle(s, t'). \quad (41)$$

Defining $\langle \varrho \rangle = \langle \bar{\varrho} \rangle + \langle \varrho^e \rangle$ in Eq. (10) from the decomposition equation (11), we obtain $\delta R_{\parallel}(t) = \delta \bar{R}_{\parallel}(t) + \delta R_{\parallel}^e(t)$. The first part obeys the deterministic equation (8b):

$$\begin{aligned} \delta \bar{R}_{\parallel}(t) &= -\hat{\zeta}^{-1} \int_0^L ds \int_0^t dt' \partial_s^2 f(s, t') \\ &= -\hat{\zeta}^{-1} [\partial_s \bar{F}(L, t) - \partial_s \bar{F}(0, t)]. \end{aligned} \quad (42)$$

It accounts only for the “slow” coarse-grained tension dynamics but neglects subdominant and stochastic contributions $\delta R_{\parallel}^e(t)$ from “fast” fluctuating boundary segments analyzed in the next section. Results for $\delta \bar{R}_{\parallel}(t)$ and $f_b(t)[f_g(t)]$ are summarized in Tables I and II.

C. Boundary effects

Because our theory applies to times $t \ll t_R$ long before the relaxation of long-wavelength modes becomes relevant, because Eq. (4) results from a coarse-grained description that averages over small-scale fluctuations, and finally because projecting the end-to-end distance onto the longitudinal axis suppresses some end effects [41], the dependence of $\delta R_{\parallel} = \delta \bar{R}_{\parallel} + \delta R_{\parallel}^e$ on the boundary conditions for the contour $\mathbf{r}(s)$ is only subdominant but still non-negligible. While the “bulk contribution” $\delta \bar{R}_{\parallel}$ is independent of boundary effects and dy-

TABLE I. Asymptotic scaling laws for the change in projected length $\delta\bar{R}_{\parallel}(t)$ from Eq. (42) for the different setups. Units have been chosen such that $\kappa \equiv \zeta_{\perp} \equiv 1$.

$\delta\bar{R}_{\parallel}(t)$	$t \ll t_f$	$t_f \ll t \ll t_L^{\parallel}$	$t_L^{\parallel} \ll t$
Force	$\frac{2^{5/8} f_{\text{pre}} t^{7/8}}{\Gamma(15/8) \hat{\zeta}^{1/2} \ell_p^{1/2}}$	$2.48 \frac{f_{\text{pre}}^{1/4} t^{1/2}}{\hat{\zeta}^{1/2} \ell_p^{1/2}}$	$\left(\frac{18Lt}{\hat{\zeta} \ell_p^2}\right)^{1/3}$
Field	$gt / \hat{\zeta}$		$\left(\frac{9Lt}{2\hat{\zeta} \ell_p^2}\right)^{1/3}$
Shear	$\gamma t L [1 - O(\ell_{\parallel}/L)]$	$\gamma t L$	$\left(\frac{18Lt}{\hat{\zeta} \ell_p^2}\right)^{1/3}$
Quench	$2.88 \frac{\theta^{3/4} t^{3/8}}{\hat{\zeta}^{1/2} \ell_p^{1/2}}$		$\left(\frac{18Lt}{\hat{\zeta} \ell_p^2}\right)^{1/3}$

namically self-averaging, this stochastic dependence is accounted for by an additional ‘‘end contribution’’ δR_{\parallel}^e , which stems from the oscillating term $c_q(s)$ in Eq. (11), and decays rapidly on much smaller length scales than that of tension variations [39]. We may therefore evaluate this part at the boundaries under zero tension [i.e., using $\chi_{\perp}(q; t, t') = e^{-2q^4(t-t')}$ instead of Eq. (9)]:

$$\delta R_{\parallel}^e(t) \approx - \int_0^L ds \int_0^{\infty} \frac{dq}{\pi \ell_p} \frac{q^2 - \theta [q^2 + \bar{f}_0(s)]}{q^2 \theta [q^2 + \bar{f}_0(s)]} (1 - e^{-2q^4 t}) c_q(s). \quad (43)$$

Consistent with this simplification, we approximate the $w_q(s)$ by eigenfunctions of the biharmonic operator ∂_s^4 (see Ref.

TABLE II. Asymptotic scaling laws for the maximum bulk tension $f_b(t) = \bar{f}(L/2, t)$ [grafting force $f_g(t) = \bar{f}(0, t)$] for different setups. Units as in Table I.

$f_b(t), f_g(t)$	$t \ll t_f$	$t_f \ll t \ll t_L^{\parallel}$	$t_L^{\parallel} \ll t$
Force		f_{pre}	$\left(\frac{3\hat{\zeta}L^2}{128\ell_p t}\right)^{2/3}$
Field		$gL [1 - O(\ell_{\parallel}/L)]$	$\left(\frac{3\hat{\zeta}L^2}{32\ell_p t}\right)^{2/3}$
Shear	$\frac{1}{8} \hat{\zeta} \gamma L^2$	$\frac{1}{8} \hat{\zeta} \gamma L^2 [1 - O(t/t_L^{\parallel})]$	$\left(\frac{3\hat{\zeta}L^2}{128\ell_p t}\right)^{2/3}$
Quench		$\frac{1}{4} \pi^{1/2} \theta t^{-1/2}$	$\left(\frac{3\hat{\zeta}L^2}{128\ell_p t}\right)^{2/3}$

[53]). Again exploiting the scale separation in this integral over the rapidly fluctuating term $c_q(s)$, we use only the spatial average \bar{f}_b of the slowly varying prestress $\bar{f}_0(s)$. This means $f_{\text{pre}} \rightarrow \bar{f}_b = \frac{1}{12} \hat{\zeta} \gamma L^2$ for the shear case, and $f_{\text{pre}} \rightarrow \bar{f}_b = \frac{1}{2} gL$ for the field setup. Because there is only one free end in the latter, the contribution to δR_{\parallel}^e is one half of the force result.

(a) *Free ends.* If $w_q'' = w_q''' = 0$ at $s=0, L$, we use

$$w_q(s) = \frac{1}{\sqrt{L}} \left[\frac{\sin qL + \sinh qL}{\cos qL - \cosh qL} (\sin qs + \sinh qs) + \cos qs + \cosh qs \right], \quad (44)$$

where q is a solution of $\cos qL \cosh qL = 1$. For $t \ll t_R$, the q integral in Eq. (43) is dominated by short wavelength contributions, and for the relevant asymptotically large modes the s integral over $c_q(s)$ reads

$$\int_0^L ds c_q(s) = \frac{6}{q} + O(e^{-qL}). \quad (45)$$

(b) *Hinged ends.* For $w_q = w_q'' = 0$ at $s=0, L$, we obtain

$$w_q(s) = \sqrt{\frac{2}{L}} \sin qs \quad (46)$$

with $\sin qL = 0$. In this case, $\int_0^L ds c_q(s) = 0$.

(c) *Clamped ends.* Here, $w_q = w_q' = 0$ at $s=0, L$, and we have

$$w_q(s) = \frac{1}{\sqrt{L}} \left[\sin qs - \sinh qs + \frac{\cos qL - \cosh qL}{\sin qL + \sinh qL} (\cos qs - \cosh qs) \right], \quad (47)$$

with $\cos qL \cosh qL = 1$ and $\int_0^L ds c_q(s) \sim -2/q$. Up to a prefactor, the contribution for clamped ends is identical to the one for free ends.

(d) *Torqued ends.* If $w_q' = w_q''' = 0$ at $s=0, L$, the eigenmodes are

$$w_q(s) = \sqrt{\frac{2}{L}} \cos qs, \quad (48)$$

with $\sin qL = 0$ and $\int_0^L ds c_q(s) = 0$.

Using the asymptotic limit of $\int_0^L c_q(s) ds$, we evaluate the end contributions in the free ends situation of our setups.

(a) *Force setup.* Here, we obtain

$$\delta R_{\parallel}^e = \frac{6 f_{\text{pre}} t}{\pi \ell_p} G(f_{\text{pre}} t^{1/2}), \quad (49)$$

where

TABLE III. (a) Characteristic time scales (given a force of $f_{\text{pre}} = 2$ pN) and (b) bounds on control parameters for typical DNA [20] ($L \approx 20$ μm , $\ell_p \approx 50$ nm) and actin [30] ($L \approx 20$ μm , $\ell_p \approx 17$ μm) in solution with viscosity $\eta \approx 10^{-3}$ Pa s at room temperature.

	DNA	Actin
(a)		
t_f	10^{-7} s	10^{-5} s
t_L^{\parallel}	0.05 s	0.003 s
t_R	≈ 6 s	≈ 10 s
(b)		
f_c	0.08 pN	0.2 fN
v_c	27 $\mu\text{m/s}$	72 nm/s
$\dot{\gamma}_c$	6.6 s $^{-1}$	0.02 s $^{-1}$

$$\begin{aligned}
 G(\phi) &= \int_0^\infty dk \frac{1 - e^{-2k^4}}{k^3(k^2 + \phi)} \\
 &= -\frac{1}{4\phi^2} \{ e^{-2\phi^2} [\pi \operatorname{erfi} \sqrt{2\phi^2} - \operatorname{Ei}(2\phi^2)] \\
 &\quad + \ln 2\phi^2 + \gamma_E - \sqrt{8\pi\phi^2} \}, \quad (50)
 \end{aligned}$$

with erfi the imaginary error function, Ei the exponential integral, and $\gamma_E \approx 0.577$ Euler's constant. The asymptotic behavior is

$$\delta R_{\parallel}^c(t) \sim \begin{cases} -\frac{3f_{\text{pre}}t}{\pi\ell_p} \ln 2f_{\text{pre}}^2 t, & t \ll f_{\text{pre}}^{-2}, \\ \frac{6t^{1/2}}{\sqrt{2\pi}\ell_p}, & t \gg f_{\text{pre}}^{-2}. \end{cases} \quad (51)$$

(b) *Quench setup.* For free ends, we obtain from Eq. (43):

$$\delta R_{\parallel}^c = \frac{6t^{1/2}}{\pi\ell_p} \left(1 - \frac{1}{\theta}\right) \int_0^\infty dk \frac{1 - e^{-2k^4}}{k^3} = \sqrt{\frac{18}{\pi}} \frac{t^{1/2}}{\ell_p} \left(1 - \frac{1}{\theta}\right). \quad (52)$$

As anticipated [41], the end contribution δR_{\parallel}^c is zero for hinged and torqued ends, while it leads to an additional reduction of R_{\parallel} for free ends and has a lengthening effect for clamped ends. Note that indeed $\delta R_{\parallel}^c \ll \delta \bar{R}_{\parallel}$ is only subdominant for $t \ll t_R$, but the quantitative relevance of this contribution becomes evident when it is directly compared to numerical solutions of Eq. (12) and simulation data in nonasymptotic regimes.

V. COMPARISON TO SIMULATION DATA

The asymptotic scaling laws of Fig. 4 are derived in the limit $f_{\text{pre}} \rightarrow \infty$, and the difference to the numerical solutions gets smaller than 20% only for $f_{\text{pre}} \gtrsim 10^{10} k_B T \ell_p^3 / L^4$. While this can easily be realized in experiments, for instance, on DNA (cf. Table III), it is not possible in simulations due to the usual tradeoff between computational efficiency and ac-

curacy. For a comparison between our theoretical results and the simulation data of Fig. 2, we therefore compute the bulk part $\delta \bar{R}_{\parallel}(t)$ and $\bar{f}_b(t)$ using numerical solutions to Eq. (12) as described previously [52]. Figure 5 shows simulation data and analytical results for all four scenarios, using $\mu = (\zeta_{\perp} b)^{-1}$ and $\zeta_{\perp} = \zeta_{\parallel}$ to relate the (isotropic) mobility of the beads in the simulation model, which does not include hydrodynamic interactions, to the anisotropic friction coefficients per length for the continuous wormlike chain used in our theory. The bulk contribution $\delta \bar{R}_{\parallel}(t)$ (dashed lines), while having the correct qualitative behavior, underestimates the contraction by as much as 50%. Including end fluctuations with $\delta R_{\parallel}^c(t)$ (solid lines) gives results for $\delta R_{\parallel}(t)$ that are slightly overestimated for longer times. This could be caused by possibly oversimplifying approximations made when evaluating Eq. (43), or by a gradual breakdown of the weakly bending limit (see also Sec. VI B).

In the quench case, we observe a strong deviation between simulation and theory for short times, both in δR_{\parallel} and \bar{f}_b . While $\bar{f}_b \propto t^{-1/2}$ diverges as $t \rightarrow 0$ in our theory, the actual tension in the simulations is finite. This is due to the extensible backbone of a bead-spring chain: the tension follows the sudden change in environmental conditions only with a temporal delay related to the finite propagation speed of longitudinal backbone strain. Because now \bar{f}_b is smaller than predicted, the contraction $\delta R_{\parallel}(t)$ is also reduced, see the scaling relation Eq. (5). It is, however, possible to include a finite extensibility correction in Eq. (4). Because this nontrivial extension is only marginally relevant for the present discussion, which is focused on differences in the relaxation dynamics from an initially straight conformation, we present a detailed discussion elsewhere [50], and merely show the corrected results for $\delta R_{\parallel}(t)$ and $\bar{f}_b(t)$ for the quench case in Fig. 5(d) (dotted lines). The analysis of this correction term allowed us to choose parameters such that our results are not affected by microscopic details, except for the quench case with its singular short-time behavior. In particular, the elastic stretching constant γ_s is large enough that the associated time scale $b/(k_B T \gamma_s \mu)$ is easily resolved by the time discretization, and the backbone springs are so stiff that the straightened filament (with a projected length of about $\delta R_{\parallel}(0)/L \sim 1 - [k_B T / (4\ell_p f_{\text{pre}})]^{1/2}$ [48]) is lengthened by less than 1% due to the mechanical stretching of backbone bonds [the latter gives a relative contribution of about $f_{\text{pre}} / (k_B T \gamma_s)$].

Altogether, we now obtain good quantitative agreement between computer simulation and theory for all four setups and both observables over six decades in time *without adjustable parameters*. Having reliable theoretical control over the relaxation dynamics, we will now present quantitative estimates for the feasible choice of control parameters in experiments and a qualitative discussion of the influence of some additional important effects.

VI. EXPERIMENTAL IMPLICATIONS

A. Time and force scales

In Table III we have compiled numerical examples for the various time and force scales introduced above based on lit-

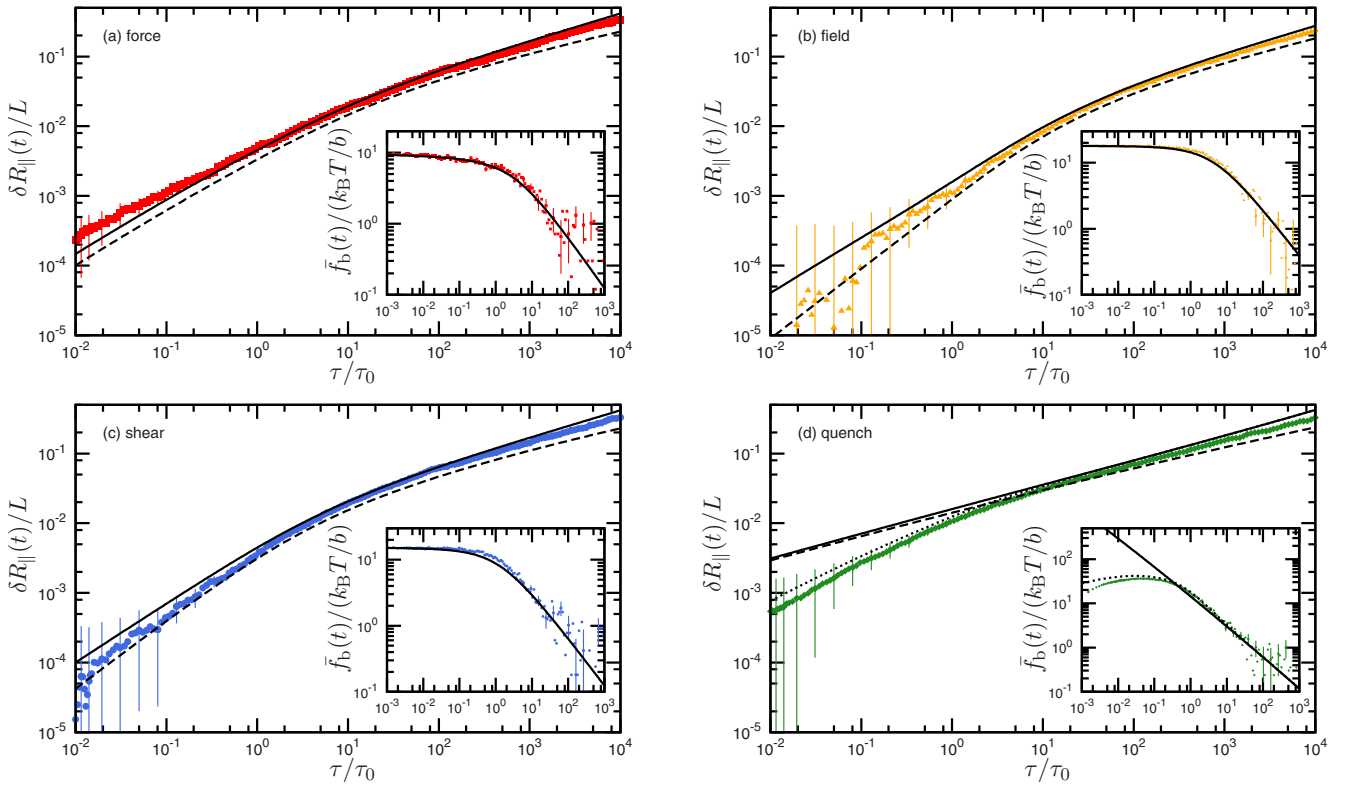


FIG. 5. (Color online) Comparison between theory and simulation data for a force (a), field (b), shear (c), and quench (d) scenario, respectively, for $\delta R_{\parallel}(t)$ and $\bar{f}_b(t)$ (insets). Note that the bulk contribution $\delta R_{\parallel}^b(t)$ from Eq. (42) (dashed lines) underestimates the contraction, which is corrected for by including the end contribution $\delta R_{\parallel}^e(t)$ from Eq. (43) (solid lines). In the simulation of the quench scenario, the tension follows the sudden change in temperature only with a delay related to the longitudinal propagation of backbone strain, which leads via Eq. (5) to a different scaling of δR_{\parallel} at short times. This can be accounted for by a correction term (dotted line) including the finite backbone extensibility of the bead-spring model [50]. Simulation data and parameters as in Fig. 2.

erature values for DNA [20] and actin [30]. In order to obtain sufficiently straight initial conformations, a conservative estimate for the control parameters f_{pre} , v , and $\dot{\gamma}$ requires them to be chosen by a factor of 25 larger than the respective values f_c , v_c , and $\dot{\gamma}_c$. The quenching strength θ should be significantly larger than $\theta_c = L/\ell_p$. The crossover times $t_L^{\parallel} \propto L^2/f_{\text{pre}}^{3/2}$ and $t_f \propto f_{\text{pre}}^{-2}$ depend strongly on the adjustable quantities L and f_{pre} ; hence the time window of interest can be varied considerably between scenario-specific and universal relaxation. The algebraic relaxation ends at times near t_R , for which we can give only a rough estimate as the unknown numerical prefactor is influenced by boundary conditions and hydrodynamic interactions and may substantially differ from unity [30].

B. Onset of the stretch-coil transition

Since experiments are often performed using quite flexible polymers like DNA with $\ell_p \ll L$, the weakly bending approximation will finally become invalid in regions near the ends, where the contour starts to (literally) coil up as the tension relaxes. Borrowing ideas from flexible polymer theory allows one to derive scaling laws accounting for the onset of the stretch-coil transition. The stem-flower picture of Brochard-Wyart [10] describes transient relaxation pro-

cesses of flexible polymers with Kuhn length a and friction coefficient ζ . Entropic forces on the order of $k_B T/a$ arising in the bulk pull the ends inwards. Balancing these forces with the associated friction gives the well-known scaling $\ell_* \approx [k_B T t / \zeta a]^{1/2}$ for the growth of “flowers” leading to an additional longitudinal contraction.

In the case of strongly stretched semiflexible polymers, this correction is negligible on time scales $t \ll t_R$. Here, the Kuhn segments are of size ℓ_p , and their Rouse-like relaxation after internal bending modes have equilibrated would generate flowers of size $\ell_* \approx L(t/t_R)^{1/2}$. However, in the relevant universal regime of homogeneous tension relaxation ($t_L^{\parallel} \ll t \ll t_R$), the bulk tension $f_b \approx k_B T(t/t_R)^{2/3}/\ell_p$ (see Table II) is much larger than $k_B T/\ell_p$, and the ends are pulled inwards so fast that a flower of the above size would be too large for the resulting drag. Observing that the associated roughly parabolic tension profiles [41] attain values of about $k_B T/\ell_p$ within distances $\ell'_* \approx L(t/t_R)^{2/3}$ from the ends, one easily confirms that this smaller value for the flower’s size indeed restores the friction balance. Altogether, we find that for times $t \ll t_R$ the $(t/t_R)^{2/3}$ growth of “flower”-like end regions, where the weakly bending approximation breaks down, is subdominant against the $(t/t_R)^{1/3}$ contraction of the remaining weakly bending part of the filament. Only at $t \approx t_R$, our assumptions finally cease to hold and more appropriate mod-

els, for conformational relaxation as well as hydrodynamic interactions, need to be employed (see, e.g., Ref. [28]). In our simulation, we do not expect a pronounced stretch-coil transition because the number L/ℓ_p is not large enough. We also checked that global rotational diffusion [40], apparently reducing the longitudinal projection of the end-to-end distance, can be neglected.

C. Hydrodynamic interactions

Finally, we want to briefly comment on hydrodynamic interactions. Their pronounced effects for strongly coiled polymers reduce to mere logarithmic corrections for relatively straight filaments [40]. As suggested previously [20], we speculate that these corrections can be summarily included via a phenomenological renormalization $L \rightarrow \ell_{\text{eff}}$ in the friction coefficient $\zeta \propto \eta/\ln(L/b)$ [40], where η is the solvent's viscosity and b the monomer size. Within our model, this has almost no further consequences than slightly shifting the time unit, cf. Eqs. (4) and (8). An appropriate time rescaling compensates for changes in the friction coefficients and could therefore easily be checked in experiments. The setups of Refs. [26,27], where initially stretched DNA relaxes with one end attached to a wall and the other fixed to a bead, can easily be modeled within our theory by appropriately adjusting the boundary conditions for the tension. It turns out that spatial inhomogeneities of the tension and end fluctuations are suppressed and hydrodynamic interactions (primarily between bead and wall) are enhanced, such that a simple quasistationary approach describes the data very well.

VII. CONCLUSION

We have presented a comprehensive theoretical analysis of the conformational relaxation dynamics of semiflexible polymers from an initially straight conformation. Special emphasis has been put on a systematic investigation of four fundamentally different realizations of “initially straight.” The sudden removal of the straightening constraint leads in all cases to strong spatial inhomogeneities of the filaments’

backbone tension. Analyzing two exemplary and easily accessible observables, we found that for short times, when these nontrivial spatial variations are restricted to the boundaries, the relaxation dynamics crucially depends on the actual initial conditions: polymers prestretched with forces display tension propagation effects, in contrast to chains straightened by fields or flows, and a quench leads to yet other effects. In the universal relaxation regime at longer times, the tension becomes quasistatically equilibrated and independent of initial conditions, but its spatial inhomogeneity remains relevant. Additionally to the derivation of asymptotic growth laws, we extended the systematic theory of Refs. [35,39,41] to include the surprisingly important influence of different boundary conditions. For nonasymptotic parameter values, quantitative and parameter-free agreement between simulation data and theory could be achieved over six time decades below the filament's longest relaxation time. In the quench case, short-time deviations could be attributed to the finite backbone extensibility of the bead-spring chains used in the simulations. Finally, we discussed quantitative implications for possible experimental realizations, adapted a widely used scaling argument for the onset of the stretch-coil transition for flexible polymers to the semiflexible case (dominated by bending energy), and commented on hydrodynamic interactions. We hope that our thorough discussion of the nonequilibrium dynamics of an initially straight polymer will help to design new quantitative single molecule experiments and lead to a better understanding of more complex phenomena such as force transduction and recoil of disrupted stress fibers in cells [54].

ACKNOWLEDGMENTS

We gratefully acknowledge financial support via the German Academic Exchange Program (DAAD) (O.H.), by the Deutsche Forschungsgemeinschaft (DFG) through Grant No. Ha 5163/1 (O.H.), and programs SFB 486 (B.O. and E.F.), FOR 877 (K.K.), and of the German Excellence Initiative via the programs “Nanosystems Initiative Munich (NIM)” (B.O. and E.F.) and Leipzig School of Natural Sciences “Building with molecules and nano-objects” (K.K.).

-
- [1] A. R. Bausch and K. Kroy, *Nat. Phys.* **2**, 231 (2006).
 - [2] B. Maher, *Nature (London)* **448**, 984 (2007).
 - [3] M. L. Gardel *et al.*, *Proc. Natl. Acad. Sci. U.S.A.* **103**, 1762 (2006).
 - [4] P. Fernandez, P. A. Pullarkat, and A. Ott, *Biophys. J.* **90**, 3796 (2006).
 - [5] C. Semmrich *et al.*, *Proc. Natl. Acad. Sci. U.S.A.* **104**, 20199 (2007).
 - [6] G. J. L. Wuite *et al.*, *Nature (London)* **404**, 103 (2000).
 - [7] A. Goel, R. D. Astumian, and D. Herschbach, *Proc. Natl. Acad. Sci. U.S.A.* **100**, 9699 (2003).
 - [8] B. van den Broek, M. C. Noom, and G. J. L. Wuite, *Nucleic Acids Res.* **33**, 2676 (2005).
 - [9] T. T. Perkins, S. R. Quake, D. E. Smith, and S. Chu, *Science* **264**, 822 (1994).
 - [10] F. Brochard-Wyart, *Europhys. Lett.* **30**, 387 (1995).
 - [11] S. Manneville *et al.*, *Europhys. Lett.* **36**, 413 (1996).
 - [12] Y.-J. Sheng, P.-Y. Lai, and H.-K. Tsao, *Phys. Rev. E* **56**, 1900 (1997).
 - [13] O. B. Bakajin, T. A. J. Duke, C. F. Chou, S. S. Chan, R. H. Austin, and E. C. Cox, *Phys. Rev. Lett.* **80**, 2737 (1998).
 - [14] F. Brochard-Wyart, A. Buguin, and P. G. de Gennes, *Europhys. Lett.* **47**, 171 (1999).
 - [15] J. W. Hatfield and S. R. Quake, *Phys. Rev. Lett.* **82**, 3548 (1999).
 - [16] B. Ladoux and P. S. Doyle, *Europhys. Lett.* **52**, 511 (2000).
 - [17] B. Maier, U. Seifert, and J. O. Rädler, *Europhys. Lett.* **60**, 622 (2002).

- [18] S. W. P. Turner, M. Cabodi, and H. G. Craighead, *Phys. Rev. Lett.* **88**, 128103 (2002).
- [19] C. M. Schroeder, H. P. Babcock, E. S. G. Shaqfeh, and S. Chu, *Science* **301**, 1515 (2003).
- [20] Y. Bohbot-Raviv, W. Z. Zhao, M. Feingold, C. H. Wiggins, and R. Granek, *Phys. Rev. Lett.* **92**, 098101 (2004).
- [21] P. Dimitrakopoulos, *Phys. Rev. Lett.* **93**, 217801 (2004).
- [22] C. M. Schroeder, E. S. G. Shaqfeh, and S. Chu, *Macromolecules* **37**, 9242 (2004).
- [23] C. H. Reccius, J. T. Mannion, J. D. Cross, and H. G. Craighead, *Phys. Rev. Lett.* **95**, 268101 (2005).
- [24] E. S. G. Shaqfeh, *J. Non-Newtonian Fluid Mech.* **130**, 1 (2005).
- [25] J. Wang and H. Gao, *J. Chem. Phys.* **123**, 084906 (2005).
- [26] E. Goshen, W. Z. Zhao, G. Carmon, S. Rosen, R. Granek, and M. Feingold, *Phys. Rev. E* **71**, 061920 (2005).
- [27] A. Crut *et al.*, *Proc. Natl. Acad. Sci. U.S.A.* **104**, 11957 (2007).
- [28] B. D. Hoffmann and E. S. G. Shaqfeh, *J. Rheol.* **51**, 947 (2007).
- [29] E. Frey, K. Kroy, J. Wilhelm, and E. Sackmann, in *Dynamical Networks in Physics and Biology*, edited by B. Beysens and G. Forgacs (EDP Sciences-Springer, Berlin, 1998).
- [30] L. LeGoff, O. Hallatschek, E. Frey, and F. Amblard, *Phys. Rev. Lett.* **89**, 258101 (2002).
- [31] D. C. Morse, *Phys. Rev. E* **58**, R1237 (1998).
- [32] L. LeGoff, F. Amblard, and E. M. Furst, *Phys. Rev. Lett.* **88**, 018101 (2001).
- [33] D. A. Koster *et al.*, *Nature (London)* **448**, 213 (2007).
- [34] U. Seifert, W. Wintz, and P. Nelson, *Phys. Rev. Lett.* **77**, 5389 (1996).
- [35] O. Hallatschek, E. Frey, and K. Kroy, *Phys. Rev. Lett.* **94**, 077804 (2005).
- [36] A. Balducci, C.-C. Hsieh, and P. S. Doyle, *Phys. Rev. Lett.* **99**, 238102 (2007).
- [37] T. T. Perkins, D. E. Smith, and S. Chu, *Science* **276**, 2016 (1997).
- [38] N. Saitô, K. Takahashi, and Y. Yunoki, *J. Phys. Soc. Jpn.* **22**, 219 (1967).
- [39] O. Hallatschek, E. Frey, and K. Kroy, *Phys. Rev. E* **75**, 031905 (2007).
- [40] M. Doi and S. F. Edwards, *The Theory of Polymer Dynamics* (Clarendon Press, Oxford, 1986).
- [41] O. Hallatschek, E. Frey, and K. Kroy, *Phys. Rev. E* **75**, 031906 (2007).
- [42] G.-M. Nam and N.-K. Lee, *J. Chem. Phys.* **126**, 164902 (2007).
- [43] O. Hallatschek, E. Frey, and K. Kroy, *Phys. Rev. E* **70**, 031802 (2004).
- [44] R. Everaers, F. Jülicher, A. Ajdari, and A. C. Maggs, *Phys. Rev. Lett.* **82**, 3717 (1999).
- [45] D. Long, J. L. Viovy, and A. Ajdari, *Phys. Rev. Lett.* **76**, 3858 (1996).
- [46] D. Stigter and C. Bustamante, *Biophys. J.* **75**, 1197 (1998).
- [47] M. G. L. van den Heuvel, M. P. de Graaff, S. G. Lemay, and C. Dekker, *Proc. Natl. Acad. Sci. U.S.A.* **104**, 7770 (2007).
- [48] J. F. Marko and E. D. Siggia, *Macromolecules* **28**, 8759 (1995).
- [49] R. Granek, *J. Phys. II* **7**, 1761 (1997).
- [50] B. Obermayer *et al.* (unpublished).
- [51] R. E. Goldstein and S. A. Langer, *Phys. Rev. Lett.* **75**, 1094 (1995).
- [52] B. Obermayer, O. Hallatschek, E. Frey, and K. Kroy, *Eur. Phys. J. E* **23**, 375 (2007).
- [53] C. H. Wiggins, D. Riveline, A. Ott, and R. E. Goldstein, *Biophys. J.* **74**, 1043 (1998).
- [54] S. Kumar *et al.*, *Biophys. J.* **90**, 3762 (2006).

Tension dynamics and viscoelasticity of extensible wormlike chains

Benedikt Obermayer and Erwin Frey*

*Arnold Sommerfeld Center and Center for NanoScience, Ludwig-Maximilians-Universität München,
Theresienstr. 37, 80333 München, Germany*

(Received 7 July 2009; published 2 October 2009)

The dynamic response of prestressed semiflexible biopolymers is characterized by the propagation and relaxation of tension, which arises due to the near inextensibility of a stiff backbone. It is coupled to the dynamics of contour length stored in thermal undulations but also to the local relaxation of elongational strain. We present a systematic theory of tension dynamics for stiff yet extensible wormlike chains. Our results show that even moderate prestress gives rise to distinct Rouse-like extensibility signatures in the high-frequency viscoelastic response.

DOI: [10.1103/PhysRevE.80.040801](https://doi.org/10.1103/PhysRevE.80.040801)

PACS number(s): 61.41.+e, 87.15.La, 87.15.H-, 87.15.ad

Recent experiments have successfully linked the viscoelastic properties of living cells to the rheological behavior of prestressed biopolymer networks [1–4]. Single filaments within these networks are well described by the wormlike chain (WLC) model, where very stiff backbones are idealized as inextensible space curves [5], giving rise to a characteristic $f^{-1/2}$ divergence of the force f required to attain full stretching [6]. Here, “stretching” needs to be seen as a “straightening” of excess length stored in thermal contour undulations [7], suggesting the phrase “pulling out stored length.” If sudden forces are applied, stored length can be pulled out at first only from growing boundary layers of size $\ell_{\parallel}(t)$ near the ends due to longitudinal friction with the viscous solvent [7–11]. The precise time dependence of $\ell_{\parallel}(t)$ is influenced in a quite subtle way by the applied prestress [12], and a nonhomogeneous distribution of stored length along the contour corresponds to a nonuniform tension profile.

Modelling prestress as prestretching force applied at the filament’s ends, a larger prestress clearly implies that an increasing contribution to the longitudinal extension stems from the microscopic elasticity of the backbone bonds and less from thermal undulations. Hence, for an extensible backbone the polymer’s response is characterized by a local competition between destroying thermal stored length and creating elongational strain. While it has long been recognized that stretching modes of long and slender elastic rods relax extremely fast [13], their local equilibrium value depends on the local tension, which in a nonequilibrium situation is in turn coupled to the much slower stored length relaxation. Especially for bead-spring simulations, where realistically stiff backbones often require unfeasibly short time steps, it is not immediately clear if and how backbone stretching affects the longitudinal relaxation. In this Rapid Communication, we present a theory of tension dynamics for stiff yet finitely extensible wormlike chains. A brief comparison of extensible and inextensible polymer models is used to motivate the ensuing systematic derivation based on the inextensible analog presented in Ref. [8]. We then calculate viscoelastic response properties and show that even moderate prestress can give rise to distinct extensibility signatures reminiscent of a Rouse-like dynamics.

In the WLC model, the polymer backbone is idealized as continuous space curve $\mathbf{r}(s)$. Contour undulations are penalized with a bending energy proportional to the squared local curvature. Strict inextensibility would require that s be the arclength such that $\mathbf{r}'(s)$ is a unit vector, and this hard constraint allows exact solutions only for special cases [5]. In general, Lagrange multipliers of varying sophistication are used to enforce miscellaneous constraints of different rigidity [14]. Specifically, for a nonequilibrium scenario with nonuniform stored length dynamics, it is inevitable to use a local constraint [7,8,11,15–18], which is intuitively interpreted as backbone tension. In the case of an extensible backbone this tension arises naturally as a spring force [19–21], and although it is generally far from trivial [22], our results will permit taking the limit from soft to rigid constraints.

For an extensible but very stiff backbone with only small stretching deformations, the Hamiltonian reads as [19]

$$\mathcal{H} = \frac{k_B T}{2} \int_0^L ds [\ell_p r'^2 + k_x u^2], \quad (1)$$

where L is the unstretched contour length, ℓ_p is the persistence length, k_x is the stretching elastic constant, and $u = |\mathbf{r}'| - 1$ is the elongational strain. Our theory relies on the weakly bending limit $\mathbf{r}(s) = (s - r_{\parallel}, \mathbf{r}_{\perp})^T$ of small transverse and longitudinal contour deviations \mathbf{r}_{\perp} and r_{\parallel} from a straight line, which gives $u \approx -r'_{\parallel} + \frac{1}{2} r_{\perp}^2$ to leading order. Observing that the polymer’s longitudinal extension in the limit of large prestress $f_0 \gg k_B T / \ell_p$ is given by [19]

$$\frac{R_{\parallel}}{L} = \int_0^L \frac{ds}{L} (1 - r'_{\parallel}) = 1 + \langle u \rangle - \left\langle \frac{1}{2} r_{\perp}^2 \right\rangle, \quad (2)$$

we can quantify the simultaneous limits of an only slightly extensible backbone and a weakly bending contour by requiring that the contributions of longitudinal strain $\langle u \rangle = f_0 / (k_B T k_x) \equiv \varepsilon_x \ll 1$ and of thermal stored length $\langle \frac{1}{2} r_{\perp}^2 \rangle = [k_B T \ell_p / (4 f_0)]^{1/2} \equiv \varepsilon_{th} \ll 1$, respectively, are both small. Although these contributions are independent, we will also assume that the force extension [Eq. (2)] is dominated by contour straightening instead of backbone stretching, i.e., that $\langle u \rangle \ll \langle \frac{1}{2} r_{\perp}^2 \rangle$, which is easily fulfilled as long as $f_0 \ll f_x$, where $f_x = k_B T k_x^{2/3} / \ell_p^{1/3}$ is the corresponding crossover force

*frey@physik.lmu.de

scale [20,23]. This assumption is reasonable in most experimental circumstances, considering that $f_x \approx 75$ pN [24] for actin and $f_x \approx 50$ pN for DNA [19], which in fact is close to the overstretching transition. For bead-spring simulations, however, this condition is much harder to obey [25] because very small time steps $\Delta t \leq k_x^{-1}$ are required. Also, in special situations such as the relaxation from a low-temperature initial condition [16], short-time transients are quite pronounced, and we will show below that even a prestress of only about $0.01f_x$ gives rise to observable effects.

To quantitatively assess the influence of backbone stretching on the dynamics, we proceed with a discussion of the equations of motion $\zeta \partial_t \mathbf{r} = -\delta H / \delta \mathbf{r} + \boldsymbol{\xi}$, with the stochastic noise $\boldsymbol{\xi}$ and the free-draining friction matrix $\boldsymbol{\zeta} = \zeta_{\perp} [\mathbf{r}' \mathbf{r}' + \hat{\zeta} (1 - \mathbf{r}' \mathbf{r}')] / \ell_p$, where $\hat{\zeta} \approx 1/2$ accounts for the anisotropy between transverse and longitudinal friction. To leading order in ε_{th} and ε_x and in the absence of external forces, we obtain

$$\partial_t \mathbf{r}_{\perp} = -\mathbf{r}_{\perp}'''' + k_x (u \mathbf{r}'_{\perp})' / \ell_p + \boldsymbol{\xi}_{\perp}, \quad (3a)$$

$$\hat{\zeta} \partial_t r_{\parallel} + (1 - \hat{\zeta}) \mathbf{r}'_{\perp} \partial_t \mathbf{r}_{\perp} = -r_{\parallel}'''' - k_x u' / \ell_p + \xi_{\parallel}. \quad (3b)$$

Here, we have introduced units such that $k_B T = \ell_p^{-1}$ and $\zeta_{\perp} = 1$, which makes time a length⁴ and force a length⁻². In the following, we are interested in the prototypical rheological experiment [1,2,4] where at time $t=0$ a small time-dependent force $\delta f(t)$ is superimposed on a static prestress f_0 , which contributes a term $[f_0 + \Theta(t) \delta f(t)] [\delta(L-s) - \delta(s)]$ on the right-hand side of Eq. (3b). In the stationary state at times $t < 0$, this gives $k_x u / \ell_p = f_0$, and the combination $k_x u / \ell_p$ plays the role of a tension in Eq. (3a) also at later times.

If we assume constant $u = \ell_p f_0 / k_x$, we find that the transverse part Eq. (3a) is correlated on length scales $\ell_{\perp}(t)$ with $\ell_{\perp} \sim t^{1/4}$ if $t \ll f_0^{-2}$ and $\ell_{\perp}(t) \sim (f_0 t)^{1/2}$ if $t \gg f_0^{-2}$ [8,10]. On the other hand, disregarding the thermal contribution r_{\parallel} to Eq. (3b) for the moment, we also find that the diffusive dynamics of the elongational strain u is correlated on length scales $\ell_x(t) \sim (k_x t / \ell_p)^{1/2}$ [19]. Given now that $\ell_p f_0 / k_x = \mathcal{O}(\varepsilon_x) \ll 1$, it turns out that $\ell_x \gg \ell_{\perp}$ except for very early times $t \leq (\ell_p / k_x)^2$, where higher-order terms become relevant. Hence, after short initial transients the elongational strain u varies slowly with arclength: stretching modes relax extremely fast but only to a local equilibrium value, which is not only nonzero for a prestressed filament but can even show nontrivial large-scale spatial variations for the previously mentioned nonequilibrium stretching experiments. Thus, elongational strain cannot globally equilibrate unless these tension variations have propagated through the filament. The latter are linked to the dynamics of thermal stored length and therefore significantly slowed down by longitudinal friction, and it has been shown that the associated characteristic length scale $\ell_{\parallel}(t) \propto \varepsilon_{\text{th}}^{-1/2} \ell_{\perp}(t)$ is much larger than the one of transverse fluctuations [8].

Our goal is now to formulate an equation for the elongational strain u that integrates over transverse fluctuations described through Eq. (3a) (on the short length scale ℓ_{\perp}) but retains both large-scale *spatial* variations in the tension $k_x u / \ell_p$ (on the scale ℓ_{\parallel}) as well as the effect of short time

transients stemming from the fast relaxation of elongational modes. To this end, we employ a multiple scale perturbation theory both in space and time: small-scale and large-scale spatial coordinates s and $\varepsilon_{\text{th}}^{1/2} \bar{s}$, respectively, account for the different *spatial* correlation lengths of transverse and longitudinal contour displacements, while slow and fast time variables t and $\tau = (\varepsilon_{\text{th}} / \varepsilon_x) t$ account for long-time stored length and short-time strain dynamics, respectively. Here, the condition $\varepsilon_x \ll \varepsilon_{\text{th}}$ (resulting from $f_0 \ll f_x$) is essential, and it entails that a τ -derivative of u is of order ε_{th} : transients from strain relaxation can become comparable to thermal stored length. We briefly sketch the analysis, which in its technical details is quite analogous to Ref. [26]. Higher-order terms of this perturbation scheme can in principle be computed, but the lowest-order results already yield a sufficiently accurate description [16]. Taking an s -derivative of Eq. (3b) and eliminating $r'_{\parallel} = -u + \frac{1}{2} r'_{\perp}{}^2$, we find to zeroth order in ε_{th} : $-\hat{\zeta} \partial_t u = \partial_s^4 u - k_x \partial_s^2 u / \ell_p$. Since $k_x u / \ell_p = \mathcal{O}(f_0)$ while everything else is $\mathcal{O}(\varepsilon_x)$, we find $\partial_s^2 u = 0$, and therefore also $\partial_s^4 u = \partial_s u = 0$. This also implies that Eq. (3a) becomes the linear equation $\partial_t \mathbf{r}_{\perp} = -\partial_s^4 \mathbf{r}_{\perp} + k_x u \partial_s^2 \mathbf{r}_{\perp} / \ell_p + \boldsymbol{\xi}_{\perp}$. To first order in ε_{th} , Eq. (3b) now gives $\hat{\zeta} \frac{1}{2} (\partial_s \mathbf{r}_{\perp})^2 - \hat{\zeta} \varepsilon_{\text{th}} \partial_{\tau} u / \varepsilon_x = -k_x \partial_s^2 u / \ell_p + H(s, \bar{s})$, where $H(s, \bar{s})$ summarizes s derivatives of terms nonlinear in \mathbf{r}_{\perp} . These vanish upon coarse graining, i.e., when averaging this equation over small-scale variations on the scale ℓ_{\perp} [26]. Denoting in such a manner spatially averaged quantities with an overbar and replacing $\tau \rightarrow t$, we obtain

$$k_x \partial_s^2 \bar{u} / \ell_p = -\hat{\zeta} \partial_t (\bar{\varrho} - \bar{u}), \quad (4)$$

where $\bar{\varrho} = \frac{1}{2} r'_{\perp}{}^2$ is the local density of contour length stored in thermal undulations. This relation, which is our main result, formalizes in an intuitive way the opposing effects thermal stored length density $\bar{\varrho}$ and elongational strain \bar{u} have on the backbone tension $k_x \bar{u} / \ell_p$: if prestress is increased, stored length is destroyed and elongational strain created and both lead temporarily to spatial tension inhomogeneities (curvature) and vice versa for decreasing prestress. Further, taking the “inextensible” limit $\varepsilon_x \rightarrow 0$ while holding the tension $k_x \bar{u} / \ell_p$ fixed leads to the inextensible analog derived in Ref. [8], and the limit $\varepsilon_{\text{th}} \rightarrow 0$ of a one-dimensional Rouse chain, although our assumptions cease to hold, nevertheless gives a simple diffusion equation for \bar{u} .

In order to solve Eq. (4), we observe that its boundary conditions are prescribed through the externally applied prestress: $\bar{u}(0, t) = \bar{u}(L, t) = \ell_p [f_0 + \Theta(t) \delta f(t)] / k_x$. Further, $\bar{\varrho}$ has to be computed from Eq. (3a), which to lowest order depends only parametrically on $\bar{u}(\bar{s}, t)$. It is thus effectively linear in \mathbf{r}_{\perp} and can be solved in Fourier space by means of the response function [26] $\chi_{\perp}(q; t, t') = e^{-q^2 [q^2(t-t') + k_x (\bar{U}(t) - \bar{U}(t')) / \ell_p]}$, where $\bar{U}(t) = \int_0^t dt' \bar{u}(t')$ is the time-integrated strain. Because spatially averaging $\bar{\varrho}$ over many effectively uncorrelated segments of length ℓ_{\perp} produces an ensemble average, the stored length density is given by [26]

$$\bar{\varrho} = \int_0^{\infty} \frac{dq}{\pi \ell_p} \left[\frac{\chi_{\perp}^2(q; t, 0)}{q^2 + f_0} + 2q^2 \int_0^t dt' \chi_{\perp}^2(q; t, t') \right]. \quad (5)$$

Solutions to Eq. (4) can now be obtained similarly to Refs. [12,16,26].

In the remainder of this Rapid Communication, we focus on a small oscillatory stress $\delta f(t) = \delta f \sin \omega t$ superimposed on a large prestress f_0 . This situation has been analyzed in Ref. [27] for an inextensible filament, and our calculation proceeds along these lines. While we cannot actually take the linear response limit $\delta f \rightarrow 0$ because then the assumptions underlying the multiple scale perturbation theory become invalid [8], we can still for small enough $\delta f \ll f_0$ linearize Eq. (5) by writing $\bar{U}(\bar{s}, t) = \ell_p f_0 t / k_x + \Delta \bar{U}(\bar{s}, t)$ and find from Eq. (4) a simple equation for the Laplace transform $\Delta \bar{U}(\bar{s}, z)$ [26,27]:

$$\partial_{\bar{s}}^2 \Delta \bar{U}(\bar{s}, z) = M(z) \Delta \bar{U}(\bar{s}, z). \quad (6)$$

The kernel $M(z) = \hat{\xi} f_0^{1/2} \hat{M}(z f_0^{-2}) / \ell_p$ is defined as

$$\hat{M}(\hat{z}) = \int_0^\infty \frac{dk}{\pi} \left[\frac{2k^2}{k^2 + 1} - \frac{4k^4}{2k^2(k^2 + 1) + \hat{z}} \right] + \phi_x^{3/2} \hat{z}, \quad (7)$$

and $\phi_x = f_0 / f_x \ll 1$ is the ratio of prestress to the critical force $f_x = k_x^{2/3} / \ell_p^{4/3}$. In contrast to the inextensible case treated in Ref. [27], where $\hat{M}(\hat{z}) \propto \hat{z}^{1/4}$ for all $\hat{z} \gg 1$, we obtain now an additional high-frequency regime $\hat{M}(\hat{z}) \sim \phi_x^{3/2} \hat{z}$ for $\hat{z} \gg \phi_x^{-2}$. Considering that $M^{-1/2}(z)$ is the analog in Laplace space to the characteristic length scale $\ell_{||}(t)$ for the large-scale spatial tension variations, we find that $\ell_{||}(t) \approx (k_x t / \ell_p)^{1/2}$ [19] shows a diffusive scaling in the corresponding extensibility-dominated short-time regime $t \ll t_x$, only then crosses over to the well-known growth law $\ell_{||}(t) \approx \ell_p^{1/2} t^{1/8}$ [10], before finally arriving at $\ell_{||}(t) \approx \ell_p^{1/2} f_0^{3/4} t^{1/2}$ [8,11] for $t \gg f_0^{-2}$ (i.e., $\hat{z} \ll 1$). We emphasize that the scaling of the crossover time $t_x = \ell_p^{8/3} / k_x^{4/3} = f_x^{-2}$ cannot simply be inferred from dimensional analysis because any combination of the lengths ℓ_p and k_x^{-1} could be used.

The observable of main interest is the change $\delta R_{||}(t)$ in projected length $R_{||}$, which is through the force-extension relation [Eq. (2)] related to the integrated change in $\bar{u} - \bar{Q}$ and thus through Eq. (4) to the features of the tension $k_x \bar{u} / \ell_p$:

$$\delta R_{||}(t) = \int_0^t dt' \int_0^L ds (\bar{u} - \bar{Q}) = \frac{k_x}{\hat{\xi} \ell_p} [\partial_{\bar{s}} \bar{U}(L, t) - \partial_{\bar{s}} \bar{U}(0, t)]. \quad (8)$$

In Laplace space, we thus obtain from a straightforward solution of Eq. (6) $\delta \bar{R}(z) = \frac{2}{\hat{\xi} z} M^{1/2}(z) \tanh[\frac{L}{2} M^{1/2}(z)] \delta \bar{f}(z)$, which can be backtransformed in the stationary limit $t \rightarrow \infty$ [27]:

$$\delta R_{||}(t) = \frac{\delta f}{\hat{\xi} L f_0^2} [\hat{J}'(\omega f_0^{-2}) \sin(\omega t) - \hat{J}''(\omega f_0^{-2}) \cos(\omega t)], \quad (9)$$

with the dimensionless compliances

$$\hat{J}'(\hat{\omega}) = \frac{2}{\hat{\omega}} \text{Im} \left[\sqrt{\phi_c^{1/2} \hat{M}(i\hat{\omega})} \tanh \sqrt{\frac{1}{4} \phi_c^{1/2} \hat{M}(i\hat{\omega})} \right],$$

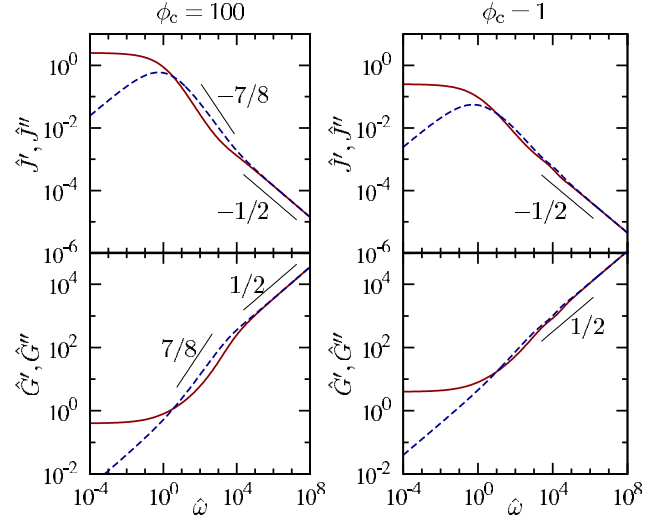


FIG. 1. (Color online) Plot of \hat{J}', \hat{J}'' (top) and \hat{G}', \hat{G}'' (bottom) from Eq. (10) for $\phi_x = f_0 / f_x = 10^{-2}$ and for $\phi_c = 100$ (left) and $\phi_c = 1$ (right), where $\phi_c = f_0 / f_c$ with $f_c = \ell_p^2 / (\hat{\xi}^2 L^4)$ and $f_x = k_x^{2/3} / \ell_p^{4/3}$. Solid lines: $\hat{J}'(\hat{G}')$ and dashed lines: $\hat{J}''(\hat{G}'')$. Short lines indicate high-frequency scaling laws of Table I.

$$\hat{J}''(\hat{\omega}) = \frac{2}{\hat{\omega}} \text{Re} \left[\sqrt{\phi_c^{1/2} \hat{M}(i\hat{\omega})} \tanh \sqrt{\frac{1}{4} \phi_c^{1/2} \hat{M}(i\hat{\omega})} \right]. \quad (10)$$

Here, $\phi_c = f_0 / f_c$ gives the ratio of f_0 to the longitudinal critical force $f_c = \ell_p^2 / (\hat{\xi}^2 L^4)$ and can be used to distinguish “long” ($\phi_c \gg 1$) and “short” ($\phi_c \ll 1$) filaments, respectively [12].

Figure 1 depicts numerical solutions of Eq. (10) for a fixed value of $\phi_x = 10^{-2}$ and different values of ϕ_c , as well as results for the corresponding viscoelastic modulus $(\hat{G}' + i\hat{G}'') = (\hat{J}' + i\hat{J}'')^{-1}$. It is straightforward to check that Eq. (10) obeys scaling laws in different intermediate asymptotic regimes, which are summarized in Table I. Most of these

TABLE I. Asymptotic scaling results [10,17,27–30] for the compliances $\hat{J}'(\hat{\omega})$ and $\hat{J}''(\hat{\omega})$ from Eq. (10) with $\hat{\omega} = \omega f_0^{-2}$ for (a) $\phi_c \gg 1$ and (b) $\phi_c \ll 1$, respectively, where $\phi_x = f_0 / f_x$ and $\phi_c = f_0 / f_c$ with $f_x = k_x^{2/3} / \ell_p^{4/3}$ and $f_c = \ell_p^2 / (\hat{\xi}^2 L^4)$.

	$\hat{J}'(\hat{\omega})$	$\hat{J}''(\hat{\omega})$
(a)		
$\hat{\omega} \gg \phi_x^{-2}$		$\phi_c^{1/4} \phi_x^{3/4} \hat{\omega}^{-1/2}$
$\phi_x^{-2} \gg \hat{\omega} \gg 1$		$\phi_c^{1/4} \hat{\omega}^{-7/8}$
$1 \gg \hat{\omega} \gg \phi_c^{-1/2}$		$\phi_c^{1/4} \hat{\omega}^{-1/2}$
$\phi_c^{-1/2} \gg \hat{\omega}$	$\phi_c^{1/2}$	$\phi_c^{1/2} \hat{\omega}^{1/2}$
(b)		
$\hat{\omega} \gg \phi_x^{-2}$		$\phi_c^{1/4} \phi_x^{3/4} \hat{\omega}^{-1/2}$
$\phi_x^{-2} \gg \hat{\omega} \gg \phi_c^{-2}$		$\phi_c^{1/4} \hat{\omega}^{-7/8}$
$\phi_c^{-2} \gg \hat{\omega} \gg 1$		$\phi_c^{1/2} \hat{\omega}^{-3/4}$
$1 \gg \hat{\omega}$	$\phi_c^{1/2}$	$\phi_c^{1/2} \hat{\omega}^{1/2}$

results have been obtained previously (cf., Refs. [10,17,27–30]), and we will therefore not comment on them in detail. We merely emphasize that for low frequencies $\hat{\omega} \leq 1$ the presence of a prestress leads to the well-known nonlinear response regime with its characteristic $\frac{1}{2}$ exponents [30,31]. The intermediate regime $\phi_c^{1/2} \ll \hat{\omega} \ll 1$ with $\hat{J}' \sim \hat{J}'' \sim \hat{\omega}^{-1/2}$ corresponds to the previously discussed regime of nonlinear tension propagation [8,11] and can only be observed for large $\phi_c \gg 1$. Also, for small prestress ($\phi_c \ll 1$), there is an intermediate regime with $\hat{J}' \sim \hat{J}'' \sim \hat{\omega}^{-3/4}$ for $\phi_c^{-2} \gg \hat{\omega} \gg 1$ equivalent to the force-free case [17,28].

The predominant effect of an extensible backbone is to produce a Rouse-like scaling in the new high-frequency regime $\omega \gg f_x^2$. Here, we find $\hat{J}'(\hat{\omega}) \sim \hat{J}''(\hat{\omega}) \sim 2^{1/2} \phi_c^{1/4} \phi_x^{3/4} \hat{\omega}^{-1/2}$, corresponding to $\hat{G}' \sim \hat{G}'' \sim 2^{-3/2} \phi_c^{-1/4} \phi_x^{-3/4} \hat{\omega}^{1/2}$. From Fig. 1

we conclude that a moderate prestress f_0 of merely 1% of the critical force f_x suffices to significantly shorten the 7/8-regime and to produce a distinct Rouse-like signature, especially if ϕ_c is not too large.

In summary, we have presented a systematic theory of tension dynamics for extensible wormlike chains including the opposing effects of thermal stored length and elongational strain relaxation at short times. These produce a Rouse-like scaling in the high-frequency viscoelastic response and are expected to be especially relevant for the proper design of bead-spring simulations.

We gratefully acknowledge helpful discussions with Klaus Kroy and Oskar Hallatschek and financial support by Deutsche Forschungsgemeinschaft Contract No. FR 850/8–1 and by Nanosystems Initiative Munich.

-
- [1] P. Fernandez, P. A. Pullarkat, and A. Ott, *Biophys. J.* **90**, 3796 (2006).
- [2] K. E. Kasza *et al.*, *Phys. Rev. E* **79**, 041928 (2009).
- [3] A. Majumdar, B. Suki, N. Rosenblatt, A. M. Alencar, and D. Stamenović, *Phys. Rev. E* **78**, 041922 (2008).
- [4] M. L. Gardel *et al.*, *Proc. Natl. Acad. Sci. U.S.A.* **103**, 1762 (2006); *Phys. Rev. Lett.* **96**, 088102 (2006).
- [5] N. Saitō, K. Takahashi, and Y. Yunoki, *J. Phys. Soc. Jpn.* **22**, 219 (1967).
- [6] J. F. Marko and E. D. Siggia, *Macromolecules* **28**, 8759 (1995).
- [7] U. Seifert, W. Wintz, and P. Nelson, *Phys. Rev. Lett.* **77**, 5389 (1996).
- [8] O. Hallatschek, E. Frey, and K. Kroy, *Phys. Rev. Lett.* **94**, 077804 (2005).
- [9] A. Ajdari, F. Jülicher, and A. Maggs, *J. Phys. (Paris)* **7**, 823 (1997).
- [10] R. Everaers, F. Jülicher, A. Ajdari, and A. C. Maggs, *Phys. Rev. Lett.* **82**, 3717 (1999).
- [11] F. Brochard-Wyart, A. Buguin, and P. G. de Gennes, *Europhys. Lett.* **47**, 171 (1999).
- [12] B. Obermayer, O. Hallatschek, E. Frey, and K. Kroy, *Eur. Phys. J. E* **23**, 375 (2007).
- [13] K. Soda, *J. Phys. Soc. Jpn.* **35**, 866 (1973).
- [14] R. A. Harris and J. E. Hearst, *J. Chem. Phys.* **44**, 2595 (1966); R. G. Winkler, P. Reineker, and L. Harnau, *ibid.* **101**, 8119 (1994); B. Y. Ha and D. Thirumalai, *ibid.* **103**, 9408 (1995); M. Hinczewski *et al.*, *Macromolecules* **42**, 860 (2009); T. B. Liverpool, *Phys. Rev. E* **72**, 021805 (2005); T. Munk, O. Hallatschek, C. H. Wiggins, and E. Frey, *ibid.* **74**, 041911 (2006).
- [15] R. E. Goldstein and S. A. Langer, *Phys. Rev. Lett.* **75**, 1094 (1995).
- [16] B. Obermayer, W. Möbius, O. Hallatschek, E. Frey, and K. Kroy, *Phys. Rev. E* **79**, 021804 (2009).
- [17] D. C. Morse, *Phys. Rev. E* **58**, R1237 (1998).
- [18] V. Shankar, M. Pasquali, and D. C. Morse, *J. Rheol.* **46**, 1111 (2002).
- [19] J. F. Marko, *Phys. Rev. E* **57**, 2134 (1998).
- [20] J. Kierfeld, O. Niamplon, V. Sa-yakanit, and R. Lipowsky, *Eur. Phys. J. E* **14**, 17 (2004).
- [21] R. R. Netz, *Macromolecules* **34**, 7522 (2001).
- [22] N. G. van Kampen and J. J. Lodder, *Am. J. Phys.* **52**, 419 (1984).
- [23] M. D. Wang *et al.*, *Biophys. J.* **72**, 1335 (1997).
- [24] H. Kojima, A. Ishijima, and T. Yanagida, *Proc. Natl. Acad. Sci. U.S.A.* **91**, 12962 (1994).
- [25] G.-M. Nam and N.-K. Lee, *J. Chem. Phys.* **126**, 164902 (2007).
- [26] O. Hallatschek, E. Frey, and K. Kroy, *Phys. Rev. E* **75**, 031905 (2007); **75**, 031906 (2007).
- [27] T. Hiraiwa and T. Ohta, *J. Phys. Soc. Jpn* **77**, 023001 (2008); e-print arXiv:0903.2095.
- [28] F. Gittes and F. C. MacKintosh, *Phys. Rev. E* **58**, R1241 (1998).
- [29] R. Granek, *J. Phys. (Paris)* **7**, 1761 (1997).
- [30] A. Caspi, M. Elbaum, R. Granek, A. Lachish, and D. Zbaida, *Phys. Rev. Lett.* **80**, 1106 (1998).
- [31] D. Mizuno, C. Tardin, C. F. Schmidt, and F. C. MacKintosh, *Science* **315**, 370 (2007).

3. Quasispecies theory for specific enzymatic replication

The RNA world theory [84] hypothesizes that RNA-like polynucleotides served both as carriers of genetic information and as metabolic enzymes at a very early stage of prebiotic evolution before these functions were largely split among DNA and proteins, respectively. For its origins from a “primordial soup”, a series of four steps has been proposed [208]: in a first step, nucleotides would be synthesized non-enzymatically, and secondly polymerize into random RNA. After acquiring the potential for non-enzymatic copying or even replication in the third step, natural selection would act on this more refined pool of RNA sequences and finally yield a set of functional RNA replicase enzymes, thus initiating Darwinian evolution. In the introduction, we discussed some recent findings regarding the diverse catalytic functions of ribozymes [49], and the experimental progress made so far towards the creation of self-replicating RNA-based systems in the lab [208, 258]. Many theoretical studies are concerned with the origins of evolution as well. The question at which point chemical kinetics turns into evolution has inspired theories of “prevolution” [198], as a description of the transition from the non-replicative generation of information-carrying polymers (“pre-life”) to the appearance of reproductive potential and evolution (“life”). We also discussed some ideas for the emergence of protocells by means of a reciprocally advantageous interaction between replicators and enclosing membranes [36, 258]. Such systems encourage a theoretical analysis by means of group selection models [3, 70].

On the level of single replicating polynucleotides, a brief account of the most relevant features of Eigen’s quasispecies model revealed that their information capacity is limited by the mutation rate μ , which must not surpass the error threshold μ_c . In this chapter, we will present a more detailed introduction to quasispecies theory, which, as a general evolution model, has also been applied in other biological contexts such as the population genetics of RNA viruses [188]. It also had a large influence on theoretical descriptions of many other dynamical processes, e.g., in chemical kinetics or language or grammar evolution [196], just to name a few. After discussing generic aspects of the underlying “fitness landscapes” and formal analogies to statistical mechanics, we will explain why these formulations of quasispecies theory pertain to “non-enzymatic” replicators, and introduce contrasting “enzymatic” models. This will finally lead us to the theory of *specific* enzymatic replication investigated in this work, and the two aspects discussed in detail: the phenomenon of an “escalation of error catastrophe” for highly specific replicators [199], and a systematic analysis of general specificity functions [201].

3.1. Eigen's quasispecies theory

Many different variants of Eigen's theory, originally proposed in the 1970s [52], exist in the literature, focusing on quite diverse aspects of evolutionary dynamics (for reviews, see Refs. [11, 27, 51, 54, 123, 196, 273]). Here, we use the formulation most appropriate for the ideas discussed in this work. In this case, quasispecies theory is a phenomenological description of molecular evolution based on deterministic chemical rate equations for the concentrations of molecules of fixed length L . Each molecule is characterized by the number of copies N_i and its sequence $S_i = (\sigma_i^{(1)} \dots \sigma_i^{(L)})$ with $\sigma_i^{(j)}$ taken from some alphabet with κ letters (for instance, $\kappa = 4$ and $\sigma \in \{A, C, G, U\}$ in the case of RNA), i.e., it is described through coordinates in the L -dimensional sequence space. These molecules replicate with replication rates R_i through some pseudo first order reaction not specified in detail. It is only assumed that the replication of sequence S_j can result in an erroneous or mutated copy S_i with probability M_{ij} . Considering that replication likely involves a stepwise polymerization reaction with a uniform error probability μ per single nucleotide and round of replication, the mutation matrix can be explicitly given as:

$$M_{ij} = (1 - \mu)^{L-d_{ij}} \left(\frac{\mu}{\kappa - 1} \right)^{d_{ij}}, \quad (3.1)$$

where d_{ij} is the Hamming distance between the sequences S_i and S_j , i.e., the number of differences. Equation (3.1) expresses the total combinatorial probability to leave $L - d_{ij}$ positions intact, while introducing one of $\kappa - 1$ different possible mutations at the other d_{ij} positions. To formulate dynamical equations for the abundances of all different species, it is further assumed that the numbers N_i (and hence their total $N = \sum_i N_i$) are all macroscopically large. In this case the equations are given in terms of their relative concentrations $X_i = N_i/N$:

$$\dot{X}_i = \sum_j M_{ij} R_j X_j - X_i \sum_j R_j X_j. \quad (3.2)$$

The second term involving the mean replication rate $\sum_j R_j X_j$ has been subtracted to keep the concentrations normalized at all times, $\sum_i X_i \equiv 1$, which makes these κ^L -dimensional equations nonlinear. It can also be seen as a constantly applied dilution flux introducing *competition* between different species, and has the consequence that a degradation term $-D_i X_i$ drops out of Eq. (3.2) if sequence-independent decay rates $D_i \equiv D$ are chosen. Measuring time in units of some reference interval like one round of replication, all quantities are dimensionless numbers.

3.1.1. Fitness landscapes

Many analogies between standard models of population genetics and quasispecies theory suggest to think of R_i as a fitness landscape, i.e., a mapping from genotype to reproductive success. More generally, the mapping involves two stages, both possibly influenced by

interactions with the environment: genotype is expressed as phenotype, which determines fitness. Within quasispecies theory, we identify genotype (i.e., the sequence S_i) with phenotype, and the replication rate R_i , which could in principle be a function of all constituents of the system, depends therefore only on the sequence S_i :

$$R_i = A_i \equiv \text{const.} \quad (3.3)$$

Although this represents a considerable simplification, it is still a complicated mapping from sequence space into the real numbers (hence, the notion of a “landscape”). Because replication rates are hardly measurable over substantial regions of genome space, which for all practical purposes is infinitely large, very little is known about general features of fitness landscapes, such as the number, distances and relative heights of local optima. Sequence space is very high-dimensional and figurative intuitions drawn from the landscape metaphor can be misleading: fitness “peaks” can be separated by deep “valleys” and at the same time connected through “ridges” of intermediate fitness. In particular, it is unclear whether these landscapes are “smooth” or “rugged”, i.e., whether single mutations generally have small or large effects, respectively. Further, the phenomenon of “neutral” networks, a set of points with identical fitness, has attracted increased interest, because these networks are expected to percolate sequence space, hence providing traversable paths between virtually any pair of points in sequence space [11, 118].

In this chapter, we will discuss some consequences of neutrality in Sec. 3.1.5, but otherwise restrict ourselves to the case of highly symmetrical and simple fitness landscapes. For more detailed reviews on these topics, see, e.g., Refs. [11, 51, 123].

3.1.2. Formal solution

For constant replication rates A_i , a formal solution to Eq. (3.2) can be obtained by standard linear algebra methods [54]. Although the rate equation are formally nonlinear due to the dilution flux term, they can be brought into linear form by means of the transformation

$$Z_i(t) = X_i(t) \exp \left[\sum_j A_j \int_0^t dt' X_j(t') \right]. \quad (3.4)$$

The new concentration variables obey the linear equation

$$\dot{Z}_i = \sum_j W_{ij} Z_j, \quad (3.5)$$

where the square matrix W is given as elementwise product of mutation matrix and fitness landscape:

$$W_{ij} = M_{ij} A_j. \quad (3.6)$$

Solutions $\tilde{Z}_i(t) = \tilde{Z}_i(0)e^{\lambda_i t}$ to Eq. (3.4) follow by diagonalizing W with an orthogonal matrix S such that $S^{-1}WS = \text{diag}(\lambda_0, \dots, \lambda_{\kappa L})$, $\tilde{Z} = S^{-1}Z$, and $S^{-1}S = S^T S = 1$. Since

W is real with positive entries, the Frobenius-Perron theorem asserts that it has a unique largest positive real eigenvalue λ_0 , and that the corresponding eigenvector has strictly positive components. In terms of the original variables $X_i(t)$, we obtain

$$X_i(t) = \frac{Z_i(t)}{\sum_k Z_k(t)} = \frac{\sum_j S_{ij} \tilde{Z}_j(0) e^{\lambda_j t}}{\sum_{kj} S_{kj} \tilde{Z}_j(0) e^{\lambda_j t}} \xrightarrow{t \rightarrow \infty} \frac{S_{i0}}{\sum_k S_{k0}}, \quad (3.7)$$

because the eigenvector to the largest eigenvalue λ_0 grows faster than all other eigenvectors (which are the columns of S). From the competitive exclusion principle [100], we would expect that in the stationary state only the single “fittest” species X_* with the largest replication rate A_* survives. In contrast, here we are left with a whole species *distribution*, given by the normalized Frobenius-Perron eigenvector of W . This motivated the notion of a “quasi-species” as the target of selection (i.e., as the steady-state result of this evolutionary dynamics), a metaphor for the formation of a cloud of mutants about this fittest sequence that are continuously generated through mutations albeit their replication rates may be smaller.

3.1.3. Simple symmetric fitness landscapes

In the following, we introduce a number of strong simplifications that have been made throughout the theoretical literature, even though their biological justification sometimes is unclear at best. First, we work only with a two-letter alphabet, $\sigma \in \{0, 1\}$, such that $\kappa = 2$. This can be motivated by classifying nucleotides as either pyrimidines (C,U) or purines (A,G), respectively, or by accounting only for the presence or absence of a certain mutation. Secondly, we consider fitness landscapes as “simple” if they exhibit only one single peak at a certain sequence with highest fitness, which is usually called the “master” sequence. The common biological scenario of having a particular “wildtype” and some (usually deleterious) “mutants” suggests such a model. Finally, we will mostly restrict ourselves to the class of “permutation invariant” fitness landscapes, which have been mainly considered in the theoretical literature (largely because of mathematical convenience). In these landscapes, fitness is only a function of the *number* of mutations relative to the master sequence, but not their *positions* along the sequence.

Exploiting this symmetry in sequence space, we reduce the original rate equations, Eq. (3.2), by lumping together sequences with k mutations relative to the master sequence into “error class” k [4, 195, 256, 283]. For the new variables x_k denoting the concentration of error class k , we obtain rate equations formally analogous to Eq. (3.2):

$$\dot{x}_k = \sum_j m_{kj} \alpha_j x_j - x_k \sum_j \alpha_j x_j. \quad (3.8)$$

Here, we use lower-case letters for all symmetrized quantities: α_j is the replication rate of error class j and m_{kj} is the symmetrized mutation matrix, denoting the probability of obtaining a sequence in error class k from mutating a sequence in error class j . It can

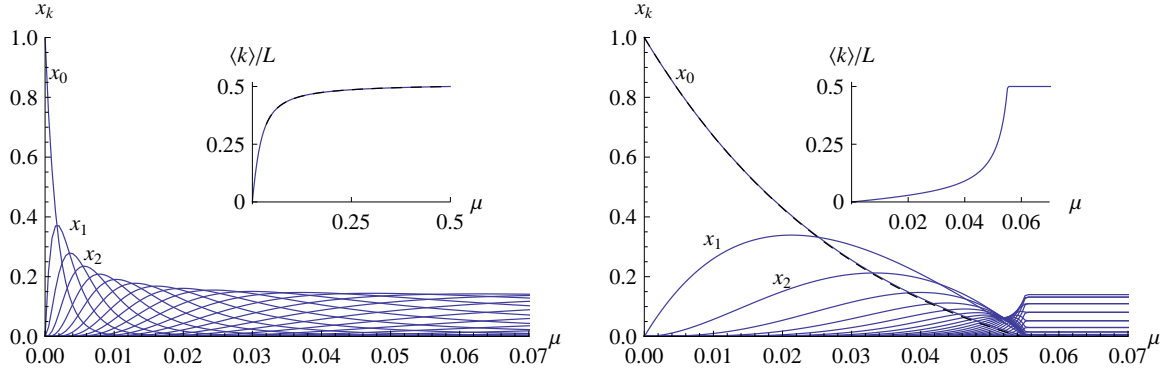


Figure 3.1: Stationary Hamming distance distribution x_k from numerical solutions to the symmetrized rate equations Eq. (3.8) for sequences of length $L = 32$: x_0 is the concentration of the master sequence, x_1 are the sequences with one mutation, x_2 those with two errors, etc. Left: a multiplicative fitness landscape $\alpha_k = (1 - s)^k$ with $s = 0.054$, where the population distribution is binomial, $x_k = \binom{L}{k} a^k (1 - a)^{L-k}$. The average Hamming distance $a = \langle k \rangle / L$ to the master sequence, shown in the inset (note the different scale on the abscissa), is given by Eq. (3.11) (dashed line). Right: the sharply peaked fitness landscape $\alpha_k = 1 + (\alpha_0 - 1)\delta_{k,0}$ with $\alpha_0 = 6$, where the dashed line depicts the result of the error-tail approximation Eq. (3.13) for x_0 .

be obtained by adding up all possibilities to appropriately distribute $0 \leq k - j + 2\ell \leq L$ mutations [4, 195, 256, 283]:

$$m_{kj} = \sum_{\ell} \binom{L-j}{k-j+\ell} \binom{j}{\ell} (1-\mu)^{L-(k-j+2\ell)} \mu^{k-j+2\ell}. \quad (3.9)$$

The reduced rate equations, Eq. (3.8), have the advantage of being only $(L+1)$ -dimensional and thus amenable to numerical solution. Figure 3.1 shows the resulting stationary Hamming distance distribution x_k under two exemplary fitness landscapes α_k .

Multiplicative landscape. If all sites are independent, each additional mutation reduces fitness by a factor $1 - s$:

$$\alpha_k = (1 - s)^k. \quad (3.10)$$

In other formulations of population genetics, where $\log \alpha_k$ is used as fitness, this is called an “additive”, hence linear, landscape; both formulations agree in the case $s \ll 1$, which is most relevant for population genetics. The stationary solution for this landscape can be obtained analytically [283]: it turns out that the Hamming distances $x_k = \binom{L}{k} a^k (1 - a)^{L-k}$ are binomially distributed, with a given by

$$a = \frac{1}{2} + \mu \frac{2-s}{2s} - \sqrt{\frac{(s(1-\mu) + 2\mu)^2}{4s^2} - \frac{\mu}{s}}. \quad (3.11)$$

This parameter (depicted in the insets of Fig. 3.1) measures the population’s mean Hamming distance to the master: $\langle k \rangle \equiv \sum_k k x_k = aL$, and thus the width of the population

distribution. It increases from $a = 0$ at $\mu = 0$, implying full localization about the master sequence, to $a = 1/2$ at $\mu = 1/2$, which means that the population consists of purely random sequences: in this case the Hamming distance distribution $x_k = 2^{-L} \binom{L}{k}$ is equal to the one obtained by randomly choosing each “bit” of a binary sequence (there are $\binom{L}{k}$ ways of having a distance of k mutations to the master).

Sharply-peaked landscape. In contrast to the above smooth case, the fitness landscape

$$\alpha_k = 1 + (\alpha_0 - 1)\delta_{k0} \quad (3.12)$$

attributes a higher replication rate α_0 only to the master, while all other sequences have unit replication rate. Because of its simplicity, this landscape has very often been used in the literature [4, 13, 32, 52, 76, 195, 225, 232, 256, 261]. A simple approximate result for the concentration x_0 of the master sequence is easily obtained by means of the error-tail approximation, which was already discussed in the introduction. It considers only the master sequence, its replication rate α_0 , and the probability $(1 - \mu)^L$ not to produce a mutant. All other sequences are part of the error tail with concentration $1 - x_0$ and identical unit fitness. Mutations in the error tail back to the master sequence are neglected, because they are very unlikely for large sequence length. The rate equations Eq. (3.8) read $\dot{x}_0 = (1 - \mu)^L \alpha_0 x_0 - x_0[1 + (\alpha_0 - 1)x_0]$ as in Eq. (1.4), and in the stationary state, the solution is

$$x_0 = \frac{\alpha_0(1 - \mu)^L - 1}{\alpha_0 - 1}, \quad (3.13)$$

in perfect agreement with the numerical solution even for moderately large L , as shown in the right panel of Fig. 3.1. With increasing mutation rate, the concentration of the master sequence decreases, while the nearest mutants are more strongly populated. From Fig. 3.1 we infer that in this landscape, compared to the multiplicative one, the population is much more localized (the mean Hamming distance $\langle k \rangle$ is much smaller).

3.1.4. The error threshold

The transition between a regime, where the population is localized about the master sequence in a quasispecies distribution, and the delocalized regime of random sequences has been termed the error threshold, because it implies that above a certain critical mutation rate the information of the master sequence is lost: even though the concentration of the master sequence itself may be very small near the error threshold, it is still present as “consensus” sequence of the population, which has at each position the most frequent letter [123], but beyond the error threshold the consensus sequence becomes random.

For the two landscapes discussed in the previous sections, these transitions are entirely different: while it appears very smooth for the multiplicative landscape, it is quite abrupt for the sharply peaked one. In more quantitative terms, we observe that in the multiplicative case the parameter a as given through Eq. (3.11) increases smoothly from

$a = 0$ to $a = 1/2$. All other observables such as the concentration of the master sequence $x_0 = (1 - a)^L$, or the population distribution's mean and variance ($\langle k \rangle = aL$ and $\langle (k - \langle k \rangle)^2 \rangle = La(1 - a)$, respectively) are also continuous, such that a distinct transition is absent. In the contrasting sharply-peaked landscape, the concentration of the master sequence x_0 , as given through Eq. (3.13), is nonzero only for $\mu < \mu_c$, with the critical mutation rate given by

$$\mu_c = 1 - \alpha_0^{-1/L} \approx \frac{\log \alpha_0}{L} \quad \text{for large } L. \quad (3.14)$$

Of course, the solution Eq. (3.13) is only approximate, because the concentrations in the stationary state are actually always positive (they are given as the components of the Frobenius-Perron eigenvector, cf. Sec. 3.1.2). However, a non-smooth transition clearly is apparent, and it can be seen also in other observables: exact results show that in the limit $L \rightarrow \infty$ the mean Hamming distance $\langle k \rangle \sim (\mu - \mu_c)^{-1}$ diverges at the error threshold [76].

General results. Generally speaking, not all fitness landscapes display an error threshold, and its characteristics depend to a certain extent on the observable [12, 123, 273]. In the last decades, considerable progress has been made in determining the existence and signatures of error thresholds for a variety of fitness landscapes (see Refs. [11, 51, 54, 123, 273] and references therein), and we will briefly account for some major results. For general bounded fitness landscapes $0 < \alpha_{\min} \leq \alpha_k \leq \alpha_{\max} < \infty$, the approximation of accounting only for unidirectional mutations (those increasing the Hamming distance to the master) gives a bound on the error threshold [273]:

$$\mu_c \leq \frac{\ln(\alpha_{\max}/\alpha_{\min})}{L}, \quad (3.15)$$

implying that μ_c generally depends inversely on sequence length and logarithmically on the selective advantage of the master (the fitness ratio relative to the “worst” mutants). Accordingly, the maximal sequence length is limited by the inverse of the mutation rate. Note, however, that the approximate result Eq. (3.15) is at variance with the absence of a threshold for the multiplicative landscape: from Eq. (3.15), we would obtain $\mu_c \leq -\ln(1 - s)$, and in Fig. 3.1 we actually chose the numerical value of s such that this result for μ_c is identical with the one for the sharply-peaked case. Because the criterion Eq. (3.15) clearly is not completely satisfactory, another necessary (but not sufficient) condition for the existence of an error threshold has been found in requiring the presence of positive epistasis, meaning that the contributions of different sites to fitness are not independent; in particular, that additional mutations do not affect fitness as much as the first one does (for the sharply-peaked fitness landscape, they have no effect at all) [12, 123, 273].

Truncation fitness. The condition Eq. (3.15) fails in the presence of lethal mutations, which means that certain sequences do not reproduce at all (i.e., that $\alpha_{\min} = 0$), and the underlying calculation shows that there is no error threshold in this case [273]. Because quasispecies theory has been applied frequently to RNA viruses, which presumably

evolve so close to the error threshold that pharmaceutically increasing their already high mutation rates might even serve as antiviral strategy [53, 188], this finding has been very controversially discussed [27, 255, 279]. Within quasispecies theory, error thresholds for truncation landscapes have been found in cases where lethality is only encountered far away from the master sequence [224], or in densely connected genome spaces [259]. In contrast, the quasispecies distribution is known as “mutation-selection” balance within population genetics theory. However, the error threshold is often confused with the related, but qualitatively different phenomenon of “Muller’s ratchet” [95], which describes the irreversible loss of the fittest genotype due to stochastic number fluctuations in a finite population. The assumption of an infinite population size is certainly a major shortfall of quasispecies theory, because it misses the probably most essential evolutionary driving force: genetic drift due to the random sampling of offspring. These finite-size effects are generally unavoidable, given that the number of different sequences is enormously larger than any realistic population size. However, the distinct quasispecies distribution is seen also when accounting for finite populations [4, 195], and quasispecies theory is formally equivalent to common models in population genetics, such that these two formulations are in principle compatible, even though the error threshold concept might be unsuitable for RNA viruses [279].

The error threshold as a phase transition. The observation that the stationary quasispecies distribution can be obtained by diagonalizing a high-dimensional matrix (see Eq. (3.7)) prompted physicists to seek analogies to statistical and quantum mechanics in order to profit from the sophisticated methods developed for these fields. In general, this is possible if the matrix W in Eq. (3.6) has the same symmetries as the Hamiltonian of a known physics problem. Although fitness has frequently been identified with (negative) energy, it is *a priori* not at all obvious that these evolution models should have the same symmetries as a physical system. For instance, fitness can be a complicated function of all sequence letters and does not arise only via next-neighbor interactions (but note that exactly this feature also implies that mean-field approximations might be exact [10]).

The first analogy found was to an anisotropic two-dimensional Ising model [154, 155], where one direction corresponds to sequence and the other one to time. Exploiting transfer matrix methods, the error threshold for a sharply-peaked landscape arises through a first-order phase transition on the “stationary” surface $t \rightarrow \infty$ [261]. A more tractable correspondence is the one to a directed polymer in a random medium [76], which gives exact results for the sharply-peaked fitness landscape. It exhibits a first-order phase transition at the error threshold in the thermodynamic limit $L \rightarrow \infty$, if the mean Hamming distance is used as order parameter, in agreement with other authors [71]. Hence, although the observable x_0 for the sharply-peaked fitness landscape (see the right panel of Fig. 3.1) is continuous at the error threshold, the order parameter $\langle k \rangle$ (shown in the inset) is actually discontinuous for $L \rightarrow \infty$ and only significantly smoothed due to finite-size effects. Later, a different formulation of the rate equations has been mapped to an Ising quantum chain [10, 12], finding second-order transitions for some other landscapes. Recently,

these different approaches based on Ising models were united using so-called “maximum principles” that are essentially based on a saddle-point approximation [106, 225].

3.1.5. Neutrality in fitness landscapes

The notoriously difficult problem how a realistic fitness landscape should be defined has been simplified considerably, even though by far not solved, in the case of RNA by the development of efficient secondary structure folding algorithms (see, e.g., Ref. [231] for a review). In contrast to the protein case, RNA folding is largely determined by secondary structure (and only little by tertiary structure), which can be decomposed into independent energetic contributions of single structural elements like hairpins, loops, etc. Hence, the computation of the partition sum of all secondary structures for a particular RNA sequence can be done efficiently by means of recursion relations, with computational time scaling (only) as the third power of sequence length. If secondary structure is taken as phenotype, and (in a heuristic approach) some function of a suitably defined difference to a specific target structure as fitness, the evolution of RNA structures can be studied *in silico* [69, 118]. The adaptative evolution towards the target then appears as a discontinuous process of major innovation steps (corresponding to structural rearrangements) separated by stationary phases, where the population diffuses randomly within a specific neutral network, which is the set of sequences that fold into a given structure (and hence have identical fitness). Because the number of possible structures of a certain length is exponentially smaller than the corresponding number of sequences, the genotype-phenotype map for RNA displays the remarkable and potentially quite generic feature that the vast majority of possible phenotypes is accessible with just a few mutations from virtually any genotype [231]. On the one hand, the possibility of finding within the neutral network of any given structure a suitable starting point for a short transition to the neutral network of any other structure provides *adaptability*. On the other hand, the presence of neutral networks also yields *mutational robustness*, i.e., an insensitivity to deleterious mutations. Theoretical calculations show that populations evolving on neutral network tend to maximize robustness [194]. Especially at enhanced mutation rates, high robustness at lower fitness can even be more favorable than high fitness at lower robustness, a phenomenon that has been termed “survival of the flattest” [281].

In general, the degree of neutrality around a certain sequence depends on the location in sequence space. For theoretical studies, two main scenarios have been discussed. In one case, fitness is insensitive to a certain *number* of mutations. This comes from the biophysics of transcription factor binding [83], where the contributions of different letters to binding *energy* are additive, but fitness is proportional to the resulting binding *probability*. The latter is given by a Fermi function of binding energy with its characteristic plateau and allows therefore for a small number of mismatches (usually between 2 and 4). A theoretical analysis within quasispecies theory attributes the observed “fuzziness” of binding motifs to the underlying quasispecies-like sequence distribution [83]. In the second case, fitness is insensitive to mutations at certain *positions*. This notion results from the observation that exchanging certain nucleotides within an RNA sequence does not necessarily affect

the structure (for instance, those in loops). Recent mutation experiments indicate that ribozymes tolerate mutations at about 25% of their positions without loss of function [147]. A full theoretical analysis of this scenario is difficult because the fitness landscape is not permutation invariant. Within a simple estimate, we can assume that if a fraction λ of all positions is selectively neutral, the effective mutation rate is only $(1 - \lambda)\mu$, because the chance to hit a non-neutral site is $1 - \lambda$ (assuming that the neutral positions are uniformly distributed and that λ and μ are small, such that multiple mutations are independent) [260]. Using this argument leads to “phenotypic error thresholds” [260], which are accordingly increased by a factor $1 - \lambda$, just as one would get if the sequence length $L(1 - \lambda)$ effectively accounted only for the non-neutral positions [54].

3.2. Enzymatic catalysis

The previous section was concerned with the results of quasispecies theory for a variety of static fitness landscapes, but it is important to note that fitness is never simply a fixed quantity. The complicated and poorly understood mapping from genotype via phenotype to fitness involves a myriad of interactions with other components of the system. In every ecosystem, the fitness of one species depends on the environment, including other species whose abundances depend on their own fitness, which in turn is a function of the whole system etc. Exemplary ecosystems include catalytic networks of reacting chemicals, highly diversified food webs, and even the behavioral strategies of different interacting species. In all those cases, ongoing evolution is probably more often than not caused by adaptation to a *changed environment* instead of independently improved reproductive success.

Of course, realistic models for changing fitness are hard to come by. In the abstract and idealized framework of quasispecies theory, some authors studied sharply-peaked fitness landscapes with temporally oscillating or fluctuating peak height [193, 280], with the result that populations follow slow changes in fitness, while they adapt to its time-averaged value for fast changes. Further, a sharply-peaked fitness landscape was studied where the peak *location* changed by a single mutation at regular time intervals [192]: besides the usual error threshold, another critical mutation rate was found *below* which the population lacks sufficient adaptability to remain close enough to the fitness peak. Motivated by the coevolution of virus and immune system, a model developed in the following had the peak location change as result of adaptation of a second population, finding a similar adaptation threshold [128]. In this work, however, we are not so much interested in the time dependence of fitness but in its concentration dependence, as will become clear in the following.

3.2.1. Non-enzymatic vs. enzymatic replication

We recall that quasispecies theory originated as a description for the prebiotic evolution of self-replicating polynucleotides (see Sec. 1.2). As evolutionary model, it has been applied also to more complex species (such as bacteria or higher organisms), which create the

sophisticated apparatus necessary for reproduction from scratch, using just the instructions given in the genetic code and substrates taken up from the environment, in order to produce all the protein components involved in replication. To a first approximation, their fitness thus depends indeed only on their genotype, and a model using fitness landscapes as in Eq. (3.3) is appropriate.

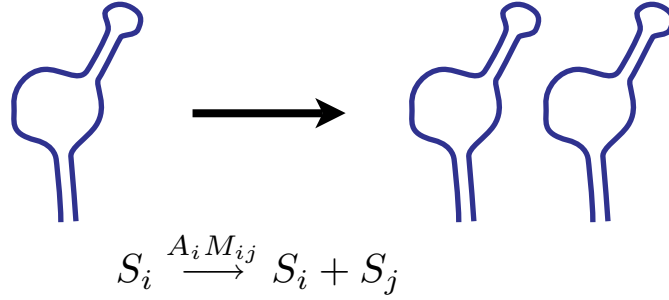
In contrast, a single replicating molecule has to perform these functions all by itself, i.e., it is genotype (template for the replication) and catalyst at the same time. Because it is not a reasonable hypothesis in a prebiotic scenario, we exclude the possibility that external replicase enzymes are present (such as the protein replicases used for *in vitro* evolution of ribozymes [126]). Hence, non-enzymatic self-replication is an autocatalytic process (no external enzymes are involved). Given that advanced catalytic functions cannot be expected from simple ribozymes, such molecules would have to rely on the spontaneous template-directed polymerization and ligation reactions illustrated in Fig. 1.5. As we discussed in the introduction, however, the polymerization reactions work reasonably well only for short molecules with rather specific sequences [1, 284]. Self-replication by ligation reactions can produce more complicated molecules [131, 134, 158, 212, 213], but only if the appropriate building blocks (which are also RNA oligomers) are provided, such that variations are rarely introduced and not heritable. In any case, Darwinian evolution has not been observed so far. One hypothesis suggested that fluidity or flexibility of RNA structures could allow template-directed polymerization at one part of the sequence to be catalyzed by another part of the same molecule [209]. These speculative ideas notwithstanding, it remains highly questionable how a single molecule should literally copy itself [126, 258].

We have illustrated the (pseudo first order) reaction scheme of non-enzymatic replication in Fig. 3.2(a). In contrast, we argue that *enzymatic* replication (shown in part (b)) is a far more likely scenario [206]. Here, the enzymatic replication of a certain sequence S_i is catalyzed by *another* molecule S_j , which could be an improved version of the polymerase ribozyme shown in Fig. 1.6. While the rate A_i of the non-enzymatic (or autocatalytic) reaction depends only on the template sequence, in the enzymatic case both genotypes (of substrate and enzyme) are potentially relevant, and the higher order rate constant is accordingly given by the matrix B_{ij} , which measures how efficiently the enzyme S_j catalyzes the replication of the template S_i . The important difference to the non-enzymatic case is that the enzyme S_j is an explicit part of the evolutionary model.

3.2.2. The replicator-mutator equation

In this section, we will set up a quasispecies model for the replication of sequence S_i through either non-enzymatic or enzymatic replication reactions. The former case gives a contribution $\dot{X}_i = A_i X_i$ as in Eq. (3.2), while the latter case involves enzymatic catalysis. At the low concentrations to be expected in a dilute prebiotic environment, we assume that these reactions are diffusion limited, such that the change \dot{X}_i through enzymatic replication is given by $\sum_j B_{ij} X_i X_j$, i.e., it is proportional to the concentrations X_j of all potential enzymes and their characteristics (entering through B_{ij}). Note that we defined the pseudo second order rate constants B_{ij} such that an additional volume dependence drops out

(a) non-enzymatic replication



(b) enzymatic replication

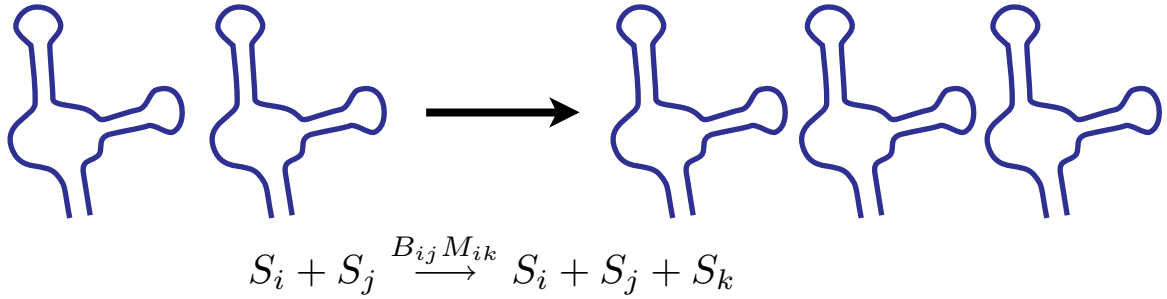


Figure 3.2: Non-enzymatic vs. enzymatic replication. In the former case (see part (a)), a molecule replicates itself autocatalytically, using only necessary substrates from the environment (no enzymes are involved). The rate A_i thus depends only on the genotype S_i , and replication may result in a different sequence S_j with probability M_{ij} . (b) The case of enzymatic replication involves (at least) two molecules: one is the template with sequence S_i , the other one (S_j) is the enzyme, catalyzing the creation of a possibly erroneous copy S_k . The rate constant B_{ij} depends therefore on both genotypes.

(recall that the concentration variables $X_i = N_i/N$ have been introduced as dimensionless quantities in Sec. 3.1).

Inserting the resulting replication rates $R_i = A_i + \sum_j B_{ij} X_j$ into the quasispecies equations, Eq. (3.2), which also account for mutations through the mutation matrix M_{ij} displayed in Eq. (3.1), gives the so-called replicator-mutator equation:

$$\dot{X}_i = \sum_j M_{ij} [A_j + \sum_k B_{jk} X_k] X_j - X_i \sum_j [A_j + \sum_k B_{jk} X_k] X_j. \quad (3.16)$$

Due to concentration-dependent replication rates, this equation is inherently nonlinear (linearization through the transformation Eq. (3.4) is not possible). In population genetics, this type of nonlinearity is called *frequency-dependent* fitness, which is usually caused by ecological interactions. It has indeed been observed for RNA viruses [59, 287].

In the contexts of ecological models and evolutionary game theory [115], where similar equations have been used, the different species S_i are not necessarily characterized by

a sequence, and the mutation matrix need not have the form Eq. (3.1). In most cases, the simpler replicator equation has been discussed, for which $M_{ij} = \delta_{ij}$ and $A_i = 0$. It lives in the concentration simplex $\sum_i X_i = 1$ and can be mapped to a Lotka-Volterra equation [115]. If the “pay-off matrix” B_{ij} is symmetric, this equation can be written as a so-called Shahshahani gradient of the Lyapunov function $\frac{1}{2} \sum_{ij} B_{ij} X_i X_j$, and if there is a fixed point in the interior in the simplex (implying coexistence of all species, i.e., positive concentrations $X_i > 0$), it is also unique and globally stable [115].

Introducing mutations can significantly change this picture. For small mutation rates, the rest point migration theorem predicts some fixed points to move into the interior of the simplex, while others are pushed to the unphysical outside; the phase portrait may thus be simplified considerably [249]. Further, also the replicator-mutator equation can be written as a gradient for special mutation matrices $M_{ij} = M_i$, where rates depend only on the target [114]. This simplification, which excludes nontrivial dynamics like limit cycles, has been used for models of grammar evolution, where the success of different grammatical variants depends on their frequency in the population and their similarity to other grammars, and new variants are chosen randomly [136, 137, 197]. In general, however, larger mutation rates such as those given in Eq. (3.1) can lead to complicated bifurcation scenarios, multiple equilibria, and even the appearance of limit cycles. Some low-dimensional examples for generic catalytic networks have been discussed in Ref. [248].

3.2.3. Hypercycles

Even the replicator equation as such gives rise to complex dynamics in cases where the matrix B_{ij} is not symmetric. One such example is the hypercycle, which has been suggested by Eigen and Schuster in the late 1970s as a possible remedy against the error catastrophe [55, 56, 57]. They imagined a specific network of n different species S_i , each of which replicates autocatalytically with rate A_i , but also catalyzes the replication of other molecules S_j with rate B_{ij} . The name “hypercycle” was chosen because a circular network topology was proposed, where each species catalyzes the replication of its next neighbor in the network, such that $B_{ij} \propto \delta_{i,i+1}$. Because a sequence containing all the information of n molecules might be too long to obey the error threshold, whereas n independently replicating shorter molecules compete with each other and cannot coexist, mutualistic catalytic interactions between different species could help to maintain their *combined* information content even in the presence of error-prone replication. Although this model was proposed as a means to beat the error threshold, mutations were initially not taken into account. In this case, it is easy to see that the resulting replicator equation admits an interior fixed point. For simplicity, we assume that all rates are equal: $A_i \equiv \alpha$, $B_{ij} = \beta \delta_{i,i+1}$, in which case the central fixed point is given by $X_i \equiv 1/n$. Its stability follows by analyzing the eigenvalues of the Jacobian, which is a circulant matrix and can easily be diagonalized. It turns out that the central fixed point loses stability for $n > 4$, giving rise to stable limit cycles with large concentration oscillations.

For a number of reasons, this model was strongly criticized. Especially John Maynard Smith raised doubts whether natural selection would actually favor the emergence and

the permanence of this quite artificial catalytic network [175]. For instance, mutations that increase the efficiency of the cycle as a whole (for instance, by making S_i a better replicase for S_{i+1}) are selected for only if they also lead to a more efficient replication of the mutated component (i.e., if the replicase S_{i-1} prefers to replicate the new S_i instead of the old one). Essentially, catalyzing the replication of *other* molecules is an altruistic property that evolves only if some higher-level selection is present, such as the one resulting from compartmentalization, which couples the growth of single species to the growth of the whole ensemble [257]. Similarly, the altruistic cooperation necessary for enzymatic replication can be exploited by parasites, i.e., molecules that are being replicated but do not catalyze the replication of others. In the hypercycle, parasites are easily created by mutations that destroy enzymatic function while retaining template potential. The spiral wave patterns that emerge from the oscillatory dynamics for $n > 4$ in a spatial hypercycle model have been shown to generate some resistance against parasites [9]. However, during the periods of very small concentrations, which are associated with these large-amplitude limit cycles, the single components of the hypercycle are very sensitive to stochastic fluctuations and may go extinct, causing the collapse of the entire cycle.

Interestingly, the deleterious effects of mutations that motivated the hypercycle concept in the first place were not investigated until many years later, when models were set up based on the error-tail approximation (see Sec. 3.1.3). Here, replication of each species results in an erroneous non-functional copy with probability $1 - (1 - \mu)^L$ [6, 7, 33, 79, 242]. It turns out that the resulting error threshold decreases logarithmically with the number of different species, such that the information capacity of a hypercycle is not as large as initially thought. Also, mutations that affect the catalytic couplings (for instance, by generating parasites) were not taken into account.

3.3. Specific enzymatic replication

The previous section has introduced some models for enzymatically catalyzed replication. Apart from the mathematical difficulties associated with the replicator-mutator equation discussed in Sec. 3.2.2, the enzymatic replication mode shown in Fig. 3.2(b) requires to specify the catalytic matrix B_{ij} , which is obviously much harder than choosing a realistic fitness landscape A_i . Trying to model how efficiently an enzyme S_j catalyzes the replication of a substrate S_i raises the question whether replication efficiency (or fitness) is a property of the enzyme or the substrate. If it depends only on the enzyme, mutations that improve its efficiency will not be selected for, because the enzyme replicates non-functional templates just as well as itself. On the other hand, if fitness is a property of the substrate, mutations that are advantageous for the substrate do not necessarily create, maintain, or improve enzymatic function. As discussed in Sec. 3.2.3, these issues are due to the fact that enzymatic function is an altruistic property, and it is therefore not clear how it should evolve in the first place, given that it is not necessarily of advantage for the enzyme itself [175]. Compartmentalization certainly is a plausible way to ensure that efficient replicators are preferentially enclosed in the same environment in order to sustain

their function, but it requires a simultaneous and coordinated evolution of protocells and replicators [36, 258]. In any case, we argue that enzymatic replicators should be good enzymes and good substrates at the same time. Enzymes should preferentially replicate functional substrates, and substrates should rather be replicated by efficient enzymes. As a possible means to enforce these necessary propensities, we propose *specific recognition*, implying that replication efficiency depends strongly on the interaction between enzyme and substrate. This hypothesized property of prebiotic replicators is not unlikely, given that ribozyme catalysis (e.g., of ligation, cleavage, or template-directed polymerization) is often strongly substrate-dependent [124, 126]. Unspecific recognition, in contrast, requires sophisticated substrate-binding properties that are probably a later evolutionary innovation [124].

In this section, we develop idealized quasispecies models for specific enzymatic replication and analyze various aspects in order to address two main questions: how can specific enzymatic replicators benefit from the altruistic property of giving catalytic help, and how does this affect the error threshold? In the first part (see Sec. 3.3.1), we investigate how highly specific recognition could be mediated via an otherwise neutral recognition region by means of a simple model. This work has been published in Ref. [199], which is reprinted in Sec. 3.6. The second part (see Sec. 3.3.2) generalizes these ideas by allowing specificity to be an arbitrary function of the Hamming distance between enzyme and substrate. Our results for error thresholds under general specificity functions, reprinted in Sec. 3.7, are published online [201] and submitted for publication in the Journal of Theoretical Biology.

3.3.1. Recognition regions and high specificity

Our study [199] is motivated by the experimental observation that catalytic and recognition regions of ribozymes such as the RNA component of RNaseP are often clearly separated [157]. Also, terminal tRNA-like structures have been speculated to act as genomic “tags” for the initiation of RNA replication [272]. While we do not actually model secondary structure in order to facilitate theoretical analysis, we assume that the corresponding sequence regions fold into distinct structural elements with either catalytic or recognition functions. We also suppose that catalytic function gives an essential contribution to non-enzymatic replication rate and that a molecule is only functional if the structural region is equal to the one of a master sequence S^* , as in a sharply-peaked fitness landscape. This catalytic property is unaffected by mutations in the recognition region, which is therefore essentially neutral. For enzymatic replication, we require that enzyme and substrate, apart from having catalytic function, also be identical in the recognition region, without specifying any particular optimal sequence. Hence, the replication rate of sequence S_i is given as

$$R_i = \begin{cases} \alpha + \gamma X_i & \text{if } S_i|_{\text{struc}} = S^*|_{\text{struc}}, \\ 1 & \text{otherwise.} \end{cases} \quad (3.17)$$

Here, $\alpha > 1$ is the selective advantage, γ is the second order rate constant, and $S|_{\text{struc}}$ denotes the restriction of the sequence S to the structural sites. Clearly, we also assume

that structural and recognition region are somehow coupled in order to ensure that non-functional substrates (those with mutations in the structural region) cannot properly be recognized by functional enzymes.

We proceed with a stochastic simulation based on the algorithm discussed in Ref. [280]. Starting with a population of functional sequences with random recognition regions, we observe stochastic fluctuations leading at some point to the emergence of a randomly chosen master sequence in the recognition region, surrounded by a quasispecies distribution of mutants. Even though initially all functional sequences have the same concentration, and by Eq. (3.17) the same replication rates, stochastic fluctuations imply fitness advantages which can lead to the “fixation” of one particular sequence (which we call the master sequence for simplicity), similar to the phenomenon of consensus formation in language evolution [21]. Hence, highly specific recognition allows enzymatic self-replicators to conserve their information content.

These results are quantitatively analyzed by means of the error-tail approximation, where we distinguish enzymatic replicators (functional molecules with a recognition sequence equal to that of the master), non-enzymatic replicators (functional molecules with random recognition sequence) and an error-tail. Mutations are only considered if they lead to the less-fitter class. Because the recognition sequence of the non-enzymatic replicators is neutral, these molecules are mutationally more robust. From this analysis, we obtain two error thresholds: one at a mutation rate $\mu_{c,n}$ separates the non-enzymatic regime from the delocalized state, and is similar to the “phenotypic” error threshold discussed in Sec. 3.1.5. The other one ($\mu_{c,e}$) delineates the enzymatic regime. For large $\gamma \gg \alpha$, we find asymptotically $\mu_{c,e} \sim \ln \gamma / (2L)$. Compared to the usual case in a static fitness landscape (where $\mu_c \approx \ln \alpha / L$, see Eq. (3.14)), the error threshold is reduced by a factor of 2, if we choose the values of the logarithms numerically equal (correspondingly, the two error thresholds are comparable only if $\gamma = \mathcal{O}(\alpha^2)$ is quite large). We explain this essential difference by an “escalation of the error catastrophe”: because the fraction of enzymatic replicators with the correct recognition sequence declines as the mutation rate is increased, their replication rate, Eq. (3.17), decreases as well, leading to an even stronger reduction in their concentration. At the error threshold, the concentration of suitable enzymes is not large enough to have them replicate with sufficient efficiency to be maintained at a macroscopic level. A similarly discontinuous transition in the concentration of the master sequence has been found in related models [33, 268].

Finally, we generalize these results to a simple hypercycle model, where different species catalyze each other’s replication if they specifically recognize each other. Analogously to the traditional case discussed in Sec. 3.2.3, we find a central coexistence fixed point, which is stable only for $n \leq 4$. Also, specific recognition via a recognition sequence can be maintained only below the error threshold, which asymptotically is given by $\mu_{c,e} \sim \ln(\gamma/n)/(2L)$. As an illustration, this implies that the supposedly larger mutational tolerance of a two-member hypercycle with two sequences of length L is actually only about equal to that of one single sequence of length $2L$ because of the reduced error threshold.

3.3.2. General specificity functions

The results discussed in the preceding section revealed that frequency-dependent replication rates give qualitatively different error thresholds, viz., a discontinuous transition of the concentration of the master sequence. We were motivated by the question how specific recognition can serve to maintain the altruistic property of catalytic function in these replicators. In our second study [201], we generalize the above model, which allowed enzymatic replication only for *identical* molecules, to arbitrary specificity functions, in order to elucidate how our findings depend on the *degree* of specificity.

To this end, we consider only recognition regions (the structural regions largely behave as in a simple fitness landscape) and assume that the catalytic matrix is a function of the Hamming distance d_{ij} between enzyme S_j and substrate S_i , while the non-enzymatic rate is a constant:

$$R_i = \alpha + \sum_j \beta f(d_{ij}) X_j. \quad (3.18)$$

Hence, we assume that replication efficiency (which could depend on both genotypes of enzyme and substrate) is only a function of the mismatches between the respective recognition regions, similar to the case of transcription factor binding briefly discussed in Sec. 3.1.5 [83], and that non-enzymatic replication rates are so small that their genotype dependence is irrelevant. Our choice implies that enzymatic function and template potential are both intrinsically coupled to the quality of recognition.

Although it is not *a priori* clear whether the associated replicator-mutator equation has a stable fixed point in the interior with all species present (cf. Sec. 3.2.2), we assume that stochastic fluctuations cause the formation of a quasispecies about a randomly chosen master sequence as in the previous section. The localization about one specific sequence allows then to perform a symmetrization of the rate equations in terms of error classes as in Sec. 3.1.3, resulting in reduced rate equations formally equivalent to the replicator-mutator equation, Eq. (3.16), with accordingly symmetrized mutation and catalytic matrices (for the former, see Eq. (3.9)). Note, however, that our frequency-dependent fitness, given through Eq. (3.18), is not strictly permutation invariant: replication rates depend on the Hamming distance between two arbitrary sequences *and* their respective concentrations, a complication that can be resolved by assuming that the error classes are homogeneously populated, which is justified by the excellent agreement with results from stochastic simulations.

In a first part, we concentrate on a specificity function for *self-specific* replication: $f_s(d) = (1 - d/L)^p$, with some exponent $p > 0$. While the limit $p \rightarrow \infty$ of high specificity relates to the situation addressed in the previous section, and corresponds to the generalized Schlögl model of autocatalytic replication partly analyzed in Ref. [248], the limit $p \rightarrow 0$ results in very low specificity (yet it is finite, because always $f_s(L) = 0$). It turns out that both cases allow localization about a master sequence for small enough mutation rates $\mu < \mu_c$. Localization is not observed if specificity is completely absent ($f_s \equiv 1$), because unspecific enzymes do not have a selective advantage. In general, stronger specificity constraints (i.e., larger p) give larger error thresholds, because the population distributions are more

localized, and the escalation of the error catastrophe is thus better controlled. However, a larger specificity degree also gives rise to bistability with the delocalized regime for mutation rates larger than a second threshold $\tilde{\mu}_c$. Utilizing a moment closure approximation, where we assume the population distribution to be binomially distributed in order to calculate the mean Hamming distance $a = \langle k \rangle / L$ for arbitrary specificity functions, we find that a pitchfork bifurcation is responsible for this effect: bistability is found in the subcritical situation where β is smaller than a critical value β^* , for which we give an explicit expression. We also analyze the case $\alpha = 0$ of vanishing non-enzymatic replication rate, where we find macroscopic (length-independent) values for the error threshold, which is a consequence of the subtleties of truncation landscapes discussed in Sec. 3.1.4.

In the second part, we analyze *cross-specific* replication with $f_c(d) = (d/L)^p$, where enzyme and substrate should be complementary, as an example for a two-member hypercycle. By means of analogous moment closure calculations, we find that the expected localization about complementary sequences is possible only if $p > 1$, i.e., if catalytic rates increase stronger than linearly with Hamming distance. In the strong-specificity limit $p \rightarrow \infty$, we obtain two equivalent and effectively independent populations, which justifies the use of the error-tail approximation in simplified models such as the one discussed in the previous section.

Although our analytical results have been obtained by means of a heuristic moment closure approximation, they are in good agreement with numerical solutions of the reduced rate equations for finite L . Further, our results for the error threshold μ_c are exact for a supercritical pitchfork bifurcation, and the asymptote of the subcritical case for $p \rightarrow \infty$ and large β agrees with the value obtained by the error-tail approximation, such that we have no reason to believe that our results should fail in the limit $L \rightarrow \infty$. Finally, we extrapolate from experimentally measured non-enzymatic and enzymatic polymerization rates to obtain a rough estimate for the maximum length L_c of the recognition region that can be used to reliably discriminate appropriate and infeasible enzymes and substrates, respectively. Depending on the degree of specificity, we find that L_c is between 11 and 33 nucleotides, given the mutation rates of about 3% observed on polymerase ribozymes [124], which implies that the error threshold severely constrains the information content of enzymatic replicators as well.

3.4. Conclusions

This chapter presented a theoretical discussion of quasispecies models for specific enzymatic self-replication. After reviewing the main results of quasispecies theory for different fitness landscapes, we argued that enzymatically catalyzed replication with frequency-dependent fitness is the more likely scenario under prebiotic conditions. However, enzymatic catalysis is an altruistic trait that is not necessarily advantageous for the enzyme itself. We propose that specific recognition could help to ensure that enzymes replicate preferentially functional substrates. We analyzed in Sec. 3.3.1 a simplified model, where specific recognition is mediated through an otherwise neutral recognition region. Our results show that

stochastic fluctuations lead to the emergence of a quasispecies-like mutant distribution about a randomly chosen master sequence. Its information content can be maintained for mutation rates smaller than an error threshold which is significantly reduced compared to the value for non-enzymatic replication due to an escalation of the error catastrophe. In Sec. 3.3.2, we generalized our model to allow for arbitrary specificity functions that depend only on the Hamming distance between enzyme and substrate. We find that a small degree of self-specificity suffices to localize a population about a master sequence, and that stronger specificity gives larger error thresholds. By means of an analytical moment closure technique, we were able to analyze the full phase diagram of localization regimes. We also analyzed the case of cross-specific replication and found that specificity needs to increase stronger than linearly with Hamming distance to allow for simultaneous localization about complementary sequences. Finally, we obtained rough numerical estimates for the maximum length of the recognition sequence permitted by the error catastrophe.

3.5. Outlook

Because the high mutation rates of RNA viruses and their enormous population sizes lead to a considerable genetic diversity even within a single host [188], the evolutionary dynamics of RNA viruses has often been described within quasispecies theory. In addition to speculations that mutagenic agents could drive these viruses into the error catastrophe [53], this approach also motivates an analysis of the coevolutionary dynamics between the virus population and the host's immune system. Previous studies have modeled the effect on the adaptive immune response as causing a shift in the location of the fitness peak for the virus [128], neglecting the essentially frequency-dependent fitness interaction between host and parasite. Similar to our work discussed in Sec. 3.3.1, this dynamics can be modeled within the error-tail approximation. It turns out that stochastic noise should not be neglected because of an intriguing interplay with slowly decaying deterministic oscillations [233].

Escalation of error catastrophe for enzymatic self-replicators

B. OBERMAYER and E. FREY^(a)

Arnold-Sommerfeld-Center for Theoretical Physics and Center for NanoScience, Ludwig-Maximilians-Universität München - Theresienstr. 37, 80333 München, Germany, EU

received 24 July 2009; accepted in final form 9 November 2009
published online 3 December 2009

PACS 87.10.-e – General theory and mathematical aspects

PACS 87.23.Kg – Dynamics of evolution

PACS 87.15.R- – Reactions and kinetics

Abstract – It is a long-standing question in origin-of-life research whether the information content of replicating molecules can be maintained in the presence of replication errors. Extending standard quasispecies models of non-enzymatic replication, we analyze highly specific enzymatic self-replication mediated through an otherwise neutral recognition region, which leads to frequency-dependent replication rates. We find a significant reduction of the maximally tolerable error rate, because the replication rate of the fittest molecules decreases with the fraction of functional enzymes. Our analysis is extended to hypercyclic couplings as an example for catalytic networks.

Copyright © EPLA, 2009

Introduction. – According to the RNA world hypothesis [1], prebiotic biochemical life is thought to have emerged through four steps: starting from the primordial non-enzymatic synthesis of nucleotides and their subsequent non-enzymatic polymerization into random RNA, which in a third step would non-enzymatically replicate, natural selection would finally produce a set of functional RNA enzymes (ribozymes), establishing exponential growth and initiating RNA evolution. Despite considerable experimental progress [2,3], as of today no truly self-replicating system has been evolved according to this hypothetical schedule. To assess its intrinsic plausibility, theory has mainly focused on the third step, usually based on the Eigen model [4] for prebiotic evolution: here, auto-catalytic self-replication of L -nucleotide sequences proceeds non-enzymatically via stepwise template-directed polymerization, with a non-negligible error probability μ per single nucleotide. Assuming that one specific “master” template replicates with the highest rate $\alpha > 1$, while all other sequences have unit replication rate, it is found that faithful replication of the master is possible only for error probabilities smaller than a critical value $\mu_c \approx \ln \alpha / L$. In this regime, the population in sequence space is concentrated about the master in a rather broad distribution, giving rise to the notion of a “quasispecies”. Larger values $\mu > \mu_c$ lead to a delocalized state with completely random sequences in the population. Many aspects of the Eigen model

depend to a large extent on the chosen fitness landscape, which assigns replication rates to genotypes. In the case of RNA, it displays a considerable degree of neutrality, because the mapping of sequences to secondary structures is decidedly many-to-one [5]. Still, although not universal, the existence of a critical mutation rate μ_c is a comparatively robust phenomenon [6,7]. It has been termed “error catastrophe” [8], because it puts possibly irreconcilable simultaneous constraints on maximally tolerable error probability and minimal functional sequence length.

Lacking actual observations of freely self-replicating RNA and hence reliable estimates for replication rates, these theoretical limitations of non-enzymatic RNA replication are not yet reasonably quantitative. However, biochemical issues [9] raise severe doubts about its plausibility as well. Although ribozymes have been discovered that catalyze most of the necessary reaction steps [2,3,10,11], it remains questionable how a ribozyme should literally copy itself [10,12]. Enzymatic replication seems the far more likely scenario, in the sense that a ribozyme copies other molecules. Presumably and most effectively, it would copy only those molecules that are exact replicas of itself, not only because known ribozymes act very substrate-specific, but also because unspecific recognition does not give a selective advantage to the replication enzymes themselves; this would require compartmentalization in vesicles to keep closely related molecules together [12]. Further, it has recently been suggested that the spontaneous emergence of RNA polymerases even without previous non-enzymatic replication

^(a)E-mail: frey@physik.lmu.de

could be promoted by a significant increase of functional complexity in a pool of random RNA due to the likely appearance of ligase activity [13].

In order to comparatively analyze non-enzymatic and enzymatic replication, their competition and their respective tolerance against mutations theoretically and by means of stochastic simulations, we employ a simplified quasispecies model, where sequences replicate both non-enzymatically and enzymatically, the latter with high specificity. We find a coexistence regime of these two replication modes, and an escalation of the error catastrophe in the enzymatic case: because the replication rate of the fittest molecules decreases with the fraction of functional enzymes, the maximally tolerable mutation rate is significantly reduced. To make contact to models of modular evolution and catalytic networks, where complex function is assumed to emerge through independent selection of small functional motives, thereby circumventing the error catastrophe [14,15], we then extend our analysis to the case of hypercycles [8,16,17].

Model. – Motivated by the observation that catalytic and recognition regions are often clearly separated in ribozymes like the RNA component of RNaseP [11], we assume that the specific recognition mediating enzymatic replication involves only a small fraction λ of otherwise selectively neutral sites. This means that the majority of sites forms the proper secondary structure of the molecule and builds its active center, which catalyzes the polymerization reactions. Although secondary structure folding algorithms provide an improved genotype-fitness mapping through an excellent approximation to RNA phenotypes, our model is formulated in terms of sequences instead of structures to allow for analytical treatment. We hence distinguish between “structural sites” and a “recognition region” on the sequence level (see fig. 1 for a schematic illustration of our model). For the former, we use a sharply-peaked fitness landscape: a master sequence S^* has the highest non-enzymatic replication rate $\alpha > 1$, while all other sequences replicate with unit rate defining the time scale. We ignore possibly neutral sites in the structural region, because on our level of approximations this merely renormalizes their total number, or, equivalently, the mutation probability (see below). However, we do account for mutations in the recognition region, which do not affect non-enzymatic replication but the specificity of enzymatic replication: idealizing “highly specific”, we require the recognition regions of enzyme and substrate to be identical for enzymatic replication to take place. Hence, ribozymes replicate only exact copies of themselves, with γ the associated rate constant. Note that we do not make any restrictions on the specific sequence of the recognition region: any molecule with the correct sequence for the structural sites can replicate enzymatically if it recognizes a suitable enzyme.

In the following, we formalize this model in the framework of quasispecies theory [4], where molecules are

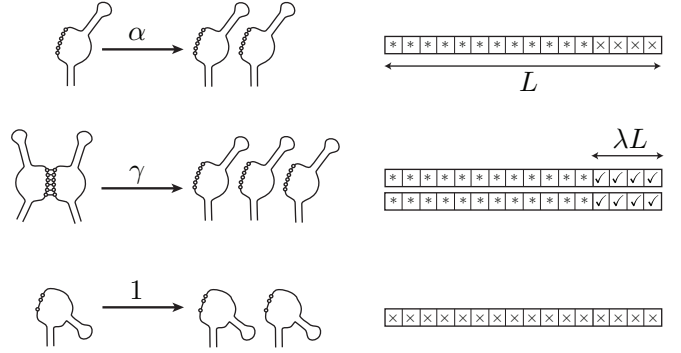


Fig. 1: Schematic illustration of the model. Left: Molecules with correct structure can replicate non-enzymatically with rate $\alpha > 1$. These molecules can also replicate enzymatically with rate γ , if they bind specifically to an identical partner within an otherwise selectively neutral recognition region of λL sites (dots). Misfolding mutant molecules replicate with unit rate. This model is formulated in terms of sequences rather than structures, as shown on the right panel: we distinguish correct “structural” nucleotides (*), matching sites in the recognition region (✓) and unmatching or random nucleotides (×).

represented by sequences $S_i = (\sigma_1^{(i)} \sigma_2^{(i)} \dots \sigma_L^{(i)})$ of L binary nucleotides $\sigma_j \in \{0, 1\}$. Their concentrations x_i evolve in the L -dimensional hypercube according to the deterministic rate equations

$$\dot{x}_i = \sum_k m_{ik} r_k x_k - x_i \bar{r}, \quad (1)$$

where r_k is the replication rate of S_k , $m_{ik} = \mu^{d_{ik}} (1 - \mu)^{L-d_{ik}}$ is the mutation probability between sequences S_i and S_k with Hamming distance d_{ik} , and μ is the single-nucleotide mutation probability. The second term in eq. (1) involves the mean replication rate $\bar{r} = \sum_k r_k x_k$ and ensures the normalization $\sum_k x_k = 1$. According to the above-defined model, the replication rates read

$$r_k = \begin{cases} \alpha + \gamma x_k, & \text{if } S_k|_{\text{struc}} = S^*|_{\text{struc}}, \\ 1, & \text{otherwise.} \end{cases} \quad (2)$$

In eq. (2), $S_k|_{\text{struc}}$ denotes the restriction of the sequence S_k to the structural sites, and $S^*|_{\text{struc}}$ is the corresponding master sequence. While replication rates are usually taken as functions only of the genotype, with one single peak at the master sequence [4,6,7,18–20], our model leads to frequency-dependent selection, which has only rarely been analyzed because it leads to mathematically challenging replicator-mutator equations (see, *e.g.*, ref. [21]).

Stochastic simulation. – For a realization of the full 2^L -dimensional system eq. (1) in a finite population of N sequences, we employ the straightforward stochastic simulation algorithm used in ref. [22]. At each time t each sequence S_k , present in n_k copies, has a probability $p_{0,k} = n_k / \sum_i n_i (1 + r_i)$ to be copied without mutations into the population at time $t+1$, and a probability

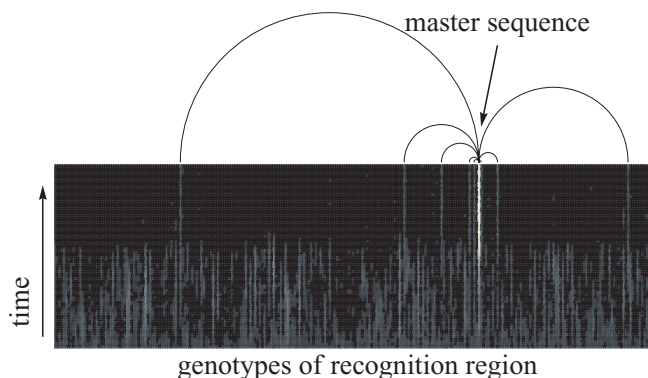


Fig. 2: Exemplary run of the stochastic simulation in a population of $N = 10^3$ sequences for $L = 32$, $\alpha = 5$, $\gamma = 10$, $\lambda = 1/4$, and $\mu = 0.005$. All sequences have been initialized with correct structural region but random recognition region. Their concentration is shown in gray level as a function of time and genotype in the recognition region (linearly arranged by reading bit strings as integer numbers). Spontaneous concentration fluctuations lead to the establishment of a quasispecies of enzymatic replicators centered about one specific yet randomly chosen master sequence. Neighboring sequences are indicated by thin lines.

$p_{\text{mut},jk} = m_{jk}r_k n_k / \sum_i n_i(1+r_i)$ to be selected and mutated into sequence S_j . The population is initialized uniformly at the master sequence, but with random recognition sequences. Because the sites of the recognition sequence are effectively neutral, a state with all possible recognition sequences present in equal concentration is stable for large sequence length [21]. But if number fluctuations sufficiently increase the concentration of one particular *yet randomly chosen* sequence, this conveys via eq. (2) a selective advantage, and its concentration will thus increase, up to the extent that mainly this sequence and its next mutational neighbors are present, in a quasispecies distribution very much like the one obtained in usual fitness landscapes. Figure 2 shows an example of this outcome, which is somewhat reminiscent of a fixation event. While its detailed dependence on the specific formulation of the underlying stochastic process and the parameter values is left for future research, the localization itself turns out to be a robust phenomenon. In the following, we will therefore without loss of generality assume that the recognition region of the most populated sequence is equal to the one of the master sequence S^* .

Results. – While analytic solutions to the $2L$ -dimensional system eq. (1) are hard to obtain, we can use the so-called “error-tail” approximation [19]: here, we introduce three different classes of molecules. In x_e , we gather enzymatic replicators identical to the master sequence, with a replication rate $r_e = \alpha + \gamma x_e$. We use a second class x_n for non-enzymatic replicators, with structural sites identical to the master sequence but random recognition sequences. Their replication rate is $r_n = \alpha$: although they are capable of enzymatic replication,

the fraction of suitable enzymes with the appropriate recognition region is negligible. Finally, $1 - x_e - x_n$ is the error-tail of molecules with incorrect structural sites and unit replication rate. The main approximation of the error-tail approximation is to consider only those mutations that lead into a less-fitter class, with the probability not to have such a mutation abbreviated as “quality factor” Q . This approximation is generally valid for large sequence length but may fail if peaks in the fitness landscape are very dense [7]. The enzymatic replicators in x_e have $Q_e = (1 - \mu)^L \equiv Q$, because a single error in L nucleotides suffices to destroy either structural or recognition region. The non-enzymatic replicators in x_n have a larger quality factor $Q_n = (1 - \mu(1 - \lambda))^L \approx Q^{1-\lambda} > Q$: because the presence of λL neutral sites in the recognition region reduces the effective mutation probability, these sequences are mutationally more robust [23–25]. Further, with probability $Q^{1-\lambda} - Q$ mutations in x_e will hit a site of the recognition region and thus contribute to x_n . Hence, the dynamical system in the error-tail approximation is given by

$$\begin{aligned} \dot{x}_e &= r_e Q x_e - x_e \bar{r}, \\ \dot{x}_n &= r_n Q^{1-\lambda} x_n + r_e (Q^{1-\lambda} - Q) x_e - x_n \bar{r}, \end{aligned} \quad (3)$$

where the mean replication rate reads $\bar{r} = (r_e - 1)x_e + (r_n - 1)x_n + 1$. Solutions to the stationary state $\dot{x}_e = \dot{x}_n = 0$ of eq. (3) for different mutation probabilities μ are shown in fig. 3, together with results from a stochastic simulation of the full system with the replication rates eq. (2) in a population of $N = 10^4$ sequences, where we initialized the sequences uniformly at the master sequence to reduce noise resulting from the intrinsically stochastic “fixation” events shown in fig. 2, and averaged the results over time after reaching a stationary state. Obviously, approximating the deterministic rate equations with the simplified eq. (3) gives an excellent description of the stochastic system. We can clearly distinguish three different regimes, separated by two error thresholds.

For high mutation probability, the population is delocalized over sequence space and only the error tail is significantly populated ($x_e = x_n = 0$). For smaller values of μ , we find a “non-enzymatic regime”, where sequences with correct structural region are present, but a stable recognition sequence cannot be maintained, such that enzymatic replication is not possible. Explicitly, we find $x_e = 0$ and $x_n = (\alpha Q^{1-\lambda} - 1)/(\alpha - 1)$. The two regimes exchange stability at $Q = \alpha^{-1/(1-\lambda)}$, corresponding to $\mu = \mu_{c,n} \approx \ln \alpha / (L(1 - \lambda))$. This is the familiar “phenotypic error threshold” [24,25]: the presence of neutral sites renormalizes the effective mutation probability, equivalent to having a shorter sequence [4].

For smaller mutation probabilities $\mu < \mu_{c,e}$ the “enzymatic regime” becomes stable. Here, the fraction x_e of enzymatic replicators is nonzero, but $x_n > 0$ as well, because this class is fed from x_e through mutations in the recognition region. Solving a third-order polynomial for x_e

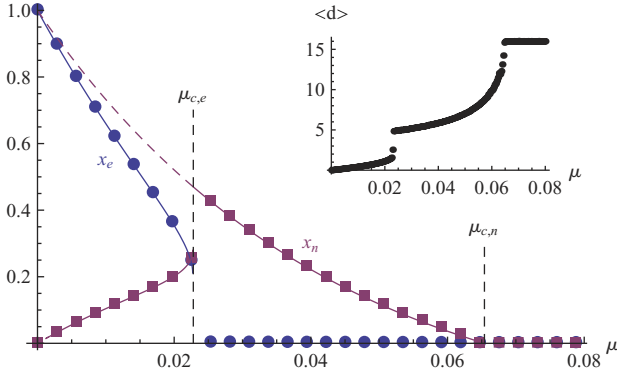


Fig. 3: (Color online) Comparison between simulation results for x_e (circles) and x_n (squares) in a population of $N = 10^4$ sequences and solutions to eq. (3) for $L = 32$, $\alpha = 5$, $\gamma = 10$ and $\lambda = 1/4$. The two error catastrophes occur at $\mu_{c,e} \approx \ln Q_c^{-1}/L$ with Q_c a solution of eq. (4) and $\mu_{c,n} \approx \ln \alpha / (L(1 - \lambda))$. The inset shows the average Hamming distance $\langle d \rangle$ to the master sequence, which increases in two steps, the first one at $\mu_{c,e}$ discontinuous, the second one at $\mu_{c,n}$ continuous.

and x_n , we find this regime is stable when the corresponding discriminant is positive, which yields a critical value $Q = Q_c$ from the condition

$$\begin{aligned} & 4 \left[3\gamma(1 + \alpha Q_c(Q_c^{-\lambda} - 2)) - (\gamma Q_c + Q_c^{-\lambda} - \alpha)^2 \right]^3 \\ & + \left[9\gamma(\alpha - \gamma Q_c - Q_c^{-\lambda})(1 + \alpha Q_c(Q_c^{-\lambda} - 2)) \right. \\ & \left. + 27\alpha\gamma(\alpha Q_c - 1)(1 - Q_c^{-\lambda}) + 2(\gamma Q_c + Q_c^{-\lambda} - \alpha)^3 \right]^2 = 0. \end{aligned} \quad (4)$$

Asymptotic solutions are given by

$$Q_c \sim \begin{cases} 1 - \frac{\gamma}{4\alpha\lambda}, & \text{if } \gamma \ll \alpha, \\ \frac{2\sqrt{\gamma} - 1}{\gamma} + \frac{\lambda}{\gamma} \ln \frac{2\sqrt{\gamma} - 1}{\gamma} + \mathcal{O}(\lambda^2), & \text{if } \gamma \gg \alpha. \end{cases} \quad (5)$$

Note that the large- γ -limit is $Q_c \sim 2/\sqrt{\gamma}$, which implies for the corresponding critical value $\mu_{c,e} \approx \ln Q_c^{-1}/L \approx \ln \gamma / (2L)$. This significant reduction by a factor of 2 can be phrased as “escalation of error catastrophe”: as the fraction x_e of enzymatically replicating sequences drops with higher mutation probability, their replication rate $r_e = \alpha + \gamma x_e$ decreases as well, leading to an even stronger reduction in x_e . Beyond the critical value $\mu_{c,e}$, the fraction of molecules with the correct recognition sequence becomes so small that their replication rate is not large enough for them to be maintained in the population at a macroscopic level.

An important difference between the transitions at $\mu_{c,n}$ and $\mu_{c,e}$ can be observed not only in the fraction x_e , but also in the width of the population distribution (measured as average Hamming distance to the master sequence), shown in the inset of fig. 3: while the delocalization transition at $\mu = \mu_{c,n}$ is continuous, the transition at $\mu_{c,e}$ is discontinuous. In the former case, this property depends

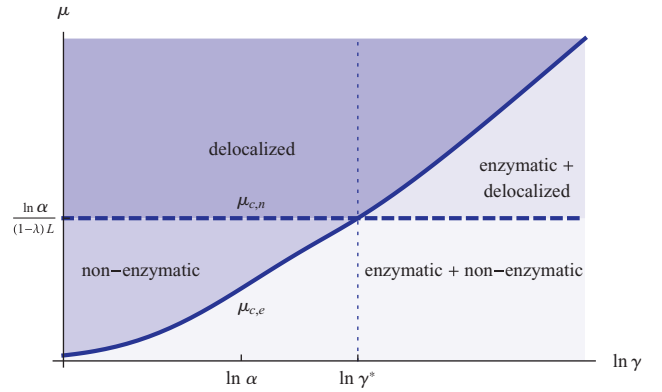


Fig. 4: (Color online) Phase diagram of stability regimes of eq. (3) in the $\ln \gamma - \mu$ -plane: the critical value $\mu_{c,n}$ (thick dashed line) separates the delocalized regime (above) and the non-enzymatic regime (below). Enzymatic replication is stable below $\mu_{c,e}$ (thick solid line) and becomes mutationally more robust than non-enzymatic replication if $\gamma > \gamma^* = \mathcal{O}(\alpha^2)$ (vertical line).

also on the choice of observable [7], but in the latter case, the discontinuity results from bistability: together with the enzymatic regime, also the non-enzymatic regime or the delocalized phase may be stable, depending on whether μ is larger or smaller than $\mu_{c,n}$, and if $\mu > \mu_{c,e}$ the enzymatic regime vanishes. The phase diagram in fig. 4 summarizes these various regimes. Note that $\mu_{c,e} = \mu_{c,n}$ at a critical value

$$\gamma^* = \alpha(\alpha - 1) + 2\lambda^{1/2}\alpha\sqrt{2\alpha(\alpha - 1)\ln \alpha} + \mathcal{O}(\lambda). \quad (6)$$

This result implies that very large rates $\gamma = \mathcal{O}(\alpha^2)$ are required if enzymatic replication is to be more error-tolerant than non-enzymatic replication [16]. Although this possibility is not contained in the approximate eq. (3), we find that in the bistability region $\mu < \min(\mu_{c,e}, \mu_{c,n})$ the enzymatic regime is easily populated by selectively advantageous concentration fluctuations from the non-enzymatic regime by randomly choosing a “master” sequence for the recognition region as shown in fig. 2.

Extension to hypercyclic couplings. – The realization that replication errors limit the maximum complexity of self-replicating molecules to a possibly paradoxical extent has led to theories of *modular* evolution, where complex functions emerge through catalytic interactions of smaller independently selected motifs [14,15], thereby also speeding up evolution by facilitating the search for complexity. While arbitrarily complex interaction networks between different modules or molecular species are conceivable, the simplest case applicable to the above system with its two-molecule interactions is the hypercycle [8]. Here, n species are arranged in a circular directed graph, where each species enzymatically catalyzes the replication of its next neighbor. This network gives rise to coexistence of all species, in a stable fixed point for $n \leq 4$ and via periodic orbits for larger n . In contrast to

previous approaches accounting for replication errors in a hypercycle [16,17], we consider distinct error tails for all species: each is present in an enzymatically active variant $x_{e,i}$ with replication rate $r_{e,i} = \alpha_i + \gamma_i x_{e,i+1}$ together with its non-enzymatic error tail $x_{n,i}$ with replication rate $r_{n,i} = \alpha_i$. In addition, there is the global error tail of misfolding mutants. For simplicity, we assume a symmetric setup with identical rate constants $\alpha_i \equiv \alpha$ and $\gamma_i \equiv \gamma$. This gives the rate equations

$$\begin{aligned} \dot{x}_{e,i} &= r_{e,i} Q x_{e,i} - x_{e,i} \bar{r}, \\ \dot{x}_{n,i} &= r_{n,i} Q^{1-\lambda} x_{n,i} + r_{e,i} (Q^{1-\lambda} - Q) x_{e,i} - x_{n,i} \bar{r}, \end{aligned} \quad (7)$$

where indices are taken modulo n and the mean fitness is now given by $\bar{r} = (\alpha - 1) \sum_i (x_{e,i} + x_{n,i}) + \gamma \sum_i x_{e,i} x_{e,i+1} + 1$. It is easy to see that this system reduces to eq. (3) if we assume that $x_{e,i} \equiv x_e^*/n$ and $x_{n,i} \equiv x_n^*/n$ and replace $\gamma \rightarrow \gamma/n$. Then, the ‘‘enzymatic’’ solution of eq. (3) corresponds to the inner fixed point of the hypercycle, where all species are present in equal concentration. Replication errors can be tolerated only if $\mu < \mu_{c,e}$, where $\mu_{c,e} \sim \ln(\gamma/n)/(2L)$ for large γ (see also ref. [16]). We emphasize that in contrast to ref. [14], where the results of unspecifically ligating functional motifs did not affect replication rates, in our model specific recognition between different species leads to frequency-dependent replication rates. This reduces the error threshold by roughly a factor of 2, which in a two-member hypercycle would cancel the putative complexity gain resulting from using two subunits of half the sequence length.

Moreover, increasing the number of hypercycle members beyond $n = 4$ changes the stability of the central fixed point. Observing that the Jacobian matrix of eq. (7) is block-circulant [26] (every block is a 2×2 -matrix for the two concentration variables $x_{e,i}$ and $x_{n,i}$ per species), its crucial eigenvalues with possibly non-negative real part are given by $\frac{1}{n} \gamma Q x_e^* e^{2im\pi/n}$, where $m = 0, \dots, n-1$ and x_e^* is the enzymatic solution of eq. (3) with $\gamma \rightarrow \gamma/n$. Hence, these eigenvalues are proportional to the n different n -th roots of unity. In close correspondence to the error-free hypercycle (and in contrast to ref. [16], where a stability region for $n = 5$ was found), the central fixed point loses stability for $n > 4$, giving rise to limit cycles with large concentration oscillations, which are vulnerable to extinction via stochastic fluctuations.

Note that the stable inner fixed point corresponding to the enzymatic regime implies coexistence of different species. However, in the non-enzymatic regime of eq. (3), the different error tails do compete against each other. As soon as the hypercycle breaks down, *e.g.*, because the recognition sequence is lost due to stochastic fluctuations, one error tail will drive the others to extinction, due to the competitive exclusion principle encountered in usual quasispecies theory [4]. This makes the reverse process, *i.e.*, a fluctuation that establishes a closed cycle, extremely unlikely.

Conclusion. – In summary, we have analyzed a simple quasispecies model for the non-enzymatic and enzymatic replication of ribozymes, where specific recognition is mediated via otherwise neutral sites. We find that the frequency-dependent replication rates associated with specific enzymatic replication lead to a discontinuous transition at the error threshold due to bistability with a partly delocalized phase. Further, hypercyclic couplings enable coexistence of at most four different species and their respective error tails in a stable fixed point.

Financial support by the Deutsche Forschungsgemeinschaft through SFB TR12 is gratefully acknowledged.

REFERENCES

- [1] ORGEL L., *Crit. Rev. Biochem. Mol. Biol.*, **39** (2004) 99.
- [2] JOHNSTON W., UNRAU P., LAWRENCE M., GLASNER M. and BARTEL D., *Science*, **292** (2001) 1319.
- [3] LINCOLN T. and JOYCE G., *Science*, **323** (2009) 1229.
- [4] EIGEN M., MCCASKILL J. and SCHUSTER P., *Adv. Chem. Phys.*, **75** (1989) 149.
- [5] HUYNEN M., STADLER P. and FONTANA W., *Proc. Natl. Acad. Sci. U.S.A.*, **93** (1996) 397.
- [6] WIEHE T., *Genet. Res. Cambridge*, **69** (1997) 127.
- [7] JAIN K. and KRUG J., *Adaptation in simple and complex fitness landscapes*, arXiv:q-bio/0508008 (2005).
- [8] EIGEN M. and SCHUSTER P., *Naturwissenschaften*, **65** (1978) 7.
- [9] ORGEL L., *Nature*, **358** (1992) 203.
- [10] JOYCE G. F., *Angew. Chem., Int. Ed.*, **46** (2007) 6420.
- [11] LILLEY D. M., *Curr. Opin. Struct. Biol.*, **15** (2005) 313.
- [12] SZOSTAK J., BARTEL D. and LUISI P. L., *Nature*, **409** (2001) 387.
- [13] BRIONES C., STICH M. and MANRUBIA S., *RNA*, **15** (2009) 743.
- [14] MANRUBIA S. C. and BRIONES C., *RNA*, **13** (2007) 97.
- [15] TAKEUCHI N. and HOGEWEG P., *Biol. Dir.*, **3** (2008) 11.
- [16] CAMPOS P., FONTANARI J. and STADLER P., *Phys. Rev. E*, **61** (2000) 2996.
- [17] SILVESTRE D. A. M. M. and FONTANARI J. F., *J. Theor. Biol.*, **254** (2008) 804.
- [18] SCHUSTER P. and SWETINA J., *Bull. Math. Biol.*, **50** (1988) 635.
- [19] NOWAK M. and SCHUSTER P., *J. Theor. Biol.*, **137** (1989) 375.
- [20] SAAKIAN D. and HU C., *Proc. Natl. Acad. Sci. U.S.A.*, **103** (2006) 4935.
- [21] STADLER P., SCHNABL W., FORST C. and SCHUSTER P., *Bull. Math. Biol.*, **57** (1995) 21.
- [22] WILKE C., RONNEWINKEL C. and MARTINETZ T., *Phys. Rep.*, **349** (2001) 395.
- [23] WILKE C., WANG J., OFRIA C., LENSKI R. and ADAMI C., *Nature*, **412** (2001) 331.
- [24] TAKEUCHI N., POORTHUIS P. and HOGEWEG P., *BMC Evol. Biol.*, **5** (2005) 9.
- [25] KUN A., SANTOS M. and SZATHMARY E., *Nat. Genet.*, **37** (2005) 1008.
- [26] TEE G., *Res. Lett. Math. Sci.*, **8** (2005) 123.

Error thresholds for self- and cross-specific enzymatic replication

Benedikt Obermayer^a, Erwin Frey^{a,*}

^a*Arnold-Sommerfeld-Center for Theoretical Physics and Center for NanoScience,
Ludwig-Maximilians-Universität München, Theresienstr. 37, 80333 München, Germany*

Abstract

The information content of a non-enzymatic self-replicator is limited by Eigen's error threshold. Presumably, enzymatic replication can maintain higher complexity, but in a competitive environment such a replicator is faced with two problems related to its twofold role as enzyme and substrate: as enzyme, it should replicate itself rather than wastefully copy non-functional substrates, and as substrate it should preferably be replicated by superior enzymes instead of less-efficient mutants. Because specific recognition may provide a solution, we thoroughly analyze an idealized quasispecies model for enzymatic replication, with replication rates that are either a decreasing (self-specific) or increasing (cross-specific) function of the Hamming distance between the recognition or "tag" sequences of enzyme and substrate. We find that very weak self-specificity suffices to localize a population about a master sequence and thus to preserve its information, while simultaneous localization about complementary sequences in the cross-specific case is more challenging. A surprising result is that stronger specificity constraints allow longer recognition sequences, because the populations are better localized. Extrapolating from experimental data, we obtain rough quantitative estimates for the maximal length of the recognition or tag sequence that can be used to reliably discriminate appropriate and infeasible enzymes and substrates, respectively.

Keywords: origin of life, quasispecies theory, enzymatic self-replication, higher-order catalysis

1. Introduction

The acclaimed experimental finding (Cech, 1990) that RNA not only stores genetic information but also provides catalytic function has inspired the RNA

*Corresponding author

Email addresses: obermayer@physik.lmu.de (Benedikt Obermayer),
frey@physik.lmu.de (Erwin Frey)

world scenario (Gilbert, 1986), a hypothesis for the starting point of Darwinian evolution at the origin of life through self-replication of RNA-like polynucleotides. Substantial progress over the last decades demonstrates the capability of RNA enzymes (ribozymes) to catalyze diverse chemical reactions (Doudna and Cech, 2002; Lilley, 2005; Joyce, 2007), among them the polymerization of as many as 20 nucleotides to a template molecule (Johnston et al., 2001; Zaher and Unrau, 2007), and even replication through template-directed ligation reactions involving short RNA oligomers as building blocks (Lincoln and Joyce, 2009). However, the currently known systems are not yet capable of Darwinian evolution, lacking either the ability to replicate molecules as long and complex as themselves or to introduce heritable variation.

For theorists, the focus has mainly been on whether the information content of a self-replicating molecule can be maintained in the presence of replication errors, usually employing Eigen’s well-known quasispecies theory (Eigen et al., 1989) for the non-enzymatic replication of L -nucleotide sequences. In this model, replication errors occur with an error probability μ per single nucleotide, and the replication rates are taken as functions only of the template sequence. A large number of such so-called fitness landscapes in genotype space, often with a single peak at one particular “master” sequence have been analyzed (Swetina and Schuster, 1982; Leuthäusser, 1986; Schuster and Swetina, 1988; Woodcock and Higgs, 1996; Galluccio, 1997; Hermisson et al., 2002; Peliti, 2002; Saakian and Hu, 2006; Saakian et al., 2009). Most of these landscapes lead to a generic result (Wiehe, 1997; Jain and Krug, 2005): the population in sequence space is characterized by a broad mutant distribution (a quasispecies) localized about the master sequence for mutation probabilities smaller than a critical value μ_c (the error threshold), while it consists of random sequences (it is delocalized) for larger values. Because the error threshold $\mu_c \sim 1/L$ is usually inversely proportional to sequence length, the problem arises whether the maximally sustainable complexity of a self-replicator suffices to perform the complex task of self-replication (Eigen and Schuster, 1978).

In a prebiotic context, it is important to emphasize that using a fitness landscape pertains to non-enzymatic rather than enzymatic replication, because in the latter case the replication rates also depend on the concentrations and the characteristics of involved enzymes. For RNA, the potential for non-enzymatic replication is questionable, given that template-directed polymerization or ligation seems limited to short molecules with rather specific sequences (v Kiedrowski, 1986; Acevedo and Orgel, 1987; Wu and Orgel, 1992; Orgel, 2004), and although there have been speculations (Pace and Marsh, 1985), it remains unclear how a single more complex RNA should literally copy itself (Joyce, 2007; Szostak et al., 2001).

Enzymatic replication is more plausible (Orgel, 1992), but raises the question whether high replication efficiency (high fitness) is a property of the substrate or the enzyme. In the latter case, a superior replicase does not enjoy a selective advantage, because it replicates non-functional mutant templates just as well as itself, while it is not guaranteed in the former case that a superior template is functional at all. Likewise, mutations generate substrates that are replicated

less efficiently, but they also produce less-efficient enzymes (Maynard Smith, 1979), thus affecting the replication rates of all potential substrates. On theoretical grounds, one should expect that a superior replicator is a good enzyme and a good substrate *at the same time*. As enzyme, it should therefore replicate only functional substrates, and as substrate, it should be replicated preferably by efficient enzymes. These propensities, necessary for survival in a competitive environment, could be enforced by a form of group selection, e.g., via compartmentalization in vesicles, to keep similar molecules closely together (Alves et al., 2001; Fontanari et al., 2006), but this requires a simultaneous and coordinated emergence of replicators and protocells (Szostak et al., 2001). Another possibility is *specific recognition*, i.e., if replication efficiency depends strongly on the interaction between enzyme and substrate. After all, known ribozymes act with moderately or even strongly substrate-specific efficiency (Joyce, 2007), and unspecific reactions require sophisticated substrate-binding properties that could well have been a rather late invention in prebiotic evolution (Johnston et al., 2001).

In this paper, we investigate the effects of specificity for enzymatic self-replication to address the consequences for the error threshold. Similar to models for the evolution of regulatory DNA motifs (Gerland and Hwa, 2002), we assume that specificity depends on the quality of binding to some recognition or tag sites (Weiner and Maizels, 1987). Idealizing this condition, we use replication rates that depend on the Hamming distance between these sequence regions of enzyme and substrate via a decreasing (self-specific) or increasing (cross-specific) function. After formulating the model, we show for these two scenarios results from stochastic simulations and numerical solutions of reduced deterministic rate equations. By means of a moment closure approximation, we analytically discuss the resulting localization conditions, error thresholds and the phase diagram. In our conclusion, we use experimental values for polymerization rates to obtain simple estimates for the maximum number of nucleotides that can be used for recognition.

2. Model

In the framework of quasispecies theory, each molecule is characterized by its sequence $S_i = (\sigma_1^{(i)} \dots \sigma_L^{(i)})$ of L binary nucleotides $\sigma_\ell^{(i)} \in \{0, 1\}$. In an infinitely large population, its concentration X_i evolves according to the deterministic rate equations (Eigen et al., 1989)

$$\dot{X}_i = \sum_j M_{ij} R_j X_j - X_i \sum_j R_j X_j. \quad (1)$$

Here, $M_{ij} = \mu^{d_{ij}} (1 - \mu)^{L - d_{ij}}$ is the mutation probability between sequences S_i and S_j with Hamming distance $d_{ij} = \sum_\ell |\sigma_\ell^{(i)} - \sigma_\ell^{(j)}|$, where μ is the error probability per single nucleotide (usually called “mutation rate”), and the

replication rate R_i of sequence S_i is given by:

$$R_i = A_i + \sum_j B_{ij} X_j. \quad (2)$$

Whereas the non-enzymatic rate A_i depends only on the genotype S_i , the second term implies frequency-dependent selection and makes our model intrinsically nonlinear. It encodes the catalytic interactions of two molecules: B_{ij} measures how well S_j catalyzes the replication of S_i . This matrix is also known as payoff matrix in evolutionary game theory (Hofbauer and Sigmund, 1998) and a related matrix has been used to describe the evolutionary compatibility of different grammars (Nowak et al., 2001; Komarova, 2004). Note that the second term in Eq. (1) ensures the normalization $\sum_j X_j = 1$, and a degradation term $-D_i X_i$ therefore drops out of Eq. (1) since we assume that the decay rate $D_i \equiv D$ is sequence-independent for simplicity.

To capture the essentials of a situation where replicase enzymes prefer to replicate themselves instead of their competitors, we assume that the quality of specific recognition influences catalytic rates more strongly than the actual genotypes of enzyme and substrate. Hence, we effectively only model the recognition regions of ribozymes, which are often clearly separated from the catalytic domains (Lilley, 2005), and neglect the consequences of mutations in the latter (see (Obermayer and Frey, 2009) for a simple model that includes these effects). We thus restrict the sequence length L to the number of nucleotides that take part in recognition. Mediated via specific base-pairing interactions (Doudna and Cech, 2002), the quality of recognition can be taken as function of the number of mismatches between the binding sites of enzyme and substrate, and we let the catalytic matrix B_{ij} therefore depend via a *specificity function* $f(d)$ only on the Hamming distance d_{ij} between enzyme and substrate. Further, because rate enhancements through ribozyme catalysis can be substantial (Doudna and Cech, 2002), such that non-enzymatic replication rates are comparably small (if nonzero at all), we neglect their genotype dependence altogether and choose a flat fitness landscape for A_i :

$$A_i \equiv \alpha, \quad B_{ij} = \beta f(d_{ij}). \quad (3)$$

Because we are interested in the stationary state, the parameter α (if nonzero) merely sets the time scale while β measures the selection strength. A decreasing function $f(d)$ corresponds to self-specific replication, while an increasing function $f(d)$ is the cross-specific case, where enzymes preferably catalyze the replication of complementary substrates.

A localized state is necessary to preserve the information content of one particular sequence S_* , but this localization is not *a priori* obvious, especially since the possibility of periodic orbits and chaos cannot be excluded for general replicator-mutator equations like Eq. (1) (Stadler et al., 1995). We did not find any signs on non-trivial dynamical behavior in our simulations, though, and one can easily convince oneself that the delocalized state, where all sequences have the same concentration and therefore identical replication rates, can lead to localization: Since replication rates are essentially proportional to concentration,

stochastic concentration fluctuations imply higher rates and can induce a transition to a state localized about some randomly chosen master sequence, which then also has the highest replication rate (see (Obermayer and Frey, 2009) for a visualization). Such “fixation” events are very similar to the phenomenon of consensus formation, e.g., in language dynamics (Blythe, 2009). Note that our idealized replication rates depend only on Hamming distances and do not predetermine any specific master sequence for localization. This symmetry would be broken in a full model where replication rates depend on the full genotypes of enzyme and substrate (and not just the Hamming distance between their recognition regions).

Given localization about some “master” sequence S_* , we can significantly reduce the dimensionality of Eq. (1) by lumping all sequences S_i with a Hamming distance k to S_* together into “error class” k . Without loss of generality, we assume that $S_* = (00 \dots 0)$. This well-known procedure (Schuster and Swetina, 1988; Woodcock and Higgs, 1996) allows one to formulate reduced rate equations formally equivalent to Eq. (1) in terms of new variables x_k denoting the concentration of error class k in the population:

$$\dot{x}_k = \sum_{ji} m_{kj} [a_j \delta_{ji} + b_{ji} x_i] x_j - x_k \sum_{ji} [a_j \delta_{ji} + b_{ji} x_i] x_j. \quad (4)$$

In our model Eq. (3) for the replication rates, $a_i \equiv \alpha$. The accordingly reduced mutation matrix and the catalytic matrix depend only on the Hamming distance between pairs of sequences in different error classes (measured with respect to the master sequence), which allows us to combinatorically assess all possibilities for their relative distance. The total probability of distributing $0 \leq k-j+2\ell \leq L$ mutations to move a sequence from error class j into error class k is given by (Woodcock and Higgs, 1996)

$$m_{kj} = \sum_{\ell} \binom{L-j}{k-j+\ell} \binom{j}{\ell} (1-\mu)^{L-(k-j+2\ell)} \mu^{k-j+2\ell}. \quad (5)$$

The replication rate Eq. (2) also depends on the frequency of each sequence in each error class. With the homogeneity assumption that all $\binom{L}{j}$ sequences in class j are equally populated, this complication can be resolved, and the reduced matrix b_{ij} reads analogously

$$b_{ij} = \beta \sum_n \binom{L-i}{j-i+n} \binom{i}{n} \frac{f(j-i+2n)}{\binom{L}{j}}. \quad (6)$$

Numerical solutions to the $(L+1)$ -dimensional rate equations given in Eq. (4) can easily be found by means of standard algorithms, while the full 2^L -dimensional system Eq. (1) can be analyzed using stochastic simulations in a finite population of N sequences. Here, we employ the straightforward stochastic simulation algorithm used by Wilke et al. (2001). At time t each sequence S_k , present in N_k copies, has a probability $p_{0,k} = N_k / \sum_i N_i (1 + R_i)$ to be copied without mutations into the population at time $t+1$, and a probability $p_{\text{mut},jk} =$

$M_{jk}R_kN_k/\sum_i N_i(1+R_i)$ to be selected and mutated into sequence S_j . Following initialization, the time averaged Hamming distance distribution x_k and its mean $\langle k \rangle = \sum_k kx_k$ and variance $\langle \Delta k^2 \rangle = \sum_k (k - \langle k \rangle)^2 x_k$ are measured after reaching a stationary state.

3. Results and Discussion

3.1. Self-specific replication

Our first scenario is concerned with self-specific replication, where replication rates increase with similarity of enzyme and substrate. In a convenient choice for the specificity function

$$f_s(d) = (1 - d/L)^p, \quad (7)$$

the degree of specificity is tunable via a parameter $p \geq 0$. Figure 1 shows results for the stationary Hamming distance distribution x_k from stochastic simulations, where we initialized all sequences at the master in order to avoid noise from the intrinsically stochastic “fixation” events, together with numerical solutions to the reduced rate equations, Eq. (4). For different degrees of specificity, from the linear case $p = 1$ to complete self-specificity $p \rightarrow \infty$, where enzyme and substrate have to be identical, we find excellent agreement between stochastic simulation results and the deterministic theory, which justifies the homogeneity assumption made in symmetrizing the specificity matrix (see Eq. (6)).

The limit $p \rightarrow \infty$ with $f_s(d) \rightarrow \delta_{d,0}$, depicted in Fig. 1(c), leads to a generalized Schlögl model of auto-catalytic replication, which has been partly analyzed by Stadler et al. (1995). Here we can employ the well-known “error-tail” approximation (Schuster and Swetina, 1988): we define x_0 as the concentration of the master sequence, $\alpha + \beta x_0$ its replication rate and $(1 - \mu)^L$ the probability not to have a mutation. All other sequences are lumped together in the error tail with concentration $1 - x_0$ and replication rate α (the concentration of suitable replication enzymes is so small that the frequency-dependent term in the replication rate does not contribute). Neglecting back mutations from the error tail into x_0 (corresponding to the large-genome limit), we obtain the simple equation

$$\dot{x}_0 = (\alpha + \beta x_0)(1 - \mu)^L x_0 - x_0 \bar{r}, \quad (8)$$

with $\bar{r} = (\alpha + \beta x_0)x_0 + \alpha(1 - x_0)$ the mean replication rate. In the stationary state, we easily find that the delocalized state $x_0 = 0$ is stable for all μ , while a branch of solutions with nonzero x_0 emerges for $(1 - \mu)^L > 2(\sqrt{\alpha(\alpha + \beta)} - \alpha)/\beta$ through a *discontinuous* transition (see also (Campos et al., 2000; Obermayer and Frey, 2009; Wagner et al., 2009) for similar results in related models). Whereas for the somewhat related sharply-peaked fitness landscape, where only the master sequence has a higher replication rate, the error threshold arises through a *continuous* bifurcation (Baake and Wiehe, 1997), the discontinuity observed here expresses the qualitatively different behavior we previously termed “escalation of error catastrophe” (Obermayer and Frey, 2009): as the mutation rate grows,

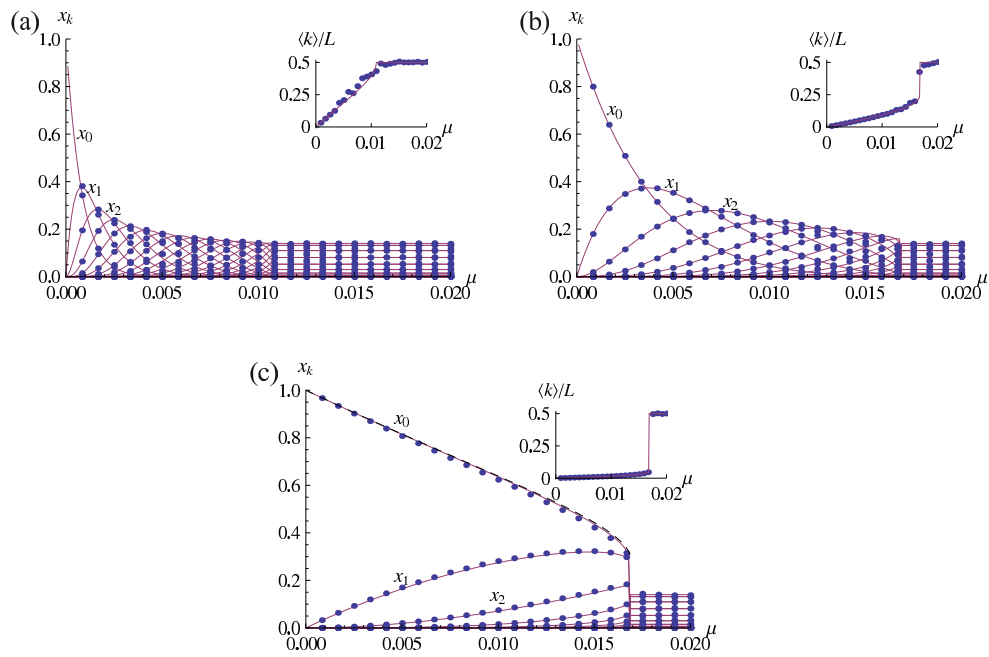


Figure 1: Solutions for self-specific replication with $f_s(d) = (1 - d/L)^p$. Stationary Hamming distance distribution x_k as function of mutation rate μ from numerical solutions to the reduced rate equations Eq. (4) (straight lines) and a stochastic simulation of the full system Eq. (1) in a population of $N = 10^4$ sequences of length $L = 32$ (dots) for $\alpha = 1$, $\beta = 5$ and (a) $p = 1$, (b) $p = 5$, and (c) $p = \infty$ (here, the dashed line shows the error-tail approximation for x_0). The insets depict the average Hamming distance $a = \langle k \rangle / L$ to the master sequence.

the proportion of fittest sequences, i.e., of the necessary replication enzymes, is diminished and therefore their replication rate. This in turn reduces their concentration, until at the error threshold the concentration of enzymes x_0 is not large enough to have them replicate with an efficiency sufficient for localization.

While Eq. (8) approximates the exact result for x_0 very well (see the dashed line in Fig. 1(c)), it is valid only for $L \rightarrow \infty$ (because back mutations are neglected) and $p \rightarrow \infty$ (because the replication rate of the error-tail is taken as concentration-independent). A more general perspective and more detailed understanding can be obtained from the population distribution's normalized first moment $a = \langle k \rangle / L = \langle \sigma \rangle$, which as the mean Hamming distance to the master $S_* = (00\dots 0)$ characterizes the width of the distribution and measures the mean value $\langle \sigma \rangle$ of each sequence's binary nucleotides. Writing down an equation for the first moment of Eq. (4) requires a hierarchy of expressions for higher moments, which can be truncated by means of a moment closure technique. Here, we assume that the stationary Hamming distance distribution is approximately binomial, $x_k \approx \binom{L}{k} a^k (1-a)^{L-k}$, because this reproduces the expected distribution in the limits $a \rightarrow 0$ (complete localization about one sequence) and $a \rightarrow 1/2$ (the delocalized state, where the binary nucleotides are random numbers). Moreover, it solves the rate equations Eq. (1) exactly for linear fitness landscapes without epistasis (Woodcock and Higgs, 1996) and for an extension of the quasispecies model to a game theory setting (Lässig et al., 2003). With this binomial ansatz, a is the population distribution's only parameter, and for our model of the replication rates Eq. (3), it obeys the equation

$$(1-2a) \left\{ \mu L [\alpha + \beta S(1-2a(1-a))] - a(1-a)(1-2\mu)\beta S'(1-2a(1-a)) \right\} = 0. \quad (9)$$

This equation for a , which is one of our main analytical results (see Appendix A.1 for a derivation), holds for *any* specificity function $f(d)$, which enters via the auxiliary function

$$S(x) = \sum_k \binom{L}{k} f(k) x^{L-k} (1-x)^k. \quad (10)$$

While Eq. (9) can be solved for $a(\mu)$ exactly only in a few special cases (see Appendix A.2), we can easily solve for $\mu(a)$ and invert graphically to obtain an approximate bifurcation diagram:

$$\mu(a) = \left[2 + \frac{\alpha + \beta S(1-2a(1-a))}{\beta a(1-a)S'(1-2a(1-a))} \right]^{-1}. \quad (11)$$

A comparison between the exact solution $a(\mu)$ obtained from the reduced rate equations Eq. (4) via numerical continuation¹ and Eq. (11) is shown in Fig. 2 for

¹AUTO software package available via <http://indy.cs.concordia.ca/auto/>.

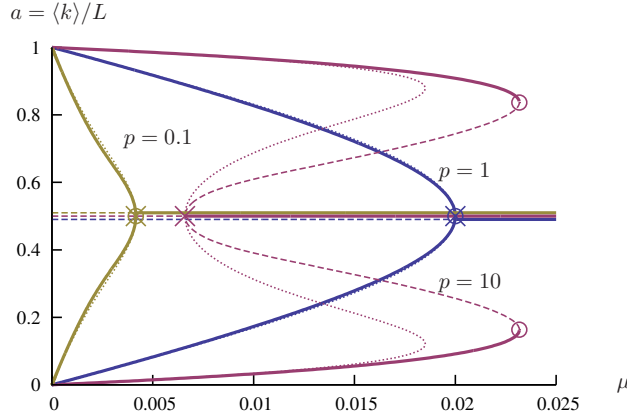


Figure 2: Bifurcation diagram of Eq. (4) for the normalized mean Hamming distance $a = \langle k \rangle / L$ with $L = 8$, $\alpha = 1$, $\beta = 1$ and different values of the specificity degree p . Thick lines indicate stable branches, dashed lines unstable branches and thin dotted lines the results of the binomial closure approximation Eq. (9), which is barely visible for $p = 1/10$ and $p = 1$. Circles indicate critical mutation rates μ_c where the localized regime vanishes, crosses show values $\tilde{\mu}_c$ where the delocalized state changes stability (horizontal branches corresponding to delocalized states are drawn slightly shifted for visualization).

$L = 8$, $\alpha = \beta = 1$ and different values of p in the specificity function Eq. (7). Recalling the symmetry of the original model, Eq. (3), namely that the population can localize about any sequence, the remaining reflection symmetry $a \rightarrow 1 - a$ about the delocalized solution $a = 1/2$ indicates that after symmetrization localization is only possible about the master sequence or its complement. The stable branches associated with localized solutions start for $\mu = 0$ at $a = 0$ (or $a = 1$), i.e., full localization about one sequence (or its complement), and higher mutation rates give rise to broader distributions with larger mean, until these localized regimes disappear at critical mutation rates μ_c denoted by circles. The delocalized solutions, on the other hand, gain stability at finite mutation rates $\tilde{\mu}_c$ (denoted by crosses), and we find bistability for $\tilde{\mu}_c < \mu < \mu_c$. A similar situation is encountered in models of grammar evolution (Nowak et al., 2001; Komarova, 2004), which are, however, mathematically considerably simpler due to the lack of a metric in “grammar space” and the resulting simpler forms for the matrices M_{ij} and B_{ij} in Eqs. (1) and (3).

Explicit expressions for the error threshold $\mu_c = \max \mu(a)$ are available when $S(x)$ in Eq. (11) has a simple form (see Appendix A.2). For instance, $\mu_c = \beta / (4\alpha L + 2\beta(L + 1))$ for $p = 1$, where specificity decreases linearly with the distance between enzyme and substrate. Although an error threshold is absent for linear fitness landscapes without epistasis (Woodcock and Higgs, 1996), here the intrinsically nonlinear model gives a transition even in this apparently similar case. For very strong specificity $p \rightarrow \infty$ we find $\mu_c = \mathcal{W}[\beta / (e\alpha)] / (2L)$ using Lambert’s \mathcal{W} -function, and we recover the result $\mu_c = \ln(\beta / \alpha) / (2L)$ that can also be obtained from the error-tail approximation in the limit $\beta \gg \alpha$.

Further, the delocalized state $a = 1/2$ is the only solution of Eq. (9) in the complete absence of specificity ($f_s(d) \equiv 1$), supporting the intuition that unspecific replication does not suffice to preferentially maintain the information of one particular sequence. Interestingly, taking $p \rightarrow 0$ in Eq. (7) gives the finite even though exponentially small value $\mu_c = \beta/(2^{L+1}(\alpha + \beta))$. This result implies that limited localization is possible even for very weak specificity (if $p = 0$ in the specificity function Eq. (7), enzymes replicate everything except their exact complement, because always $f_s(L) = 0$).

From the bifurcation diagram obtained via Eq. (11), we easily read off exact results for the value $\tilde{\mu}_c = \mu(1/2)$ where the delocalized state gains stability. E.g., for the generalized Schlögl model $p \rightarrow \infty$, we get $\tilde{\mu}_c = \beta/(\alpha 2^{L+1} + 4\beta)$ (Stadler et al., 1995). This exponentially small yet finite value is consistent with our previous conclusion that the delocalized regime is stable for all values of μ within the error-tail approximation, Eq. (8), which holds for $L \rightarrow \infty$. Further, we find that the two critical values $\tilde{\mu}_c$ and μ_c are identical for $p = 0, 1, 2$. Recognizing that Fig. 2 describes a pitchfork bifurcation at $a = 1/2$ and $\mu = \tilde{\mu}_c$, we infer that the two critical mutation rates are equal ($\mu_c = \tilde{\mu}_c$) whenever the pitchfork is supercritical, whereas bistability between localized and delocalized states for intermediate mutation rates $\tilde{\mu}_c < \mu < \mu_c$ is possible in the subcritical case, leading to the discontinuous transition observed in Fig. 1. The bistability regime vanishes as the curvature $\mu''(1/2)$ in the bifurcation diagram changes sign, which gives from Eq. (11) an approximate expression for the corresponding critical value of β :

$$\beta^* = \alpha \left[\frac{S'^2(1/2)}{S''(1/2) - 2S'(1/2)} - S(1/2) \right]^{-1}. \quad (12)$$

This generally applicable result can readily be evaluated for our specificity function Eq. (7), predicting bistability for all values $\beta < \beta^* = \alpha 2^{L-1}(L-2)$ for strong specificity $p \rightarrow \infty$, and no bistability for weak specificity because $\beta^* \leq 0$ for $p < p_{\min} = 2 + \mathcal{O}(L^{-1})$.

The results of the binomial closure approximation Eq. (9) are summarized in the phase diagram Fig. 3, where the two critical mutation rates μ_c and $\tilde{\mu}_c$ are shown as functions of the selection strength β and the specificity degree p for $\alpha = 1$. The thick line denoted β^* indicates the boundary of the bistability regime $\mu_c > \tilde{\mu}_c$. Fig. 2 indicates that the binomial approximation is quantitatively excellent in the supercritical situation $\beta > \beta^*$, and qualitatively correct otherwise, where the values for μ_c are somewhat underestimated: near the error threshold, the variance of the population distribution is considerably larger than that of a binomial. The performance of the binomial closure approximation can be appreciated in more detail from the projected phase diagrams shown in Fig. 4.

A remarkable feature of these phase diagrams is that the error threshold μ_c *increases* for stronger specificity p (see Fig. 4(b)), which implies that higher mutation rates can be tolerated, i.e., that longer sequences can be maintained. This seems at first counter-intuitive, because weaker specificity constraints on the recognition sequence should allow more mutational “freedom”.

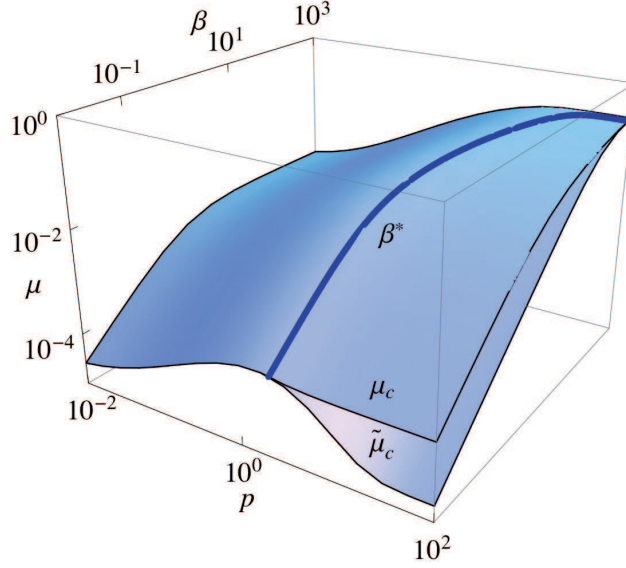


Figure 3: Phase diagram of localization regimes in the parameter space of mutation rate μ , selection strength β and specificity degree p (log-log-log scale) obtained from Eq. (9) for $L = 8$ and $\alpha = 1$: below the upper plane μ_c , a localized solution exists, while above the lower plane $\tilde{\mu}_c$ the delocalized state becomes stable. Bistability ($\mu_c > \tilde{\mu}_c$) is possible only for $\beta < \beta^*(p)$.

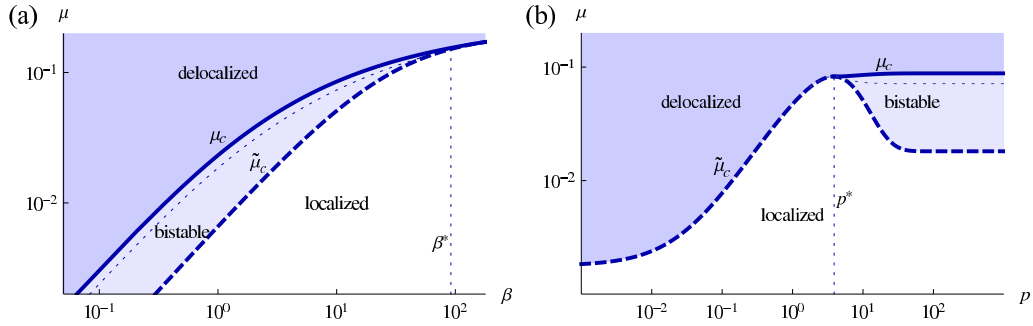


Figure 4: Projected phase diagrams of localization regimes for self-specific replication with $L = 8$ and $\alpha = 1$: (a) as function of β with $p = 10$ fixed; (b) as function of p with $\beta = 10$ fixed. Below μ_c (thick line), a localized solution exists, while above $\tilde{\mu}_c$ (thick dashed line) the delocalized state becomes stable. The dotted lines denote the result for μ_c obtained via the binomial closure approximation. Bistability ($\mu_c > \tilde{\mu}_c$) is possible only for $\beta < \beta^*(p)$ (or $p > p^*(\beta)$).

However, as shown in Fig. 2 and Fig. 1, smaller values for p lead to much broader distributions: mutants are still reasonably well replicated by master enzymes, but the master is only moderately well (but not quite as efficiently) replicated by the mutants. The resulting broadening of the distribution effectively reduces the replication rate of the master and escalates the error catastrophe (Obermayer and Frey, 2009). Thus, the necessity for an enzymatic replicator to discriminate not only between functional and non-functional *substrates*, but also between efficient and unproductive *enzymes*, is again emphasized.

We finally want to remark on the case $\alpha = 0$, i.e., no background level for the non-enzymatic replication rate. Most of the above results obtained from the binomial closure approximation can be simply evaluated for $\alpha = 0$ (note that then β sets the timescale and drops out), but the strong specificity limit $p \rightarrow \infty$ deserves extra attention. The error-tail approximation indicates that the error threshold vanishes ($\mu_c \rightarrow 1$), but from Eq. (9) we find $\mu_c = \tilde{\mu}_c = 1/6$ for $L \gg 1$, i.e., a macroscopic yet finite value (see Appendix A.2). This remarkable result can be explained by recalling that the traditional result $\mu_c \approx \ln r/L$ (Eigen et al., 1989) for the error threshold depends on the replication advantage r of the master relative to a possibly small but finite value for the mutants. In our case, rates are directly proportional to concentration, and because the master sequence has a concentration of order 1, while in an infinitely large population distant mutants have concentrations of order 2^{-L} , this relative advantage itself is of order 2^L , and cancels the length dependence of the error threshold. In the corresponding non-enzymatic case, results for so-called “truncation” fitness landscapes have led to some debate about the applicability of the error threshold concept in the presence of lethal mutations (Wilke, 2005; Summers and Litwin, 2006; Takeuchi and Hogeweg, 2007; Saakian et al., 2009). Accordingly, we should cautiously note that our results for $\alpha = 0$ will probably be affected when accounting for the effects of finite populations and the full dependence of the replication rates on the genotypes of enzyme and substrate.

3.2. Cross-specific replication

To increase the information content of replicating systems beyond the limited complexity of a single replicator, auto-catalytic reaction networks such as Hypercycles (Eigen and Schuster, 1978; Stadler et al., 1995) have been proposed, where different molecular species catalyze each other’s replication in a possibly complex interaction graph. Only very little is known for these systems regarding the issue of reaction specificity and the cross-interactions of each species’ mutant clouds. The simplest conceivable networks are 2-member cross-catalytic hypercycles, which could rely on complementary base-pairing for recognition. This suggests to analyze a specificity function where replication rates increase with Hamming distance between enzyme and substrate:

$$f_c(d) = (d/L)^p. \quad (13)$$

If enzyme and substrate should be complementary for efficient replication, we expect the formation of two sub-populations localized about complementary

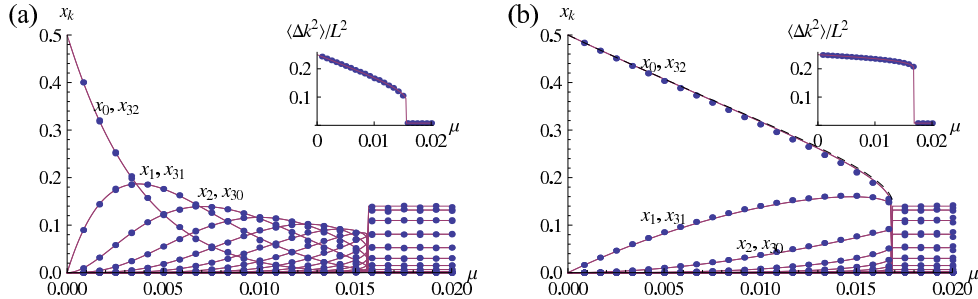


Figure 5: Hamming distance distribution x_k as function of mutation rate μ as in Fig. 1, but for cross-specific replication with $\alpha = 1$, $\beta = 10$, $L = 32$, and (a) $p = 5$ or (b) $p = \infty$. The insets show the variance $\langle \Delta k^2 \rangle = \sum_k (k - \langle k \rangle)^2 x_k$ (in a symmetric population, $\langle k \rangle = L/2$).

sequences, each catalyzing the replication of the other. The main question to be answered is how specificity affects coexistence. In the standard Eigen model (Swetina and Schuster, 1982), quasispecies coexistence is prevented by competitive exclusion except in degenerate cases, because the “fittest” individuals take over the population. In our case, we expect non-trivial coexistence results, because each subpopulation depends on the presence of the other for efficient replication, but it is unclear how the possibly broad distributions influence each other.

From numerical solutions to the reduced rate equations and simulation results, where we initialized the population split between the master sequence and its complement (see Fig. 5), we find that localization is only possible for $p > 1$. The case $p \rightarrow \infty$ essentially looks like having two equivalent self-specifically replicating subpopulations, in the sense that in the localized state the sum $x_k + x_{L-k}$ of the cross-specific case is equal to x_k in the self-specific situation once we replace $\beta \rightarrow \beta/2$. We will now corroborate these two findings using the binomial closure approximation.

Two equivalent subpopulations localized about complementary sequences correspond to a superposition of binomial distributions: $x_k \approx \frac{1}{2} \binom{L}{k} [a^k (1-a)^{L-k} + (1-a)^k a^{L-k}]$. To obtain an equation similar to Eq. (9) for their mean widths a , we cannot use the first moment of the reduced rate equations (it is constant by construction, because the distribution is symmetric about $a = 1/2$), but use the second moment, leading to a lengthy result explicitly given in Appendix B.1 (see Eq. (B.5)). Most importantly, for $p = 1$ we obtain only the solution $a = 1/2$. Because the complementary distributions overlap too much if catalytic rates increase only linearly with Hamming distance, the populations are not localized strongly enough to ensure coexistence.

The resulting bifurcation diagram $\mu(a)$ (see Appendix B.2) is shown in comparison with the exact result in Fig. 6 for different values of p . We obtain information about a from the variance, in the case of two complementary binomials given by $\langle \Delta k^2 \rangle = L^2/4 - L(L-1)a(1-a)$. Using this expression gives very good agreement between binomial closure approximation and exact numerical results

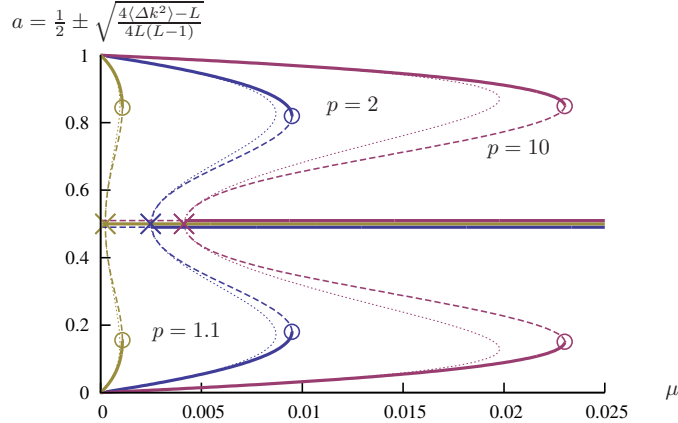


Figure 6: Bifurcation diagram of Eq. (4) as in Fig. 2, but for cross-specific replication in terms of the population parameter a , which denotes the width of the two subpopulations and is calculated from the variance $\langle\Delta k^2\rangle$ in the Hamming distance distribution. Parameters are $L = 8$, $\alpha = 1$, and $\beta = 1$.

especially for small p , because now the first *two* moments are correct. The critical mutation rates μ_c and $\tilde{\mu}_c$ can be found from the bifurcation diagram, e.g., $\mu_c = \mathcal{W}[\beta/(2\alpha e)]/(2L)$ for $p \rightarrow \infty$, which is identical to the corresponding result for self-specific replication if we replace $\beta \rightarrow \beta/2$. Hence, in this limit we obtain two clearly separated binomial distributions representing two equivalent and catalytically coupled populations, and the “coupling constant” is only half as large because only one half of the population is available as enzymes for the other. In particular, the negligible interaction between the respective mutant clouds allows one to employ the error-tail approximation assuming independent species and error tails as in (Campos et al., 2000; Obermayer and Frey, 2009). Further, we find that the pitchfork bifurcation is always subcritical, i.e., that $\mu_c > \tilde{\mu}_c$. We summarize our main results by plotting projected phase diagrams of μ_c and $\tilde{\mu}_c$ as functions of $p - 1$ and β in Fig. 7. This confirms that both critical mutation rates μ_c and $\tilde{\mu}_c$ vanish linearly with $p - 1$, because $\mu(a) \propto p - 1$ as $p \rightarrow 1$, which gives the sharp bound $p > 1$ for coexistence of two populations. Finally, the case $\alpha = 0$ of zero non-enzymatic replication rate is similar the self-specific case: the slight chance of distant mutants to find an appropriate enzyme gives an enormous replication advantage to the mainly populated master sequences and therefore macroscopic values for the error threshold (see Appendix B.3 for details).

4. Conclusion

Because enzymatic replication provokes the necessity for enzymes to favor functional substrates and for substrates to prefer efficient enzymes, we analyzed a model of specific replication, where replication rates depend on the Hamming

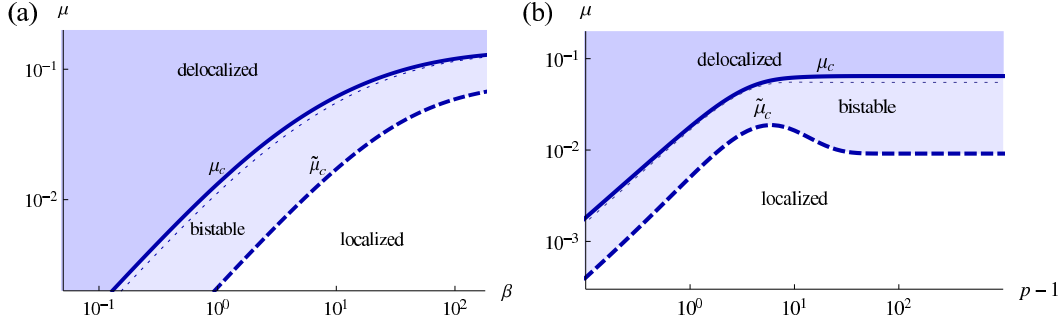


Figure 7: Projected phase diagrams of localization regimes as in Fig. 4, but for cross-specific replication with $L = 8$ and $\alpha = 1$: (a) as function of β with $p = 10$ fixed; (b) as function of p with $\beta = 10$ fixed.

distance between recognition regions of enzyme and substrate via an adjustable degree of specificity. Combining stochastic simulations, numerical solutions of reduced rate equations and analytical solutions to a binomial closure approximation, we could analyze the entire phase diagram and assess how mutation rate μ , selection strength β and specificity degree p influence the localization about a master sequence in order to preserve its information content. We found that for self-specific replication very weak specificity suffices for localization, whereas stronger specificity gives more tolerance against mutations but leads to bistability with the delocalized regime of random sequences. In particular, the binomial closure approximation allows one to obtain analytical expressions for the bifurcation diagram and an upper bound β^* for the bistability regime, which can be evaluated for any specificity function $f_s(d)$. Apart from our special choice, Eq. (7), a mesa-shaped function would also be conceivable, in correspondence to fitness landscapes for transcription factor binding allowing for some “fuzziness” or neutrality in the binding sequence (Gerland and Hwa, 2002). Preliminary results indicate that in this case the binomial closure approximation gives at least qualitative agreement as well. While our approximation is not restricted to large L , this limit can probably be more systematically be described using the maximum principle employed previously in quasispecies theory (Hermisson et al., 2002; Saakian and Hu, 2006). In the case of cross-specificity, we found that co-existence of subpopulations localized about complementary sequences is possible only if replication rates increase faster than linearly with Hamming distance.

Although our model is based on idealizing assumptions, we can extrapolate from currently available experimental data to obtain rough quantitative estimates for the maximal length L_c of the recognition or tag sequences that can be used by replication enzymes to specifically and reliably discriminate appropriate and useless templates (and vice versa). Considering that non-enzymatic template-directed polymerization rates are on the order of several hours to days per base (Acevedo and Orgel, 1987; Wu and Orgel, 1992), while ribozyme-catalyzed polymerization gives rates in the hour range (Johnston et al., 2001;

Zaher and Unrau, 2007), we can estimate the ratio β/α somewhere near 5-20 if polymerization is the rate-limiting step. Assuming a self-specific enzymatic replicator with a mutation rate on the order of 3% as in (Johnston et al., 2001), we obtain a critical length $L_c = 11-15$ for weak specificity $p = 1$, and a larger value $L_c = 18-33$ for $p \rightarrow \infty$, because stronger specificity constraints allow longer sequences due to better localization. These values are significantly smaller than the lengths of, e.g., the 154-nucleotide specificity domain of *Bacillus subtilis* RNase P (Lilley, 2005) or the tRNA-like structures supposed to act as “genomic tags” for the replication of RNA viruses (Weiner and Maizels, 1987). Many of the nucleotides in these instances have a structural role, which makes them effectively redundant or neutral in our model, and only a minority is actually involved in recognition. Also, recent research indicates that “stalling” of polymerization after mismatch incorporation might significantly reduce the error threshold (Rajamani et al., unpublished). Nevertheless, our result suggests that the error threshold puts hard constraints on the information content of enzymatic replicators as well.

Acknowledgements

We gratefully acknowledge helpful discussions with Joachim Krug and Irene Chen and financial support by the German Excellence Initiative via the program “Nanosystems Initiative Munich” and by the Deutsche Forschungsgemeinschaft through SFB TR12.

Appendix A. Self-specific replication

Appendix A.1. Derivation of Eq. (9)

To obtain Eq. (9), we compute the first moment $\sum_k k \dot{x}_k$ of the reduced rate equations Eq. (4) under the assumption that $x_k = x_k^b \equiv \binom{L}{k} a^k (1-a)^{L-k}$ is binomially distributed. This gives four terms

$$\begin{aligned} T_1 &= \sum_{jk} k m_{kj} a_j x_j^b & T_2 &= \sum_{ijk} k m_{kj} b_{ji} x_i^b x_j^b \\ T_3 &= - \sum_k k x_k^b \sum_j a_j x_j^b & T_4 &= - \sum_k k x_k^b \sum_{ij} b_{ji} x_i^b x_j^b. \end{aligned} \quad (\text{A.1})$$

The reduced mutation matrix m_{kj} and the catalytic matrix b_{ij} are given in Eqs. (5) and (6). Note that although not immediately obvious, the catalytic matrix $b_{ij} = b_{ji}$ is symmetric, because the binomial in the denominator of Eq. (6) normalizes it to the single sequence level. We further keep in mind that $\binom{n}{k} = 0$ if $k < 0$ or $k > n$ if n and k are integer, so we do not need to keep track of the summation limits in the following calculations.

While it is straightforward to find $T_1 = \alpha L(a + \mu(1 - 2a))$ and $T_3 = -\alpha a L$, we concentrate first on T_4 , which reads after performing the summation over k

$$T_4 = -\beta a L \sum_{ijn} \binom{L-j}{i-j+n} \binom{L}{j} \binom{j}{n} f_s(i-j+2n) a^{i+j} (1-a)^{2L-(i+j)}. \quad (\text{A.2})$$

Replacing $i' = i - j + 2n$ and rearranging $\binom{L-j}{i'-n} \binom{L}{j} \binom{j}{n} = \binom{L-i'}{j-n} \binom{L}{i'} \binom{i'}{n}$, we can sum over j and n , and are left with

$$\begin{aligned} T_4 &= -\beta a L \sum_{i'} \binom{L}{i'} f_s(i') (1 - 2a(1-a))^{L-i'} (2a(1-a))^{i'} \\ &= -\beta a L S(1 - 2a(1-a)). \end{aligned} \quad (\text{A.3})$$

The term T_2 can after similar rearrangements be written as the product of two generalized Vandermonde matrices:

$$T_2 = \beta \sum_{i'} \binom{L}{i'} f_s(i') \sum_{jk} k \begin{bmatrix} \mu & 1-\mu \\ 1-\mu & \mu \end{bmatrix}_{L-k,j} \begin{bmatrix} (1-a)^2 & a(1-a) \\ a^2 & a(1-a) \end{bmatrix}_{j,i}, \quad (\text{A.4})$$

where the L^{th} Vandermonde matrix with parameters a, b, c , and d is defined as

$$\begin{bmatrix} a & b \\ c & d \end{bmatrix}_{i,j} \equiv \sum_{\ell} \binom{L-j}{i-\ell} \binom{j}{\ell} a^{L+\ell-i-j} b^{j-\ell} c^{i-\ell} d^{\ell}. \quad (\text{A.5})$$

This allows us to use a nice multiplication identity (Rawlings and Sze, 2005) for these matrices:

$$\begin{bmatrix} a & b \\ c & d \end{bmatrix} \begin{bmatrix} e & f \\ g & h \end{bmatrix} = \begin{bmatrix} ae + bg & af + bh \\ ce + dg & cf + dh \end{bmatrix}, \quad (\text{A.6})$$

which gives:

$$T_2 = \beta \sum_{i'} \binom{L}{i'} f_s(i') \sum_k k \begin{bmatrix} a^2 + \mu(1-2a) & a(1-a) \\ (1-a)^2 - \mu(1-2a) & a(1-a) \end{bmatrix}_{L-k,i'} \quad (\text{A.7})$$

$$= \beta [L(a + \mu(1-2a))S(1-2a(1-a)) \quad (\text{A.8})$$

$$- (1-2a)a(1-a)(1-2\mu)S'(1-2a(1-a))]. \quad (\text{A.9})$$

Adding up $T_1 + T_2 + T_3 + T_4 = 0$ gives Eq. (9).

Appendix A.2. Solutions of Eq. (9)

This equation can be solved whenever $S(x)$, defined in Eq. (10), assumes a simple form. For $f_s(d) = (1-d/L)^p$ as in Eq. (7), $S(x)$ is a polynomial of order L , except for integer $0 < p < L$, where it is of order p . A few instances for $L > 2$ are given by

$$S(x) = \begin{cases} 1 - (1-x)^L, & p = 0, \\ x, & p = 1, \\ \frac{1}{L}x + \frac{L-1}{L}x^2, & p = 2, \\ x^L, & p = \infty. \end{cases} \quad (\text{A.10})$$

To find solutions $a(\mu) \neq 1/2$, we write $x = a(1-a)$ and solve Eq. (9) for x :

$$x = \begin{cases} \frac{1}{2} \left(2\mu \frac{\alpha+\beta}{\beta} \right)^{1/L}, & p = 0 \\ \frac{\alpha+\beta}{\beta} \frac{\mu L}{1+2\mu(L-1)}, & p = 1 \\ \mu - \frac{1}{2L} \mathcal{W} \left(-\frac{2\alpha\mu L}{\beta} e^{2\mu L} \right), & p = \infty. \end{cases} \quad (\text{A.11})$$

For the last case, we approximated $(1 - 2x)^L \approx e^{-2xL}$ and $\mu/(1 - 2\mu) \approx \mu$ for the important asymptote $L \gg 1$ with μL fixed, and used Lambert's \mathcal{W} -function. A more complicated expression is obtained for $p = 2$. The solution $a = \frac{1}{2} (1 \pm \sqrt{1 - 4x})$ is then easily computed, and the error thresholds μ_c follow from evaluating the condition $x = 1/4$ (for $p = 0, 1, 2$), or from requiring the \mathcal{W} -function to give a real result (for $p = \infty$):

$$\mu_c = \begin{cases} \frac{\beta}{\alpha + \beta} 2^{-(L+1)}, & p = 0, \\ \frac{\beta}{4\alpha L + 2\beta(L+1)}, & p = 1, \\ \frac{\beta}{4\alpha L + \beta(L+3)}, & p = 2, \\ \frac{1}{2L} \mathcal{W}\left(\frac{\beta}{e\alpha}\right), & p = \infty. \end{cases} \quad (\text{A.12})$$

Finally, it is easy to evaluate the bifurcation diagram at $a = 1/2$ to get the critical mutation rate $\tilde{\mu}_c = \mu(1/2)$:

$$\tilde{\mu}_c = \frac{\beta S'(1/2)}{2\beta S'(1/2) + 4L(\alpha + \beta S(1/2))}. \quad (\text{A.13})$$

For our specificity function $f_s(d) = (1 - d/L)^p$, we obtain explicitly

$$\tilde{\mu}_c = \begin{cases} 2^{-(L+1)} \frac{\beta}{\alpha + \beta}, & p = 0 \\ \frac{\beta}{4\alpha L + 2\beta(L+1)}, & p = 1 \\ \frac{\beta}{4\alpha L + \beta(L+3)}, & p = 2 \\ \frac{\beta}{\alpha 2^{L+1} + 4\beta}, & p = \infty. \end{cases} \quad (\text{A.14})$$

Note that $\mu_c = \tilde{\mu}_c$ for $p \leq 2$.

While most of these results can be evaluated also for $\alpha = 0$, the case $p \rightarrow \infty$ is special. Here, Eq. (9) gives $x = \mu/(1 - 2\mu)$ if we again approximate $(1 - 2x)^L \approx e^{-2xL}$, hence the error threshold is $\mu_c = 1/6$, independent of β and L .

Appendix B. Cross-specific replication

Appendix B.1. Derivation of an equation for a

To obtain an equation for the parameter a , we compute the second moment $\sum_k k^2 \dot{x}_k$ of the reduced rate equations under the assumption that $x_k = x_k^c \equiv \frac{1}{2} \binom{L}{k} [a^k (1 - a)^{L-k} + a^{L-k} (1 - a)^k]$ is a sum of two complementary binomials, because in this case the first moment vanishes by construction. The four terms T_1 - T_4 are defined and evaluated analogously to Eq. (A.1), and after some algebra

we find:

$$T_1 = \frac{1}{2}\alpha L [L - 2(L-1)(a(1-a)(1-2\mu)^2 + \mu(1-\mu))] \quad (\text{B.1})$$

$$T_2 = \frac{1}{2}\beta \left[L(L-2(L-1)(a + \mu(1-2a))(1-a - \mu(1-2a)))C(1-2a(1-a)) \right. \\ \left. + 2a(1-a)(1-2a)^2(1-2\mu)^2(L-1)C'(1-2a(1-a)) \right. \\ \left. + 2(a(1-a)(1-2a)(1-2\mu))^2C''(1-2a(1-a)) \right] \quad (\text{B.2})$$

$$T_3 = -\frac{1}{2}\alpha L [L - 2(L-1)a(1-a)] \quad (\text{B.3})$$

$$T_4 = -\frac{1}{2}\beta L [L - 2(L-1)a(1-a)]C(1-2a(1-a)). \quad (\text{B.4})$$

Here, we have defined $C(x) = \frac{1}{2} \sum_k \binom{L}{k} [f_c(k) + f_c(L-k)]x^{L-k}(1-x)^k$. Adding up $T_1 + T_2 + T_3 + T_4 = 0$ gives the condition

$$(1-2a)^2 \left\{ \begin{aligned} &\mu(1-\mu)L(L-1)[\alpha + \beta C(1-2a(1-a))] \\ &- \beta a(1-a)(1-2\mu)^2[(L-1)C'(1-2a(1-a)) \\ &+ a(1-a)C''(1-2a(1-a))] \end{aligned} \right\} = 0. \quad (\text{B.5})$$

Most importantly, Eq. (B.5) reads for $p = 1$ in the specificity function $f_c(d) = (d/L)^p$:

$$-(1-2a)^2 L(L-1)\mu(1-\mu)(\alpha + \beta/2) = 0, \quad (\text{B.6})$$

which has only the solution $a = 1/2$.

Appendix B.2. Bifurcation diagram

Solving Eq. (B.5) for μ gives the bifurcation diagram:

$$\mu(a) = \frac{1}{2} \left[1 \pm \left(1 + \frac{4\beta a(1-a)[(L-1)C'(1-2a(1-a)) + a(1-a)C''(1-2a(1-a))]}{L(L-1)[\alpha + \beta C(1-2a(1-a))]} \right)^{-1/2} \right], \quad (\text{B.7})$$

where we take the negative sign and the positive root to obtain values μ near zero (values near unity imply complementary replication and give equivalent results for cross-specific replication).

We readily find that $\mu''(1/2) > 0$ if $\beta > 0$, which implies that the pitchfork bifurcation described through Eq. (B.7) is always subcritical.

Appendix B.3. Solutions of Eq. (B.5)

The auxiliary function $C(x)$ can be evaluated for small integer p as in Eq. (A.10). There is no solution to Eq. (B.5) except $a = 1/2$ for $p = 1$, and the

expression for $p = 2$ is quite lengthy. For $p = \infty$ and $\alpha > 0$, we get

$$x = a(1 - a) = \mu - \frac{1}{2L} \mathcal{W} \left(\frac{4\alpha\mu L}{\beta} e^{2\mu L} \right), \quad (\text{B.8})$$

which is exactly the result for the self-specific case if we replace $\beta \rightarrow \beta/2$. Accordingly, we get $\mu_c = \mathcal{W}[\beta/(2e\alpha)]/(2L)$ for the error threshold.

Observing that $C'(1/2) = 0$, the critical mutation rate $\tilde{\mu}_c = \mu(1/2)$ is given by

$$\tilde{\mu}_c = \frac{1}{2} \left[1 - \left(1 + \frac{\beta C''(1/2)}{4L(L-1)(\alpha + \beta C(1/2))} \right)^{-1/2} \right], \quad (\text{B.9})$$

which reads explicitly

$$\tilde{\mu}_c = \begin{cases} 0, & p = 1 \\ \frac{1}{2} \left[1 - \left(1 + \frac{2\beta}{4\alpha L^2 + \beta L(L+1)} \right)^{-1/2} \right], & p = 2 \\ \frac{1}{2} \left[1 - \left(1 + \frac{\beta}{\alpha 2^L + \beta} \right)^{-1/2} \right], & p = \infty. \end{cases} \quad (\text{B.10})$$

We can simply take $\alpha = 0$ in most of the above expressions to investigate the case of zero non-enzymatic replication rate. In the limits $p \rightarrow \infty$ and $L \rightarrow \infty$, we find that the bifurcation diagram $\mu(a)$ converges towards

$$\mu(a) \rightarrow a(1 - a), \quad (\text{B.11})$$

except for a region near $a = 1/2$, where $\mu(a)$ has to coincide with the exact value $\tilde{\mu}_c = (2 - \sqrt{2})/4$. Because this region becomes infinitesimally small as $L \rightarrow \infty$, we conclude that $\mu_c \rightarrow 1/4$ in this limit.

References

- Acevedo, O., Orgel, L., 1987. Non-enzymatic transcription of an oligodeoxynucleotide 14 residues long. *J Mol Biol* 197, 187–93.
- Alves, D., Campos, P., Silva, A., Fontanari, J., 2001. Group selection models in prebiotic evolution. *Phys. Rev. E* 63, 011911.
- Baake, E., Wiehe, T., 1997. Bifurcations in haploid and diploid sequence space models. *J Math Biol* 35, 321–343.
- Blythe, R., 2009. Generic modes of consensus formation in stochastic language dynamics. *J Stat Mech-Theory E*, P02059.
- Campos, P., Fontanari, J., Stadler, P., 2000. Error propagation in the hypercycle. *Phys. Rev. E* 61, 2996–3002.
- Cech, T., 1990. Nobel lecture. Self-splicing and enzymatic activity of an intervening sequence RNA from *tetrahymena*. *Biosci Rep* 10, 239–61.

- Doudna, J., Cech, T., 2002. The chemical repertoire of natural ribozymes. *Nature* 418, 222–228.
- Eigen, M., McCaskill, J., Schuster, P., 1989. The molecular quasi-species. *Adv Chem Phys* 75, 149–263.
- Eigen, M., Schuster, P., 1978. The hypercycle – a principle of natural self-organization. Part B: The abstract hypercycle. *Naturwissenschaften* 65, 7–41.
- Fontanari, J., Santos, M., Szathmari, E., 2006. Coexistence and error propagation in pre-biotic vesicle models: A group selection approach. *J Theor Biol* 239, 247–256.
- Galluccio, S., 1997. Exact solution of the quasispecies model in a sharply peaked fitness landscape. *Phys. Rev. E* 56, 4526–4539.
- Gerland, U., Hwa, T., 2002. On the selection and evolution of regulatory DNA motifs. *J Mol Evol* 55, 386–400.
- Gilbert, W., 1986. Origin of life – the RNA world. *Nature* 319, 618–618.
- Hermisson, J., Redner, O., Wagner, H., Baake, E., 2002. Mutation-selection balance: Ancestry, load, and maximum principle. *Theor Popul Biol* 62, 9–46.
- Hofbauer, J., Sigmund, K., 1998. *Evolutionary games and population dynamics*. Cambridge University Press.
- Jain, K., Krug, J., 2005. Adaptation in simple and complex fitness landscapes. arXiv: q-bio/0508008.
- Johnston, W., Unrau, P., Lawrence, M., Glasner, M., Bartel, D., 2001. RNA-catalyzed RNA polymerization: accurate and general RNA-templated primer extension. *Science* 292, 1319–25.
- Joyce, G.F., 2007. Forty years of in vitro evolution. *Angew Chem Int Ed* 46, 6420–36.
- v Kiedrowski, G., 1986. A self-replicating hexadeoxynucleotide. *Angew Chem Int Ed* 25, 932–935.
- Komarova, N., 2004. Replicator-mutator equation, universality property and population dynamics of learning. *J Theor Biol* 230, 227–239.
- Lässig, M., Tria, F., Peliti, L., 2003. Evolutionary games and quasispecies. *Europhys Lett* 62, 446–451.
- Leuthäusser, I., 1986. An exact correspondence between Eigen’s evolution model and a two-dimensional Ising system. *J Chem Phys* 84, 1884–1885.
- Lilley, D.M., 2005. Structure, folding and mechanisms of ribozymes. *Curr Opin Struc Biol* 15, 313–23.

- Lincoln, T., Joyce, G., 2009. Self-sustained replication of an RNA enzyme. *Science* 323, 1229–1232.
- Maynard Smith, J., 1979. Hypercycles and the origin of life. *Nature* 280, 445–446.
- Nowak, M., Komarova, N., Niyogi, P., 2001. Evolution of universal grammar. *Science* 291, 114–118.
- Obermayer, B., Frey, E., 2009. Escalation of error catastrophe for enzymatic self-replicators. *Europhys Lett* 88, 48006.
- Orgel, L., 1992. Molecular replication. *Nature* 358, 203–209.
- Orgel, L., 2004. Prebiotic chemistry and the origin of the RNA world. *Crit Rev Biochem Mol* 39, 99–123.
- Pace, N., Marsh, T., 1985. RNA catalysis and the origin of life. *Origins Life Evol B* 16, 97–116.
- Peliti, L., 2002. Quasispecies evolution in general mean-field landscapes. *Europhys Lett* 57, 745–751.
- Rawlings, D., Sze, L., 2005. On the metamorphosis of vandermonde’s identity. *Mathematics Magazine* 78, 232–238.
- Saakian, D.B., Biebricher, C.K., Hu, C.K., 2009. Phase diagram for the Eigen quasispecies theory with a truncated fitness landscape. *Phys. Rev. E* 79, 041905.
- Saakian, D.B., Hu, C.K., 2006. Exact solution of the Eigen model with general fitness functions and degradation rates. *P Natl Acad Sci USA* 103, 4935–4939.
- Schuster, P., Swetina, J., 1988. Stationary mutant distributions and evolutionary optimization. *Bull Math Biol* 50, 635–660.
- Stadler, P., Schnabl, W., Forst, C., Schuster, P., 1995. Dynamics of small autocatalytic reaction networks. 2. Replication, mutation and catalysis. *Bull Math Biol* 57, 21–61.
- Summers, J., Litwin, S., 2006. Examining the theory of error catastrophe. *J Virol* 80, 20–26.
- Swetina, J., Schuster, P., 1982. Self-replication with errors – a model for polynucleotide replication. *Biophys Chem* 16, 329–345.
- Szostak, J., Bartel, D., Luisi, P.L., 2001. Synthesizing life. *Nature* 409, 387–309.
- Takeuchi, N., Hogeweg, P., 2007. Error-threshold exists in fitness landscapes with lethal mutants. *BMC Evol Biol* 7, 15.

- Wagner, N., Tannenbaum, E., Ashkenasy, G., 2009. Second-order catalytic quasispecies yields first-order phase transition. arXiv: q-bio/0912.4960.
- Weiner, A., Maizels, N., 1987. Transfer RNA-like structures tag the 3' ends of genomic RNA molecules for replication – implications for the origin of protein-synthesis. *P Natl Acad Sci USA* 84, 7383–7387.
- Wiehe, T., 1997. Model dependency of error thresholds: the role of fitness functions and contrasts between the finite and infinite sites models. *Genet Res* 69, 127–136.
- Wilke, C., 2005. Quasispecies theory in the context of population genetics. *BMC Evol Biol* 5, 44.
- Wilke, C., Ronnewinkel, C., Martinetz, T., 2001. Dynamic fitness landscapes in molecular evolution. *Phys Rep* 349, 395–446.
- Woodcock, G., Higgs, P., 1996. Population evolution on a multiplicative single-peak fitness landscape. *J Theor Biol* 179, 61–73.
- Wu, T., Orgel, L., 1992. Nonenzymatic template-directed synthesis on oligodeoxycytidylate sequences in hairpin oligonucleotides. *J Am Chem Soc* 114, 317–322.
- Zaher, H.S., Unrau, P.J., 2007. Selection of an improved RNA polymerase ribozyme with superior extension and fidelity. *RNA* 13, 1017–1026.

A. Calculation details for Chapter 2

This appendix compiles some technical calculations for the nonlinear dynamic response of semiflexible polymers discussed in Chapter 2.

A.1. Asymptotic force-extension relations

In the stationary state at $t < 0$, the stored length density for scenarios involving an external force follows as high-force asymptote from Eq. (2.22) as

$$\langle \bar{\varrho} \rangle (s) = \frac{1}{2\ell_p \sqrt{f_0(s)}} - \frac{\ell_p}{k_x} f_0(s), \quad (\text{A.1})$$

while $\varrho = L/(6\theta\ell_p)$ for the “quench” case. Fortunately, the potential singularity of Eq. (A.1) near force-free ends is unproblematic. For the setups analyzed in Ref. [204] we have therefore

$$\frac{R_{\parallel}}{L} = 1 - \frac{1}{L} \int_0^L ds \langle \bar{\varrho} \rangle (s) = \begin{cases} 1 - \frac{1}{2\ell_p \sqrt{f_{\text{pre}}}} + \frac{\ell_p f_{\text{pre}}}{k_x}, & \text{“force”,} & (\text{A.2a}) \\ 1 - \frac{1}{2\ell_p \sqrt{\frac{1}{4}\hat{\zeta}vL}} + \frac{\frac{1}{2}\hat{\zeta}vL\ell_p}{k_x}, & \text{“field”,} & (\text{A.2b}) \\ 1 - \frac{1}{2\ell_p \sqrt{\frac{1}{2\pi^2}\hat{\zeta}\dot{\gamma}L^2}} + \frac{\frac{1}{12}\hat{\zeta}\dot{\gamma}L^2\ell_p}{k_x}, & \text{“shear”,} & (\text{A.2c}) \\ 1 - \frac{L}{6\theta\ell_p}, & \text{“quench”.} & (\text{A.2d}) \end{cases}$$

This allows to choose the control parameters such as to have comparable initial extension R_{\parallel} : for instance, for an inextensible filament ($k_x \rightarrow \infty$) one would take $f_{\text{pre}} = \frac{1}{4}\hat{\zeta}vL = \frac{1}{2\pi^2}\hat{\zeta}\dot{\gamma}L^2 = (3\theta/L)^2$.

A.2. Discretization effects

In order to include discretization effects, we assume that the mode decomposition of Eq. (2.17a) is cut off at some highest mode $q_{\text{max}} \simeq \pi/b$, where b is a microscopic length scale

(the polymer thickness, the bond length, the bead size, the rod length, etc.), which is assumed to be small enough ($N = L/b \gg 1$) to justify the approximation $L^{-1} \sum_q \approx \pi^{-1} \int dq$. For a “force” scenario as in Sec. 2.5, Eq. (2.24) reads

$$\partial_s^2 F(s, t) = \hat{\zeta} \int_0^{\pi/b} \frac{dq}{\pi \ell_p} \left[\frac{1 - \chi_{\perp}^2(q; t, 0)}{q^2 + f_{\text{pre}}} - 2q^2 \int_0^t dt' \chi_{\perp}^2(q; t, t') \right]. \quad (\text{A.3})$$

From the response function Eq. (2.19), we get the asymptotic scaling for the wave number $Q \simeq \ell_{\perp}^{-1}$ of the mode that relaxes at time t :

$$Q \simeq \begin{cases} t^{-1/4}, & \text{if } F^2/t \ll 1 \quad (\text{“linear”}) \\ F^{-1/2}, & \text{if } F^2/t \gg 1 \quad (\text{“nonlinear”}) \end{cases} \quad (\text{A.4})$$

Normally, we would expect relevant discretization effects only in the regime $Q \gg \pi/b$, when the cutoff mode π/b suppresses essential parts of the response function χ_{\perp} . In this case, the longitudinal relaxation is dominated by normal diffusive relaxation of (compared to Q) long wavelength modes, which are essentially uninhibited by the elastic (bending and tension) forces that would otherwise lead to anomalous diffusion. But the initial mode spectrum $1/[q^2 + f_{\text{pre}}]$ in the first term on the right hand side of Eq. (A.3) behaves differently, depending on the magnitude of f_{pre} . It turns out that discretization effects are much more relevant than normally expected for larger forces $f_{\text{pre}} \gg b^{-2}$, see Table A.1.

A.2.1. Small force ($f_{\text{pre}} \ll b^{-2}$)

In the case $Q \gg \pi/b \gg f_{\text{pre}}^{1/2}$, we can perform an expansion of the right hand side of Eq. (A.3) with respect to the integrated tension F and to the force f_{pre} [99, 203]:

$$\partial_s^2 F(s, t) \approx \hat{\zeta} \int_0^{\pi/b} \frac{dq}{\pi \ell_p} \left[-\frac{f_{\text{pre}}}{q^4} \left(1 - e^{-2q^4 t} \right) + 2F(s, t) - 4q^4 \int_0^t dt' F(s, t') e^{-2q^4(t-t')} \right]. \quad (\text{A.5})$$

Using the Laplace transform $\tilde{F}(s, z) = \mathcal{L}\{F(s, t)\}$, this reads

$$\partial_s^2 \tilde{F}(s, z) = \hat{\zeta} \int_0^{\pi/b} \frac{dq}{\pi \ell_p} \left[-\frac{2f_{\text{pre}}}{z(z + 2q^4)} + \tilde{F}(s, z) \frac{2z}{z + 2q^4} \right], \quad (\text{A.6})$$

which, after performing the q -integral, reduces to:

$$\lambda^2 \partial_s^2 \tilde{F} = \tilde{F} - \frac{f_{\text{pre}}}{z^2}. \quad (\text{A.7})$$

Since initially $Q \simeq t^{-1/4} \simeq z^{1/4}$ and therefore $bz^{1/4} \gg 1$, the characteristic length is given by $\lambda = [\ell_p b / (2\hat{\zeta})]^{1/2}$ independent of z . The solution in real space reads

$$F(s, t) = f_{\text{pre}} t \left(1 - \frac{\cosh[(L - 2s)/(2\lambda)]}{\cosh[L/(2\lambda)]} \right). \quad (\text{A.8})$$

The tension profile $f(s, t) = \partial_t F(s, t)$ is *stationary*, there is *no propagation*. For polymers with $\ell_p < L$ (or sufficiently fine discretization $b \ll L^2/\ell_p$ otherwise), we find that $\lambda \ll L$. In this case, the change in end-to-end distance is given by

$$\Delta_{\parallel}(t) = -\sqrt{\frac{8}{\hat{\zeta}\ell_p b}} f_{\text{pre}} t \quad \text{for } t \ll b^4 \quad (\text{A.9})$$

At $t = b^4$, there is a crossover to the linear propagation regime $b^4 \ll t \ll f_{\text{pre}}^{-2}$, where discretization effects are irrelevant.

A.2.2. Intermediate force ($b^{-2} \ll f_{\text{pre}} \ll L^2/(\ell_p b^3)$).

In the case $Q, f_{\text{pre}}^{1/2} \gg \pi/b$, we can also linearize Eq. (A.3) in F , but *not in* f_{pre} as before in Eq. (A.6). The leading order terms are

$$\partial_s^2 F \approx \hat{\zeta} \int_0^{\pi/b} \frac{dq}{\pi\ell_p} \left[\frac{2q^2 F}{f_{\text{pre}}} - 2q^2 t \right] = \lambda^{-2} [F - f_{\text{pre}} t], \quad (\text{A.10})$$

with the solution Eq. (A.8), but a different length $\lambda = [3\ell_p f_{\text{pre}} b^3 / (2\hat{\zeta}\pi^2)]^{1/2}$. Again, there is no propagation. The change in end-to-end distance is given by

$$\Delta_{\parallel}(t) = -\sqrt{\frac{8f_{\text{pre}}\pi^2}{3\hat{\zeta}\ell_p b^3}} t \quad \text{for } t \ll \frac{b^2}{f_{\text{pre}}}, \quad (\text{A.11})$$

and $Q \simeq \pi/b$ at $t = b^2/f_{\text{pre}} \gg f_{\text{pre}}^{-2}$.

In the following regime, $\pi/b \gg Q \simeq F^{-1/2}$ holds, and we find the response function $\chi_{\perp}(q; t, t')$ from Eq. (2.19) finite only near $t' \approx t$. We can thus linearize $F(s, t) - F(s, t') \approx [\partial_t F(s, t)](t - t')$ in the exponent. In contrast to the case $Q \gg \pi/b$, where we expanded the exponential of the response function Eq. (2.19) in a series, we now set it to zero:

$$\partial_s^2 F \approx \hat{\zeta} \int_0^{\pi/b} \frac{dq}{\pi\ell_p} \left[\frac{1}{q^2 + f_{\text{pre}}} - \frac{1}{q^2 + \partial_t F} \right]. \quad (\text{A.12})$$

The integrals have different asymptotes, depending on the products $b f_{\text{pre}}^{1/2}$ and $b[\partial_t F]^{1/2}$, i.e., even for $t \gg f_{\text{pre}}/b^2$ discretization effects may be important.

Intermediate time regime. Initially $F \simeq f_{\text{pre}} t$, and because $f_{\text{pre}} \gg b^{-2}$ was assumed, we find from Eq. (A.12)

$$\partial_s^2 F \approx \frac{\hat{\zeta}}{\ell_p b} [f_{\text{pre}}^{-1} - (\partial_t F)^{-1}]. \quad (\text{A.13})$$

Taking a time derivative gives

$$\partial_s^2 f = \frac{\hat{\zeta}}{\ell_p b} \frac{\partial_t f}{f^2}. \quad (\text{A.14})$$

This can be solved in two limits. During the propagation regime $t \ll t_L^\parallel$, the scaling ansatz $f(s, t) = f_{\text{pre}}\varphi(s/\ell_\parallel(t))$ with a growing boundary layer $\ell_\parallel(t) = (\ell_p b/\hat{\zeta})^{1/2} f_{\text{pre}} t^{1/2}$ gives

$$\partial_\xi^2 \varphi(\xi) = -\frac{1}{2} \xi \varphi^{-2}(\xi) \partial_\xi \varphi(\xi), \quad (\text{A.15})$$

with boundary conditions $\varphi(0) = 0$, $\varphi(\xi \rightarrow \infty) = 1$. A numerical solution yields $\varphi'(0) \approx 4.501$, and the change in end-to-end distance follows as:

$$\Delta_\parallel(t) \approx -18 \sqrt{\frac{t}{\hat{\zeta} \ell_p b}}. \quad (\text{A.16})$$

At $t = \hat{\zeta} L^2 / (\ell_p b f_{\text{pre}}^2)$ when $\ell_\parallel = L$, this propagation regime ends. For the relaxation regime, we choose the asymptotic separation ansatz $f(s, t) = [\hat{\zeta} L^2 / (\ell_p b t)]^{1/2} h(s/L)$ where $h(\xi)$ solves

$$h'' = -\frac{1}{2h} \quad \text{with } h(0) = h(1) = 0. \quad (\text{A.17})$$

Unfortunately, near the boundaries this equation gives a pathological singularity: Although we obtain a finite value $h(1/2) = (4\pi)^{-1/2}$, the slope at the boundary diverges, $h'(0) \rightarrow \infty$, such that we cannot find a reasonable numerical prefactor for the growth law of the change in projected length:

$$\Delta_\parallel(t) = -4h'(0) \sqrt{\frac{t}{\hat{\zeta} \ell_p b}}. \quad (\text{A.18})$$

This complication arises because the condition $b[\partial_t F]^{1/2} \gg 1$ for the asymptotic Eq. (A.13) is violated very close to the boundary where $\partial_t F = f$ is near zero. However, our numerical solutions to Eq. (A.3) agree excellently with this scaling and they further suggest a numerically stable value of about $h'(0) \approx 1.9$. We conclude:

1. The crossover at $t = t_L^\parallel$ does not change the scaling of $\Delta_\parallel(t)$.
2. The condition $b[\partial_t F]^{1/2} \gg 1$ holds up to times $t = \hat{\zeta} L^2 b^3 / \ell_p \ll b^4$.
3. Discretization effects matter therefore for much longer times than in the case of small force.
4. This time regime $b^2/f_{\text{pre}} \ll t \ll L^2 b^3 / \ell_p$ is formally equivalent to the regime of nonlinear propagation ($f_{\text{pre}}^{-2} \ll t \ll L^2 / (\ell_p f_{\text{pre}}^{3/2})$) of the ‘‘force’’ setup if $b \rightarrow f_{\text{pre}}^{-1/2}$ is replaced.

Long-time regime. For times $t \gg L^2 b^3 / \ell_p$, the tension becomes so small that $b[\partial_t F]^{1/2} \ll 1$. In this case, Eq. (A.12) reads

$$\partial_s^2 F \approx \frac{\hat{\zeta}}{2\ell_p} \left[\frac{2}{f_{\text{pre}} b} - (\partial_t F)^{-1/2} \right]. \quad (\text{A.19})$$

(a)	$t \ll b^4$	$b^4 \ll t \ll t_f$	$t_f \ll t \ll t_L^{\parallel}$	$t_L^{\parallel} \ll t$
	$\frac{f_{\text{pre}} t}{(\hat{\zeta} \ell_p b)^{1/2}}$	$\frac{f_{\text{pre}} t^{7/8}}{(\hat{\zeta} \ell_p)^{1/2}}$	$\frac{f_{\text{pre}}^{1/4} t^{1/2}}{(\hat{\zeta} \ell_p)^{1/2}}$	$\left(\frac{Lt}{\hat{\zeta} \ell_p^2}\right)^{1/3}$
(b)	$t \ll \frac{b^2}{f_{\text{pre}}}$	$\frac{b^2}{f_{\text{pre}}} \ll t \ll \frac{L^2 b^3}{\ell_p}$	$\frac{L^2 b^3}{\ell_p} \ll t$	
	$\frac{f_{\text{pre}}^{1/2} t}{(\hat{\zeta} \ell_p b^3)^{1/2}}$	$\frac{t^{1/2}}{(\hat{\zeta} \ell_p b)^{1/2}}$	$\left(\frac{Lt}{\hat{\zeta} \ell_p^2}\right)^{1/3}$	
(c)	$t \ll \frac{\ell_p b^5}{L^2}$	$\frac{\ell_p b^5}{L^2} \ll t \ll \frac{L^2 b^3}{\ell_p}$	$\frac{L^2 b^3}{\ell_p} \ll t$	
	$\frac{Lt}{b^3 \ell_p}$	$\frac{t^{1/2}}{(\hat{\zeta} \ell_p b)^{1/2}}$	$\left(\frac{Lt}{\hat{\zeta} \ell_p^2}\right)^{1/3}$	

Table A.1: Asymptotic scaling laws for the change in projected length $|\Delta_{\parallel}(t)|$ for a “force” setup, including discretization effects for (a) $f_{\text{pre}} \ll b^{-2}$, (b) $b^{-2} \ll f_{\text{pre}} \ll L^2/(\ell_p b^3)$, and (c) $L^2/(\ell_p b^3) \ll f_{\text{pre}}$.

Again taking a time derivative, we arrive at:

$$\partial_s^2 f = \frac{\hat{\zeta} \partial_t f}{4 \ell_p f^{3/2}}. \quad (\text{A.20})$$

Here, we try the separation ansatz $f(s, t) = g(t)h(\xi)$ with $\xi = s/L$, which gives [99]

$$g(t) = \left(\frac{\hat{\zeta} L^2}{\ell_p t}\right)^{2/3}, \quad (\text{A.21})$$

and the function $h(\xi)$ solves

$$h'' = -\frac{1}{6h^{1/2}} \quad \text{with } h(0) = h(1) = 0. \quad (\text{A.22})$$

For the almost parabolic profile $h(\xi)$ we find the characteristics [99]

$$h'(0) = 12^{-1/3}, \quad h(1/2) = \left(\frac{3}{128}\right)^{2/3}. \quad (\text{A.23})$$

A.2.3. Large force ($f_{\text{pre}} \gg L^2/(\ell_p b^3)$).

For large forces $f_{\text{pre}} \gg L^2/(\ell_p b^3)$, the characteristic length $\lambda = [3\ell_p b f_{\text{pre}}/(2\hat{\zeta}\pi^2)]^{1/2} \gg L$ in the initial regime described by Eq. (A.10), is very large, and the tension profile Eq. (A.8) therefore simply parabolic. This gives

$$\Delta_{\parallel}(t) \simeq -\frac{2\pi^2 Lt}{3b^3 \ell_p} \quad (\text{A.24})$$

for times up to $t = b^5 \ell_p / L^2$ when $Q \simeq \pi/b$. The following regimes are similar to the case of intermediate force: Eq. (A.13) holds, but its solution yields Eq. (A.18). At $t = \hat{\zeta} L^2 b^3 / \ell_p$, finally, this regime is followed by the regime of homogeneous tension relaxation, similar to Eqs. (A.21), (A.22), (A.23). Since there is no dependence on f_{pre} left, we conclude that forces larger than $\hat{\zeta} L^2 / (\ell_p b^3)$ are equivalent to *infinite forces*, i.e., an *exactly straight initial conformation*, where initially parabolic tension profiles are to be expected [92].

Bibliography

- [1] O. L. Acevedo and L. E. Orgel, “Non-enzymatic transcription of an oligodeoxynucleotide 14 residues long”, *J Mol Biol*, **197**, 187 (1987)
- [2] A. Ajdari, F. Jülicher, and A. Maggs, “Pulling on a filament”, *J Phys I*, **7**, 823 (1997)
- [3] D. Alves, P. R. A. Campos, A. T. C. Silva, and J. F. Fontanari, “Group selection models in prebiotic evolution”, *Phys Rev E*, **63**, 011911 (2001)
- [4] D. Alves and J. F. Fontanari, “Error threshold in finite populations”, *Phys Rev E*, **57**, 7008 (1998)
- [5] F. Amblard, A. C. Maggs, B. Yurke, A. N. Pargellis, and S. Leibler, “Subdiffusion and anomalous local viscoelasticity in actin networks”, *Phys Rev Lett*, **77**, 4470 (1996)
- [6] M. A. Andrade, A. J. García-Tejedor, and F. Montero, “Study of an error-prone hypercycle formed from two kinetically distinguishable species”, *Biophys Chem*, **40**, 43 (1991)
- [7] M. A. Andrade, J. C. Nuño, F. Morán, F. Montero, and G. J. Mpitsos, “Complex dynamics of a catalytic network having faulty replication into error-species”, *Physica D*, **63**, 21 (1993)
- [8] S. R. Aragón and R. Pecora, “Dynamics of wormlike chains”, *Macromolecules*, **18**, 1868 (1985)
- [9] C. S. O. Attolini and P. F. Stadler, “Evolving towards the hypercycle: A spatial model of molecular evolution”, *Physica D*, **217**, 134 (2006)
- [10] E. Baake, M. Baake, and H. Wagner, “Ising quantum chain is equivalent to a model of biological evolution”, *Phys Rev Lett*, **78**, 559 (1997)
- [11] E. Baake and W. Gabriel, “Biological evolution through mutation, selection, and drift: An introductory review”, *Ann Rev Comp Phys VII*, 203 (2000)
- [12] E. Baake and H. Wagner, “Mutation-selection models solved exactly with methods of statistical mechanics”, *Genet Res*, **78**, 93 (2001)
- [13] E. Baake and T. Wiehe, “Bifurcations in haploid and diploid sequence space models”, *J Math Biol*, **35**, 321 (1997)

- [14] P. Baaske, F. M. Weinert, S. Duhr, K. H. Lemke, M. J. Russell, et al., “Extreme accumulation of nucleotides in simulated hydrothermal pore systems”, *P Natl Acad Sci USA*, **104**, 9346 (2007)
- [15] O. B. Bakajin, T. A. J. Duke, C. F. Chou, S. S. Chan, R. H. Austin, et al., “Electrohydrodynamic stretching of DNA in confined environments”, *Phys Rev Lett*, **80**, 2737 (1998)
- [16] A. Balducci, C.-C. Hsieh, and P. S. Doyle, “Relaxation of stretched DNA in slitlike confinement”, *Phys Rev Lett*, **99**, 238102 (2007)
- [17] G. K. Batchelor, “Slender-body theory for particles of arbitrary cross-section in Stokes flow”, *J Fluid Mech*, **44**, 419 (1970)
- [18] A. R. Bausch and K. Kroy, “A bottom-up approach to cell mechanics”, *Nat Phys*, **2**, 231 (2006)
- [19] D. Bensimon, A. J. Simon, V. Croquette, and A. Bensimon, “Stretching DNA with a receding meniscus: Experiments and models”, *Phys Rev Lett*, **74**, 4754 (1995)
- [20] K. Bloom and A. Joglekar, “Towards building a chromosome segregation machine”, *Nature*, **463**, 446 (2010)
- [21] R. A. Blythe and A. J. McKane, “Stochastic models of evolution in genetics, ecology and linguistics”, *J Stat Mech-Theory E*, P07018 (2007)
- [22] Y. Bohbot-Raviv, W. Z. Zhao, M. Feingold, C. H. Wiggins, and R. Granek, “Relaxation dynamics of semiflexible polymers”, *Phys Rev Lett*, **92**, 098101 (2004)
- [23] C. Bouchiat, M. D. Wang, J.-F. Allemand, T. Strick, S. M. Block, et al., “Estimating the persistence length of a worm-like chain molecule from force-extension measurements”, *Biophys J*, **76**, 409 (1999)
- [24] F. Brochard-Wyart, “Polymer chains under strong flows – stems and flowers”, *Europhys Lett*, **30**, 387 (1995)
- [25] F. Brochard-Wyart, A. Buguin, and P. G. de Gennes, “Dynamics of taut DNA chains”, *Europhys Lett*, **47**, 171 (1999)
- [26] B. van den Broek, M. C. Noom, and G. J. L. Wuite, “DNA-tension dependence of restriction enzyme activity reveals mechanochemical properties of the reaction pathway”, *Nucleic Acids Res*, **33**, 2676 (2005)
- [27] J. J. Bull, L. A. Meyers, and M. Lachmann, “Quasispecies made simple”, *Plos Comput Biol*, **1**, 450 (2005)
- [28] C. Bustamante, Z. Bryant, and S. B. Smith, “Ten years of tension: Single-molecule DNA mechanics”, *Nature*, **421**, 423 (2003)

- [29] C. Bustamante, J. C. Macosko, and G. J. L. Wuite, “Grabbing the cat by the tail: Manipulating molecules one by one”, *Nat Rev Mol Cell Bio*, **1**, 130 (2000)
- [30] C. Bustamante, J. F. Marko, E. D. Siggia, and S. Smith, “Entropic elasticity of λ -phage DNA”, *Science*, **265**, 1599 (1994)
- [31] C. Bustamante, S. B. Smith, J. Liphardt, and D. Smith, “Single-molecule studies of DNA mechanics”, *Curr Opin Struc Biol*, **10**, 279 (2000)
- [32] P. R. A. Campos and J. F. Fontanari, “Finite-size scaling of the quasispecies model”, *Phys Rev E*, **58**, 2664 (1998)
- [33] P. R. A. Campos, J. F. Fontanari, and P. F. Stadler, “Error propagation in the hypercycle”, *Phys Rev E*, **61**, 2996 (2000)
- [34] A. Caspi, M. Elbaum, R. Granek, A. Lachish, and D. Zbaida, “Semiflexible polymer network: A view from inside”, *Phys Rev Lett*, **80**, 1106 (1998)
- [35] T. R. Cech, “Nobel lecture. Self-splicing and enzymatic activity of an intervening sequence RNA from *Tetrahymena*”, *Biosci Rep*, **10**, 239 (1990)
- [36] I. A. Chen, “The emergence of cells during the origin of life”, *Science*, **314**, 1558 (2006)
- [37] I. A. Chen, R. W. Roberts, and J. W. Szostak, “The emergence of competition between model protocells”, *Science*, **305**, 1474 (2004)
- [38] I. A. Chen, K. Salehi-Ashtiani, and J. W. Szostak, “RNA catalysis in model protocell vesicles”, *J Am Chem Soc*, **127**, 13213 (2005)
- [39] I. A. Chen and J. W. Szostak, “A kinetic study of the growth of fatty acid vesicles”, *Biophys J*, **87**, 988 (2004)
- [40] I. A. Chen and J. W. Szostak, “Membrane growth can generate a transmembrane pH gradient in fatty acid vesicles”, *P Natl Acad Sci USA*, **101**, 7965 (2004)
- [41] P. Cizeau and J.-L. Viovy, “Modeling extreme extension of DNA”, *Biopolymers*, **42**, 383 (1997)
- [42] P. Cluzel, A. Lebrun, C. Heller, R. Lavery, J.-L. Viovy, et al., “DNA: An extensible molecule”, *Science*, **271**, 792 (1996)
- [43] A. Crut, D. A. Koster, R. Seidel, C. H. Wiggins, and N. H. Dekker, “Fast dynamics of supercoiled DNA revealed by single-molecule experiments”, *P Natl Acad Sci USA*, **104**, 11957 (2007)
- [44] A. Crut, P. A. Nair, D. A. Koster, S. Shuman, and N. H. Dekker, “Dynamics of phosphodiester synthesis by DNA ligase”, *P Natl Acad Sci USA*, **105**, 6894 (2008)

- [45] P. G. de Gennes, P. Pincus, R. M. Velasco, and F. Brochard, “Remarks on polyelectrolyte conformation”, *J Phys-Paris*, **37**, 1461 (1976)
- [46] P. Dimitrakopoulos, “Conformational evolution of initially straight flexible and stiff polymers over extended time periods via the scaling law methodology”, *J Chem Phys*, **119**, 8189 (2003)
- [47] P. Dimitrakopoulos, “Longitudinal relaxation of initially straight flexible and stiff polymers”, *Phys Rev Lett*, **93**, 217801 (2004)
- [48] M. Doi and S. F. Edwards, “The Theory of Polymer Dynamics”, (Oxford University Press, 1986)
- [49] J. A. Doudna and T. R. Cech, “The chemical repertoire of natural ribozymes”, *Nature*, **418**, 222 (2002)
- [50] J. A. Doudna and J. W. Szostak, “RNA-catalyzed synthesis of complementary-strand RNA”, *Nature*, **339**, 519 (1989)
- [51] B. Drossel, “Biological evolution and statistical physics”, *Adv Phys*, **50**, 209 (2001)
- [52] M. Eigen, “Selforganization of matter and evolution of biological macromolecules”, *Naturwissenschaften*, **58**, 465 (1971)
- [53] M. Eigen, “Error catastrophe and antiviral strategy”, *P Natl Acad Sci USA*, **99**, 13374 (2002)
- [54] M. Eigen, J. McCaskill, and P. Schuster, “The molecular quasi-species”, *Adv Chem Phys*, **75**, 149 (1989)
- [55] M. Eigen and P. Schuster, “The hypercycle. A principle of natural self-organization. A. Emergence of the hypercycle”, *Naturwissenschaften*, **64**, 541 (1977)
- [56] M. Eigen and P. Schuster, “The hypercycle. A principle of natural self-organization. B. The abstract hypercycle”, *Naturwissenschaften*, **65**, 7 (1978)
- [57] M. Eigen and P. Schuster, “The hypercycle. A principle of natural self-organization. C. The realistic hypercycle”, *Naturwissenschaften*, **65**, 341 (1978)
- [58] E. H. Eklund and D. P. Bartel, “RNA-catalysed RNA polymerization using nucleoside triphosphates”, *Nature*, **382**, 373 (1996)
- [59] S. F. Elena, R. Miralles, and A. Moya, “Frequency-dependent selection in a mammalian RNA virus”, *Evolution*, **51**, 984 (1997)
- [60] R. Everaers, F. Jülicher, A. Ajdari, and A. C. Maggs, “Dynamic fluctuations of semiflexible filaments”, *Phys Rev Lett*, **82**, 3717 (1999)

-
- [61] B. Fabry, G. N. Maksym, J. P. Butler, M. Glogauer, D. Navajas, et al., “Scaling the microrheology of living cells”, *Phys Rev Lett*, **87**, 148102 (2001)
- [62] E. Farge and A. C. Maggs, “Dynamic scattering from semiflexible polymers”, *Macromolecules*, **26**, 5041 (1993)
- [63] M. Feingold, “Single-molecule studies of DNA and DNA-protein interactions”, *Physica E*, **9**, 616 (2001)
- [64] P. Fernandez, P. A. Pullarkat, and A. Ott, “A master relation defines the nonlinear viscoelasticity of single fibroblasts”, *Biophys J*, **90**, 3796 (2006)
- [65] J. P. Ferris, “Montmorillonite catalysis of 30-50 mer oligonucleotides: Laboratory demonstration of potential steps in the origin of the RNA world”, *Origins Life Evol B*, **32**, 311 (2002)
- [66] J. Fisher, M. Ballenger, E. O’Brien, J. Haase, R. Superfine, et al., “DNA relaxation dynamics as a probe for the intracellular environment”, *P Natl Acad Sci USA* (2009)
- [67] M. Fixman, “Simulation of polymer dynamics. II. Relaxation rates and dynamic viscosity”, *J Chem Phys*, **69**, 1538 (1978)
- [68] D. A. Fletcher and R. D. Mullins, “Cell mechanics and the cytoskeleton”, *Nature*, **463**, 485 (2010)
- [69] W. Fontana and P. Schuster, “Continuity in evolution: on the nature of transitions”, *Science*, **280**, 1451 (1998)
- [70] J. F. Fontanari, M. Santos, and E. Szathmáry, “Coexistence and error propagation in pre-biotic vesicle models: A group selection approach”, *J Theor Biol*, **239**, 247 (2006)
- [71] S. Franz and L. Peliti, “Error threshold in simple landscapes”, *J Phys A-Math Gen*, **30**, 4481 (1997)
- [72] E. Frey, “Physics in cell biology: On the physics of biopolymers and molecular motors”, *ChemPhysChem*, **3**, 270 (2002)
- [73] E. Frey, K. Kroy, and J. Wilhelm, “Physics of solutions and networks of semiflexible macromolecules and the control of cell function”, (1998), [arxiv:cond-mat/9808022](https://arxiv.org/abs/cond-mat/9808022)
- [74] E. Frey, K. Kroy, J. Wilhelm, and E. Sackmann, “Statistical mechanics of semiflexible polymers: Theory and experiment”, (1997), [arxiv:cond-mat/9707021](https://arxiv.org/abs/cond-mat/9707021)
- [75] S. Gago, S. F. Elena, R. Flores, and R. Sanjuán, “Extremely high mutation rate of a hammerhead viroid”, *Science*, **323**, 1308 (2009)

- [76] S. Galluccio, “Exact solution of the quasispecies model in a sharply peaked fitness landscape”, *Phys Rev E*, **56**, 4526 (1997)
- [77] T. Gánti, “Organization of chemical reactions into dividing and metabolizing units: The chemotons”, *BioSystems*, **7**, 15 (1975)
- [78] H. G. Garcia, P. Grayson, L. Han, M. Inamdar, J. Kondev, et al., “Biological consequences of tightly bent DNA: The other life of a macromolecular celebrity”, *Biopolymers*, **85**, 115 (2007)
- [79] A. García-Tejedor, F. Morán, and F. Montero, “Influence of the hypercyclic organization on the error threshold”, *J Theor Biol*, **127**, 393 (1987)
- [80] M. L. Gardel, F. Nakamura, J. Hartwig, J. C. Crocker, T. P. Stossel, et al., “Stress-dependent elasticity of composite actin networks as a model for cell behavior”, *Phys Rev Lett*, **96**, 088102 (2006)
- [81] M. L. Gardel, F. Nakamura, J. H. Hartwig, J. C. Crocker, T. P. Stossel, et al., “Prestressed F-actin networks cross-linked by hinged filamins replicate mechanical properties of cells”, *P Natl Acad Sci USA*, **103**, 1762 (2006)
- [82] G. J. Gemmen, R. Millin, and D. E. Smith, “Tension-dependent DNA cleavage by restriction endonucleases: Two-site enzymes are ”switched off” at low force”, *P Natl Acad Sci USA*, **103**, 11555 (2006)
- [83] U. Gerland and T. Hwa, “On the selection and evolution of regulatory DNA motifs”, *J Mol Evol*, **55**, 386 (2002)
- [84] R. F. Gesteland, T. R. Cech, and J. F. Atkins (editors), “The RNA world”, (Cold Spring Harbor Laboratory Press, 2006)
- [85] W. Gilbert, “Origin of life – the RNA world”, *Nature*, **319**, 618 (1986)
- [86] F. Gittes and F. C. MacKintosh, “Dynamic shear modulus of a semiflexible polymer network”, *Phys Rev E*, **58**, R1241 (1998)
- [87] F. Gittes, B. Schnurr, P. D. Olmsted, F. C. MacKintosh, and C. F. Schmidt, “Microscopic viscoelasticity: Shear moduli of soft materials determined from thermal fluctuations”, *Phys Rev Lett*, **79**, 3286 (1997)
- [88] A. Goel, R. D. Astumian, and D. Herschbach, “Tuning and switching a DNA polymerase motor with mechanical tension”, *P Natl Acad Sci USA*, **100**, 9699 (2003)
- [89] R. E. Goldstein and S. A. Langer, “Nonlinear dynamics of stiff polymers”, *Phys Rev Lett*, **75**, 1094 (1995)
- [90] E. Goshen, W. Z. Zhao, G. Carmon, S. Rosen, R. Granek, et al., “Relaxation dynamics of a single DNA molecule”, *Phys Rev E*, **71**, 061920 (2005)

-
- [91] R. Granek, “From semi-flexible polymers to membranes: Anomalous diffusion and reptation”, *J Phys II*, **7**, 1761 (1997)
- [92] P. Grassia and E. J. Hinch, “Computer simulations of polymer chain relaxation via Brownian motion”, *J Fluid Mech*, **308**, 255 (1996)
- [93] B.-Y. Ha and D. Thirumalai, “A mean-field model for semiflexible chains”, *J Chem Phys*, **103**, 9408 (1995)
- [94] B.-Y. Ha and D. Thirumalai, “Semiflexible chains under tension”, *J Chem Phys*, **106**, 4243 (1997)
- [95] J. Haigh, “The accumulation of deleterious genes in a population – Muller’s ratchet”, *Theor Popul Biol*, **14**, 251 (1978)
- [96] O. Hallatschek, E. Frey, and K. Kroy, “Overdamped stress relaxation in buckled rods”, *Phys Rev E*, **70**, 031802 (2004)
- [97] O. Hallatschek, E. Frey, and K. Kroy, “Propagation and relaxation of tension in stiff polymers”, *Phys Rev Lett*, **94**, 077804 (2005)
- [98] O. Hallatschek, E. Frey, and K. Kroy, “Tension dynamics in semiflexible polymers. I. Coarse-grained equations of motion”, *Phys Rev E*, **75**, 031905 (2007)
- [99] O. Hallatschek, E. Frey, and K. Kroy, “Tension dynamics in semiflexible polymers. II. Scaling solutions and applications”, *Phys Rev E*, **75**, 031906 (2007)
- [100] G. Hardin, “The competitive exclusion principle”, *Science*, **131**, 1292 (1960)
- [101] L. Harnau, R. G. Winkler, and P. Reineker, “Dynamic properties of molecular chains with variable stiffness”, *J Chem Phys*, **102**, 7750 (1995)
- [102] L. Harnau, R. G. Winkler, and P. Reineker, “Dynamic structure factor of semiflexible macromolecules in dilute solution”, *J Chem Phys*, **104**, 6355 (1996)
- [103] R. A. Harris and J. E. Hearst, “On polymer dynamics”, *J Chem Phys*, **44**, 2595 (1966)
- [104] J. W. Hatfield and S. R. Quake, “Dynamic properties of an extended polymer in solution”, *Phys Rev Lett*, **82**, 3548 (1999)
- [105] J. E. Hearst, R. A. Harris, and E. Beals, “On polymer dynamics II”, *J Chem Phys*, **45**, 3106 (1966)
- [106] J. Hermisson, O. Redner, H. Wagner, and E. Baake, “Mutation-selection balance: Ancestry, load, and maximum principle”, *Theor Popul Biol*, **62**, 9 (2002)

- [107] M. G. L. van den Heuvel, M. P. de Graaff, S. G. Lemay, and C. Dekker, “Electrophoresis of individual microtubules in microchannels”, *P Natl Acad Sci USA*, **104**, 7770 (2007)
- [108] E. J. Hinch, “Perturbation Methods”, (Cambridge University Press, 1991)
- [109] M. Hinczewski and R. R. Netz, “Anisotropic mean-field theory for semiflexible polymer dynamics under tension”, (2009), [arxiv:0908.0376v1](https://arxiv.org/abs/0908.0376v1)
- [110] M. Hinczewski and R. R. Netz, “Global cross-over dynamics of single semiflexible polymers”, *Europhys Lett*, **88**, 18001 (2009)
- [111] M. Hinczewski, X. Schlagberger, M. Rubinstein, O. Krichevsky, and R. R. Netz, “End-monomer dynamics in semiflexible polymers”, *Macromolecules*, **42**, 860 (2009)
- [112] H. Hirsch, J. Wilhelm, and E. Frey, “Quantitative tube model for semiflexible polymer solutions”, *Eur Phys J E*, **24**, 35 (2007)
- [113] T. Hiraiwa and T. Ohta, “Viscoelasticity of a single semiflexible polymer chain”, *Macromolecules*, **42**, 7553 (2009)
- [114] J. Hofbauer, “The selection mutation equation”, *J Math Biol*, **23**, 41 (1985)
- [115] J. Hofbauer and K. Sigmund, “Evolutionary Games and Population dynamics”, (Cambridge University Press, 1998)
- [116] B. D. Hoffman and E. S. G. Shaqfeh, “The dynamics of the coil-stretch transition for long, flexible polymers in planar mixed flows”, *J Rheol*, **51**, 947 (2007)
- [117] J. J. Hopfield, “Kinetic proofreading: A new mechanism for reducing errors in biosynthetic processes requiring high specificity”, *P Natl Acad Sci USA*, **71**, 4135 (1974)
- [118] M. A. Huynen, P. F. Stadler, and W. Fontana, “Smoothness within ruggedness: The role of neutrality in adaptation”, *P Natl Acad Sci USA*, **93**, 397 (1996)
- [119] G. O. Ibáñez-García and S. Hanna, “Relaxation of an initially-stretched, tethered polymer under shear flow: A Brownian dynamics simulation”, *Soft Matter*, **5**, 4464 (2009)
- [120] B. Ibarra, Y. R. Chemla, S. Plyasunov, S. B. Smith, J. M. Lázaro, et al., “Proof-reading dynamics of a processive DNA polymerase”, *Embo J*, **28**, 2794 (2009)
- [121] D. E. Ingber, “Tensegrity I. Cell structure and hierarchical systems biology”, *J Cell Sci*, **116**, 1157 (2003)
- [122] D. E. Ingber, “Tensegrity II. How structural networks influence cellular information processing networks”, *J Cell Sci*, **116**, 1397 (2003)

- [123] K. Jain and J. Krug, “Adaptation in simple and complex fitness landscapes”, (2005), arxiv:q-bio/0508008v1
- [124] W. K. Johnston, P. J. Unrau, M. S. Lawrence, M. E. Glasner, and D. P. Bartel, “RNA-catalyzed RNA polymerization: Accurate and general RNA-templated primer extension”, *Science*, **292**, 1319 (2001)
- [125] G. F. Joyce, “RNA evolution and the origins of life”, *Nature*, **338**, 217 (1989)
- [126] G. F. Joyce, “Forty years of *in vitro* evolution”, *Angew Chem Int Edit*, **46**, 6420 (2007)
- [127] S. Jun and B. Mulder, “Entropy-driven spatial organization of highly confined polymers: Lessons for the bacterial chromosome”, *P Natl Acad Sci USA*, **103**, 12388 (2006)
- [128] C. Kamp and S. Bornholdt, “Coevolution of quasispecies: B-cell mutation rates maximize viral error catastrophes”, *Phys Rev Lett*, **88**, 068104 (2002)
- [129] A. Kanavarioti, P. A. Monnard, and D. W. Deamer, “Eutectic phases in ice facilitate nonenzymatic nucleic acid synthesis”, *Astrobiology*, **1**, 271 (2002)
- [130] K. E. Kasza, G. H. Koenderink, Y. C. Lin, C. P. Broedersz, W. Messner, et al., “Nonlinear elasticity of stiff biopolymers connected by flexible linkers”, *Phys Rev E*, **79** (2009)
- [131] G. von Kiedrowski, “A self-replicating hexadeoxynucleotide”, *Angew Chem Int Edit*, **25**, 932 (1986)
- [132] G. von Kiedrowski, B. Wlotzka, J. Helbing, M. Matzen, and S. Jordan, “Parabolic growth of a self-replicating hexadeoxynucleotide bearing a 3'-5'-phosphoamidate linkage”, *Angew Chem Int Edit*, **30**, 423 (1991)
- [133] J. Kierfeld, O. Niamploy, V. Sa-yakanit, and R. Lipowsky, “Stretching of semiflexible polymers with elastic bonds”, *Eur Phys J E*, **14**, 17 (2004)
- [134] D.-E. Kim and G. F. Joyce, “Cross-catalytic replication of an RNA ligase ribozyme”, *Chem Biol*, **11**, 1505 (2004)
- [135] H. Kojima, A. Ishijima, and T. Yanagida, “Direct measurement of stiffness of single actin-filaments with and without tropomyosin by *in-vitro* nanomanipulation”, *P Natl Acad Sci USA*, **91**, 12962 (1994)
- [136] N. L. Komarova, “Replicator-mutator equation, universality property and population dynamics of learning”, *J Theor Biol*, **230**, 227 (2004)
- [137] N. L. Komarova, P. Niyogi, and M. A. Nowak, “The evolutionary dynamics of grammar acquisition”, *J Theor Biol*, **209**, 43 (2001)

- [138] E. V. Koonin, “An RNA-making reactor for the origin of life”, *P Natl Acad Sci USA*, **104**, 9105 (2007)
- [139] D. A. Koster, K. Palle, E. S. M. Bot, M.-A. Bjornsti, and N. H. Dekker, “Antitumour drugs impede DNA uncoiling by topoisomerase I”, *Nature*, **448**, 213 (2007)
- [140] S. Köster, H. Stark, T. Pfohl, and J. Kierfeld, “Fluctuations of single confined actin filaments”, *Biophys Rev Lett*, **2**, 155 (2007)
- [141] O. Kratky and G. Porod, “Röntgenuntersuchung gelöster Fadenmoleküle”, *Recl Trav Chim Pay B*, **68**, 1106 (1949)
- [142] K. Kroy, “Dynamics of wormlike and glassy wormlike chains”, *Soft Matter* (2008)
- [143] K. Kroy and E. Frey, “Force-extension relation and plateau modulus for wormlike chains”, *Phys Rev Lett*, **77**, 306 (1996)
- [144] K. Kroy and E. Frey, “Dynamic scattering from solutions of semiflexible polymers”, *Phys Rev E*, **55**, 3092 (1997)
- [145] K. Kroy and J. Glaser, “The glassy wormlike chain”, *New J Phys*, **9**, 416 (2007)
- [146] S. Kumar, I. Z. Maxwell, A. Heisterkamp, T. R. Polte, T. P. Lele, et al., “Viscoelastic retraction of single living stress fibers and its impact on cell shape, cytoskeletal organization, and extracellular matrix mechanics”, *Biophys J*, **90**, 3762 (2006)
- [147] A. Kun, M. Santos, and E. Szathmáry, “Real ribozymes suggest a relaxed error threshold”, *Nat Genet*, **37**, 1008 (2005)
- [148] B. Ladoux and P. S. Doyle, “Stretching tethered DNA chains in shear flow”, *Europhys Lett*, **52**, 511 (2000)
- [149] P.-Y. Lai, Y.-J. Sheng, and H.-K. Tsao, “Releasing a stretched polymer chain: Scaling and Monte Carlo studies”, *Physica A*, **254**, 280 (1998)
- [150] P. S. Lang, Diploma Thesis, LMU München (2010)
- [151] R. G. Larson, H. Hu, D. E. Smith, and S. Chu, “Brownian dynamics simulations of a DNA molecule in an extensional flow field”, *J Rheol*, **43**, 267 (1999)
- [152] L. Le Goff, O. Hallatschek, E. Frey, and F. Amblard, “Tracer studies on F-actin fluctuations”, *Phys Rev Lett*, **89**, 258101 (2002)
- [153] N. K. Lee and D. Thirumalai, “Pulling-speed-dependent force-extension profiles for semiflexible chains”, *Biophys J*, **86**, 2641 (2004)
- [154] I. Leuthäusser, “An exact correspondence between Eigen’s evolution model and a two-dimensional Ising system”, *J Chem Phys*, **84**, 1884 (1986)

-
- [155] I. Leuthäusser, “Statistical mechanics of Eigen’s evolution model”, *J Stat Phys*, **48**, 343 (1987)
- [156] P. Levi and K. Mecke, “Radial distribution function for semiflexible polymers confined in microchannels”, *Europhys Lett*, **78**, 38001 (2007)
- [157] D. M. J. Lilley, “Structure, folding and mechanisms of ribozymes”, *Curr Opin Struc Biol*, **15**, 313 (2005)
- [158] T. A. Lincoln and G. F. Joyce, “Self-sustained replication of an RNA enzyme”, *Science*, **323**, 1229 (2009)
- [159] J. Liu, M. L. Gardel, K. Kroy, E. Frey, B. D. Hoffman, et al., “Microrheology probes length scale dependent rheology”, *Phys Rev Lett*, **96**, 118104 (2006)
- [160] L. Livadaru, R. R. Netz, and H. J. Kreuzer, “Stretching response of discrete semiflexible polymers”, *Macromolecules*, **36**, 3732 (2003)
- [161] T. B. Liverpool, “Dynamics of inextensible semiflexible filaments”, *Phys Rev E*, **72**, 021805 (2005)
- [162] T. B. Liverpool and A. C. Maggs, “Dynamic scattering from semiflexible polymers”, *Macromolecules*, **34**, 6064 (2001)
- [163] D. Long, J.-L. Viovy, and A. Ajdari, “Simultaneous action of electric fields and nonelectric forces on a polyelectrolyte: Motion and deformation”, *Phys Rev Lett*, **76**, 3858 (1996)
- [164] D. Long, J.-L. Viovy, and A. Ajdari, “Stretching DNA with electric fields revisited”, *Biopolymers*, **39**, 755 (1996)
- [165] D. Lumma, S. Keller, T. Vilgis, and J. O. Rädler, “Dynamics of large semiflexible chains probed by fluorescence correlation spectroscopy”, *Phys Rev Lett*, **90**, 218301 (2003)
- [166] F. C. MacKintosh, J. Käs, and P. A. Janmey, “Elasticity of semiflexible biopolymer networks”, *Phys Rev Lett*, **75**, 4425 (1995)
- [167] B. Maier, D. Bensimon, and V. Croquette, “Replication by a single DNA polymerase of a stretched single-stranded DNA”, *P Natl Acad Sci USA*, **97**, 12002 (2000)
- [168] B. Maier, U. Seifert, and J. O. Rädler, “Elastic response of DNA to external electric fields in two dimensions”, *Europhys Lett*, **60**, 622 (2002)
- [169] A. Majumdar, B. Suki, N. Rosenblatt, A. M. Alencar, and D. Stamenović, “Power-law creep behavior of a semiflexible chain”, *Phys Rev E*, **78**, 041922 (2008)

- [170] S. Manneville, P. Cluzel, J.-L. Viovy, D. Chatenay, and F. Caron, “Evidence for the universal scaling behaviour of a freely relaxing DNA molecule”, *Europhys Lett*, **36**, 413 (1996)
- [171] J. F. Marko, “Stretching must twist DNA”, *Europhys Lett*, **38**, 183 (1997)
- [172] J. F. Marko, “DNA under high tension: Overstretching, undertwisting, and relaxation dynamics”, *Phys Rev E*, **57**, 2134 (1998)
- [173] J. F. Marko and S. Cocco, “The micromechanics of DNA”, *Phys World*, **16**, 37 (2003)
- [174] J. F. Marko and E. D. Siggia, “Stretching DNA”, *Macromolecules*, **28**, 8759 (1995)
- [175] J. Maynard Smith, “Hypercycles and the origin of life”, *Nature*, **280**, 445 (1979)
- [176] J. Maynard Smith, “Models of evolution”, *P Roy Soc Lond B Bio*, **219**, 315 (1983)
- [177] J. Maynard Smith and E. Szathmary, “The major transitions in evolution”, (Oxford University Press, 1995)
- [178] A. K. Mazur, “Wormlike chain theory and bending of short DNA”, *Phys Rev Lett*, **98**, 218102 (2007)
- [179] K. E. McGinness and G. F. Joyce, “RNA-catalyzed RNA ligation on an external RNA template”, *Chem Biol*, **9**, 297 (2002)
- [180] C. P. McKay, “What is life – and how do we search for it in other worlds?”, *Plos Biol*, **2**, E302 (2004)
- [181] J. C. Meiners and S. R. Quake, “Femtonewton force spectroscopy of single extended DNA molecules”, *Phys Rev Lett*, **84**, 5014 (2000)
- [182] D. Mizuno, D. A. Head, F. C. MacKintosh, and C. F. Schmidt, “Active and passive microrheology in equilibrium and nonequilibrium systems”, *Macromolecules*, **41**, 7194 (2008)
- [183] D. Mizuno, C. Tardin, C. F. Schmidt, and F. C. MacKintosh, “Nonequilibrium mechanics of active cytoskeletal networks”, *Science*, **315**, 370 (2007)
- [184] A. Montesi, D. C. Morse, and M. Pasquali, “Brownian dynamics algorithm for bead-rod semiflexible chain with anisotropic friction”, *J Chem Phys*, **122**, 084903 (2005)
- [185] D. C. Morse, “Viscoelasticity of concentrated isotropic solutions of semiflexible polymers. 2. Linear response”, *Macromolecules*, **31**, 7044 (1998)
- [186] D. C. Morse, “Viscoelasticity of tightly entangled solutions of semiflexible polymers”, *Phys Rev E*, **58**, R1237 (1998)

-
- [187] D. C. Morse, “Theory of constrained Brownian motion”, *Adv Chem Phys*, **128**, 65 (2004)
- [188] A. Moya, E. C. Holmes, and F. González-Candelas, “The population genetics and evolutionary epidemiology of RNA viruses”, *Nat Rev Micro*, **2**, 279 (2004)
- [189] T. Munk, O. Hallatschek, C. H. Wiggins, and E. Frey, “Dynamics of semiflexible polymers in a flow field”, *Phys Rev E*, **74**, 041911 (2006)
- [190] G.-M. Nam and N.-K. Lee, “Kinetics of a semiflexible chain under external force”, *J Chem Phys*, **126**, 164902 (2007)
- [191] R. R. Netz, “Strongly stretched semiflexible extensible polyelectrolytes and DNA”, *Macromolecules*, **34**, 7522 (2001)
- [192] M. Nilsson and N. Snoad, “Error thresholds for quasispecies on dynamic fitness landscapes”, *Phys Rev Lett*, **84**, 191 (2000)
- [193] M. Nilsson and N. Snoad, “Quasispecies evolution on a fitness landscape with a fluctuating peak”, *Phys Rev E*, **65**, 031901 (2002)
- [194] E. van Nimwegen, J. P. Crutchfield, and M. Huynen, “Neutral evolution of mutational robustness”, *P Natl Acad Sci USA*, **96**, 9716 (1999)
- [195] M. Nowak and P. Schuster, “Error thresholds of replication in finite populations. Mutation frequencies and the onset of Muller’s ratchet”, *J Theor Biol*, **137**, 375 (1989)
- [196] M. A. Nowak, “From quasispecies to universal grammar”, *Z Phys Chem*, **216**, 5 (2002)
- [197] M. A. Nowak, N. L. Komarova, and P. Niyogi, “Evolution of universal grammar”, *Science*, **291**, 114 (2001)
- [198] M. A. Nowak and H. Ohtsuki, “Prevolutionary dynamics and the origin of evolution”, *P Natl Acad Sci USA*, **105**, 14924 (2008)
- [199] B. Obermayer and E. Frey, “Escalation of error catastrophe for enzymatic self-replicators”, *Europhys Lett*, **88**, 48006 (2009)
- [200] B. Obermayer and E. Frey, “Tension dynamics and viscoelasticity of extensible worm-like chains”, *Phys Rev E*, **80**, 040801(R) (2009)
- [201] B. Obermayer and E. Frey, “Error thresholds for self- and cross-specific enzymatic replication”, submitted to *J Theor Biol* (2010), [arxiv:1003.1304](https://arxiv.org/abs/1003.1304)
- [202] B. Obermayer and O. Hallatschek, “Coupling of transverse and longitudinal response in stiff polymers”, *Phys Rev Lett*, **99**, 098302 (2007)

- [203] B. Obermayer, O. Hallatschek, E. Frey, and K. Kroy, "Stretching dynamics of semi-flexible polymers", *Eur Phys J E*, **23**, 375 (2007)
- [204] B. Obermayer, W. Möbius, O. Hallatschek, E. Frey, and K. Kroy, "Freely relaxing polymers remember how they were straightened", *Phys Rev E*, **79**, 021804 (2009)
- [205] T. Odijk, "On the statistics and dynamics of confined or entangled stiff polymers", *Macromolecules*, **16**, 1340 (1983)
- [206] L. E. Orgel, "Molecular replication", *Nature*, **358**, 203 (1992)
- [207] L. E. Orgel, "The origin of life. A review of facts and speculations", *Trends Biochem Sci*, **23**, 491 (1998)
- [208] L. E. Orgel, "Prebiotic chemistry and the origin of the RNA world", *Crit Rev Biochem Mol*, **39**, 99 (2004)
- [209] N. R. Pace and T. L. Marsh, "RNA catalysis and the origin of life", *Origins Life Evol B*, **16**, 97 (1985)
- [210] F. Pampaloni, G. Lattanzi, A. Jonás, T. Surrey, E. Frey, et al., "Thermal fluctuations of grafted microtubules provide evidence of a length-dependent persistence length", *P Natl Acad Sci USA*, **103**, 10248 (2006)
- [211] M. Pasquali, V. Shankar, and D. C. Morse, "Viscoelasticity of dilute solutions of semiflexible polymers", *Phys Rev E*, **64**, 020802 (2001)
- [212] N. Paul and G. F. Joyce, "A self-replicating ligase ribozyme", *P Natl Acad Sci USA*, **99**, 12733 (2002)
- [213] N. Paul and G. F. Joyce, "Minimal self-replicating systems", *Curr Opin Chem Biol*, **8**, 634 (2004)
- [214] T. T. Perkins, S. R. Quake, D. E. Smith, and S. Chu, "Relaxation of a single DNA molecule observed by optical microscopy", *Science*, **264**, 822 (1994)
- [215] T. T. Perkins, D. E. Smith, R. G. Larson, and S. Chu, "Stretching of a single tethered polymer in a uniform flow", *Science*, **268**, 83 (1995)
- [216] S. Pino, F. Ciciriello, G. Costanzo, and E. D. Mauro, "Nonenzymatic RNA ligation in water", *J Biol Chem*, **283**, 36494 (2008)
- [217] S. R. Quake, H. Babcock, and S. Chu, "The dynamics of partially extended single molecules of DNA", *Nature*, **388**, 151 (1997)
- [218] S. Rajamani, A. Vlassov, S. Benner, A. Coombs, F. Olasagasti, et al., "Lipid-assisted synthesis of RNA-like polymers from mononucleotides", *Origins Life Evol B*, **38**, 57 (2008)

- [219] P. Ranjith and P. B. S. Kumar, “Dynamics of a semiflexible filament under external force”, *Physica A*, **318**, 220 (2003)
- [220] C. H. Reccius, J. T. Mannion, J. D. Cross, and H. G. Craighead, “Compression and free expansion of single DNA molecules in nanochannels”, *Phys Rev Lett*, **95**, 268101 (2005)
- [221] W. Reisner, K. J. Morton, R. Riehn, Y. M. Wang, Z. N. Yu, et al., “Statics and dynamics of single DNA molecules confined in nanochannels”, *Phys Rev Lett*, **94**, 196101 (2005)
- [222] M. W. Rochlin, M. E. Dailey, and P. C. Bridgman, “Polymerizing microtubules activate site-directed F-actin assembly in nerve growth cones”, *Mol Biol Cell*, **10**, 2309 (1999)
- [223] N. Rosenblatt, A. M. Alencar, A. Majumdar, B. Suki, and D. Stamenović, “Dynamics of prestressed semiflexible polymer chains as a model of cell rheology”, *Phys Rev Lett*, **97**, 168101 (2006)
- [224] D. B. Saakian, C. K. Biebricher, and C.-K. Hu, “Phase diagram for the Eigen quasispecies theory with a truncated fitness landscape”, *Phys Rev E*, **79**, 041905 (2009)
- [225] D. B. Saakian and C.-K. Hu, “Exact solution of the Eigen model with general fitness functions and degradation rates”, *P Natl Acad Sci USA*, **103**, 4935 (2006)
- [226] N. Saitô, K. Takahashi, and Y. Yunoki, “Statistical mechanical theory of stiff chains”, *J Phys Soc Jpn*, **22**, 219 (1967)
- [227] E. Schrödinger, “What is Life?”, (Cambridge University Press, 1948)
- [228] C. M. Schroeder, H. P. Babcock, E. S. G. Shaqfeh, and S. Chu, “Observation of polymer conformation hysteresis in extensional flow”, *Science*, **301**, 1515 (2003)
- [229] C. M. Schroeder, E. S. G. Shaqfeh, and S. Chu, “Effect of hydrodynamic interactions on DNA dynamics in extensional flow: Simulation and single molecule experiment”, *Macromolecules*, **37**, 9242 (2004)
- [230] C. M. Schroeder, R. E. Teixeira, E. S. G. Shaqfeh, and S. Chu, “Dynamics of DNA in the flow-gradient plane of steady shear flow: Observations and simulations”, *Macromolecules*, **38**, 1967 (2005)
- [231] P. Schuster, “Prediction of RNA secondary structures: From theory to models and real molecules”, *Rep Prog Phys*, **69**, 1419 (2006)
- [232] P. Schuster and J. Swetina, “Stationary mutant distributions and evolutionary optimization”, *Bull Math Biol*, **50**, 635 (1988)
- [233] A. Seeholzer, Diploma Thesis, LMU München (2010)

- [234] D. Segré, D. Ben-Eli, and D. Lancet, “Compositional genomes: Prebiotic information transfer in mutually catalytic noncovalent assemblies”, *P Natl Acad Sci USA*, **97**, 4112 (2000)
- [235] D. Segré, D. Lancet, O. Kedem, and Y. Pilpel, “Graded autocatalysis replication domain (GARD): Kinetic analysis of self-replication in mutually catalytic sets”, *Origins Life Evol B*, **28**, 501 (1998)
- [236] U. Seifert, W. Wintz, and P. Nelson, “Straightening of thermal fluctuations in semi-flexible polymers by applied tension”, *Phys Rev Lett*, **77**, 5389 (1996)
- [237] C. Semmrich, T. Storz, J. Glaser, R. Merkel, A. R. Bausch, et al., “Glass transition and rheological redundancy in F-actin solutions”, *P Natl Acad Sci USA*, **104**, 20199 (2007)
- [238] V. Shankar, M. Pasquali, and D. C. Morse, “Theory of linear viscoelasticity of semi-flexible rods in dilute solution”, *J Rheol*, **46**, 1111 (2002)
- [239] E. S. G. Shaqfeh, “The dynamics of single-molecule DNA in flow”, *J Non-Newton Fluid*, **130**, 1 (2005)
- [240] E. S. G. Shaqfeh, G. H. McKinley, N. Woo, D. A. Nguyen, and T. Sridhar, “On the polymer entropic force singularity and its relation to extensional stress relaxation and filament recoil”, *J Rheol*, **48**, 209 (2004)
- [241] Y.-J. Sheng, P.-Y. Lai, and H.-K. Tsao, “Nonequilibrium relaxation of a stretched polymer chain”, *Phys Rev E*, **56**, 1900 (1997)
- [242] D. A. M. M. Silvestre and J. F. Fontanari, “The information capacity of hypercycles”, *J Theor Biol*, **254**, 804 (2008)
- [243] D. E. Smith, H. P. Babcock, and S. Chu, “Single-polymer dynamics in steady shear flow”, *Science*, **283**, 1724 (1999)
- [244] S. B. Smith, Y. J. Cui, and C. Bustamante, “Overstretching B-DNA: The elastic response of individual double-stranded and single-stranded DNA molecules”, *Science*, **271**, 795 (1996)
- [245] S. B. Smith, L. Finzi, and C. Bustamante, “Direct mechanical measurements of the elasticity of single DNA-molecules by using magnetic beads”, *Science*, **258**, 1122 (1992)
- [246] K. Soda, “Dynamics of stiff chains. 1. Equation of motion”, *J Phys Soc Jpn*, **35**, 866 (1973)
- [247] M. Somasi, B. Khomami, N. J. Woo, J. S. Hur, and E. S. G. Shaqfeh, “Brownian dynamics simulations of bead-rod and bead-spring chains: Numerical algorithms and coarse-graining issues”, *J Non-Newton Fluid*, **108**, 227 (2002)

- [248] P. F. Stadler, W. Schnabl, C. V. Forst, and P. Schuster, “Dynamics of small autocatalytic reaction networks. II. Replication, mutation and catalysis”, *Bull Math Biol*, **57**, 21 (1995)
- [249] P. F. Stadler and P. Schuster, “Mutation in autocatalytic reaction networks – an analysis based on perturbation theory”, *J Math Biol*, **30**, 597 (1992)
- [250] D. Stigter and C. Bustamante, “Theory for the hydrodynamic and electrophoretic stretch of tethered B-DNA”, *Biophys J*, **75**, 1197 (1998)
- [251] C. Storm and P. C. Nelson, “Theory of high-force DNA stretching and overstretching”, *Phys Rev E*, **67**, 051906 (2003)
- [252] T. Strick, J.-F. Allemand, V. Croquette, and D. Bensimon, “Twisting and stretching single DNA molecules”, *Prog Biophys Mol Bio*, **74**, 115 (2000)
- [253] T. R. Strick, V. Croquette, and D. Bensimon, “Single-molecule analysis of DNA uncoiling by a type II topoisomerase”, *Nature*, **404**, 901 (2000)
- [254] S. Sturm, B. Obermayer, and K. Kroy, in preparation (2010)
- [255] J. Summers and S. Litwin, “Examining the theory of error catastrophe”, *J Virol*, **80**, 20 (2006)
- [256] J. Swetina and P. Schuster, “Self-replication with errors – a model for polynucleotide replication”, *Biophys Chem*, **16**, 329 (1982)
- [257] E. Szathmáry and J. Maynard Smith, “From replicators to reproducers: The first major transitions leading to life”, *J Theor Biol*, **187**, 555 (1997)
- [258] J. W. Szostak, D. P. Bartel, and P. L. Luisi, “Synthesizing life”, *Nature*, **409**, 387 (2001)
- [259] N. Takeuchi and P. Hogeweg, “Error-threshold exists in fitness landscapes with lethal mutants”, *BMC Evol Biol*, **7**, 15 (2007)
- [260] N. Takeuchi, P. H. Poorthuis, and P. Hogeweg, “Phenotypic error threshold; additivity and epistasis in RNA evolution”, *BMC Evol Biol*, **5**, 9 (2005)
- [261] P. Tarazona, “Error thresholds for molecular quasispecies as phase transitions: From simple landscapes to spin-glass models”, *Phys Rev A*, **45**, 6038 (1992)
- [262] K. M. Taute, F. Pampaloni, E. Frey, and E.-L. Florin, “Microtubule dynamics depart from the wormlike chain model”, *Phys Rev Lett*, **100**, 028102 (2008)
- [263] F. Thüroff, E. Frey, and B. Obermayer, in preparation (2010)
- [264] F. Thüroff, F. Wagner, and E. Frey, “Boundary effects on the end-to-end distance statistics of confined semiflexible polymers”, (2010), [arxiv:1002.1826v1](https://arxiv.org/abs/1002.1826v1)

- [265] S. W. P. Turner, M. Cabodi, and H. G. Craighead, “Confinement-induced entropic recoil of single DNA molecules in a nanofluidic structure”, *Phys Rev Lett*, **88**, 128103 (2002)
- [266] V. Vasas, E. Szathmáry, and M. Santos, “Lack of evolvability in self-sustaining autocatalytic networks constraints metabolism-first scenarios for the origin of life”, *P Natl Acad Sci USA*, **107**, 1470 (2010)
- [267] F. Wagner, G. Lattanzi, and E. Frey, “Conformations of confined biopolymers”, *Phys Rev E*, **75**, 050902 (2007)
- [268] N. Wagner, E. Tannenbaum, and G. Ashkenasy, “Second-order catalytic quasispecies yields first-order phase transition”, (2009), [arxiv:0912.4960v1](https://arxiv.org/abs/0912.4960v1)
- [269] J. Z. Wang and H. J. Gao, “A generalized bead-rod model for Brownian dynamics simulations of wormlike chains under strong confinement”, *J Chem Phys*, **123**, 084906 (2005)
- [270] M. D. Wang, H. Yin, R. Landick, J. Gelles, and S. M. Block, “Stretching DNA with optical tweezers”, *Biophys J*, **72**, 1335 (1997)
- [271] N. Wang, K. Naruse, D. Stamenović, J. J. Fredberg, S. M. Mijailovich, et al., “Mechanical behavior in living cells consistent with the tensegrity model”, *P Natl Acad Sci USA*, **98**, 7765 (2001)
- [272] A. M. Weiner and N. Maizels, “tRNA-like structures tag the 3’ ends of genomic RNA molecules for replication: Implications for the origin of protein synthesis”, *P Natl Acad Sci USA*, **84**, 7383 (1987)
- [273] T. Wiehe, “Model dependency of error thresholds: The role of fitness functions and contrasts between the finite and infinite sites models”, *Genet Res*, **69**, 127 (1997)
- [274] C. H. Wiggins, D. Rivelino, A. Ott, and R. E. Goldstein, “Trapping and wiggling: Elastohydrodynamics of driven microfilaments”, *Biophys J*, **74**, 1043 (1998)
- [275] P. A. Wiggins, T. van der Heijden, F. Moreno-Herrero, A. Spakowitz, R. Phillips, et al., “High flexibility of DNA on short length scales probed by atomic force microscopy”, *Nat Nanotechnol*, **1**, 137 (2006)
- [276] P. A. Wiggins and P. C. Nelson, “Generalized theory of semiflexible polymers”, *Phys Rev E*, **73**, 031906 (2006)
- [277] J. Wilhelm and E. Frey, “Radial distribution function of semiflexible polymers”, *Phys Rev Lett*, **77**, 2581 (1996)
- [278] J. Wilhelm and E. Frey, “Elasticity of stiff polymer networks”, *Phys Rev Lett*, **91**, 108103 (2003)

-
- [279] C. O. Wilke, “Quasispecies theory in the context of population genetics”, *BMC Evol Biol*, **5**, 44 (2005)
- [280] C. O. Wilke, C. Ronnewinkel, and T. Martinetz, “Dynamic fitness landscapes in molecular evolution”, *Phys Rep*, **349**, 395 (2001)
- [281] C. O. Wilke, J. L. Wang, C. Ofria, R. E. Lenski, and C. Adami, “Evolution of digital organisms at high mutation rates leads to survival of the flattest”, *Nature*, **412**, 331 (2001)
- [282] R. G. Winkler, P. Reineker, and L. Harnau, “Models and equilibrium properties of stiff molecular chains”, *J Chem Phys*, **101**, 8119 (1994)
- [283] G. Woodcock and P. G. Higgs, “Population evolution on a multiplicative single-peak fitness landscape”, *J Theor Biol*, **179**, 61 (1996)
- [284] T. F. Wu and L. E. Orgel, “Nonenzymatic template-directed synthesis on oligodeoxycytidylate sequences in hairpin oligonucleotides”, *J Am Chem Soc*, **114**, 317 (1992)
- [285] G. J. Wuite, S. B. Smith, M. Young, D. Keller, and C. Bustamante, “Single-molecule studies of the effect of template tension on T7 DNA polymerase activity”, *Nature*, **404**, 103 (2000)
- [286] C. Yuan, H. Chen, X. W. Lou, and L. A. Archer, “DNA bending stiffness on small length scales”, *Phys Rev Lett*, **100**, 018102 (2008)
- [287] E. Yuste, A. Moya, and C. Lopez-Galindez, “Frequency-dependent selection in human immunodeficiency virus type 1”, *J Gen Virol*, **83**, 103 (2002)
- [288] H. S. Zaher and P. J. Unrau, “Selection of an improved RNA polymerase ribozyme with superior extension and fidelity”, *RNA*, **13**, 1017 (2007)

Danksagung

An erster Stelle möchte ich mich bei meinem Betreuer Prof. Dr. Erwin Frey bedanken, insbesondere für die vertrauensvolle Unterstützung, die Ermöglichung einer flexiblen Zeiteinteilung und die vielen Gelegenheiten, in München oder auf verschiedenen Konferenzen mit diversen Thematiken in Berührung zu kommen und schließlich einige davon mit großer wissenschaftlicher Freiheit bearbeiten zu können.

Außerdem danke ich Prof. Dr. Klaus Kroy für die langjährige und auch wegen seines ausdauernden Enthusiasmus' sehr ergiebige Zusammenarbeit im Bereich der Polymerdynamik. Dr. Oskar Hallatschek danke ich für die intensive Hilfe nicht nur während der Diplomarbeit, die es mir ermöglicht hat, spätere Projekte eigenständig anzugehen. Besonders schätze ich auch seine Einladung ans Kavli Institute for Theoretical Physics in Santa Barbara, wo ich faszinierende Einblicke in die Populationsgenetik bekommen konnte. Bei Prof. Dr. Ulrich Gerland möchte ich mich für die Arbeit an spannenden laufenden Projekten bedanken, die keinen Platz mehr in dieser Arbeit gefunden haben.

Schließlich möchte ich meinen Kollegen am Lehrstuhl danken: Karen Alim für über drei Jahre höchst angenehmer Bürogemeinschaft, Wolfram Möbius für Computersimulationen und vielfältige Ratschläge, Florian Thüroff, Anna Melbinger und Jonas Cremer nebst anderem auch für das Korrekturlesen der Arbeit, und allen anderen für die offene und hilfsbereite Atmosphäre. Dankbar bin ich auch für finanzielle Förderung durch ein Stipendium nach dem bayerischen Eliteförderungsgesetz.

Curriculum Vitae

Personal

born July 13, 1980 in Gräfelfing near Munich, Germany

Academic Track

- PhD thesis at Ludwig-Maximilians-Universität Munich since October 2006
Supervisor: Prof. Dr. Erwin Frey
- Research assistant at Leipzig University (October 2005 – April 2006)
- Diploma of physics at Freie Universität Berlin (October 2005)
Thesis on “Nonequilibrium dynamics of semiflexible polymers”
Supervisor: Prof. Dr. Erwin Frey
- Studies of physics at Wake Forest University, NC, USA (September 2002 – May 2003)
- Studies of physics at Freie Universität Berlin (October 2000 – September 2005)
- School until May 1999